



UNIVERSITAT_{DE}
BARCELONA

Tailored immunotherapies on 3D models of non-Hodgkin lymphoma

Ferran Araujo Ayala



Aquesta tesi doctoral està subjecta a la llicència **Reconeixement 4.0. Espanya de Creative Commons.**

Esta tesis doctoral está sujeta a la licencia **Reconocimiento 4.0. España de Creative Commons.**

This doctoral thesis is licensed under the **Creative Commons Attribution 4.0. Spain License.**

DOCTORAL PROGRAMME IN BIOMEDICINE

Research line – Molecular and cellular biology of cancer



UNIVERSITAT DE
BARCELONA

2020 – 2024

University of Barcelona – Faculty of Medicine

Tailored immunotherapies on 3D models of non-Hodgkin lymphoma

Doctoral thesis presented by:

Ferran Araujo Ayala

Institut d'Investigacions Biomèdiques August Pi i Sunyer (IDIBAPS)

Ferran Araujo Ayala

PhD candidate

Patricia Pérez Galán

Thesis director

Armando López Guillermo

Thesis tutor

Barcelona, 2024

Als que m'han acompanyat en aquest camí

TABLE OF CONTENTS

TABLE OF CONTENTS

TABLE OF CONTENTS	1
LIST OF ABBREVIATIONS	6
ABSTRACT	13
INTRODUCTION	19
1. B-CELL NON-HODGKIN LYMPHOMA.....	21
2. MANTLE CELL LYMPHOMA.....	24
2.1. Pathogenesis	24
2.2. Tumor microenvironment	25
2.2.1. Mesenchymal stromal cells	26
2.2.2. Follicular dendritic cells.....	27
2.2.3. Macrophages	27
2.3. Non-nodal vs indolent Mantle Cell Lymphoma.....	29
2.4. Diagnosis and prognosis	30
2.5. Treatment.....	31
3. FOLLICULAR LYMPHOMA	35
3.1. Pathogenesis	35
3.2. Tumor microenvironment	37
3.2.1. T cells	39
3.2.2. Lymphoid stromal cells.....	42
3.2.3. Tumor associated macrophages (TAMs)	43
3.3. Diagnosis and prognosis	44
3.4. Treatment.....	47
3.5. Histological transformation	50
4. MODELS TO STUDY B-NHL.....	52
4.1. Culture of primary samples	52
4.1.1. Cell lines and mouse models	52
4.1.2. MCL primary cultures	53

TABLE OF CONTENTS

4.1.3. FL primary cultures	54
4.2. 3D models	55
4.2.1. 3D models in NHL	57
5. CD70 AS A TARGET FOR CAR-T THERAPY	59
5.1. CD70	59
5.2. CD70 as a target in B-NHL	60
5.3. CAR-T cells	64
5.3.1. CD19 CAR-T	66
5.3.2. Dual CAR-T	67
5.4. Anti-CD70 CAR-T strategies	68
5.4.1. Ligand-based CAR-Ts	69
5.4.2. scFv-based CAR-Ts	70
5.4.3. Fratricide	71
5.4.4. Allogenic CAR-T	72
OBJECTIVES	75
MATERIAL, METHODS AND RESULTS	79
CHAPTER 1. DEVELOPMENT OF NOVEL 3D MODELS IN NON-HODGKIN LYMPHOMA	81
STUDY 1. A novel patient-derived 3D model recapitulates mantle cell lymphoma lymph node signaling, immune profile and in vivo ibrutinib responses	82
STUDY 2. Patient-Derived Follicular Lymphoma Spheroids recapitulate lymph node signaling and immune profile uncovering galectin-9 as a novel immunotherapeutic target	96
CHAPTER 2. IDENTIFICATION OF TAILORED IMMUNOTHERAPIES IN FOLLICULAR LYMPHOMA	111
STUDY 3. CD70 deregulation in follicular lymphoma at diagnosis is associated with relapse and opens new avenues for dual CD19-CD70 CAR-T therapy	112
AUTHOR CONTRIBUTIONS	157
SUMMARY OF THE RESULTS	158
DISCUSSION	163
PDLs as a 3D system to culture NHL samples mimicking the lymph node	165

TABLE OF CONTENTS

Drug testing in PDLS recapitulate <i>in vivo</i> responses and may be used for immunotherapeutic treatment	169
CD70 is up-regulated in FL-LN in patients that will relapse	172
CD70 as a target for CAR-T cells in B-cell lymphoma	176
CONCLUSIONS	181
REFERENCES	187
ANNEXES.....	225
SUPPLEMENTAL MATERIAL STUDY 1.....	227
SUPPLEMENTAL MATERIAL STUDY 2.....	243
SUPPLEMENTAL MATERIAL STUDY 3.....	256
ADDITIONAL PUBLICATIONS.....	266
ACKNOWLEDGEMENTS	295

TABLE OF CONTENTS

LIST OF ABBREVIATIONS

A

ADC: antibody-drug conjugate

ADCC: antibody-dependent cellular cytotoxicity

ADCP: antibody-dependent cellular phagocytosis

AID: activation-induced cytidine deaminase

ALL: acute lymphoblastic leukemia

AML: acute myeloid leukemia

B

BAFF: B-cell activating factor

BAFF-R: B-cell activating factor receptor

BCR: B-cell receptor

BITE: bispecific T-cell engaging antibody

BL: Burkitt lymphoma

BM: bone marrow

BTK: Bruton's tyrosine kinase

C

CAF: cancer-associated fibroblast

CAR: chimeric antigen receptor

ccRCC: clear cell renal cell carcinoma

CD27L: CD27 ligand

CD40L: CD40 ligand

CLL: chronic lymphocytic leukemia

cMCL: conventional mantle cell lymphoma

CR: complete response

CSF-1: colony stimulating factor 1

CT: computed tomography

CTL: cytotoxic T lymphocyte

D

DC-SIGN: dendritic cell-specific intracellular adhesion molecule-3-grabbing nonintegrin

DLBCL: diffuse-large B-cell lymphoma

DOR: duration of response

E

ECD: extracellular domain

ECM: extracellular matrix

F

FAK: focal adhesion kinase

FDC: follicular dendritic cells

FL: follicular lymphoma

FRC: fibroblastic reticular cell

TABLE OF CONTENTS

G

GC: germinal center

GEMM: genetically-engineered mouse model

GvHD: graft versus host disease

H

HLA: human leukocyte antigen

HT: histological transformation

I

IFRT: involved field radiation therapy

IG: immunoglobulin

IGHV: variable region of immunoglobulin gene

K

KO: knock-out

L

LN: lymph node

LT: lymphotoxine

M

MALC: multicellular aggregate of lymphoma cells

MCL: mantle cell lymphoma

MSC: mesenchymal stromal cells

N

NHL: non-Hodgkin lymphoma

nnMCL: non-nodal mantle cell lymphoma

O

ORR: overall response rate

OS: overall survival

P

PCNS: primary central nervous system

PDLs: patient-derived lymphoma spheroids

PDX: patient-derived xenograft

PFS: progression free survival

PI3Ki: PI3K inhibitor

POD: progression of disease

R

R/R: relapsed / refractory

S

sCD27: soluble CD27

scFv: single-chain variable fragment

scRNA: single-cell RNA

SLO: secondary lymphoid organs

TABLE OF CONTENTS

SMH: somatic hypermutation

T

TAM: tumor-associated macrophage

TFH: T follicular helper

tFL: transformed follicular lymphoma

TFR: T follicular regulatory

TLR: toll-like receptor

TME: tumor microenvironment

TNFRSF: tumor necrosis receptor superfamily

TNF α : tumor necrosis factor alpha

TNSF: tumor necrosis superfamily

trCD27: truncated CD27

Treg: T regulatory

U

ULA: ultra-low attachment

ABSTRACT

ABSTRACT

B-cell non-Hodgkin lymphoma (B-NHL) represent the most frequent group of hematologic tumors. Follicular lymphoma (FL) is usually indolent; however, some patients relapse after standard chemotherapy, increasing risk of transformation to aggressive lymphoma. Mantle cell lymphoma (MCL) is less frequent but very aggressive. In this thesis, we set up 3D models to culture primary cells (named as Patient-Derived Lymphoma Spheroids, PDLS) from B-NHL *in vitro* by mixing FL/MCL cells with healthy donors' monocytes and specific cytokine cocktails in ultra-low attachment (ULA) plates. After 7 days, PDLS were highly viable and had an enhanced proliferation. RNA-seq and gene-set enrichment analysis determined PDLS strongly recapitulate the pathological LN as well as pathways involved in lymphoma pathogenesis. Remarkably, MCL-PDLS reproduces *in vivo* responses to ibrutinib, and its resistance may be overcome by adding anti-PD1 nivolumab. Besides, these models are suitable to test novel immunotherapies, which let us uncover a potential therapeutic benefit of anti-galectin9 antibodies in FL. In parallel, we used Nanostring technology to analyze the transcriptomic immune profile of FL-LN samples. In a cohort of patients at diagnosis, homogeneously treated with immunochemotherapy, we discovered *CD70* is up-regulated in patients that eventually relapse. Furthermore, we validated this over-expression at protein level and determined, by multiplex immunofluorescence, it is highly expressed in tumor B cells, but also in a subset of T cells from the microenvironment. Our results showed the generation of a dual CD19-CD27 CAR-T by combining an academic, approved CD19 CAR-T (ARI-0001) and a ligand-based anti-CD70 CAR-T using a truncated CD27 protein.

ABSTRACT

RESUM

El limfoma no Hodgkin de cèl·lules B (B-NHL) representa el grup més freqüent de tumors hematològics. El limfoma fol·licular (FL) normalment és indolent, però alguns pacients recauen de la quimioimmunoteràpia estàndard, el que incrementa el risc de transformació a un limfoma agressiu. El limfoma de cèl·lules de mantell (MCL) és menys freqüent però molt agressiu. En aquesta tesi, hem generat models 3D per cultivar *in vitro* cèl·lules primàries de B-NHL (anomenats com Esferoids de Limfoma Derivats de Pacients, PDLS) barrejant cèl·lules de FL/MCL amb monòcits de donants sans i còctels de citoquines específics, en plaques de molt baixa adherència (ULA). Després de 7 dies, els PDLS eren altament viables i tenien una proliferació incrementada. Els anàlisis de RNA-seq i enriquiment de vies han determinat que els PDLS altament recapitulen el gangli limfàtic (LN) patològic així com vies involucrades en la patogènesi del limfoma. Cal destacar que els MCL-PDLS reproduïen les respostes *in vivo* de l'ibrutinib, i la seva resistència pot ser superada afegint l'anti-PD1 nivoulamb. A més, aquests models poden ser utilitzats per provar noves immunoteràpies, el que ens ha permès descobrir un potencial benefici terapèutic a l'afegir anticossos anti-galectina-9 en FL. En paral·lel, hem utilitzat la tecnologia de Nanostring per analitzar el perfil immune a nivell transcriptòmic en mostres de FL-LN. En una cohort de pacients en el diagnòstic, homogèniament tractats amb quimioimmunoteràpia, hem descobert que *CD70* està sobreexpressat en pacients que acaben recaient. També hem validat aquesta sobreexpressió a nivell de proteïna i hem determinat, amb immunofluorescència múltiple, que està altament expressat en cèl·lules B tumorals, però també en una part de les cèl·lules T del microambient. Els nostres resultats han impulsat la generació d'un CAR-T

dual CD19-CD27 combinant un CAR-T CD19 acadèmic i aprovat (ARI-0001) amb un CAR-T anti-CD70 basat en lligand, utilitzant una proteïna CD27 truncada.

INTRODUCTION

INTRODUCTION

1. B-CELL NON-HODGKIN LYMPHOMA

Non-Hodgkin lymphomas (NHL) are a heterogeneous group of hematologic malignancies that represent the majority of lymphomas (around 90% of cases) and constitute the seventh more prevalent cancer type and has the sixth highest mortality.¹ Non-Hodgkin lymphomas are classified, according to the cell type, in B-cell and T/NK-cell lymphoma.² The work from this thesis is based on B-cell lymphoma, which arise from mature B cells within the secondary lymphoid organs and account for 90% of cases.³

B cells differentiate in the bone marrow from a hematopoietic stem cell (HSC) that commits to a common lymphoid progenitor.⁴ Contrary to T lymphocytes, which mature in the thymus, B lymphocytes are characterized by exiting the bone marrow into the bloodstream once they have completed their maturing process.

In the blood, B cells circulate as naïve lymphocytes but, given their role in the adaptive immune system as major players in humoral, they have the capacity to recirculate through secondary lymphoid organs (SLO) to encounter antigens, and are able to experience the germinal center (GC) reaction in a T-cell dependent process.⁵ Germinal centers are specialized structures within lymphoid secondary organs (lymph nodes, spleen, Peyer's patches and mucosal associated lymphoid tissues) in which B cells undergo somatic hypermutation (SMH) and are selected based on antigen affinity.⁶

Hematoxylin-eosin staining allows the identification of the germinal center, and its division between the dark zone, composed by centroblasts, and the

INTRODUCTION

light zone, containing mainly centrocytes (**Figure 1**). Moreover, by immunohistochemistry, cells are mostly CD20+CD10+, with CD3+ cells surrounding the GC area, highly proliferative (Ki67+), BCL2- (with the exception of some T follicular helper, TFH, cells) and with presence of follicular dendritic cells (FDC) in the light zone, characterized by the expression of CD21.⁷

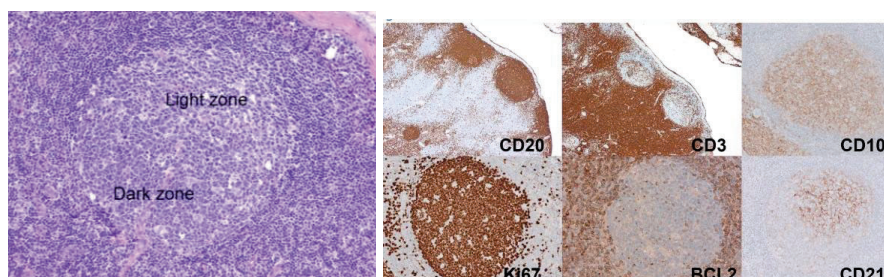


Figure 1. Germinal center immunohistochemistry. At the left, visualization of a germinal center using hematoxylin-eosin staining, indicating dark and light zones. At the right, IHQ staining of common population markers. Van den Brand *et al*, Hematopathology 2020⁷

In the dark zone of GCs, centroblasts proliferate and experience the immunoglobulin somatic hypermutation process, which enables the introduction of single nucleotide exchanges in the genes encoding for the variable regions of the immunoglobulin receptors. On the other hand, centrocytes in the light zone interact with follicular dendritic cells and are selected based on the antigen affinity.⁸⁵ B cells have the capacity to recirculate between compartments or to exit GC to differentiate to memory B cells and plasma cells in a highly controlled genetic and epigenetic network;⁹¹⁰ nevertheless, these same mechanisms are prone to mutational events, making GC B cells very sensitive to lymphomagenesis as observed in **Figure 2**.⁸¹¹

Indeed, a majority of NHL are derived from B cells transiting the germinal center, and include diffuse large B-cell lymphoma (DLBCL), follicular lymphoma (FL) and Burkitt lymphoma (BL)^{12, 10}. As SHM rearranges immunoglobulin (IG) genes, which encode for the B-cell receptor (BCR), B-cell lymphomas can be classified according whether they have undergone or not GC reaction, which has prognostic value in some pathologies as chronic lymphocytic leukemia (CLL) or mantle cell lymphoma (MCL)^{13, 14}

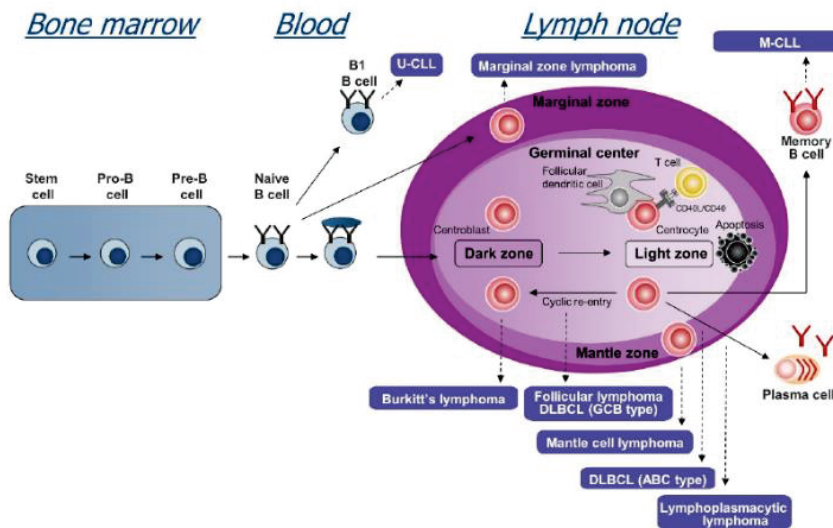


Figure 2. Development of B-NHL malignancies. Efremov *et al* Cancers 2020¹⁴

INTRODUCTION

2. MANTLE CELL LYMPHOMA

Mantle cell lymphoma is a rare and aggressive lymphoma that arise from small B lymphocytes within the mantle zone in the lymph node, an anatomical structure which is surrounding the germinal center.¹⁵

MCL is phenotypically characterized by frequent CD5 positivity and accounts for 3-10% of NHL, with an incidence of 0.51-0.55 / 100,000. Patients are more usually males (ratio 2.5:1) and the median age at diagnosis is 68 years old.^{16, 13} The clinical behavior is usually aggressive, with a median overall survival (OS) of 4-5 years.¹⁷

2.1. Pathogenesis

The primary mutation in Mantle cell lymphoma is, in most patients, the translocation t(11;14)(q13;q32) in the bone marrow, which causes the overexpression of the cyclin D1. This genetic alteration occurs between the *BCL-1* locus and the immunoglobulin heavy chain locus in the bone marrow.^{18, 19} Cyclin D1 is closely related to proliferation, as promote G1 to S transition by inactivating retinoblastoma protein.²⁰ Strikingly, patients negative for the t(11;14) translocation present *CCND2* or *CCND3* arrangements.²¹

With the development of massive sequencing techniques, the complex mutational landscape of MCL have been uncovered.²² Recurrent mutations may be classified in different processes: ¹³

- **Cell cycle.** Apart from *CCND1* (95% rearrangement and 14-34% mutation), we can highlight deletions in *RB1* (25-55%), *LATS1* (19-37%) and *CDKN2A/B* (10-36%), while gains have been detected in *BCL2* (3-17%) and *BM11* (6-12%).

- **DNA repair.** Deletions and mutations in *TP53* (21-45% and 14-31% respectively) and *ATM* (11-57% and 6-10%) are frequently detected.
- **BCR – NFkB.** *BIRC3* (11-57% deletions and 6-10% mutations) and *CARD11* (mutations in 3-15%) are the most frequent altered genes.
- **Apoptosis.** Deletions in *FBXO25* (17-34%) and gains in *MYC* (6-32%).
- **Epigenetic modifiers.** Mutations have been detected in *KMT2D* (12-23%), *KMT2C* (5-16%), *NSD2* (10-13%) and *SMARCA4* (8%).

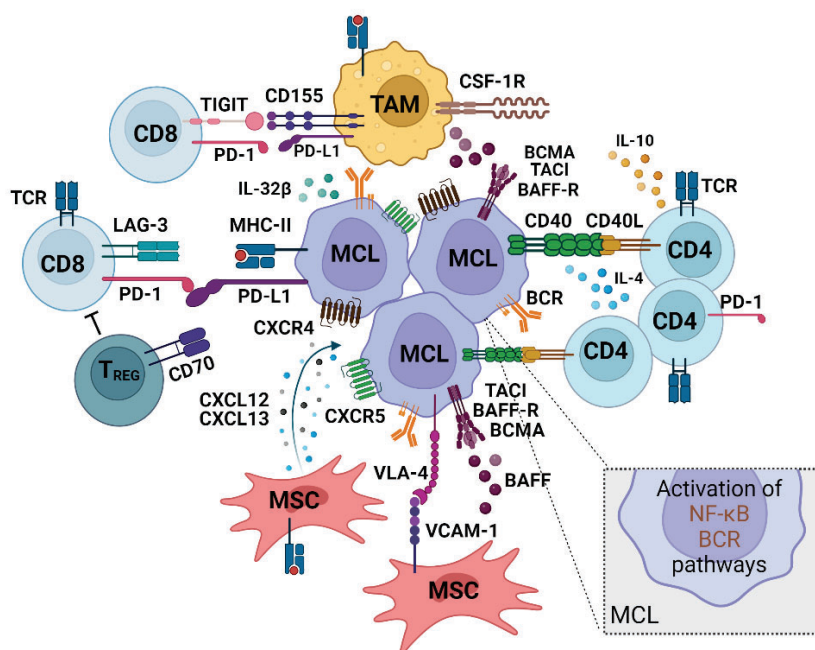
2.2. Tumor microenvironment

The cellular milieu in the mantle cell lymphoma tumor microenvironment (MCL-TME) includes immune cells (T cells, macrophages, NK cells), fibroblasts, endothelial cells, mesenchymal stromal cells (MSCs) and soluble cytokines and growth factors. (**Figure 3**)

Recently, a detailed study by Jain et al shed light in MCL-TME. As done in solid tumors but also in other hematological malignancies as DLBCL,²³ MCL samples could be classified according the immune infiltration: i) normal LN-like (high CD4+ cells, stroma-rich, FDC, TFH and lymphatic endothelium), ii) immune-enriched or hot (low stromal expression and overexpression of immune and checkpoint molecules), iii) mesenchymal (increased stromal signature and tumor-promoting cytokines), and iv) immune-depleted or cold. This depleted group was related to resistance to Bruton's tyrosine kinase (BTK) inhibitors and had the worse overall survival.²⁴

By comparing lymph node (LN) and peripheral blood tissues from MCL patients, activation of B-cell receptor (BCR) and NF-kB signaling were identified as relevant factors in MCL pathogenesis induced by LN microenvironment. Moreover, genes up-regulated in the LN also were related

to proliferation, stemness, invasion, BAFF-APRIL and PI3K-AKT.²⁵ Interestingly, BCR and PI3K pathways are highly activated but no mutations have been detected; thus, this observation remarks the importance of the TME.²⁶



2.2.1. Mesenchymal stromal cells

Microenvironment interactions also determine B-cell trafficking into the secondary lymphoid organs in a process orchestrated by stromal cells.²⁸ Both normal and malignant B cells highly express CXCR4 (a receptor of CXCL12) and

CXCR5, which has CXCL13 as a ligand.^{29, 30} CXCR4 has also been related to *SOX11* expression, together with focal adhesion kinase (FAK).³¹

Moreover, CD49d (commonly known as VLA-4) has also been defined as a key adhesion molecule. Besides, MSCs are also capable to confer drug resistance to chemotherapeutic drugs.³² Endothelial cells are also responsible in the migration process, as they secrete CCL19, a chemotactic molecule for MCL cells but not for normal B cells.³⁰

2.2.2. Follicular dendritic cells

Despite follicular dendritic cells (FDC) are not found in mantle zones within normal lymph nodes, they are present in MCL samples. Strikingly, the pattern of FDC correlates with survival, as nodular FDC pattern has a better prognosis than a diffuse one.³³ Furthermore, the degree of overlap between MCL tumor area and CD21+ FDC meshwork is also an independent factor and correlates with good prognosis.³⁴

2.2.3. Macrophages

Monocytes are not fully differentiated cells that shortly circulate in the bloodstream before they extravase and infiltrate a diversity of tissues, including lymph nodes.³⁵ Monocytes can secret CXCL12 but also express its receptors CXCR4 and CXCR7, establishing an autocrine/paracrine loop.³⁶ In cancer, tumor-associated macrophages have been usually described to possess pro-tumoral characteristics such as proliferation, extracellular matrix remodeling, angiogenesis and immunosuppression.³⁷

Macrophages are found in MCL-LN and their abundance seems to be related to disease aggressiveness, suggesting a role as tumor-associated macrophages^{26, 38} Their function as pro-tumorigenic is also supported by *in*

INTRODUCTION

vivo data published by Le K and colleagues, in which they found that MCL cells polarize monocytes to M2 macrophages, which are able to produce IL-10.³⁹

IL-10, together with colony stimulating factor 1 (CSF1) were also described as major drivers of monocyte polarization into CD163+ M2 macrophages. Of note, CD163 was up-regulated in monocytes from MCL patients compared to healthy donors, and CSF-1 and IL-10 are also increased in MCL patients' plasma.⁴⁰

In Decombis *et al*, it was identified IL-32 β as a cytokine secreted by tumor cells that enables the polarization of monocytes into tumor-associated macrophages, which favors tumor survival. In addition, these macrophages are able to secrete BAFF thus stimulating MCL cells, in a process dependent on alternative NF κ B, NIK pathway.⁴¹

T cells

There are many evidences that T cells support MCL viability and proliferation. MCL cells are highly responsive to CD40 ligand (CD40L) and IL-4^{42, 43}. CD40L, also known as CD154, is found in the surface of T cells and binds to activate CD40.

The abundance of T cells and, concretely, CD4+ cells, is associated to histology: nodular and especially diffuse variants are related to lower levels.⁴⁴ Moreover, a CD4:CD8 ratio correlated with longer overall survival.^{44, 45}

In a longitudinal single-cell RNA (scRNA) analysis, CD8 was found to be down-regulated in non-responder patients after they were treated with ibrutinib, indicating CD8 dysfunction as a therapeutic resistance mechanism.⁴⁶

In the study of Yang *et al*, T-cell infiltration was deeply studied in B-cell NHL, including two MCL patients and it was described the presence of intratumoral CD4+CD25+ T regulatory (Treg) cells, which are capable to hijack proliferation and cytokine production of CD4+ T cells. These immunosuppressor cells may be actively recruited by lymphoma B cells secreting CCL22.⁴⁷ In the same line, Treg cells are higher infiltrated in aggressive SOX11+ MCL tumors, a phenomenon also related to an increase in CD70 expression and down-modulation of antigen processing and T-cell presentation.⁴⁸ Finally, high Treg infiltration was also confirmed as a poor prognosis marker by immunohistochemistry analysis, together with IL17A and low IL2.⁴⁹

2.3. Non-nodal vs indolent Mantle Cell Lymphoma

Firstly, the analysis of the variable region of immunoglobulin gene (IGHV) determined mantle cell lymphoma cell of origin was a naïve pre-germinal center B cell, as somatic mutations were almost absent.⁵⁰ Nevertheless, it was later identified a subset of patients characterized with non-nodal (nnMCL) disease (i.e.: absence of lymphadenopathy), the presence of IGHV mutations and frequent indolent disease, reflected in a prolonged overall survival.⁵¹ Moreover, indolent MCL was associated to a non-complex karyotype and the absence of SOX11 protein expression.⁵² Then, subsequent studies confirmed the positivity of SOX11 in unmutated MCL as well as its identification as an independent risk factor that predicted poor survival.⁵³

An extensive study by Navarro *et al* identified *SOX11* as an independent risk factor that predicted for poor survival, and positivity for *SOX11* was associated with unmutated MCL.⁵⁴

INTRODUCTION

Nowadays, these two different subgroups (nodal or conventional MCL, cMCL, and leukemic non-nodal MCL) are recognized⁵⁵ Interestingly, conventional MCL has a higher degree of genomic instability and epigenetic alterations compared to non-nodal MCL.^{56, 57}

2.4. Diagnosis and prognosis

Patients with mantle cell lymphoma typically present with non-localized lymphadenopathy (in the case of conventional MCL) and the possibility of systemic B symptoms such as fever, sweats, weight loss or fatigue. Presence of circulating tumor cells and bone marrow involvement are common; thus, the study of the immunophenotype is necessary for a differential diagnosis. Tumor MCL cells are CD5+, CD20bright, CD19+, sIgM/IgD+, FMC-7+, CD23-, CD200-, although some leukemic non-nodal cases may have aberrant CD200 expression and loss of CD5.^{57, 58}

Hematopathological study is crucial as blastoid and pleomorphic histological variants, which represent around 10% of cases, have been described to be more aggressive than classical MCL and may require a more intensive treatment.⁵⁹

In order to stratify non-Hodgkin patient's prognosis, the International Prognostic Index (IPI) was developed.⁶⁰ Specifically to mantle cell lymphoma, MIPI prognostic index was assessed and nowadays is widely used.⁶¹ By combining different clinical factors, it stratifies patients in better, intermediate or worse prognosis, and may also condition therapeutic approach. Finally, Ki-67 proliferation index and *TP53* mutation or deletion are also important as they are related to bad prognosis.⁵⁸

2.5. Treatment

Treatment of mantle cell lymphoma is variable according to the clinic features of the patient, the subtype (conventional vs non-nodal), the histology, the percentage of Ki-67 positivity and alterations in *TP53* gene.⁵⁷ (Figure 4)

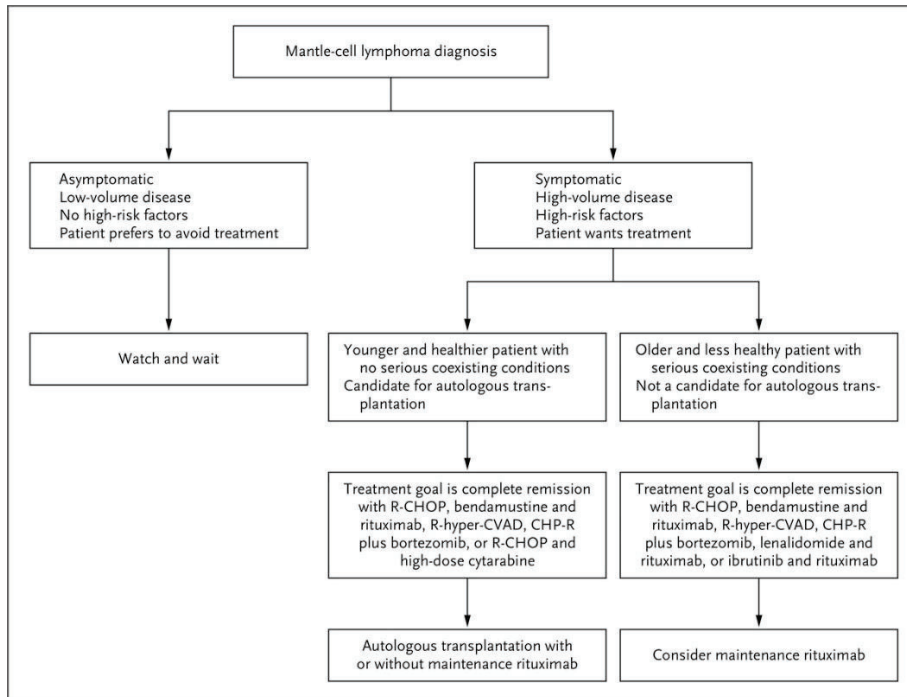


Figure 4. Algorithm for primary therapy in patients with mantle cell lymphoma.

Armitage and Longo, NEJM 2022⁵⁸

As described in observational studies, some MCL patients presenting an indolent disease, may benefit from a wait and watch strategy if they do not require immediate systemic treatment.^{62, 63}

First-line treatment is based on chemoimmunotherapy regimens, combining anti-CD20 rituximab and a combination of chemotherapeutic drugs. Almost all patients achieve an objective response, with overall response rates (ORR) superior to 90%, while complete response (CR) is achieved by >60% of

INTRODUCTION

patients. According to the risk factors previously mentioned and the age and fitness of the patient, an autologous bone marrow transplantation may be performed after intensive chemoimmunotherapy.⁵⁷ Importantly, rituximab is also frequently used as a maintenance therapy, and meta-analysis data indicate longer progression free survival and lower hazard ratio of death.⁶⁴

For the treatment of relapsed / refractory (R/R) mantle cell lymphoma, BTK inhibitors have emerged as a common therapeutic option. BTK is a member of TEC family of non-receptor kinases involved which is involved in BCR pathway.⁶⁵ Ibrutinib is an approved first-in-class covalent BTK inhibitor that demonstrated high activity in mantle cell lymphoma, with an ORR of 68% in clinical trials⁶⁶ but also in other B-cell malignancies such as chronic lymphocytic leukemia.⁶⁷ **(Figure 5)**

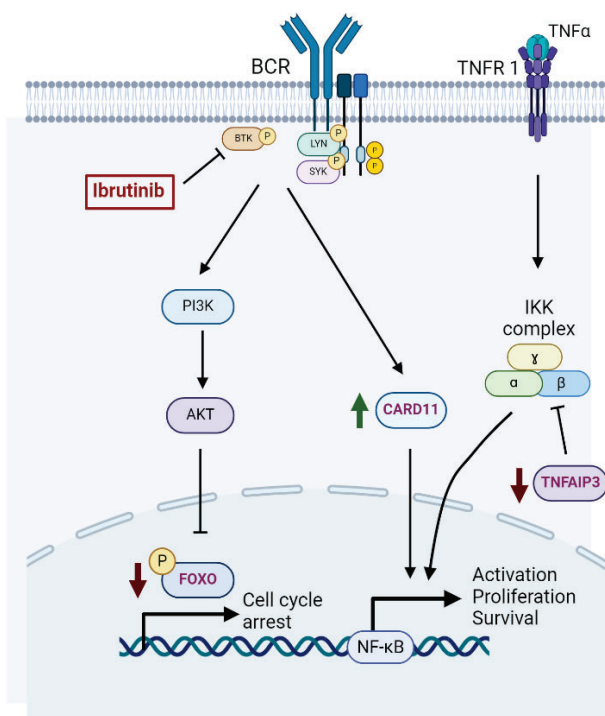


Figure 5. BCR pathway signaling and inhibition by ibrutinib. Created with BioRender.com

The mechanisms underlying ibrutinib resistances, which can be either primary or acquired, includes point mutations in BTK pathway (BTK^{C481S} and PCLG2^{R665W}) but also in other signaling pathways, such as NFkB (mutations in *TRAF2*, *TRAF3*, *MAPK3K14*, *CARD11*, *MYD88*) and cell cycle (*CCND1*).⁶⁸ Furthermore, microenvironment interactions including PI3K-AKT-mTOR axis, integrin-B1-ILK signaling and BAFF have also been described as mediators of ibrutinib resistance.^{69, 27}

Ibrutinib has been recently proposed to be used in first-line. In a phase II clinical trial, in which ibrutinib was combined with rituximab to treat indolent clinical forms of MCL, CR was achieved in 87% of patients, and after 2 years of treatment ibrutinib could be discontinued in 69% of cases as disease was undetectable by minimal residual disease.⁷⁰ Ibrutinib and rituximab combination was also investigated in older patients in a clinical trial which concluded it was effective as 96% patients had ORR including 71% of complete responses.⁷¹

BCL-2 is an anti-apoptotic protein frequently overexpressed in non-Hodgkin lymphoma. In mantle cell lymphoma, gene amplification 18q21 was identified in 9 out of 39 patients.⁷² Later, other mechanisms such as defective protein degradation and transcriptional upregulation have also been described. For this reason, the BCL-2 inhibitor venetoclax was tested in B-NHL. Results showed a high heterogeneity among the different lymphomas; in the case of MCL, ORR was higher (75%) and a progression free survival (PFS) longer (14 months) compared to germinal center-derived lymphomas.⁷³ To date, venetoclax has been approved for chronic lymphocytic leukemia and small

INTRODUCTION

lymphocytic lymphoma, but still is in phase III clinical trials for MCL. (NCT03112174)

Recently, other immunotherapeutic options have emerged as promising for the treatment of R/R MCL. Bispecific antibodies targeting both tumor and T cells are able to activate cytotoxic response. In this frame, different products have been successfully tested in MCL as well as in other B-NHL. Finally, treatment with chimeric antigen receptor (CAR)-T cells directed to CD19 expressing cells achieve high rates of response and a percentage of CR superior to 60%, emerging as a very effective option in BTKi resistance patients.⁷⁴

3. FOLLICULAR LYMPHOMA

Follicular Lymphoma is the most common indolent lymphoma and the second most prevalent after diffuse large B-cell lymphoma (DLBCL), representing 15-20% of diagnoses and an incidence of 4/100,000/year.¹³ Despite it is considered an incurable disease, up to 40% of patients enjoy remission durations longer than 10 years and an overall survival of approximately 20 years.⁷⁵ The median age at diagnosis is 65 years.⁷⁶

FL is a nodal disease, with a usually progressive and slowly clinical course, with waxing and waning adenopathy. (Rosenquist). Besides lymphadenopathy, it commonly presents with bone marrow involvement and splenomegaly^{77, 78}. Moreover, leukemic disease may also be detected in a subset of patients.⁷⁹

3.1. Pathogenesis

FL is a lymphoproliferative disorder that arises from developmentally blocked germinal center B cells, as the result of the cooperation of genetic alterations with a permissive tumor microenvironment.⁸⁰

The first oncogenic hit, also used for diagnostic purposes, is the translocation t(14;18)(q32;q21), which occurs in the Pro/Pre B phase during the B-cell development within the bone marrow. This translocation causes the over-expression of the antiapoptotic protein BCL-2 as passes to be controlled by the IGHV promoter.⁸¹ Despite this translocation is also found in healthy individuals,⁸² a large study presented by Roulland and collaborators validated its utility as a predictive biomarker and demonstrated that disease progression occurred from t(14;18) positive precursors.⁸³

Importantly, there is a fraction of patients (~10-15%) who do not present t(14;18), indicating the existence of alternative pathogenic mechanisms.⁸⁴

INTRODUCTION

The existence of t(14;18) in healthy people indicates that this translocation *per se* is not enough to develop an overt disease. B cells that overexpress BCL2 protein avoid cell death by apoptosis, but require multiple GC reentries before acquiring the characteristic development arrest.⁸⁵ These developmentally blocked B cells, which constitutively express BCL-6 protein and activation-induced cytidine deaminase (AID), are able to acquire complementary oncogenic hits and progress to FL.^{86, 80}

Thanks to recent advances in sequencing techniques, including whole genome and exon sequencing and single-cell sequencing, the genomic landscape of FL has been deeply analyzed, unraveling mutations in epigenetic genes as early events in the disease development, present in the common precursor cell (CPC) population.⁸⁷ CPC is a pool of tumor-initiating cells that harbor a shared set of mutations and alterations and acts as a disease reservoir for relapse or histological transformation.^{80, 87} Intriguingly, most of the high-prevalence mutations not only have a direct impact on tumor B cells, but also on the surrounding microenvironment.⁸⁸ The most frequent altered pathways in FL are the following:

- **Chromatin regulation.** Virtually all patients present mutations in chromatin-modifying genes. The most frequent one is the histone methyltransferase *KMT2D*, in which 79-89% patients have loss-of-function mutations^{89, 90, 91, 92}. Inactivating mutations are also frequent in histone acetyltransferases *CREBBP* (up to 70%) and *EP300* (9-19%), and are related to reduced p53 activation and BCL6 maintenance, as well as to diminished antigen presentation.^{93, 90, 91, 94, 95}. On the contrary, the methyltransferase *EZH2* presents gain-of-function mutations in 17-27% of patients. Its alteration implies GC light zone

cells lose dependency on TFH and favor its interaction with FDC^{96, 90, 92, 97}

- **Immune regulation / evasion.** *TNFRSF14* (also known as HVEM) is a tumor suppressor frequently inactivated (around 30% FL patients) and associated with bad prognosis.⁹⁸
- **BCR/NF-κB signaling.** One third of patients present alterations in genes encoding for proteins in this pathway; the most frequently mutated gene is *CARD11* (10% FL patients), followed by *CD79B* (9%) and *TNFAIP3* (9%).^{13, 89, 90}
- **JAK-STAT pathway.** 21% of FL patients present activating mutations in *STAT6* gene, which enhances IL-4 induced activation of target genes.⁹⁹
- **mTor signaling.** Activating mutations in *RRAGC* have been described in up to 17% of patients, representing a mechanism that bypasses amino acid deprivation and activates mTORC1 signaling.^{100, 101, 102}

3.2. Tumor microenvironment

Follicular lymphoma is considered a paradigm of a B-cell malignancy dependent on a germinal center-like permissive microenvironment.¹⁰³ The importance of the TME is not only important on the pathogenesis, but is also relevant in prognosis, and some cells have an impact in histological transformation.¹⁰⁴

In 2004, Dave *et al* developed gene-expression signatures to predict at diagnosis the survival of FL patients. Remarkably, the length of survival correlates with the molecular features of non-malignant immune cells. The immune-response 1 signature is associated with favorable prognosis (relative risk of death = 0.15) and includes genes expressed in T cells and macrophages. On the other hand, the immune-response 2 signature is associated with poor

INTRODUCTION

prognosis (relative risk of death = 9.35) and the genes are associated with macrophages and dendritic cells.¹⁰⁵

The tumor microenvironment is composed by follicular dendritic cells, fibroblastic reticular cells (FRCs), mesenchymal stromal cells, tumor-associated macrophages (TAMs) and a great diversity of T cells, including T follicular helper (TFH), T regulatory (Treg), T follicular regulatory (TFR) and CD8+ cytotoxic T cells (CTL).⁸⁸ **(Figure 6)**

In conclusion, there are many evidences that support the existence of a dynamic bidirectional crosstalk between FL tumor cells and the surrounding non-malignant cells. These cells constitute specialized tumor niches in the lymph node but also in the bone marrow.¹⁰⁶

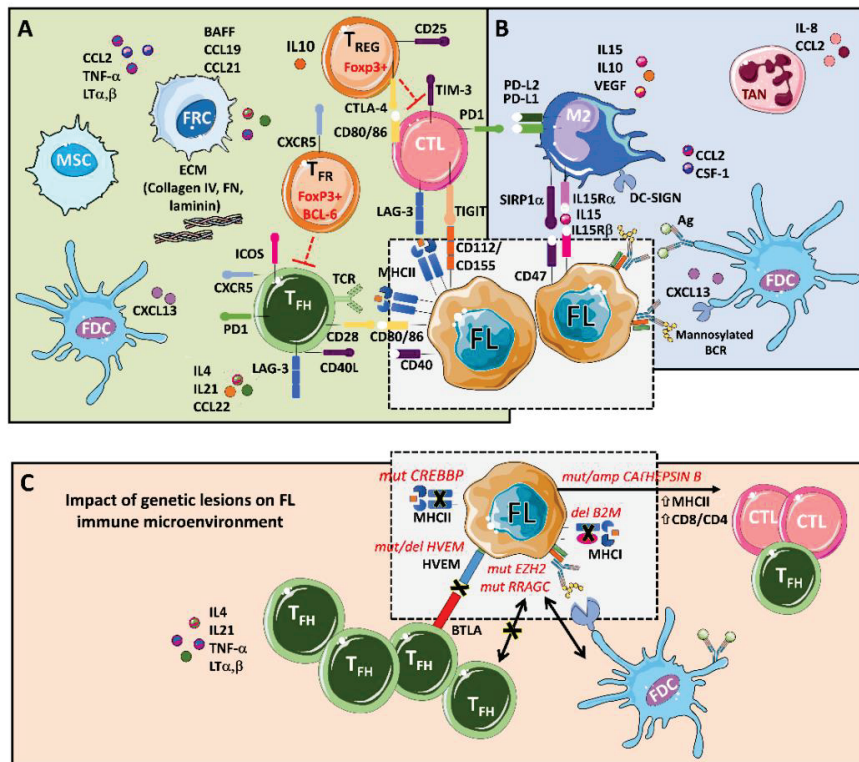


Figure 6. An integrative view of follicular lymphoma microenvironment. (A) A variety of T-cell populations interact with FL cells. **(B)** FL cells are supported by myeloid cells (M2-TAM, TAN) and follicular dendritic cells (FDC). **(C)** Some of the most prevalent mutations in FL notably impact in the TME. Dobaño-López *et al.* Cancers 2021

3.2.1. T cells

T cells represent the most frequent non-malignant cell type in the FL-LN. In a single-cell study by Han and collaborators, T cells represented a median of 87.6% of non-tumoral cells, in a range comprised between 73.8 and 98.9%.¹⁰⁷ As follicular lymphoma maintains the structure of germinal centers, in which B cells are highly activated after their interaction with T cells, proliferation of FL cells is dependent on CD4+ cells.¹⁰⁸

INTRODUCTION

T cells comprise a high diversity of specialized subtypes. In FL, different clusters of CD4+ cells (naïve, T regulatory, T follicular helper and cytotoxic) and CD8+ cells (naïve, effector and exhausted) have been identified.¹⁰⁷ Based on this clustering, FL-TME was classified in four different groups, as similarly done in other lymphomas.^{23, 24} This classification includes naïve, warm, intermediate and depleted groups, having the last an inferior survival outcome.¹⁰⁷

CD8+ cells are cells with cytotoxic capacity as they express cytotoxic molecules such as granzymes and perforin and its low frequency has been correlated with a poor prognosis.¹⁰⁹ Nevertheless, in cancer, CD8+ cells are frequently dysfunctional due to the expression of immune checkpoint inhibitors, among other factors.¹¹⁰ In FL, it has been reported a high percentage of TIM-3 within CD8+, but also coexpression of PD1 and LAG3 and TIGIT^{111, 112, 113} Interestingly, it was recently described a CD4+ population with cytotoxic capacity.¹⁰⁷

Immune checkpoint expression has also been observed in CD4+ population. IL-12, a cytokine increased in FL patients' serum, induces TIM-3 expression, leading to an impairment of T-cell function^{114, 112} High expression of TIGIT correlates with bad prognosis in both CD4+ and CD8+ populations, and is abundantly expressed in Treg and TFH populations.¹¹³

T regulatory cells (Treg), a CD4+ population characterized by expression of CD25, CTLA4 and the transcription factor FOXP3, suppresses anti-tumor immunity.¹¹⁵ In NHL, including FL, they are overrepresented compared to normal tonsils, and their cell distribution predicts survival and transformation to DLBCL.^{47, 116} Interestingly, tumor B cells actively recruit Treg cells within the

tumor niche by secretion of CCL22. Moreover, these cells are able to suppress the proliferation and infiltration of other T cells and impair the secretion of IFN γ .¹¹⁷

T follicular helper cells (TFH) are a specialized CD4⁺ population found within the germinal center and play a crucial role in FL pathogenesis. They are characterized by expression of CXCR5, PD1, ICOS and BCL6, while are negative for CD25, CCR7.^{118, 88} As demonstrated by Amé-Thomas *et al*, TFH support tumor B cells and protect them from apoptosis by providing CD40 signaling through CD40 ligand (CD40L) and secreting IL4. TFH represent a high amount of CD4⁺ fraction in FL-LN (~30%) and are significantly increased compared to reactive LN but not to tonsils.¹¹⁹ In addition, TFH cells have a major role remodeling the TME, as IL4 and CD40L induce the expression of CCL17 and CCL22 chemokines, which recruit Treg cells, thus creating a positive feedback of immune suppression.¹²⁰

T follicular regulatory cells (TFR) is a subset of CXCR5⁺BCL6⁺ cells that also express FOXP3.¹²¹ It has been described this TFR population may be originated from both natural Treg precursors (Wing JB PNAS 2017) or from naïve FOXP3⁻ precursors.¹²² This TFR population has mainly been described as a suppressor of GC reaction by inhibiting TFH and B cell activation.^{121 123 124} However, it has been recently described that TFR are also capable of producing IL10, which stimulates GC B cells, thus playing a dual role of stimulation / inhibition of the germinal center reaction.^{125, 126} Interestingly, it represents an enriched population in follicular lymphoma LN compared to follicular hyperplasia and tonsils.¹¹⁹ Overall, the significance of T regulatory FOXP3⁺ cells is controversial in FL,¹²⁷ and this may be explained by the heterogeneity of FOXP3⁺ cells as well as the different roles they may have.

INTRODUCTION

3.2.2. Lymphoid stromal cells

Stromal cells are characterized by a mesenchymal, non-hematopoietic origin, and include follicular dendritic cells (FDC), mesenchymal stromal cells (MSC) and fibroblastic reticular cells (FRC).⁸⁸ In FL, there exists an active, bidirectional crosstalk between malignant B cells and stromal cells, which show a specific transcriptomic signature in FL.¹²⁸

Follicular dendritic cells are stromal CD21⁺CD23⁺ cells that retain antigens and present antigen – antibody complexes on their cell surface which can be recognized by B cells; those able to bind to the immune complexes will survive and complete the GC reaction and progress in the differentiation process.¹²⁹ Their differentiation from mesenchymal stromal cells is induced by tumor necrosis factor alpha (TNF α) and lymphotoxins (LT) LT α 1 β 2, two cytokines produced by activated B cells.¹³⁰ Interestingly, mutations in HVEM increase the production of these cytokines, reflecting in a higher number of FDC and type I collagen density.¹³¹ FDCs also express the chemokine CXCL13, which binds to CXCR5, expressed in both TFH and FL cells.¹³² Moreover, in FL-LN is enriched in CXCL12 expression and may be produced by stromal cells, including FDCs, after IL-4 stimulation.¹³³

Fibroblastic reticular cells are also capable to produce CXCL12, as well as other chemokines such as CCL19 and CCL21.^{133, 134} Contrary to FDCs, they are located in the T-cell zone of the lymph node, providing strength and flexibility and compartmentalizing B and T zones. Moreover, they stimulate B cells by secreting IL-7 and BAFF, and produce CCL19 and CCL21, enhancing T-cell regulatory functions.¹³⁵ Finally, FRC are also capable to produce CXCL13 after interaction of CCL19 (chemokine secreted by fibroblasts) and IL-4R, found in B cells.¹³⁶

In the bone marrow (BM) tumor microenvironment, mesenchymal stromal cells have a major role. FL patients frequently present with BM involvement, and it has been observed an ectopic development of stromal cells associated with tumor B cells.¹²⁸ MSCs sustain B-cell viability through the secretion of BAFF.¹³⁷ Furthermore, MSCs in FL have a specific gene signature, with enhanced production of CCL2.¹³⁸ and IL-8,¹³⁹ pointing out a role of neutrophils in FL-TME that has been poorly described. As other stromal cell types, they are able to recruit FL cells through the secretion of CXCL12, which is increased compared to healthy donors' tonsils.¹³³ In response to TNF and lymphotoxines, secreted by FL cells, they differentiate into FRCs.¹³⁷

3.2.3. Tumor associated macrophages (TAMs)

Monocytes are circulating, non-fully differentiated myeloid cells that are able to extravase and differentiate into a variety of specialized cell types in the tissues, such as macrophages, dendritic cells and myeloid-derived suppressor cells.¹⁴⁰ Their role in cancer has been extensively studied, as can induce immune tolerance and angiogenesis, and enhance dissemination. Tumor-associated macrophages exhibit its own transcriptional profile and are enriched in genes associated with immunosuppression.¹⁴¹

In FL, the prognostic value of macrophages has been controversial: in studies from the pre-rituximab era they were reported to have a bad prognosis,^{142, 143} consistent with the immune response 2 described in Dave *et al*, rich in myeloid genes.¹⁰⁵ Moreover, in a study published in 2010, in which only two patients had received rituximab, it was described a pro-angiogenic function related to the number of macrophages.¹⁴⁴ In contrast, in the rituximab era, the macrophage marker CD163 has been associated with favorable prognosis.¹⁴⁵

INTRODUCTION

In previous work from our group, we have demonstrated that macrophages support B-cell viability.¹⁴⁶ FL cells actively recruit monocytes through CCL2 and CSF-1 production; then, in the FL niche, these monocytes differentiate into pro-tumoral M2-like macrophages.^{146 138} (Yang ZZ and Ansell Clin Adv Hematol Oncol). These macrophages trans-present IL-15 to B cells,¹⁴⁷ which induce B-cell proliferation in combination with CD40L, and activate the B-cell receptor in an antigen-independent manner by dendritic cell-specific intracellular adhesion molecule-3-grabbing nonintegrin (DC-SIGN).¹⁴⁸

Macrophages are cells with phagocytic capacity, able to kill tumor cells; however, many tumor cells overexpress CD47 protein, known as “do not eat me” signal, which bind to SIRP α in myeloid cells.¹⁴⁹ In FL, it has been identified a CD14+SIRP α ^{high} population and is associated with an inferior survival.¹⁵⁰ Another mechanism of immune escape induced by TAMs is the overexpression of PD-L1 in an intrafollicular CD68+ population, related to a shorter time to transformation.¹⁵¹

3.3. Diagnosis and prognosis

Follicular lymphoma patients typically present with adenopathy; thus, a computed tomography (CT) scan of the neck, thorax and abdomen in the initial work-up is necessary. FL diagnosis is based on pathological review of a surgical specimen.¹⁵² LN have a nodal architecture, with tumor cells growing in a follicular pattern (**Figure 7A**). FL cells are highly positive for BCL-2 protein (**Figure 7B**) due to the translocation t(14;18), which can also be detected by fluorescence *in situ* hybridization (FISH). Determination of the immunophenotype is also useful for differential diagnosis, as FL cells are CD20bright, CD19+, CD10+, CD79b+ and BCL-6+; while are negative for CD5 and CD23.⁷⁶

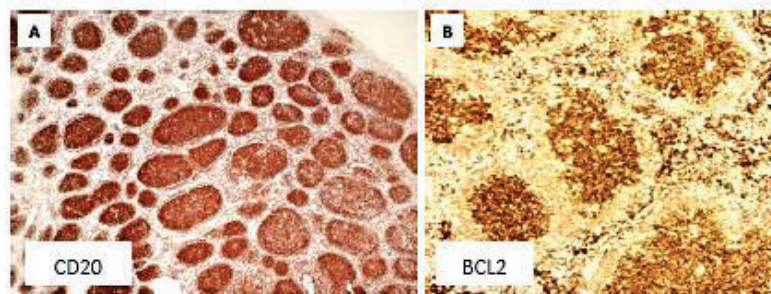


Figure 7. Follicular lymphoma histopathology. (A) IHC of CD20+ cells creating follicle structures. (B) IHC of BCL2+ cells. Courtesy of Dr. Elias Campo, Secció Hematopatologia, Hospital Clínic de Barcelona.

FL malignant cells are a mixture of centrocytes and centroblasts, both with a germinal center origin. While centrocytes are small/medium cells localized in the light zone of GC in physiological conditions, centroblasts are larger and have a dark zone origin. Determining the proportion of both cell types is crucial in the diagnosis of FL, as the number of centroblasts determines the clinical aggressiveness of the tumor.⁷⁶ The histological grading of FL is determined by the number of centroblasts per high power field (hpf): Grade I FL has less than 5 blasts/hpf, Grade II has 6 to 15 and Grade III has more than 15. Grade III is divided in 3A and 3B according whether centrocytes are observed or not, respectively.^{76, 152} According to ESMO guidelines, FL grade IIIB should be treated as an aggressive lymphoma, while other grades have to be treated as an indolent disease. Given the possibility of bone marrow involvement and presence of the disease in the peripheral blood, a BM aspirate and biopsy as well as a complete blood count are also recommended.¹⁵² Nevertheless, bone marrow assessment is controversial as recent data indicate it is no longer prognostic in the disease.⁷⁵

INTRODUCTION

FL patients' prognosis have improved since the introduction of rituximab in the early 2000s. In an extensive study analyzing US and French cohorts, ten-year overall survival was 77% and 80% respectively; however, histological transformation was highlighted as a major cause of death.¹⁵³

Multiple clinical-biologic risk models have been developed for FL¹⁵⁴ The Follicular Lymphoma International Prognostic Index (FLIPI) has been widely used, and integrates five adverse prognostic factors: age, Ann Arbor stage, hemoglobin level, number of nodal areas and serum LDH level.¹⁵⁵ With the standardization of rituximab, FLIPI score was updated by including bone marrow involvement, bulky disease and beta2 microglobulin.¹⁵⁶ Furthermore, the m7-FLIPI takes into account genomic alterations in 7 genes (*EZH2*, *ARID1A*, *MEF2B*, *EP300*, *FOXO1*, *CREBBP* and *CARD11*).⁹²

In the rituximab era, follicular lymphoma patients experience in many cases complete and durable responses. Nevertheless, a fraction of patients is primary refractory to the treatment or rapidly relapse, which worsens the prognosis. In 2015, a study in patients treated at first line with R-CHOP defined as high-risk population those patients who experienced progression of disease (POD) within 2 years of treatment, also known as POD24. Concretely, 19% of patients relapsed in this timeframe, and had a five-year overall survival of 50%, much lower to the 90% in the reference group.¹⁵⁷ Recently, POD24 has been further validated in a pooled analysis of 13 randomized clinical trials.¹⁵⁸

3.4. Treatment

Although follicular lymphoma remains to be considered as an incurable disease, the introduction of novel treatments in the last years has improved clinical management of FL patients.¹⁵⁹

In a minority of patients (less than 20%) that present with localized FL (Ann Arbor stage I / II) and have low tumor burden a radiotherapy-based treatment called involved field radiation therapy (IFRT) is the preferred approach as may be curative.^{152 159} Radiotherapy may also be combined with rituximab as single-agent.¹⁶⁰ In selected cases, watch-and-wait strategy or rituximab monotherapy treatment are also performed.¹⁵² (**Figure 8**)

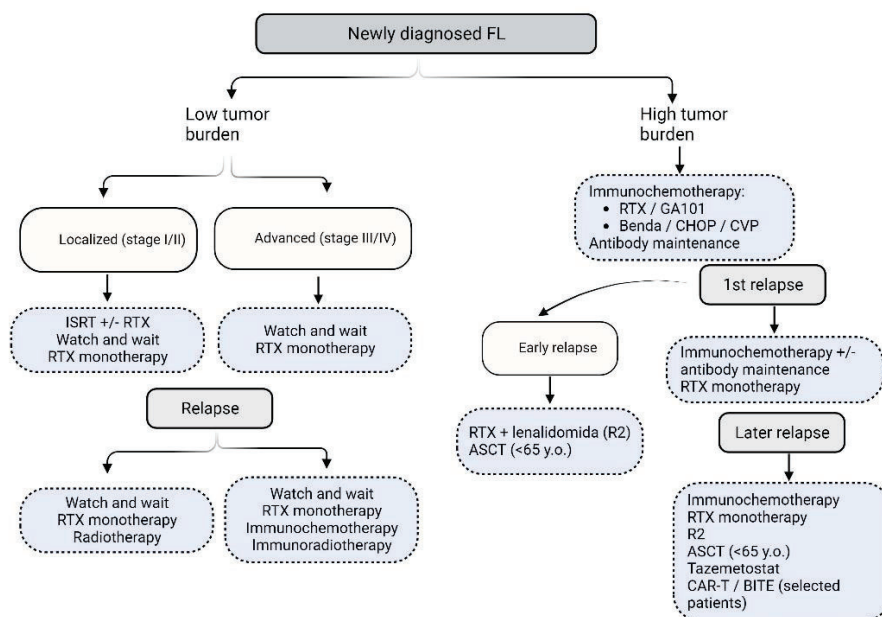


Figure 8. Algorithm of follicular lymphoma treatment. Created with BioRender.com

Nevertheless, patients usually are diagnosed in an advanced stage (III / IV). The decision to start or delay treatment is based on clinical criteria, including B symptoms (unexplained fever, night sweats, weight loss), hematopoietic

INTRODUCTION

impairment or bulky disease, among others.^{152, 159} In asymptomatic cases, watch-and-wait is usually done, as early initiation of therapy does not result in a clear therapeutic benefit;¹⁶¹ however, rituximab as a single-agent could result in longer progression free survival.¹⁶²

In symptomatic patients, immunochemotherapy has become the standard-of-care. Despite rituximab is still the most commonly used anti-CD20 antibody, GA101 or obinutuzumab, which has an enhanced direct and immune effector cell-mediated cytotoxicity, is approved since 2017.^{159, 163} **(Figure 9)** Chemotherapy regimens include CHOP (cyclophosphamide, vincristine, doxorubicin, prednisone), bendamustine or CVP (cyclophosphamide, vincristine, prednisone), being the last inferior in PFS compared to CHOP.^{159, 152, 164} After the induction phase, a maintenance during 2 years with rituximab has been demonstrated to prolong PFS.¹⁶⁵

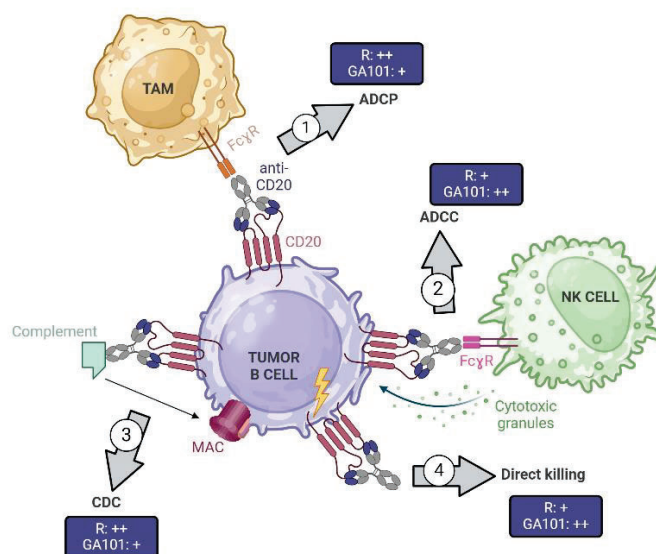


Figure 9. Mechanism of action of anti-CD20 antibodies.

In relapse, it is recommended to perform a new biopsy so a transformation to an aggressive lymphoma can be excluded. Treatment depends on the initial response and its duration, and frequently are bendamustine / CHOP (depending on the first-line) with addition of rituximab / obinituzumab.¹⁵² Combination of rituximab and lenalidomide (R2) is also often used.¹⁵⁴ Lenalidomide is an immunomodulatory agent effective for the treatment of both first-line and relapsed follicular lymphoma.¹⁶⁶ Nevertheless, superiority over standard immunochemotherapy could not be demonstrated, meaning it will not replace standard-of-care therapy.¹⁵⁹ Autologous stem-cell transplantation (ASCT) after high-dose chemotherapy prolongs PFS and may be considered in younger patients that experienced an early relapse.¹⁵²

Targeted and immunotherapies are used in third-line. PI3K inhibitor (PI3Ki) were commonly used, after it was assessed idelalisib is highly active in follicular lymphoma and other indolent lymphomas.¹⁶⁷ Even so, concerns related to toxicity led to a withdrawal of this group of drugs from the U.S. market.¹⁵⁴

Nowadays, PI3Ki have been replaced for tazemetostat, an EZH2 inhibitor approved for r/r FL patients who had received at least two previous treatments.¹⁶⁸ In a phase II clinical trial, the ORR was 69% in *EZH2*^{mut} patients while decreased to 35% in *EZH2*^{mut} individuals.¹⁶⁹

Anti-CD19 CAR-T therapy has been approved for relapsed follicular lymphoma. Due to described toxicities, its use remains reserved for transformed cases or relapsing patients with poor prognostic features.¹⁵² For this reason, data is still limited, but a clinical trial denotes follicular lymphoma

INTRODUCTION

patients are highly responsive and experience long-term responses, with 71% of them achieving a CR compared to the 43% in the DLBCL cohort.¹⁷⁰

Finally, the regulatory agencies have recently approved mosunetuzumab, a bispecific T-cell engaging antibody (BITE), as clinical trials data indicates a high efficacy, with an ORR of 80% including 60% of CR.^{171, 172}

3.5. Histological transformation

A subset of follicular lymphoma patients suffer a histological transformation (HT) to an aggressive lymphoma, mostly, GCB-DLBCL.¹⁷³ HT occurs in a rate of around 2% patients per year, meaning an overall transformation rate of 10.7% at 5 years.¹⁷⁴ Importantly, treatment with rituximab (with or without chemotherapy) is associated to a significant lower risk of transformation compared to watch and wait strategy.¹⁷⁴ Subsequent series confirmed that observation and assessed a lower risk of transformation, of 8.7% at ten years.¹⁷⁵

Transformed FL (tFL) represent a challenge for the clinical management, as transformed FL (tFL) patients have a worse prognosis, especially those who suffered an early transformation.¹⁷⁶ Histological changes are easily observed, as the typical follicular pattern (**Figure 7**) is completely lost due to the FDC network disappears and the cells acquire a diffuse pattern of centroblasts.^{177, 178}

Moreover, genetic changes also occur: it increase the mutational burden, the genomic complexity and tFL patients commonly harbor alterations in DNA damage response and cell cycle regulation genes such as *MYC*, *CDKN2A/B* and *TP53*.^{179, 91, 176} Even though the pathogenic process is still unknown, it has been assessed it occurs after divergent evolution from a common mutated

precursor.⁹¹ Furthermore, mutations in *EBF1* and in regulators of NF- κ B (*MYD88*, *TNFAIP3*) signaling are also acquired in transformation.⁹⁰

4. MODELS TO STUDY B-NHL

4.1. Culture of primary samples

B-cell non-Hodgkin lymphoma, including mantle cell lymphoma and follicular lymphoma are characterized by a strong dependence on tumor microenvironment.^{26, 88} This means that, in order to study both the pathogenesis and novel treatments, it is necessary to develop complex models that englobe both the tumor cells and the surrounding TME.

4.1.1. Cell lines and mouse models

Cell lines represent quick, easy to use and non-expensive methods to work with many cancer types. However, several limitations compromise its use, as do not represent intratumoral heterogeneity (including clonal variability and absence of TME) and their serial passage may cause variations in genotype and phenotype.¹⁸⁰ Moreover, in indolent lymphomas including follicular lymphoma, there is a lack of accurate cellular models due to the need of additional transforming events to achieve cell immortalization.¹⁸¹ For this reason, FL cell lines often represent a transformation stage into aggressive lymphoma. On the other hand, cell lines from aggressive lymphomas better recapitulate the disease. In mantle cell lymphoma, they carry mutations in *CCND1*, *ATM* and *TP53* genes, while other relevant mutations such as *KMT2D* and *NOTCH2* are poorly or not represented.²²

Cell lines have also been engrafted into mouse models to perform *in vivo* experiments in the so-called xenograft models.¹⁸² In the last years, patient-derived xenografts (PDX) have been successfully established from primary cells in different tumors.¹⁸³ In NHL, they are still scarce but their use has been reported for both FL (n=2) and MCL (n=8).¹⁸⁴ Nevertheless, it requires the use

of NOD/SCID mice, an immunodeficient model, which limits their use for immunotherapeutic and TME studies. Thus, humanized models that include a human immune system, such as humanized PDX (hu-PDX) have emerged as an interesting but still costly alternative.¹⁸²

As an alternative to PDX, there are syngeneic and genetically-engineered mouse models (GEMM). In syngeneic models, a murine cancer cell line has been isolated, expanded and inoculated in new immune-competent individuals from the same strain.¹⁸² In NHL, we have to highlight A20 lymphoma line from BALB/c mice.²³

At last, GEMMs consist on the development of a transgenic mice that usually incorporates specific genomic alterations, which let a gradual tumor development and progression in immune-competent mice, allowing for an autologous development of a complex TME.¹⁸² In mantle cell lymphoma, there is the E μ^{CycD1} /E μ -Myc double transgenic mice; however, it resembles the single E μ -Myc, representing a rare genetic rearrangement, only found in some blastoid cases. Similarly, the tumors observed in the *Cdk4*^{R24C}/Myc-3'RR mice also resemble to the blastoid subtype. On the other hand, in follicular lymphoma the VavP-*Bcl2* model not only recapitulates critical aspects on the disease, but has been widely used in combination with genetic alterations (*Crebbp*^{fl/fl}, *Kmt2d*^{fl/fl} and *Ezh2*^{Y641N}) that are concomitantly mutated with *BCL2*.¹⁸⁵

4.1.2. MCL primary cultures

In contrast to immortalized cancer cell lines, primary cells alone hardly survive or proliferate without the addition of specific signals or microenvironment cells that support its growth.

INTRODUCTION

As previously mentioned, CD40L is a crucial stimulus for MCL cells; for this reason, it can be used to induce proliferation *ex vivo*. In the model published by Chiron *et al*, stromal cells expressing CD40L were used in combination to the addition of the following cytokines: IGF-1, BAFF, IL-6 and IL-10. Altogether, proliferation as well as relevant pathways in MCL, such as NFkB, were induced. Furthermore, regulation of apoptotic proteins and loss of mitochondrial priming were observed, which led to drug resistance.¹⁸⁶

Other models are based in the co-culture with cells from the microenvironment, as bone marrow stromal cells, which activate pro-survival and proliferation pathways.^{187, 27} Given the high relevance of the myeloid compartment, MCL primary cells are also highly viable if co-cultured with monocytes or macrophages.¹⁸⁸

4.1.3. FL primary cultures

In previous studies from our laboratory, we co-cultured FL primary cells together with monocytes and confirm that FL cells actively differentiate and polarize monocytes to M2 macrophages and identified CSF-1R as a therapeutic target.¹⁴⁶

In order to mimic the germinal center microenvironment, a non-immortalized FDC cell line, HK, has been extensively used.^{189 190 191} By co-culturing HK cells with FL primary cells we could study the impact of idelalisib in the angiogenesis and migration processes induced by FDC, as well as the FL-T cell crosstalk and the recruitment of relevant populations in the FL-TME such as Treg and TFH.¹⁹²

Remarkably, HK cells alone do not induce proliferation in B-cell population but they do if combined with CD40 stimulation.¹⁸⁹ In Caesar *et al*, immortalized YK6 were engineered from HK cells, and are able to express CD40L and IL21 in the cell membrane. YK6 cells allow for a robust stimulation of GC-derived B cells, thus broaden the experimental options to study GC-derived lymphomas.¹⁹³

Tonsil stromal cells have also been used to culture primary FL cells in a 3D model.¹⁹⁴ These cells were previously characterized and it was determined they exhibited characteristics of follicular reticular cells.¹³⁷ Recently, a novel 3D model that recapitulates immune exhaustion features from FL-LN has also been published. In this case, non-purified FL samples were cultured with a cytokine cocktail containing IL-2, IL-4 and CD40L.¹⁹⁵

4.2. 3D models

In cancer research, 2D cultures represent a limitation, as they fail to represent the heterogeneity of tumor specimens and the original architecture.¹⁹⁶ *In vivo*, tumors grow within an interactive 3D microenvironment that regulates cell function due to cell-cell and cell-ECM interactions, adhesive, topographical and mechanical forces and are subjected to local gradients of nutrients, oxygen and growth factors.¹⁹⁷

Different methods have been reported to generate tridimensional models, and may be classified in scaffold-free, scaffold-based or microfluidic devices. Based on the cellular composition and the dynamics of the system the models can also be classified in multicellular tumor spheroids, organoids and organ-on a chip models.¹⁹⁶

INTRODUCTION

Multicellular tumor spheroids represent the most common scaffold-free model as its intermediate complexity between 2D *in vitro* cultures and *in vivo* models and its relatively low cost makes them suitable for drug testing. Spheroids may reproduce cellular heterogeneity, cell interactions and cell processes (migration, invasion). Importantly, they maintain a physical barrier for drug penetration, a metabolic and oxygen gradient and the tumor organization, with dividing cells in the periphery and apoptotic cells in a necrotic core.¹⁹⁸ **(Figure 10)**

Many methods are available to generate a 3D multicellular spheroid; however, we highlight i) the hanging-drop technique, in which a small droplet (10-50 μ l) of cell suspension is placed onto a culture dish lip or a glass coverslip, and then inverted upside down; and ii) ultra-low attachment (ULA) microplates, treated with a hydrophilic coating covalently bound to the well surface that enables the formation of spheroids.^{198, 199}

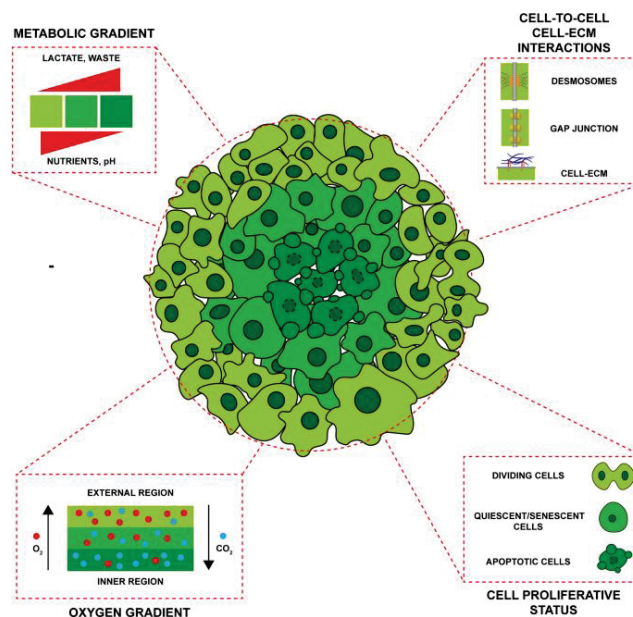


Figure 10. Representation of a spheroid model. Zanoni *et al* 2020.

Spheroids usually refer to scaffold-free or anchorage-independent models. Nevertheless, the addition of a scaffold to provide physical support is feasible. These anchorage-dependent spheroids (also called tumoroids), intend to mimic a native ECM in which tumor cells adhere, proliferate and migrate in 3D.¹⁹⁷

Organoids are self-organized structures containing adult or embryonic stem cells and reflects the original tissue architecture and characteristics, including cell differentiation. In summary, it is necessary to reproduce organogenesis cues *in vitro*. To date, organoids from many solid cancers have been generated.¹⁹⁶

Finally, organ-on-a-chip technology consist on a cell culture device design to reproduce functional units of human organs *in vitro*. They are composed by micro-channels that mimic a certain tissue-specific environment, meaning that parameters as temperature, pH and oxygen can be controlled.²⁰⁰

4.2.1. 3D models in NHL

Although lymphoma growth in the lymph nodes possess characteristics of a solid tumor, 3D models in the field are still very scarce.

The first tridimensional models in follicular lymphoma were based on culturing cell lines in 3D. In 2013, Decaup and colleagues published a multicellular aggregate of lymphoma cells (MALC) using a hanging drop method to compare different anti-CD20 antibodies.²⁰¹ In this line, our group has assessed a good antibody penetrance in this model by using anti-CD38 daratumumab.²⁰²

Recently, we demonstrated that MALC could also be generated by using ULA plates, resulting in regular and viable spheroids useful for drug testing.²⁰³

INTRODUCTION

Lately, the culture of primary samples in the ULA plates has represented a step forward in the development of 3D models in FL and was named as patient-derived lymphoma spheroids (PDLS). This model maintains crucial markers of FL: CD79a, BCL2, CD10 and CD20, which could be analyzed by immunohistochemistry, and different populations from the TME (CD4+ T cells, CD8+ T cells and NK cells).

In the model presented by Lamaison *et al*, a microfluidic method based on the encapsulation of cells inside alginate microspheres was used. Both cell lines (from DLBCL and FL) and primary samples (FL) were tested, and stromal cells and matrigel to mimic ECM were included.¹⁹⁴

Apart from follicular lymphoma, attempts to create tridimensional models have been done in other malignancies including DLBCL and CLL. Regarding chronic lymphocytic leukemia, ULA plates have been used in a similar way than FL, in a model containing IL-2, IL-15, IL-21, CpG and anti-CD3/CD28 for T-cell stimulation.²⁰⁴ A sophisticated bioprinting method published by Sbrana and collaborators consists on mixing cell lines or primary CLL cells with an hydrogel to generate a scaffold that allows cell viability for up to 28 days.²⁰⁵

In Foxall *et al*, DLBCL grew in spheroids using a scaffold-based (collagen I) hanging-drop system, which enabled the study of adherent populations from the TME like cancer-associated fibroblasts (CAF) and TAMs.²⁰⁶ Finally, a lymphoma-on-chip model with a vascularized and perfusable microchannel has been reported.²⁰⁷

5. CD70 AS A TARGET FOR CAR-T THERAPY

5.1. CD70

CD70, also known as CD27 ligand (CD27L) or TNFSF7, is a membrane protein that belongs to the tumor necrosis superfamily (TNFSF).²⁰⁸²⁰⁹ Even though in physiological conditions it is only found on activated T and B lymphocytes, it is frequently deregulated in a variety of B-cell malignancies, including follicular lymphoma and mantle cell lymphoma,^{210 211 48} as well as other solid and hematologic cancers.²¹²

In first place, CD70 was defined as the ligand of CD27, a tumor necrosis factor receptor superfamily (TNFRSF) expressed in non-experienced antigen T cells and memory B cells. In T cells, CD27 acts as a coactivator, providing a second signal for T cell activation and revealing as a key component in the expansion and maintenance of adaptive immune system.^{213 214215} In parallel, a role in B-cell activation, proliferation and immunoglobulin synthesis by CD27/CD70 axis was also described.²¹⁶

Nevertheless, CD27-CD70 interactions may be bidirectional, as first described by Lens et al, meaning that CD70 not only works as a ligand for CD27, but also could initiate a reverse signaling in which, after encountering CD27, induces PI3K and MEK pathways downstream.²¹⁷ (**Figure 11**). Remarkably, this reverse signaling enhances B-cell proliferation and synergizes with CD40L and IL-4, known as GC stimuli, while the terminal differentiation to plasma cells was decreased.^{217 218}

INTRODUCTION

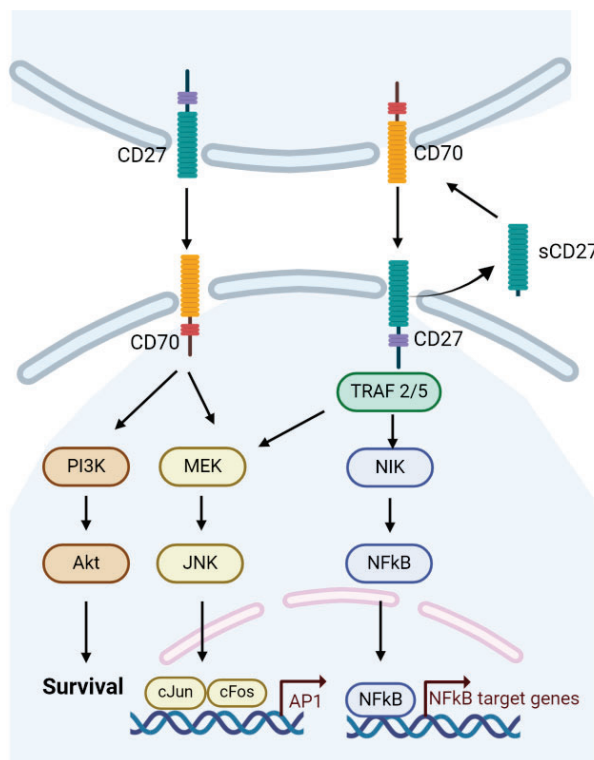


Figure 11. CD27/CD70 axis signaling. Created with BioRender.com

Altogether, CD27-CD70 axis has gained attention as an interesting novel target for cancer treatment, especially for immunotherapy intervention.²¹⁹

5.2. CD70 as a target in B-NHL

In the recent years, therapies targeting CD70 in B-cell lymphoma are being studied and some of them reached clinical trials (**Table 1**). Even so, clinical development of anti-CD70 drugs was already progressed for acute myeloid leukemia (AML), characterized by *de novo* CD70 expression in malignant cells.²²⁰ In this way, ARGX-110 (also known as Cusatuzumab) is a monoclonal antibody that targets and neutralizes CD70, disrupting CD27/CD70 axis and promoting antibody-dependent cellular cytotoxicity (ADCC) and antibody-dependent cellular phagocytosis (ADCP)²²¹ with interesting results in clinical

trials for AML treatment: NCT03030612²²², NCT03030612²²³, NCT04241549²²⁴. Apart from AML, it has been tested in different CD70+ malignancies, including cutaneous T-cell lymphoma and other solid tumors (NCT01813539, NCT01813539)^{225 226} Even though no data is available for B-NHL, promising results have recently been presented in a preclinical model of chronic lymphocytic leukemia.²²⁷

Clinical Trial ID	Pathology	Product	Phase	Start date
NCT05667155	DLBCL, tFL, PMBCL, MCL, other indolent and transforming B-NHL	Cord Blood-derived dualCAR-NK19/70	I	15-12-2022
NCT04429438	B-cell lymphoma including PMBCL, CNS-BCL	CAR-T cells targeting different antigens (CD19, CD20, CD22, CD70, CD13, CD79b, GD2, PSMA)	I / II	01-06-2020
NCT05842707	DLBCL, tFL, PMBCL, MCL, other indolent and transforming B-NHL	dualCAR-NK19/70 cell	I / II	18-01-2023
NCT02216890	DLBCL, FL3b, MCL	SGN-CD70A	I	08-2014 (completed 15-02-2017)

INTRODUCTION

NCT03307746	DLBCL, FL, MCL, MZL	Varlilumab in combination with Rituximab	I / II	23-11-2017
NCT04502446	DLBCL	Anti-CD70 Allogeneic CRISPR-Cas9-Engineered T Cells (CTX130)	I	31-07-2020
NCT00944905		MDX-1203, a human monoclonal antibody drug conjugate		07-2009 (completed 11-2012)

Table 1. Clinical trials targeting CD70 in B-NHL. Information extracted from ClinicalTrials.gov

In contrast to Cusatuzumab, which has not reached clinical trials in B-cell lymphoma, antibody drug conjugate (ADC) strategies have been more successful. That is the case of SGN-CD70A, a compound formed by an anti-CD70 antibody, a protease-cleavable linker and a DNA-crosslinking pyrrolobenzodiazepine dimer drug, which has been used for patients with CD70+ DLBCL and MCL (NCT02216890²²⁸). Nevertheless, its limited efficacy (ORR=20%) and frequent thrombocytopenia have limited its therapeutic applicability. MDX-1203, also known as BMS-936561, is another example of an ADC: there is an anti-CD70 antibody linked to a duocarmycin derivative containing a DNA binding domain, which acts as a cytotoxic agent, and a dipeptide linker.²²⁹ In a first-in-human clinical trial in clear cell renal cell carcinoma (ccRCC) or relapsed or refractory B-NHL any CR/PR were observed (NCT00944905²³⁰).

Finally, varlilumab (CDX-1127) is a human mAb that targets CD27 developed to target CD27-expressing leukemias or lymphomas.²³¹ Given the role of CD27 cells as a coactivator in CD3+, it has also been purposed that varlilumab could have an anti-tumoral effect by activating T lymphocytes through an agonistic effect on CD27.^{232 233 234} To date, safety and activity results from 2 clinical trials in solid tumors have been published with modest response rates (NCT01460134²³⁵, NCT02335918²³⁶), while similar results were recently observed in hematological malignancies. However, a durable CR was observed on an advanced Hodgkin lymphoma patient, whose tumor cells were characterized by a high CD27 expression.²³⁷

A novel strategy that has revolutionized the management of hematologic tumors in the latest years, chimeric antigen receptor (CAR) T cells, has not been excluded in the development of CD70-targeting therapies. A prove of that is the fact that out of the seven active clinical trials targeting CD70 for B-cell lymphoma, four of them are CAR-based. **(Table 1) (Figure 12)**

INTRODUCTION

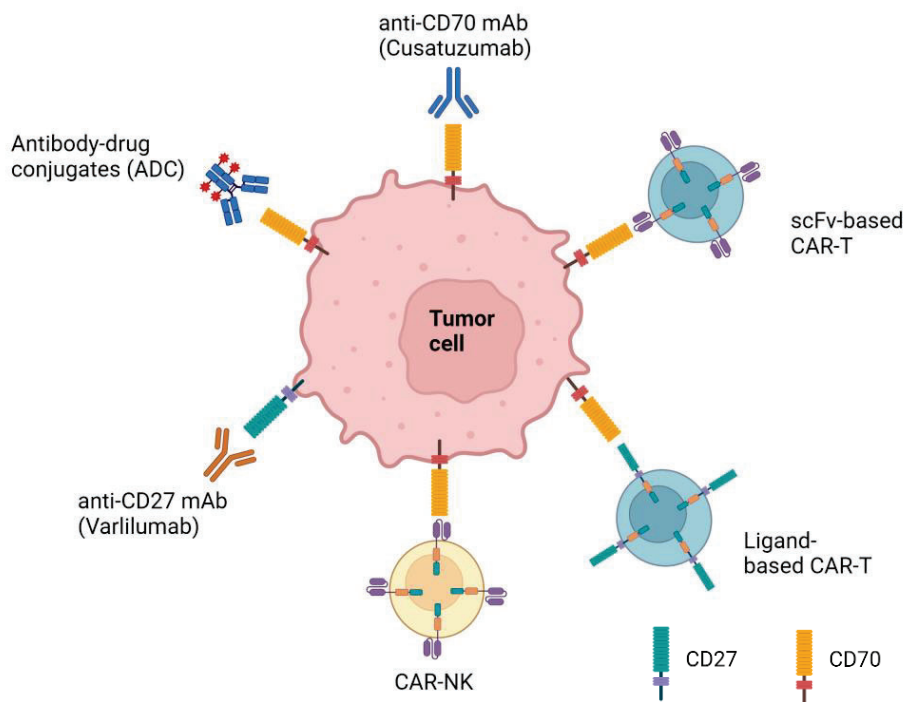


Figure 12. Different strategies targeting CD70 in hematologic tumors.

Created with BioRender.com

5.3. CAR-T cells

Chimeric antigen receptor T-cell (CAR-T) treatment is a cellular immunotherapy based on combining an effector cell with antitumor properties (T cell) with a synthetic receptor with high capacity to recognize antigens.²³⁸ **(Figure 13)**

First-generation CAR-T, composed only by the following domains: extracellular antigen recognition, hinge, transmembrane and intracellular signaling (CD3 ζ) were not able to induce clinical responses.^{238 239} For this reason, second-generation CAR-T cells that include a costimulatory domain were developed. In first place, CD28 was used as a costimulatory signaling

domain;^{240 241} however, 4-1BB domain also was demonstrated to be effective.²⁴² Finally, third-generation CAR-T are the result to combine CD28 and 4-1BB in the same construct; while fourth-generation CAR-T include a transgene, usually encoding for a cytokine that may be useful to overcome an immunosuppressive tumor microenvironment.^{243 244}

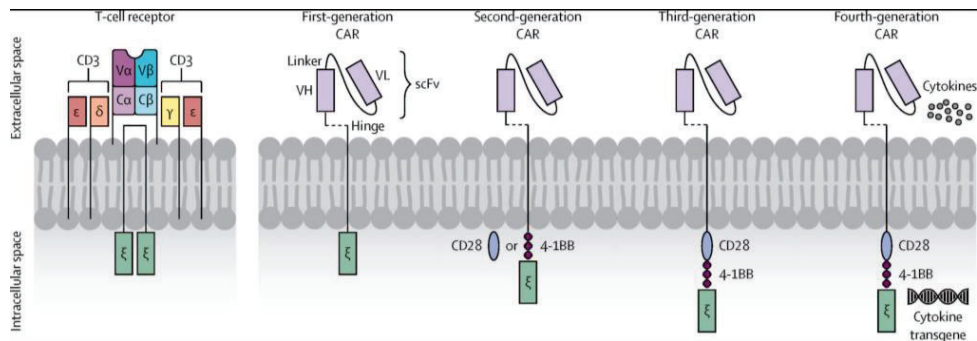


Figure 13. CAR-T constructs. At left, a normal TCR. At right, 1st to 4th generation of chimeric antigen receptor constructs. Singh and McGuirc Lancet Oncol 2020

CAR-T cells are activated due to antigen recognition, without the need of human leukocyte antigen (HLA) presentation, avoiding a crucial mechanism of immune evasion in cancer.²⁴⁵ Even though the chimeric receptor usually consists of a single-chain variable fragment (scFv) containing the variable regions of the heavy (VH) and light (VL) of an antibody connected by a peptide linker, there are also CAR-T products not based on antibodies.^{246 247}

Aiming to overcome some limitations in scFv-based CAR-T, ligand-based CAR-T have emerged as a promising alternative.²⁴⁸ Importantly, they maintain the capacity to recognize antigens in a non-HLA based manner and, compared to antibody-based CAR-T, are likely to present an increased stability, decreased dimerization, and lower immunogenicity. To date, ligand-based CAR-T cells

INTRODUCTION

directed into many targets have entered into clinical trials, including anti-CD70 CAR-T based on its natural ligand CD27.^{246 247}

To date, most CAR-T clinically tested use autologous T cells. These T cells are isolated from the patient and genetically modified to express the CAR and the desired domains. Then, CAR-T cells are expanded *ex vivo* and reinfused into the patient.²⁴⁹ (Figure 14)

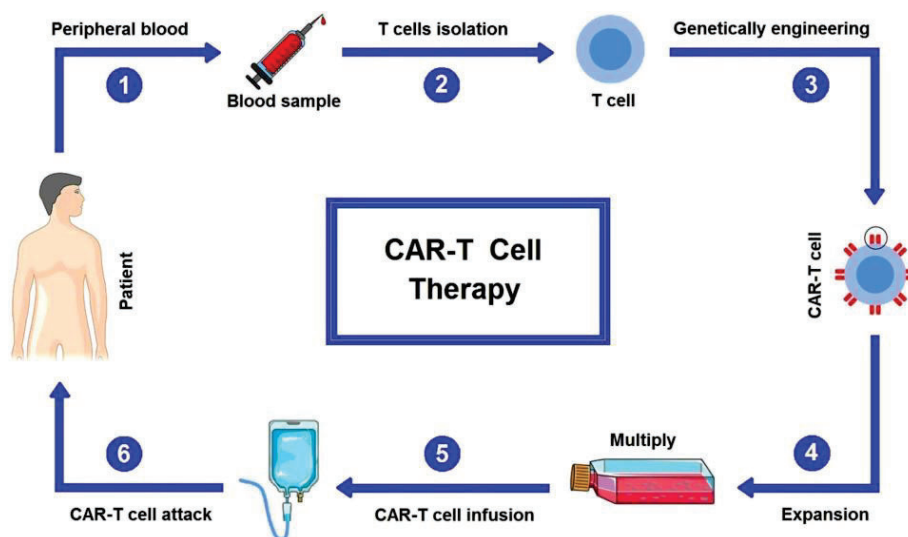


Figure 14. CAR-T therapy generation in the clinics. Abbasi S et al Cancer Medicine 2022

5.3.1. CD19 CAR-T

CD19 is a surface molecule restricted to the B-cell lineage that has been widely used as a target for CAR-T cell therapy for the treatment of B-acute lymphoblastic leukemia (ALL) and lymphoma (B-NHL).²³⁹ Nowadays, many anti-CD19 CAR-T products have been approved for the treatment of B-NHL by regulatory agencies, including the following: tisagenlecleucel (tisa-cel), axicabtagene ciloleucel (axi-cel), lisocabtagene maraleucel (liso-cel) and brexucabtagene, being the last only for R/R MCL.²⁴⁶

Additionally, the academic CAR-T ARI-0001, developed at Hospital Clínic de Barcelona, received the approval by the Spanish Agency of Medicines and Medical Devices (AEMPS) as a hospital exemption to treat R/R B-ALL patients older than 25 years old.^{250 251} In the clinical trial (NCT03144583) also 8 NHL (4 DLBCL, 2 primary mediastinal B cell lymphoma, 2 FL) were included with ORR = 75%. Recently, data published from nine CLL patients treated with ARI-0001, six of them with Richter's transformation, indicate a good overall response rate of 87.5%, including a CR in four patients.²⁵² Overall, ARI-0001 efficacy is comparable to available commercial CAR-Ts.²⁵³

5.3.2. Dual CAR-T

CAR-T therapy has been proved to be highly effective in B-NHL; however, long-term data is still scarce. In a recent review by Cappell and Kochenderfer, in which are reported ten studies with more than 24 months of follow-up, ORR was superior to 60% in most cases, with the exception of a tFL cohort in which the ORR was 46%.²⁵⁴ Complete response was slightly lower, in a range of 40-70%.²⁵⁵

One of the most complete studies determined a duration of response (DOR) in a cohort composed by B-NHL and CLL patients treated with axi-cel superior to 3 years of 51%, with a slight superiority in low grade lymphoma (63%).²⁵⁶

Whether a patient achieve or not a durable remission is associated, among other factors, to a deep initial response.²⁵⁵ While overall DOR > 3 years was 51%, in patients which experienced a CR was increased to 76%.²⁵⁶ Furthermore, up to 25% of patients who first respond to CD19 CAR-T treatment, experience a CD19-negative relapse, showing antigen-escape

INTRODUCTION

resistance mechanisms in CAR-T cell therapy.^{254 247} For this reason, dual CAR-Ts able to target two different antigens are being developed.

The frequent loss of CD19 antigen in lymphoma has led to the recent development of novel CAR-Ts that are able to target different antigens simultaneously. In this way, Hospital Clínic de Barcelona has combined anti-CD19 CAR-T (ARI-0001) with anti-BCMA (hARI-0002), the last used for multiple myeloma,²⁵⁷ generating a new product, ARI-0003.²⁵⁸

Nevertheless, to date, the most frequent strategy has been the development of dual CAR-T targeting CD19 and CD22, a protein also found in the membrane of B cells²⁵⁹²⁶⁰²⁶¹²⁶². An extensive clinical trial reported in Spiegel JY *et al* demonstrated a similar PFS rate of dual CAR-T compared to tisa-cel; nevertheless, they observed an inferior cytokine release after CD22 scFv ligation compared to CD19.²⁶³ In another study, anti-CD19 CAR-T also induced higher levels of IL2 and TNF α in vitro; however, the dual CD19-CD22 CAR-T produced more granzyme B. It was also included a clinical trial with comparable responses to anti-CD19 CAR-T in aggressive B lymphoma with 87.5% ORR and 62.5% CR.²⁶¹ Finally, dual bicistronic CD19-CD22 CAR-T has also been tested in a clinical trial in combination with anti-PD1 pembrolizumab with similar results (ORR = 66%, CR = 48.9%) without avoiding relapse.²⁶⁴

5.4. Anti-CD70 CAR-T strategies

CD70 has been proposed as an interesting target for lymphoma in the context of CD19 antigen escape.²⁶⁵ Nevertheless, to date, development of dual CD19-CD70 CAR-T have been limited in a coadministration of both single CAR-T cells in a patient diagnosed of primary central nervous system (PCNS)-DLBCL.²⁶⁶

Besides, in the recent years, anti-CD70 CAR-T cells have been considered, not only for the treatment of hematologic tumors, but also for some solid tumors as head and neck squamous cell carcinoma²⁶⁷ and gliomas.²⁶⁸

5.4.1. Ligand-based CAR-Ts

Ligand-based strategies to generate CAR-T cells that target CD70 have been broadly used. In 2011, Shaffer and colleagues generated a first-generation CAR fusing CD27 with CD3- ζ chain. This CAR-T was tested against cell lines from NHL and other hematologic malignancies, showing an increase in cytokines (IL-2, IFN γ). Mild specific lysis was observed and patient samples from B-cell lymphoma were included in the study.²⁶⁹

However, strategies to modify CD27 protein by using a truncated version (without intracellular domain) as well to include 4-1-BB and/or CD28 costimulatory domains have been evaluated.²⁷⁰ In this paper it was suggested that CD28 signaling led to lower reactivity, while a truncated CD27 with 4-1-BB costimulatory domain was selected to be tested against a clear cell renal carcinoma cell line. Interestingly, similar efficacy was observed compared to full length 1st generation CAR-T described in Shaffer *et al.* This product has also been used in head and neck models²⁶⁷ and in glioblastoma.²⁷¹

Given the fact that AML cells highly express CD70, it has become a good model to study a-CD70 CAR-Ts. Strikingly, it was demonstrated a superior activity of a ligand-based strategy using CD27 compared to the six scFv constructs studied. Although one of the scFv constructs, LF-27z, also induced similar levels of cytotoxicity and cytokine production *in vitro*, it had poorer results *in vivo*.²⁷² Moreover, T-cell expansion was also diminished and viability was comprised when IM spacer and 41BB costimulatory domain were present,

INTRODUCTION

while a differentiation towards effector memory T cells was observed in scFv-based CAR-Ts with the exception of LF-27z.

In order to optimize CD27 CAR-Ts, Leick et al describe a novel strategy based on substituting CD27 transmembrane residues by a CD8 hinge and transmembrane domain. This novel CAR-T induced a superior *in vitro* specific lysis as well as an increased survival in *in vivo* experiments compared to all products tested, including the native truncated form described in *Wang et al*. Moreover, this construct was not released into supernatants, as had similar levels than untransduced cells. Finally, it was demonstrated that this CAR-T had an enhanced binding avidity.²⁷³

5.4.2. scFv-based CAR-Ts

scFv-based strategy has also been used in other studies, such as in Ji F et al, in which they generated a CAR-T containing a CD8 hinge and a 4-1BB costimulatory domain to treat RCC or in Seyfrid *et al*, in which a similar construct was developed to target cancer stem cells in glioblastoma.²⁷⁴

An antibody-based CAR-T was also used in AML with high efficacy *in vitro* but, even though attenuated leukemia progression *in vivo*, failed persist and mice eventually died due to the disease.²⁷⁵

Two antibodies (one of them, based on cusatuzumab, and the other on P91 antibody) were compared to truncated CD27 with comparable levels of cytotoxicity and differences among lung cancer models in the case of cusatuzumab-based, while P91-based had inferior results.²⁷⁶

Finally, a novel emergent strategy has been the development of nanobodies to target CD70 that also were CD70-knockout (KO).²⁷⁷ These nanobodies

represent an alternative to scFv and contain a single-variable domain on heavy chain (VHH).

5.4.3. Fratricide

As CD70 is a protein that may be also expressed by T cells, fratricide could constitute a limitation in the context of CAR-T therapy. Fratricide is the process by which CAR-T cells can kill each other and it has been especially studied in constructs that target CD7 as a therapy for T-cell malignancies.²⁷⁸

(Figure 15)

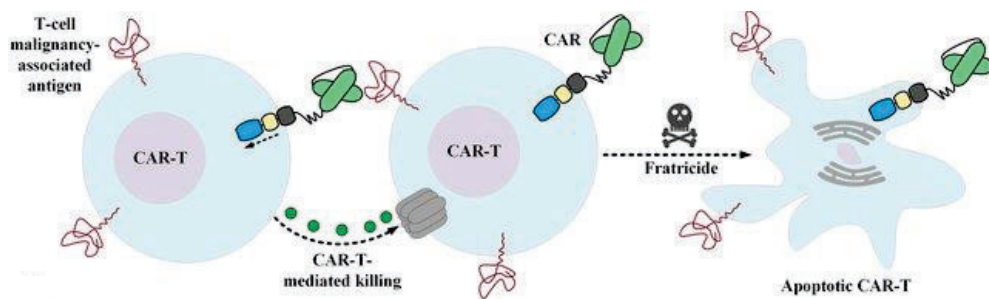


Figure 15. CAR-T fratricide. Modified from Kozani *et al* Stem Cell Res Ther 2021

According to Park YP *et al*, fratricide was not observed; nevertheless, it has been suggested in Seyfrid *et al*, as lower CD70 was found in CAR-T transduced cells. CD70 knockdown using shRNA was performed to avoid this limitation in Jurkat cells and it improved the viability.²⁶⁷²⁷⁴

To prevent fratricide and a potential exhaustion during CAR-T generation and expansion, KO has been tested.²⁷⁹ However, there was not clear data that demonstrated an improvement.

Interestingly, CD70 KO has been compared to wild-type in an anti-CD70 CAR-T designed to treat AML: knock-out slightly increased T-cell expansion, viability and functionality. Intriguingly, it was seen by scRNAseq that KO

INTRODUCTION

product contained a higher proportion of CD4+ central memory cells and CD4+ naïve cells as well as higher TCR clonal diversity but lower CD8 cytotoxic.²⁷⁷

5.4.4. Allogenic CAR-T

By now, all approved CAR-T therapies have been based on modifying autologous T cells from the patients. However, cost of production represents a limitation on the standardization of these therapies. For this reason, the use of allogenic CAR-Ts, also called universal or “off the shelf” (ref) have been explored. In the case of CD70, an allogenic CAR-T with disrupted CD52 and TRAC to prevent graft versus host disease (GvHD) has been published for RCC treatment.²⁷⁹

OBJECTIVES

OBJECTIVES

The **main objective** of this thesis is to develop three-dimensional models of non-Hodgkin lymphoma to test novel immunotherapies. B-cell Non-Hodgkin lymphomas are a heterogeneous group of malignancies with high dependence of the tumor microenvironment. Immunotherapy represents a promising novel strategy in B-NHL treatment but is necessary to determine which patients

To achieve this aim, the **first objective** is to generate and characterize in vitro 3D models of NHL, which better recapitulate the TME. The **second objective** is to identify novel actionable immune modulators by analyzing the immune profile at transcriptomic and protein level of FL and MCL patients. Finally, the **third objective** is to explore novel combinations of selected immunotherapies in 3D cultures tailored for each disease and clinical group.

MATERIAL, METHODS AND RESULTS

MATERIAL, METHODS AND RESULTS

CHAPTER 1. DEVELOPMENT OF NOVEL 3D MODELS IN NON-HODGKIN LYMPHOMA

This first chapter is focused on the generation and characterization of new models to culture primary B-NHL cells from mantle cell lymphoma (**Study 1**) and follicular lymphoma (**Study 2**) in three-dimensions to test conventional and immunotherapeutic drugs.

STUDY 1. A novel patient-derived 3D model recapitulates mantle cell lymphoma lymph node signaling, immune profile and in vivo ibrutinib responses

Araujo-Ayala F*, Dobaño-López C*, Valero JG, Nadeu F, Gava F, Faria C, Norlund M, Morin R, Bernes-Lasserre P, Serrat N, Playa-Albinyana H, Giménez R, Campo E, Lagarde JM, López-Guillermo A, Gine E, Colomer D, Bezombes C, Pérez-Galán P. A novel patient-derived 3D model recapitulates mantle cell lymphoma lymph node signaling, immune profile and in vivo ibrutinib responses.

Leukemia. 2023 Jun;37(6):1311-1323. doi: 10.1038/s41375-023-01885-1. Epub 2023 Apr 8. PMID: 37031299; PMCID: PMC10244172.

*These authors contributed equally to this work

ARTICLE OPEN



LYMPHOMA

A novel patient-derived 3D model recapitulates mantle cell lymphoma lymph node signaling, immune profile and in vivo ibrutinib responses

Ferran Araujo-Ayala^{1,2,11}, Cèlia Dobano-López^{1,2,11}, Juan García Valero^{1,2}, Ferran Nadeu^{1,2}, Fabien Gava^{3,4,5,6,7}, Carla Faria^{3,4,5,6,7}, Marine Norlund⁸, Renaud Morin⁸, Pascale Bernes-Lasserre⁸, Neus Serrat¹, Heribert Playa-Albinyana^{1,2}, Rubén Giménez^{1,2}, Elias Campo^{1,2,9,10}, Jean-Michel Lagarde⁸, Armando López-Guillermo^{1,2,9,10}, Eva Gine^{1,2,9}, Dolors Colomer^{1,2,9,10}, Christine Bezombes^{3,4,5,6,7} and Patricia Pérez-Galán^{1,2,11}

© The Author(s) 2023

Mantle cell lymphoma (MCL), a rare and aggressive B-cell non-Hodgkin lymphoma, mainly develops in the lymph node (LN) and creates a protective and immunosuppressive niche that facilitates tumor survival, proliferation and chemoresistance. To capture disease heterogeneity and tumor microenvironment (TME) cues, we have developed the first patient-derived MCL spheroids (MCL-PDLS) that recapitulate tumor oncogenic pathways and immune microenvironment in a multiplexed system that allows easy drug screening, including immunotherapies. MCL spheroids, integrated by tumor B cells, monocytes and autologous T-cells self-organize in disc-shaped structures, where B and T-cells maintain viability and proliferate, and monocytes differentiate into M2-like macrophages. RNA-seq analysis demonstrated that tumor cells recapitulate hallmarks of MCL-LN (proliferation, NF-κB and BCR), with T cells exhibiting an exhaustion profile (PD1, TIM-3 and TIGIT). MCL-PDLS reproduces in vivo responses to ibrutinib and demonstrates that combination of ibrutinib with nivolumab (anti-PD1) may be effective in ibrutinib-resistant cases by engaging an immune response with increased interferon gamma and granzyme B release. In conclusion, MCL-PDLS recapitulates specific MCL-LN features and in vivo responses to ibrutinib, representing a robust tool to study MCL interaction with the immune TME and to perform drug screening in a patient-derived system, advancing toward personalized therapeutic approaches.

Leukemia (2023) 37:1311–1323; <https://doi.org/10.1038/s41375-023-01885-1>

INTRODUCTION

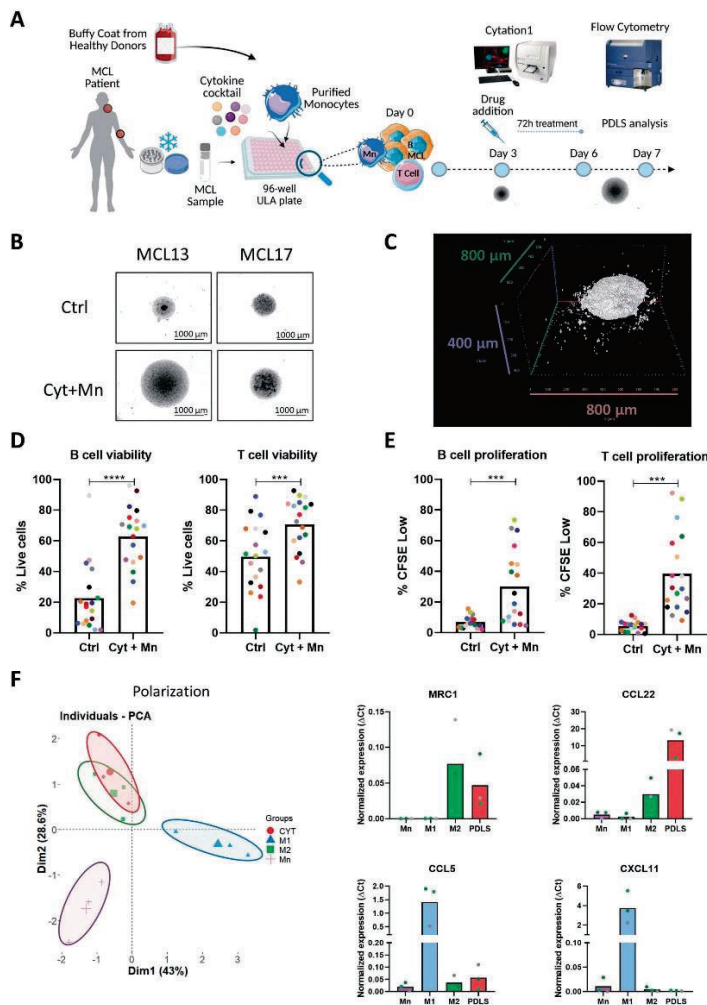
Mantle cell lymphoma (MCL) is a rare and aggressive B-cell non-Hodgkin lymphoma characterized by CCND1 deregulation caused by the t(11;14)(q13;q32) translocation as the first oncogenic hit. Moreover, MCL is characterized by genomic instability and high number of secondary genetic aberrations that are necessary to engage lymphomagenesis. MCL is an heterogeneous disease “per se” and World Health Organization recognizes 2 molecular subtypes that differ in their clinical and biological features: the most common and aggressive conventional MCL (cMCL; SOX11+ and unmutated immunoglobulin heavy chain (IGHV), naïve-like B-cell) and the indolent leukemic non-nodal MCL (nnMCL; SOX11– and mutated IGHV, memory-like B-cell) [1–3]. Besides, both forms differ in the underlying genomic and epigenomic abnormalities [4].

In the last decade, next generation sequencing studies have deciphered the MCL mutational landscape identifying recurrent

mutations (*TP53*, *ATM*, *NOTCH1/2*, *CCND1*, *HNRNP1*, *KMT2D*, *ARID1A*, *SMARCA4*) [5, 6] that contribute to MCL pathogenesis and resistance to chemoimmunotherapy or targeted therapies [7]. These genomic alterations often impact molecular pathways that are involved in DNA damage response, cell proliferation and cell survival [8, 9]. In addition to these genomic abnormalities it is fundamental to consider MCL-tumor microenvironment (TME) crosstalk within the lymph node (LN) [10, 11]. This dialog, together with genomic alterations, leads to the activation of MCL hallmarks pathways of cell proliferation, DNA repair, apoptosis inhibition, NF-κB and BCR signaling [12], with a different representation among patients. In this regard, a study combining genomic and transcriptomic profiling has revealed distinct patients subsets, grouped by genomic alterations and activated pathways [6], associated with differential outcomes, thus reflecting the cooperation between genome aberrations and TME on disease development and outcomes.

¹Fundació de Recerca Clínic Barcelona (FCRB)-IDIBAPS, Barcelona, Spain. ²Centro de Investigación Biomédica en Red-Oncología (CIBERONC), Madrid, Spain. ³Centre de Recherches en Cancérologie de Toulouse (CRCT), INSERM UMR1037, Toulouse, France. ⁴Université de Toulouse, Inserm, CNRS, Université Toulouse III Paul Sabatier, Centre de Recherches en Cancérologie de Toulouse, Toulouse, France. ⁵UCT-Oncopole, Toulouse, France. ⁶Laboratoire d'Excellence “TOUCAN-2”, Toulouse, France. ⁷Institut Carnot Lymphome CALYM, Pierre-Bénite, France. ⁸MACTIV-3D, Toulouse, France. ⁹Hospital Clínic, Barcelona, Spain. ¹⁰University of Barcelona, Medical School, Barcelona, Spain. ¹¹These authors contributed equally: Ferran Araujo-Ayala, Cèlia Dobano-López. [✉]email: pperez@recercaclinic.cat

Received: 2 February 2023 Revised: 13 March 2023 Accepted: 21 March 2023
Published online: 8 April 2023



In the LN ecosystem, the interaction between MCL tumor cells and T cells through CD40L and IL-4 is fundamental to promote tumor proliferation and viability [13]. Likewise, stromal cells as follicular dendritic cells (FDC) [14, 15], through integrin receptors and secreted factors as CXCL12/13 or BAFF [16–18] maintain

MCL viability. In addition, macrophages play a fundamental role in this scenario, as their number is associated with poor prognosis [19], support MCL cell growth in vitro [20] as well as in vivo [21], and may induce immune exhaustion through PD-L1 expression [22].

Fig. 1 MCL-PDLS as a novel 3D model to culture MCL samples *ex vivo*. **A** Representative scheme showing the workflow for MCL-PDLS generation. Created with BioRender.com. **B** Brightfield images (magnification $\times 40$) captured in the Cytation 1 of PDLS generated with cytokines (Cyt) and monocytes (Mn) stimuli compared to non-stimulated PDLS control (Ctrl) after 7 days of culture. **C** 3D reconstruction of a representative PDLS (MCL 1) from an image obtained by SPIM microscopy. **D** Cell viability in tumor B cells and autologous T cells from PDLS determined by percentage of negative LIVE/DEAD fixable Aqua staining ($n = 18$) after 7 days of culture. **E** Cell proliferation in B cells and T cells, calculated as percentage of CFSE low cells, after 7 days of culture ($n = 18$). **F** PCA analysis using normalized expression values of six genes related to macrophage polarization obtained by RT-qPCR in macrophages isolated from MCL-PDLS and 2D-differentiated macrophages polarized to M1 or M2 phenotype as references. Undifferentiated monocytes were used as a control. *MRC1* and *CCL22* are used as M2 markers while *CCL5* and *CXCL11* are used as M1 markers.

In view of the heterogeneity of this rare disease and the critical contribution of TME, powerful preclinical systems using patient-derived material and recapitulating microenvironment cues are mandatory. Several attempts have been described in order to maintain lymphoma patient-derived cultures and induce their proliferation in 2D co-culture systems [17, 23–25]. In the last years there has been an evolution toward patient-derived 3D cultures and organoids (PDO) in many cancer types [26]. However, those systems are scarce in lymphoma [27, 28] and not previously generated in MCL. In the era of personalized medicine and with the rapid evolution of immunotherapies, there is an urgent need to establish these systems that recapitulate disease activated pathway and immune profile, and are able to induce T-cell mediated responses. In this work, we aimed to develop a novel 3D spheroid-based model to culture MCL primary cells together with autologous T cells and healthy donor monocytes, recreating the immune TME. This MCL Patient Derived Lymphoma Spheroid (MCL-PDLS) reproduces a specific MCL-LN signature [12] making it a suitable tool to study MCL biology, and to test both conventional and immunotherapeutic drugs together with identification of biomarkers of response and relapse.

METHODS

PDLS generation

Peripheral blood mononuclear cells (PBMCs) isolated from MCL ($n = 19$) samples were thawed in sterile conditions, resuspended in enriched medium [29] and counted using Neubauer chamber system with trypan blue to assess cell viability. In order to assess proliferation, cells were labeled with 0.5 μ M carboxyfluorescein succinimidyl ester (CFSE) cell tracker (Thermo Fisher Scientific, Waltham, MA, USA) following manufacturer's instructions.

The workflow for MCL-PDLS generation is detailed in Fig. 1A. CFSE-labeled MCL samples were mixed with monocytes at a 4:1 ratio (MCL:monocytes), seeding 5×10^4 MCL cells/well and 1.25×10^4 monocytes/well in a final volume of 200 μ l/well in Nunclon™ Sphera™ 96-wells Ultra-Low Attachment (ULA) microplates (Thermo Fisher Scientific) in enriched medium supplemented with the following cytokines: 50 ng/ml CD40L-HA tagged (R&D Systems, Minneapolis, MN, USA), 1 μ g/ml anti-HA-Tag antibody (Merck, Darmstadt, Germany), 10 ng/ml IL-4 (Peprotech, Cranbury, NJ, USA) and 50 ng/ml B-cell activating factor (BAFF) (Miltenyi Biotec), referred hereafter as "PDLS medium" and maintained at 37 °C 5% CO₂ up to 7 days.

Drug assays

PDLS generated as indicated above were cultured in 150 μ l of PDLS medium, drugs were added at day 3 (50 μ l/well in PDLS medium). Ibrutinib (Selleck Chemicals LLC, Houston, TX, USA) was added to a final concentration of 500 nM and nivolumab (Selleck Chemicals LLC) at 10 μ g/ml. Six PDLS replicates were assessed per each condition. After 3 days of treatment, MCL-PDLS were mechanically disaggregated and analyzed by flow cytometry (BD LSRFortessa SORP-HTS, BD Biosciences, Franklin Lakes, NY, USA) to assess cell viability (LIVE/DEAD Fixable Aqua) and cell population distribution (CD20, CD3, CD4, CD8). To determine cell number of viable cells, disaggregated PDLS were analyzed using a High Throughput Sampler (HTS) integrated in the flow cytometry reading a fix volume.

Detailed description of additional methods is included in the Supplementary Material. These materials include: patient samples, monocyte-macrophage differentiation and polarization analysis, PDLS immune profile

and activation, RNA-seq, metadata comparative analysis and a table of antibodies used to characterize the populations by flow cytometry (Table S1).

RESULTS

Patient-derived MCL spheroids: cellular composition, distribution and 3D structure

In secondary lymphoid organs (SLO) as the LN, lymphoma B cells are in close contact with cells of immune origin, including CD40L-expressing T cells, and macrophages together with endothelial and stromal cells [30]. Thus, in order to generate a system that recapitulates microenvironment cues in SLO, we cultured MCL samples (Table 1), most of them from PB, in an optimized medium (PDLS medium) containing CD40L, IL-4 and BAFF, which are known to be fundamental to mimic interactions with T cells and stromal cells [16, 17]. Macrophages are often not recovered from biopsies and the number of monocytes in Peripheral Blood (PB) is highly variable and does not correlate with macrophage infiltration of SLO in MCL [31]. For this reason, monocytes from healthy donors were also included to account for the myeloid compartment, fundamental in this pathology [20, 21]. This multicellular suspension was seeded in ULA plates, as shown in Fig. 1A, to facilitate cell aggregation and growth (Fig. 1B). Nineteen MCL-PB samples were used to successfully generate PDLS. Spheroid formation occurs in the first 24 h after seeding (Supplementary Video 1). SPIM microscopy demonstrated that these structures self-organize in a real spheroid, with a mean volume of 0.16 mm³ (MCL1) (Fig. 1C and Supplementary Video 2). As shown in Fig. S1A, B, after 7 days of culture the viability of lymphoma B cells (mean 22.5) and accompanying T cells (mean 49.7), was significantly increased by both the cytokine cocktail (mean B cells 62.5; mean T cells 57.8) and the monocytes (mean B cells 55.45; mean T cells 73.92), separately. However, B-cell proliferation was only engaged by cytokines (mean 32.95). In the case of T cells, both cytokines (mean 21.47), and monocytes (mean 23.64) induced proliferation (Fig. S1A, B), albeit with a great variability and similarly to previous studies in 2D MCL stimulated with other cocktails [17]. This proliferation was also reflected in the spheroid diameter (Fig. S1C). Interestingly, this cytokine cocktail not only induced B-cell proliferation, but also activation, as revealed by flow cytometry changes in size (FSC) and complexity (SSC) and by the upregulation of CD69 and CD86, as seen in SLO (Fig. S1D). Thus, we chose to combine both cytokine cocktail and monocytes with the lymphoma B cells and T cells, which similarly increased viability in B and T cells (mean 62.88 and 70.9, respectively) and proliferation in B cells (mean 30.17), while improved the T-cell proliferation induced by cytokines alone (mean 39.57) (Fig. 1D, E). After 7 days, MCL PDLS were mostly composed of B cells (mean 82%) and similar proportion of T cells (mean 9.8%) and monocytes (mean 8.2%) (Fig. S1E).


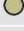


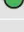
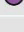
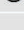

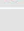
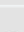
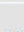
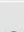
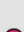




It has been previously recognized that MCL cells induce differentiation of monocytes to M2 macrophages [12, 21]. Similarly, we observed that monocytes progressively differentiate into macrophages as shown by the increase in size and complexity (FSC/SSC) (Fig. S1F). These macrophages displayed high expression of M2-like markers as the mannose receptor *CD206* (*MRC1*)

MATERIAL, METHODS AND RESULTS

F. Araujo-Ayala et al.

1314



Table 1. MCL patient characteristics.

Study label	Sex/ Age ^a	Sample type ^a	% IgVH homology ^c	Stage ^d	MCL variant ^e	Disease status ^f	MIPI ^g	nnMCL/ cMCL ^h	TP53 altered ⁱ	Color
MCL1	M/63	PB	96.18 ^k	IV	NA	R	Medium	nnMCL	Y	
MCL2	M/76	PB	97.92 ^j	IV	C	D	High	cMCL	Y	
MCL4	M/NA	PB	98.11 ^j	IV	NA	D	High	cMCL	NA	
MCL5	M/73	PB	99.6 ^j	IV	NA	D	NA	cMCL	NA	
MCL6	M/43	PB	99.65 ^j	IV	B	D	High	cMCL	NA	
MCL8	M/NA	PB	NA	NA	B	NA	NA	NA	NA	
MCL10	F/73	PB	100 ^j	IV	C	R	High	cMCL	NA	
MCL11	M/71	PB	100 ^j	IV	C	D	High	cMCL	N	
MCL12	M/64	PB	100 ^k	IV	C	R	High	cMCL	N	
MCL13	M/70	PB	98.60 ^k	IV	C	R	High	cMCL	N	
MCL14	M/75	PB	95.14 ^k	IV	NA	R	High	nnMCL	Y	
MCL16	M/80	PB	97.22 ^k	IV	NA	D	High	nnMCL	Y	
MCL17	F/78	PB	95.83 ^k	NA	NA	R	NA	nnMCL	N	
MCL18	M/65	PB	91.58 ^k	IV	NA	Pt	Medium	nnMCL	N	
MCL19	F/60	BM	97.32 ^j	NA	NA	Pt	NA	nnMCL	NA	
MCL20	M/52	PB	NA	I	NA	R	Low	nnMCL	NA	
MCL21	F/59	PB	96.18 ^j	IV	C	R	Low	cMCL	N	

SPRINGER NATURE

Leukemia (2023) 37:1311–1323

Table 1. continued

Study label	Sex/ Age ^a	Sample type ^a	% IgVH homology ^c	Stage ^d	MCL variant ^e	Disease status ^f	MIPI ^g	nnMCL/ cMCL ^h	TP53 altered ⁱ	Color
MCL22	M/60	BM	93.47 ^k	IV	NA	R	Medium	nnMCL	Y	
MCL24	F/59	LN	NA	IV	C	R	Low	cMCL	NA	

^aF: female, M: male.^bPB: peripheral blood, LN: lymph node, BM: bone marrow.^c% of homology with the germline, assessed by Sanger sequencing or ^hIgCaller [59].^dAnn Arbor stage.^eEvaluated by two independent pathologists. C: conventional, B: blastoid; NA cases did not have tissue available.^fSamples were obtained at D: diagnosis, R: relapse, Pt: pretreatment, NA: not available.^gMIPI: Mantle cell Lymphoma International Prognostic Index (High: 6–11; Medium: 4–5; Low: 0–3).^hnnMCL: non-nodal MCL; cMCL: conventional MCL.ⁱMutated and/or deleted at the time of sampling. Y: yes, N: no, NA: not available.

and CCL22 (Fig. 1F), while M1-like markers were underrepresented (Fig. 1F). Moreover, the macrophages from the MCL-PDLS clearly clustered with M2-like macrophages in the PCA analysis generated with the expression of monocytes (*PMAIP1* and *RGS2*), M1 (*CCL5* and *CXCL1*) and M2 markers (*CCL22* and *MRC1*). These genes were selected from studies analyzing their differential expression [32, 33].

In summary, we have established for the first time a patient-derived 3D system integrating fundamental cellular and signaling component of MCL-TME with viable and proliferative B and T cells.

Patient-derived MCL spheroids recapitulate MCL-LN signaling pathways

We next sought to determine if these MCL-PDLS engage a transcriptional program close to that of LN-resident MCL cells. Thus, we performed RNA-seq of purified B cells from unstimulated samples (MCL-PB) and compared with B cells isolated from the generated PDLS after 7 days of culture ($n=4$). Differential expression analysis of paired samples indicated that 4262 genes were upregulated and 3365 downregulated in the PDLS (Fig. 2A, B), highlighting a significant transcriptome modulation. We next proceeded to validate if MCL-PDLS recapitulate MCL-LN signaling pathways. A recent study from Saba [12] and cols established MCL-PB and MCL-LN compartment-specific signatures. Using these signatures, as well as BCR, NF- κ B and NIK pathway and proliferation signatures [12, 34], we demonstrated that the expression levels of the genes involved in those signatures (signature score) were significantly upregulated in the MCL-PDLS compared to original MCL-PB, while PB signature was downregulated. The leading-edge genes of these signatures are presented in a heatmap (Fig. 2C) and gene names are included in Table S2. Moreover, we confirmed by GSEA analysis that these pathways were significantly enriched in the PDLS while PB signature was enriched in MCL-PB samples (Fig. S2A).

BCR signature was also increased in 3 out of the 4 patients analyzed (Fig. S2B) but did not reach significance. Of note, the sample that behaves differently (MCL 10) belongs to a post-ibrutinib case at the time of relapse that may explain this outlier behavior. In fact, the down-regulation of BCR signaling after treatment with BTK inhibitors has been recently described in Richter transformation patients [35].

Furthermore, GSEA analysis using canonical pathways [36] uncovered that B cells from PDLS, compared to MCL-PB, exhibited an overrepresentation of relevant pathways in MCL pathogenesis including two fundamental blocks. The first one, composed of proliferation (E2F, MYC, KRAS), survival (NF- κ B, TNF), metabolic

pathways (OXPHOS, glucose and amino acid metabolism), “house-keeping” cellular processes (protein and RNA synthesis), DNA damage/repair, altogether reflecting the active state of these MCL tumors. The second block was composed of immune pathways including activation, antigen presentation together with cytokines and chemokines fundamental for a LN-like immune microenvironment (Figs. 2D and S2C and Tables S3 and S4).

Moreover, we confirmed that the optimized culture conditions for primary MCL cells in 3D (PDLS) were superior to a conventional 2D approach including the same cytokine cocktail and monocytes. In this regard, differential expression analysis of 3D (PDLS) vs. 2D (MCL-2D) approaches allowed the identification of 90 genes upregulated in the PDLS condition, while only 32 genes were increased in the 2D culture (Fig. 3A, B). Noteworthy, PDLS was superior than MCL-2D in recapitulating MCL hallmark pathways (BCR, NF- κ B, NIK and proliferation) (Fig. 3C). Moreover, GSEA highlighted additional pathways upregulated in PDLS compared to MCL-2D including angiogenesis, cell cycle, oncogene activation (KRAS and MYC), cell adhesion, stemness, post-translational modification (O-glycosylation) and extracellular matrix (ECM) involvement (Table S5 and Fig. 3D). The leading-edge genes of representative signatures from Fig. 3C are presented in heatmaps (Fig. 3E) and gene names are included in Table S6. In this regard, it is noteworthy the reorganization of the ECM that occurs in 3D including the upregulation of several collagens (*COL12A1*, *COL22A1*, *COL6A3* and *COL7A1*), the immunosuppressive tenascin (*TNC*) together with metalloproteinases (*MMP9*, *MMP16* and *MMP19*) (Table S6).

Altogether, these results support that MCL-PDLS represent a robust 3D model recapitulating fundamental biological pathways of MCL in secondary lymphoid organs such as the LN.

Patient-derived MCL spheroids exhibit a T-cell immune exhaustion profile reminiscent of MCL-LN

It has been described that MCL exhibits features of exhaustion, including high expression of PD-1 and TIGIT in both CD4 and CD8 T cells [22], as well as the presence of the corresponding ligands PD-L1, CD155 and CD112 in lymphoma cells and/or macrophages. By means of a bioinformatics analyses of public databases we compared the expression of a wide panel of immune checkpoints and its ligands in normal tonsils and in LN from MCL patients (MCL-LN), and we confirmed those published results and identified additional immune regulators overexpressed in MCL-LN. Among the receptor-ligand pairs analyzed, we highlight the increase in RNA levels of CD66a and TIM3, SIRP α , CD27, together with the already known PD-L1 and TIGIT (Fig. 4A). We next sought

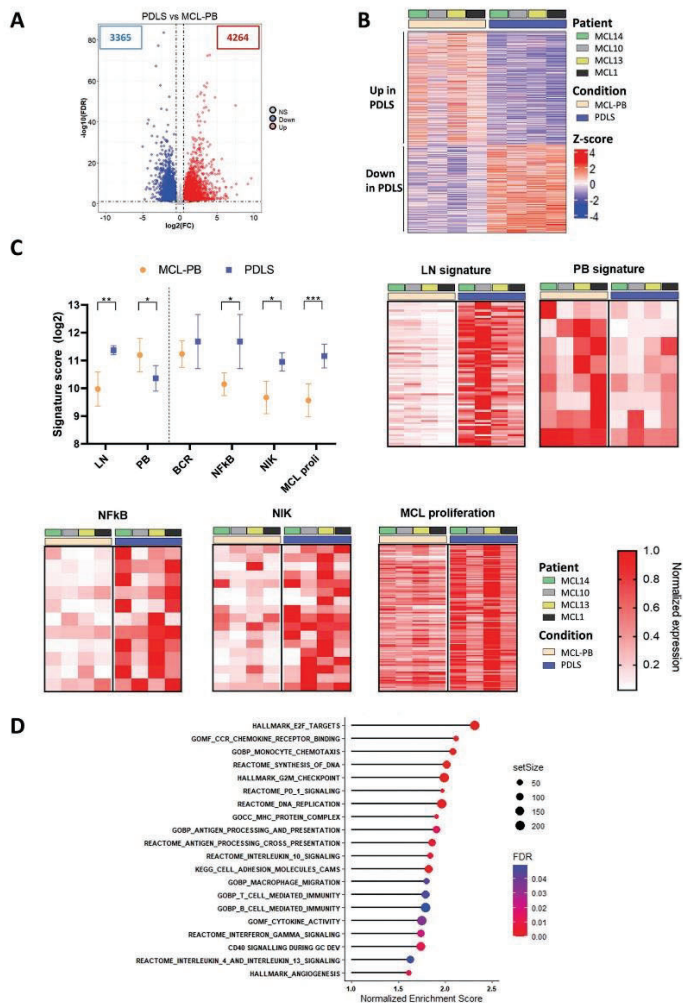


Fig. 2 MCL-PDLS transcriptome recapitulates lymph node hallmarks. **A** Volcano plot representing the differentially expressed genes (DEG) comparing PDLS after 7 days of culture with the original MCL peripheral blood (MCL-PB) sample. DEG were obtained by a paired ($n = 4$) DESeq2 analysis ($FDR < 0.1$ and absolute $\log_2FC > 0.5$). **B** Heatmap of DEG for the individual patients ($n = 4$). **C** Signature score of MCL hallmark pathways as described by Saba and Rosenwald [12, 34]. Values were calculated as the geometric mean of the normalized counts for the genes involved in each pathway. For each significantly upregulated gene set, the leading genes are represented in a heatmap. **D** Bubble plot representing the most significant and representative GSEA pathways upregulated in MCL-PDLS compared to MCL-PB.

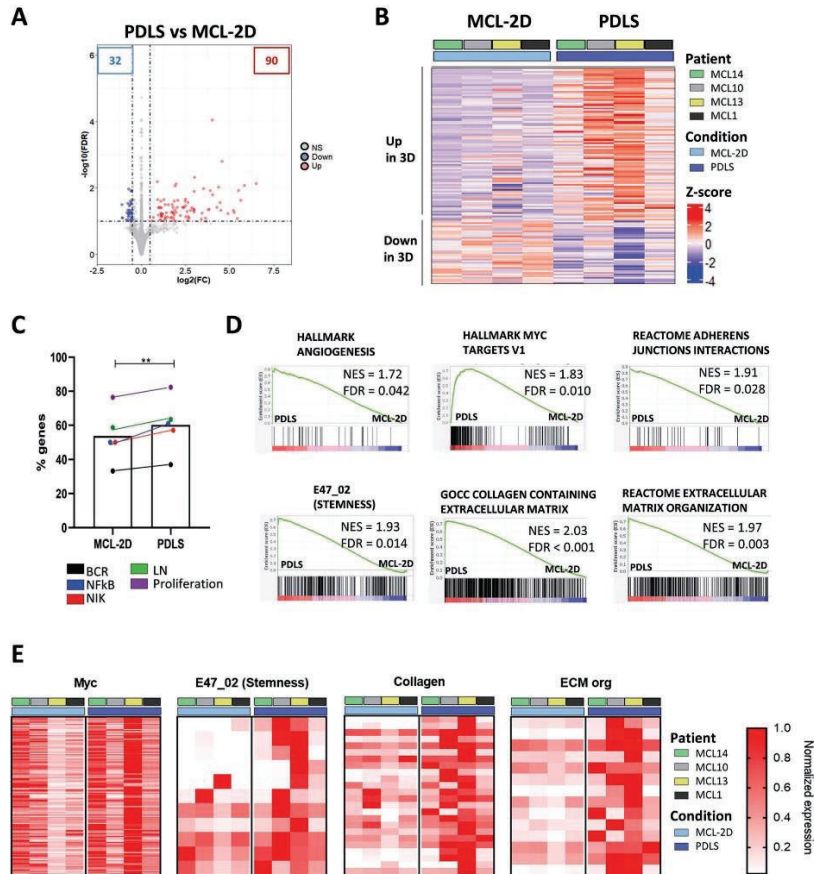


Fig. 3 PDLS transcriptome compared to MCL-2D. **A** Volcano plot representing the differentially expressed genes (DEG) between MCL-PDLS after 7 days of culture to 2D-MCL culture with monocytes and cytokines. DEG were obtained by a paired ($n = 4$) DESeq2 analysis (FDR < 0.1 and absolute $\log_2FC > 0.5$). **B** Heatmap of DEG for the individual patients ($n = 4$). **C** Percentage of genes described in each pathway (as in Fig. 2) [12, 34] which are upregulated in the PDLS or in MCL-2D. **D** GSEA plots representing significantly enriched pathways (FDR < 0.05) in the PDLS compared to 2D-MCL. **E** Heatmaps of leading genes of the indicated gene sets in (D).

to determine if MCL-PDLS recapitulate this immune exhaustion profile by flow cytometry analysis of these immune regulators and their ligands, including those whose expression levels were not significantly different between MCL and normal tonsils. We performed this analysis in the PB sample just after thawing (MCL-PB) and in PDLS after 3- and 7-days culture. Moreover, we added a control of PBMCs from healthy donors. Likewise, in the case of monocytes, we compared the immune regulators

expression before their inclusion in the PDLS, and after being in the PDLS for 3 or 7 days. We observed that MCL-PB profile is quite similar to PBMCs control for the expression of many immune regulators in CD4 or CD8 T cells and B cells. After the PDLS culture, there was an increase of most immune checkpoints and their ligands including: TIM-3 and TIGIT in both CD4 and CD8 cells, CD70 in CD8 and PD-1 in CD4. SIRPa, CD27 and CD47 expression was basically maintained. The increase of PD-L1, CD112 and

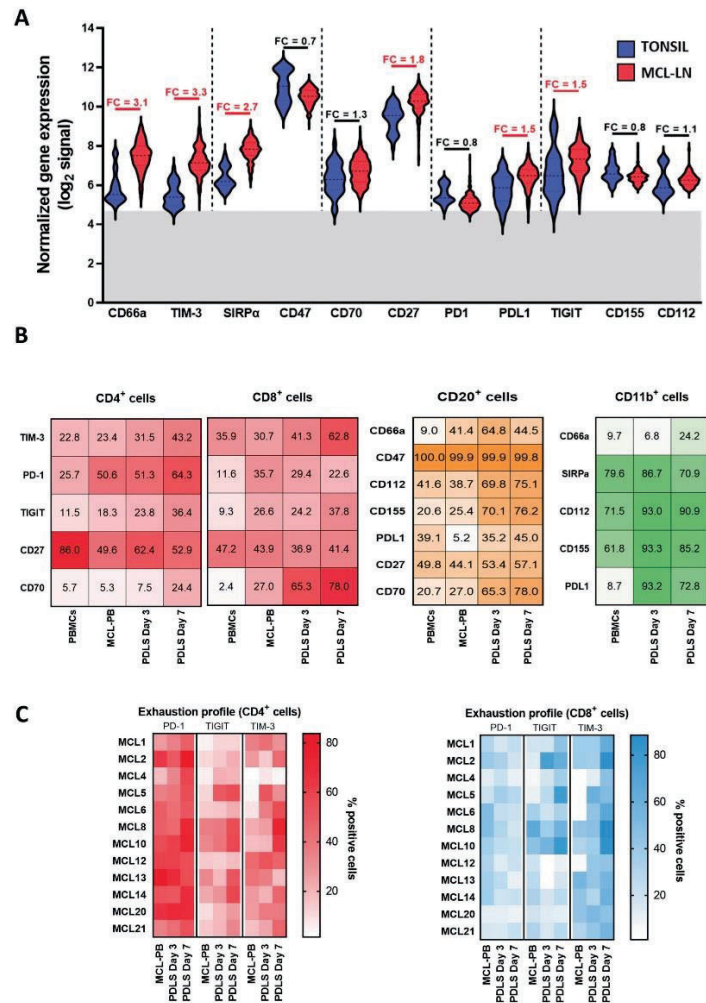


Fig. 4 Evolution of the immune profile in the MCL-PDLs. **A** Differential gene expression analysis from microarray data obtained from public repositories (detailed in Supplementary Methods) showed upregulation of several immune regulators in MCL-LN ($n = 199$) compared to a normal tonsil ($n = 30$). In red those comparatives that are statistically significant (p value < 0.001 and absolute $FC > 1.5$). **B** Percentage of positive cells assessed by flow cytometry for the immune regulators represented in **(A)** in B, T cells and monocytes. Data are represented as mean values after thawing (MCL-PB or monocytes) or in the PDL5 after 3 and 7 days of culture. PBMCs from healthy donors were included as reference. **C** Expression levels of immune exhaustion markers in CD4⁺ and CD8⁺ T cells in each individual patient in the same experimental conditions as in **(B)**. Data are represented as percentage of positive cells.

CD155 was also significant in both B (CD20+) cells and monocytes/macrophages (CD11b+) in the PDLs (Figs. 4B and 5B) compared to MCL-PB. As expected, the level of immune exhaustion generally increases with the days of culture. The heatmap in Fig. 4C illustrates this phenomenon for PD-1, TIM-3 and TIGIT and also shows the interpatient variability.

Overall, we can conclude that MCL-PDLs generated from PB recapitulate the immune exhaustion features of MCL-LN and may represent a good tool for immune-oncology studies.

Patient-derived MCL spheroids recapitulate in vivo response to ibrutinib treatment

BTK inhibitors as ibrutinib represent the standard of care to treat relapsed MCL, and is currently moving to frontline combined with standard first-line therapy (NCT02858258). Thus, we sought to determine if we could recapitulate clinical responses to ibrutinib in the MCL-PDLs system. First, we checked if the inhibitor was active in the PDLs. As shown in Fig. 5A, ibrutinib decreases tumor burden significantly, almost 50% on average albeit with inter-patient variability ($n = 17$). This depletion was associated in the sensitive cases with a decrease in tumor cell proliferation and viability induced by ibrutinib (Fig. 5A, C).

Then, we generated MCL-PDLs with samples from patients who received the drug at our institution and thus can be classified into responder patients (including partial response) and non-responder patients. After 3 days, MCL-PDLs were treated with ibrutinib or not (control condition) and cell count and viability were determined by flow cytometry. Noteworthy, MCL-PDLs reproduced with high degree of accuracy the in vivo response (Fig. 5A), and only the PDLs derived from ibrutinib-responder patients showed a decrease in their viability in B-cell fraction when adding ibrutinib (Fig. 5B).

Interestingly, one of the patients included in this study, MCL10, received ibrutinib as 2nd line treatment after relapsing from R-CHOP initial treatment. At first, MCL10 was responsive to ibrutinib achieving a partial response, followed by a new progression 9 months later. We were able to generate PDLs from MCL10 from the sensitive pre-ibrutinib sample and with the samples of the second relapse, post-ibrutinib, when the patient was longer responding to ibrutinib. PDLs recapitulate this in vivo scenario faithfully, as displayed in Fig. 5C. Ibrutinib induced more than 30% B-cell depletion in the PDLs from the first relapse that initially responded to ibrutinib, while no effect was seen when treating the PDLs from ibrutinib progression. Similar results were obtained when viability was assessed in these two PDLs (Fig. 5C).

These results support the PDLs model as a robust system to predict the response to BTK inhibitors.

Patient-derived MCL spheroids engage immune activation in response to immune checkpoint inhibitors

Ibrutinib is known to be an effective drug for MCL treatment, but most patients acquire resistance and eventually relapse. Therefore, effective therapeutic alternatives represent an unmet clinical need for MCL. In this scenario, the combination of ibrutinib with the anti-PD1 nivolumab has been studied in clinical trials [37] in several types of NHL but not in MCL, showing good results in CLL Richter transformation [38]. Thus, we analyzed the efficacy of this combination compared to ibrutinib in the PDLs system. As shown in Fig. 6A, B-cell depletion induced by the combination was slightly higher than ibrutinib monotherapy, but without reaching statistical significance. However, we noticed that those MCL cases with limited responses to ibrutinib (B-cell depletion below the mean (31.9%)), were those that benefit most from the combination, and B-cell depletion was significantly superior than ibrutinib alone (Fig. 6A, right).

Furthermore, in vivo non-responder patients to ibrutinib achieved a higher B-cell depletion with nivolumab combination,

while the in vivo responder patients did not benefit from nivolumab addition in vitro (Fig. 6B).

Next, we classified our patients according to TP53 status between wild-type and mutated (Table 1). Interestingly, addition of nivolumab only benefited those cases who did not have altered TP53, while patients who carried mutations or deletions showed a similar B-cell depletion (fold change = 1) when comparing the combination or ibrutinib as monotherapy (Fig. 55A).

Finally, we investigated whether addition of nivolumab activated the immune system toward an anti-tumoral response by analyzing the release of IFN γ and Granzyme B in the MCL-PDLs supernatants as a read-out of immune activation. Interestingly, the combination led to significant higher IFN γ concentrations in PDLs supernatants compared to ibrutinib alone, suggesting that the MCL-PDLs system may engage a Th1 anti-tumoral response (Fig. 6C). Granzyme B levels were also increased but without reaching statistical significance (Fig. 55B). However, when patients were classified into sensitive or refractory to the combination, according to the in vitro response (fold change depletion (ibru + nivo vs. ibru) > 1.2), we observed the increase of granzyme B levels in supernatants from sensitive PDLs, while not in those from refractory PDLs (Fig. 6D). Likewise, the percentage of CD8 T cells increased in PDLs sensitive to the combination (Fig. 55C).

Thus, we found evidence that a cytotoxic response (Granzyme B release) is activated by the addition of nivolumab to the PDLs system and it is associated to the efficacy of the combination.

DISCUSSION

B lymphoma mainly develop within LN as aggregates of tumor cells densely packed with their surrounding microenvironment, creating a tumor specific niche. In the precise case of LN-resident MCL cells, they rely mostly on BCR-mediated signaling and NF- κ B pathways and have therefore a clear role in proliferation of LN-MCL cells [12]. These signaling pathways are the results of MCL crosstalk with the TME in the LN, mainly T cells, macrophages and resident stromal cells as FDCs. In order to recapitulate these complex interactions in vitro, patient-derived 2D co-cultures supplemented with specific cytokines and growth factor cocktails have been established [17]. However, it is currently accepted that 3D models better represent cancer biology, signaling pathways [39, 40], and specially B and T-cell activation, as they are influenced by physical forces that are not recapitulated in 2D cultures [41]. Thus, in the era of precision medicine, it is mandatory to establish robust and reproducible patient-derived 3D systems. This is even more urgent in a rare and heterogeneous disease as MCL, where preclinical efficacy of novel agents and combinations will ease the design of clinical trials where patient recruitment is always challenging.

For all these reasons, we endeavored to set the first patient-derived MCL lymphoma 3D system as a real alternative to costly Patient-Derived Xenograft (PDX) model. MCL-PDX have been successfully established in this disease and have proven to be useful for antibody therapy [42–44]. However, they do not represent the best option for large screenings and do not recapitulate a human microenvironment, unless using humanized (hu-PDX) mice, which elevates the cost and complicates the design. Thus, one can envision PDX and hu-PDX as a last step of validation before clinical translation.

MCL-PDLs represents an affordable and robust system for a number of reasons:

First, both tumor B cells and autologous T cells maintain good viability and engage proliferation for at least 1-week, a window which allows to analyze the efficacy of most therapeutic agents. It is fundamental to consider the myeloid compartment as a part of the MCL niche, disease pathogenesis and a source of immunosuppressive signals [20, 21, 45]. As the percentage of autologous monocytes in the original PB sample was extremely low due to

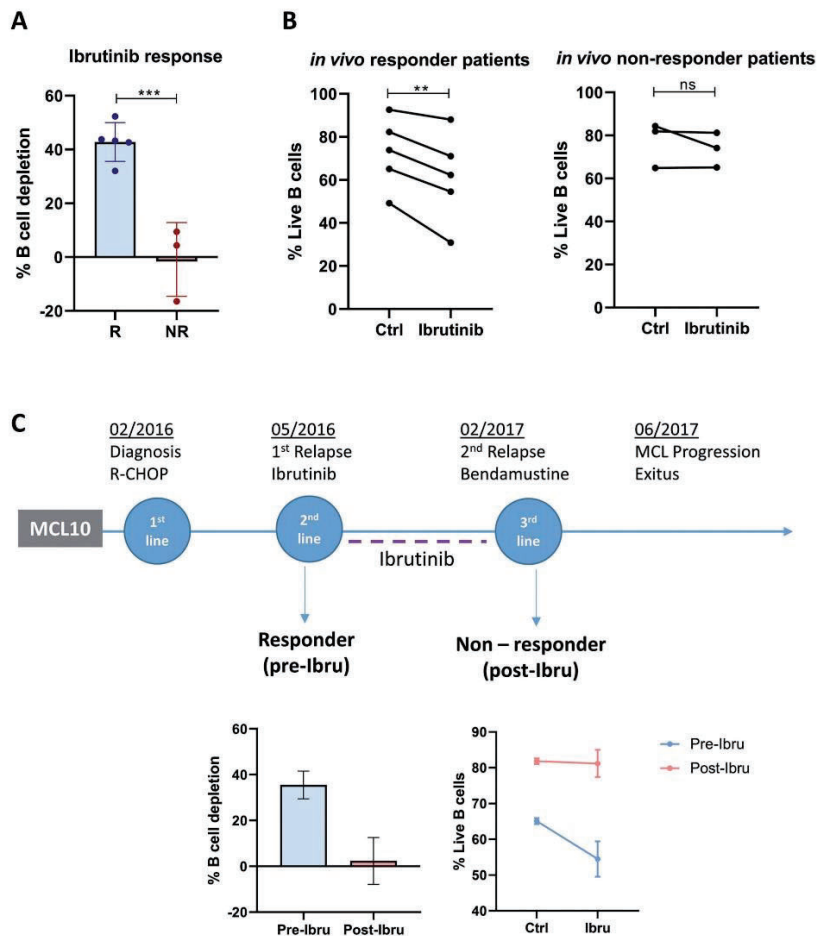


Fig. 5 MCL-PDLS reproduces in vivo response to ibrutinib. **A** Tumor B-cell depletion after 72 h of ibrutinib treatment compared to untreated condition in PDLS generated from MCL patients who in vivo responded to ibrutinib (R) or patients who did not respond to the drug (NR). **B** B-cell viability in untreated (Ctrl) or after in vitro ibrutinib treatment (72 h) in PDLS from in vivo responder or non-responder patients. **C** Clinical case of MCL10 including timeline with the different lines of treatment. Graphs showed B-cell depletion and viability of PDLS after 72 h of treatment with ibrutinib referred to untreated control.

tumor B-cell expansion [46], we decided to introduce monocytes from healthy donors in a ratio that reflects macrophage infiltration in MCL biopsies [31].

Second, in this study most of the samples were PBMCs from PB, both from cMCL ($n = 10$) and nnMCL ($n = 8$). PB samples represent

the most common and abundant material available as a high proportion of MCL patients present with leukemic disease [47]. Thanks to the optimized culture conditions, PDLS fairly recapitulate MCL-LN signature and fundamental hallmarks as NF- κ B, BCR and proliferation signature. This is of special interest considering the

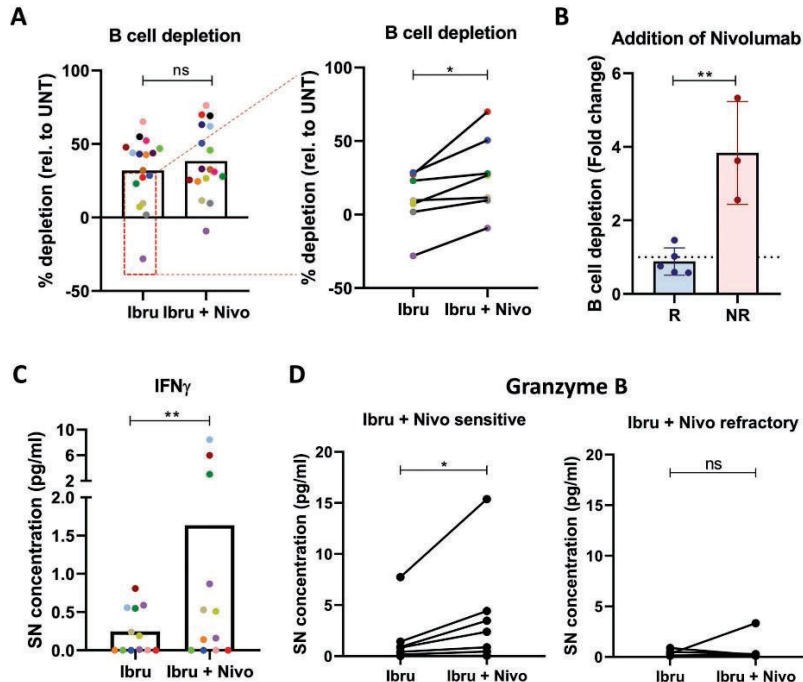


Fig. 6 Ibrutinib and nivolumab combination is effective in ibrutinib-resistant patients by activating the immune system. **A** B-cell depletion of ibrutinib and nivolumab combination (Ibru + Nivo) compared to ibrutinib monotherapy (Ibru) ($n = 17$), with a significant benefit in most resistant patients ($n = 7$). **B** Effect of adding nivolumab to ibrutinib treatment in in vivo responder (R) or non-responder (NR) patients, represented as the fold change of B-cell depletion induced by the combination compared to ibrutinib monotherapy. **C** Interferon gamma (IFN γ) concentration in PDLS supernatants comparing ibrutinib monotherapy or in combination with Nivolumab in MCL-PDLS. **D** Granzyme B secretion comparing ibrutinib monotherapy with ibrutinib and nivolumab combo, in sensitive or resistant patients to the combination. Cytometric Bead Array (CBA) analysis of cell culture supernatants was used in (C) and (D) ($n = 12$).

scarce availability of MCL-LN samples. Moreover, additional relevant pathways identified include metabolic pathways (OXPHOS [48], glucose and amino acids metabolism) and housekeeping processes (protein/RNA synthesis), reflecting that MCL-PDLS are a living and dynamic system. In addition, despite the absence of external additional of ECM in the system, we were able to demonstrate that the 3D conformation together with monocytes that differentiate into macrophages in the MCL-PDLS, favor the generation of ECM components including several types collagen (COL12A1, COL22A1, COL6A3 and COL7A1), the immunosuppressive tenascin (TNC) together with metalloproteinases (MMP9, MMP16 and MMP19), creating a more fibrotic TME typical of M2-like macrophages [49, 50].

Third, MCL-PDLS recapitulate the immune TME exhaustion features of MCL-LN [51] and may represent a good tool for immune-oncology studies. It is noteworthy the overrepresentation of gene sets related to immune pathways identified by RNA-seq (Tables S3 and S4). Thus, PDLS may be useful to test bi-specific antibodies and T-cell engagers due to the presence of autologous

T-cells. Moreover, this MCL-PDLS has the advantage of including myeloid immunosuppressive cells expressing key ICP ligands such as PDL1, CD66a, SIRP α and the TIGIT ligands CD112 and CD155.

Fourth, PDLS recapitulate in vivo responses to biological agents targeting tumor cells and TME such as ibrutinib, and represents a platform to study novel combination of BTK inhibitors. Ibrutinib is approved and very active in relapse/refractory (R/R) MCL [52], but most patients eventually develop resistance. Thus, second and third generation BTKi have been developed and will offer an advantage in certain settings [53]. Likewise, new combinatorial approaches have been investigated, including anti-CD20 mAb [54] and/or BH3 mimetics [55, 56]. In this context we propose the combination with the anti-PD1 mAb nivolumab specifically for those patients with limited ibrutinib responses. This has been analyzed in the phase I/IIa LYM1002 study (NCT02329847) for several relapsed/refractory B-cell malignancies. The best responses (>60%) were obtained for chronic lymphocytic leukemia (CLL) and Richter Syndrome [57], and current efforts are driven toward the

identification of potential biomarkers of response to identify beforehand those patients who will benefit from this combination [58]. Likewise, the preliminary efficacy of the anti-PD1 pembrolizumab in combination with ibrutinib is under investigation in a phase I/IIa trial (NCT03153202) in R/R CLL and R/R MCL. Thus, we envision our MCL-PDLS system as a complementary *in vitro* tool for phase I/2 trials to help identifying biomarkers of response and mechanisms of resistance.

In summary, MCL-PDLS represents a novel 3D model maintaining fundamental hallmarks of MCL-LN, that may serve as a platform to perform preclinical screening of novel targeted therapies, immunotherapies and cell therapies in a robust, 96-well format and affordable patient-derived 3D system. Future perspectives we are approaching to improve and complexify these systems include: the integration of ECM and relevant stromal cells (FDC), and the inclusion of these tumoroids in a microvascularized system.

DATA AVAILABILITY

RNA sequencing data generated and analyzed during the current study are available in the European Genome-phenome Archive (<http://ebi.ac.uk/ega/>) under accession number EGAS00001006964. The datasets generated and/or analyzed during the current study are available from the corresponding author on reasonable request.

REFERENCES

1. Fernández V, Salameo O, Espinet B, Solé F, Royo C, Navarro A, et al. Genomic and gene expression profiling defines indolent forms of mantle cell lymphoma. *Cancer Res*. 2010;70:1408–18.
2. Navarro A, Clot G, Royo C, Jares P, Hadzidimitriou A, Agathangelidis A, et al. Molecular subsets of mantle cell lymphoma defined by the IGHV mutational status and SOX11 expression have distinct biologic and clinical features. *Cancer Res*. 2012;72:5307–16.
3. Royo C, Navarro A, Clot G, Salaverria I, Giné E, Jares P, et al. Non-nodal type of mantle cell lymphoma is a specific biological and clinical subgroup of the disease. *Leukemia*. 2012;26:1895–8.
4. Nadeu F, Martín-García D, Clot G, Díaz-Navarro A, Duran-Ferrer M, Navarro A, et al. Genomic and epigenomic insights into the origin, pathogenesis, and clinical behavior of mantle cell lymphoma subtypes. *Blood*. 2020;136:1419–32.
5. Beà S, Valdés-Mas R, Navarro A, Salaverria I, Martín-García D, Jares P, et al. Landscape of somatic mutations and clonal evolution in mantle cell lymphoma. *Proc Natl Acad Sci USA*. 2013;110:18250–5.
6. Yi S, Yan Y, Jin M, Bhattacharya S, Wang Y, Wu Y, et al. Genomic and transcriptomic profiling reveals distinct molecular subsets associated with outcomes in mantle cell lymphoma. *J Clin Invest*. 2022;132:e153283.
7. Ferrero S, Rossi D, Rinaldi A, Bruscazzini A, Spina V, Eskeland CW, et al. KMT2D mutations and TP53 disruptions are poor prognostic biomarkers in mantle cell lymphoma receiving high-dose therapy: a FFL study. *Haematologica*. 2020;105:1604–12.
8. Jares P, Colomer D, Campo E. Molecular pathogenesis of mantle cell lymphoma. *J Clin Invest*. 2012;122:3416–23.
9. Pérez-Galán P, Dreyling M, Wiestner A. Mantle cell lymphoma: biology, pathogenesis, and the molecular basis of treatment in the genomic era. *Blood*. 2011;117:26–38.
10. Puente XS, Jares P, Campo E. Chronic lymphocytic leukemia and mantle cell lymphoma: crossroads of genetic and microenvironment interactions. *Blood*. 2018;131:2283–96.
11. Burger JA, Ford RJ. The microenvironment in mantle cell lymphoma: cellular and molecular pathways and emerging targeted therapies. *Semin Cancer Biol*. 2011;21:308–12.
12. Saba NS, Liu D, Herman SEM, Underbayev C, Tian X, Behrend D, et al. Pathogenic role of B-cell receptor signaling and canonical NF- κ B activation in mantle cell lymphoma. *Blood*. 2016;128:82–92.
13. Castillo R, Mascarenhas J, Telford W, Chadburn A, Friedman SM, Schattner EJ. Proliferative response of mantle cell lymphoma cells stimulated by CD40 ligation and IL-4. *Leukemia*. 2000;14:292–8.
14. Schrader C, Meusers P, Brittinger G, Janssen D, Teymourtash A, Siebmann JU, et al. Growth pattern and distribution of follicular dendritic cells in mantle cell lymphoma: a clinicopathological study of 96 patients. *Virchows Arch: Int J Pathol*. 2006;448:151–9.
15. Lwin T, Lin J, Choi YS, Zhang X, Moscinski LC, Wright KL, et al. Follicular dendritic cell-dependent drug resistance of non-Hodgkin lymphoma involves cell adhesion-mediated Bim down-regulation through induction of microRNA-181a. *Blood*. 2010;116:5228–36.

16. Medina DJ, Goodell L, Glod J, Gélinas C, Rabson AB, Strair RK. Mesenchymal stromal cells protect mantle cell lymphoma cells from spontaneous and drug-induced apoptosis through secretion of B-cell activating factor and activation of the canonical and non-canonical nuclear factor κ B pathways. *Haematologica*. 2012;97:1255–63.
17. Chiron D, Bellanger C, Papin A, Tessoulin B, Dousset C, Maiga S, et al. Rational targeted therapies to overcome microenvironment-dependent expansion of mantle cell lymphoma. *Blood*. 2016;128:2808–18.
18. Kurtova AV, Tamayo AT, Ford RJ, Burger JA. Mantle cell lymphoma cells express high levels of CXCR4, CXCR5, and VLA-4 (CD49d): importance for interactions with the stromal microenvironment and specific targeting. *Blood*. 2009;113:4604–13.
19. Pham LV, Pogue E, Ford RJ. The role of macrophage/B-cell interactions in the pathophysiology of B-cell lymphomas. *Front Oncol*. 2018;8:147.
20. Papin A, Tessoulin B, Bellanger C, Moreau A, Bris YL, Maisonneuve H, et al. CSF1R and BTK inhibitors as novel strategies to disrupt the dialog between mantle cell lymphoma and macrophages. *Leukemia*. 2019;33:2442–53.
21. Le K, Sun J, Khawaja H, Shibata M, Maggiorari SB, Smith MR, et al. Mantle cell lymphoma polarizes tumor-associated macrophages into M2-like macrophages, which in turn promote tumorigenesis. *Blood Adv*. 2021;5:2863–78.
22. Josefsson SE, Belske K, Blaker YN, Forsund MS, Holte H, Stenstad B, et al. TIGIT and PD-1 mark intratumoral T cells with reduced effector function in B-cell non-Hodgkin lymphoma. *Cancer Immunol Res*. 2019;7:355–62.
23. Vidal-Crespo A, Rodríguez V, Matas-Céspedes A, Lee E, Rivas-Delgado A, Giné E, et al. The Bruton tyrosine kinase inhibitor CC-292 shows activity in mantle cell lymphoma and synergizes with lenalidomide and NIK inhibitors depending on nuclear factor- κ B mutational status. *Haematologica*. 2017;102:e447–51.
24. Valero JG, Matas-Céspedes A, Arenas F, Rodríguez V, Carreras J, Serrat N, et al. The receptor of the colony-stimulating factor-1 (CSF-1R) is a novel prognostic factor and therapeutic target in follicular lymphoma. *Leukemia*. 2021;35:2635–49.
25. Serrat N, Guerrero-Hernández M, Matas-Céspedes A, Yahiaoui A, Valero JG, Nadeu F, et al. PI3K δ inhibition reshapes follicular lymphoma-immune microenvironment cross talk and unleashes the activity of venetoclax. *Blood Adv*. 2020;4:4217–31.
26. Schutgens F, Clevers H. Human organoids: tools for understanding biology and treating diseases. *Annu Rev Pathol*. 2020;15:211–34.
27. Lamaison C, Latour S, Hélène N, Le Morvan V, Saint-Vanne J, Mahouche I, et al. A novel 3D culture model recapitulates primary FL B-cell features and promotes their survival. *Blood Adv*. 2021;5:5372–86.
28. Maura R, Francesco A, Simona R, Elena S, Claudio A. Three-dimensional models: a novel approach for lymphoma research. *J Cancer Res Clin Oncol*. 2022;148:753–65.
29. Mongini PKA, Gupta R, Boyle E, Nieto J, Lee H, Stein J, et al. TLR-9 and IL-15 synergy promotes the *in vitro* clonal expansion of chronic lymphocytic leukemia B cells. *J Immunol*. 2015;195:901–23.
30. Papin A, Le Gouill S, Chiron D. Rationale for targeting tumor cells in their microenvironment for mantle cell lymphoma treatment. *Leuk Lymphoma*. 2018;59:1064–72.
31. Koh YW, Shin SJ, Park C, Yoon DH, Suh C, Huh J. Absolute monocyte count predicts overall survival in mantle cell lymphomas: correlation with tumour-associated macrophages. *Hematol Oncol*. 2014;32:178–86.
32. Martinez FO, Gordon S, Locati M, Mantovani A. Transcriptional profiling of the human monocyte-to-macrophage differentiation and polarization: new molecules and patterns of gene expression. *J Immunol*. 2006;177:7303–11.
33. Jaguin M, Houlbert N, Fardel O, Lecœur V. Polarization profiles of human M-CSF-generated macrophages and comparison of M1-markers in classically activated macrophages from GM-CSF and M-CSF origin. *Cell Immunol*. 2013;281:51–61.
34. Rosenwald A, Wright G, Wiestner A, Chan WC, Connors JM, Campo E, et al. The proliferation gene expression signature is a quantitative integrator of oncogenic events that predicts survival in mantle cell lymphoma. *Cancer Cell*. 2003;3:185–97.
35. Nadeu F, Royo R, Massoni-Badosa R, Playa-Albinyana H, García-Torre B, Duran-Ferrer M, et al. Detection of early seeding of Richter transformation in chronic lymphocytic leukemia. *Nat Med*. 2022;28:1662–71.
36. Überzon A, Subramanian A, Pinchback R, Thorvaldsdóttir H, Tamayo P, Mesirov JP. Molecular signatures database (MSigDB) 3.0. *Bioinformatics*. 2011;27:1739–40.
37. Lesokhin AM, Ansell SM, Armand P, Scott EC, Halwani A, Gutierrez M, et al. Nivolumab in patients with relapsed or refractory hematologic malignancy: preliminary results of a phase Ib study. *J Clin Oncol*. 2016;34:2698–704.
38. Jain N, Senapati J, Thakral B, Ferrajoli A, Thompson PA, Burger JA, et al. A phase 2 study of nivolumab combined with ibrutinib in patients with diffuse large B-cell Richter transformation of CLL. *Blood Adv*. 2022;bloodadvances.2022008790.
39. Decaup E, Jean C, Laurent C, Gravelle P, Fruchon S, Capilla F, et al. Anti-tumor activity of obinutuzumab and rituximab in a follicular lymphoma 3D model. *Blood Cancer J*. 2013;3:e131.

40. Riedl A, Schiederer M, Pudelko K, Stadler M, Walter S, Unterleuthner D, et al. Comparison of cancer cells in 2D vs 3D culture reveals differences in AKT-mTOR-S6K signaling and drug responses. *J Cell Sci.* 2017;130:203–18.
41. Apoorva F, Loiben AM, Shah SB, Purwada A, Fontan L, Goldstein R, et al. How biophysical forces regulate human B cell lymphomas. *Cell Rep.* 2018;23:499–511.
42. Zhang L, Nornie K, Zhang H, Bell T, Pham L, Kadri S, et al. B-cell lymphoma patient-derived xenograft models enable drug discovery and are a platform for personalized therapy. *Clin Cancer Res.* 2017;23:4212–23.
43. Jiang VC, Liu Y, Jordan A, McIntosh J, Li Y, Che Y, et al. The antibody drug conjugate VLS-101 targeting ROR1 is effective in CAR T-resistant mantle cell lymphoma. *J Hematol Oncol.* 2021;14:132.
44. Jiang VC, Liu Y, Jordan A, Leeming A, McIntosh J, Huang S, et al. Targeting FcγRIIB by antagonistic antibody B1-206 improves the efficacy of rituximab-based therapies in aggressive mantle cell lymphoma. *J Hematol Oncol.* 2022;15:42.
45. Saleh K, Cheminant M, Chiron D, Burroni B, Ribrag V, Sarkozy C. Tumor micro-environment and immunotherapy-based approaches in mantle cell lymphoma. *Cancers.* 2022;14:1–21.
46. Aprile von Hohenstaufen K, Conconi A, de Campos CP, Franceschetti S, Bertoni F, Margiotta Casaluci G, et al. Prognostic impact of monocyte count at presentation in mantle cell lymphoma. *Br J Haematol.* 2013;162:465–73.
47. Cohen PL, Kurtin PJ, Donovan KA, Hanson CA. Bone marrow and peripheral blood involvement in mantle cell lymphoma. *Br J Haematol.* 1998;101:302–10.
48. Fuhr V, Heidenreich S, Srivastava M, Riedel A, Düll J, Gerhard-Hartmann E, et al. CD52 and OXPHOS-potential targets in ibritinib-treated mantle cell lymphoma. *Cell Death Discov.* 2022;8:505.
49. Schnoor M, Cullen P, Lorkowski J, Stolle K, Robenek H, Troyer D, et al. Production of type VI collagen by human macrophages: a new dimension in macrophage functional heterogeneity. *J Immunol.* 2008;180:5707–19.
50. Sica A, Mantovani A. Macrophage plasticity and polarization: in vivo veritas. *J Clin Invest.* 2012;122:787–95.
51. Laurent C, Charmpi K, Gravelle P, Tosolini M, Franchet C, Ysebaert L, et al. Several immune escape patterns in non-Hodgkin's lymphomas. *Oncimmunology.* 2015;4:0–14.
52. Wang ML, Rule S, Martin P, Goy A, Auer R, Kahl BS, et al. Targeting BTK with ibrutinib in relapsed or refractory mantle-cell lymphoma. *N Engl J Med.* 2013;369:507–16.
53. Nakhoda S, Vistapop A, Wang YL. Resistance to Bruton tyrosine kinase inhibition in chronic lymphocytic leukaemia and non-Hodgkin lymphoma. *Br J Haematol.* 2023;200:137–49.
54. Giné E, de la Cruz F, Jiménez Ubieta A, López Jimenez J, Martín García-Sancho A, Terol MJ, et al. Ibrutinib in combination with rituximab for indolent clinical forms of mantle cell lymphoma (IMCL-2015): a multicenter, open-label, single-arm, phase II trial. *J Clin Oncol.* 2022;40:1196–205.
55. Le Gouill S, Morschhauser F, Chiron D, Bouabdallah K, Cartron G, Casasnovas O, et al. Ibrutinib, obinutuzumab, and venetoclax in relapsed and untreated patients with mantle cell lymphoma: a phase 1/2 trial. *Blood.* 2021;137:877–87.
56. Tam CS, Anderson MA, Pott C, Agarwal R, Handunnetti S, Hicks RJ, et al. Ibrutinib plus venetoclax for the treatment of mantle-cell lymphoma. *N Engl J Med.* 2018;378:1211–23.
57. Younes A, Brody J, Carpio C, Lopez-Guillermo A, Ben-Yehuda D, Ferhanoglu B, et al. Safety and activity of ibrutinib in combination with nivolumab in patients with relapsed non-Hodgkin lymphoma or chronic lymphocytic leukaemia: a phase 1/2a study. *Lancet Haematol.* 2019;6:e67–78.
58. Hodgkinson BP, Schaffer M, Brody JD, Jurczak W, Carpio C, Ben-Yehuda D, et al. Biomarkers of response to ibrutinib plus nivolumab in relapsed diffuse large B-cell lymphoma, follicular lymphoma, or Richter's transformation. *Transl Oncol.* 2021;14:100977.
59. Nadeu F, Mas-de-Les-Valls R, Navarro A, Royo R, Martín S, Villamor N, et al. IgGallier for reconstructing immunoglobulin gene rearrangements and oncogenic translocations from whole-genome sequencing in lymphoid neoplasms. *Nat Commun.* 2020;11:3390.

ACKNOWLEDGEMENTS

We thank Ariadna Giró and Fabian Arenas for their technical assistance, the IDIBAPS genomics facility for gene expression data generation and the IDIBAPS Flow

Cytometry and Cell Sorting Core facility. We are indebted to the HCB-IDIBAPS Biobank, integrated in the Spanish National Biobanks Network, for the biological human samples and data procurement. This work was carried out at the Esther Koplowitz Center, Barcelona. Grants that contributed to this work included: this work was part of an Interreg POCTEFA program (IMLINFO EFA281/16). Spanish Ministry of Economy and Competitiveness & European Regional Development Fund (ERDF) "Una manera de hacer Europa" for SAF2017/88275R to PP-G. CD-L was supported by a personal FPI fellowship from the Ministry of Economy and competitiveness (PRE2018-083797) associated to the project SAF2017-88275-R. Additional grants are: CIBERONC (CB16/12/00334 to DC and CB16/12/00225 to EC), and finally Generalitat de Catalunya support for AGAUR 2017SGR1009 to DC. PP-G and CB belong to the imCORE network on behalf of F. Hoffmann-La Roche (TALYIES, R21080BB).

AUTHOR CONTRIBUTIONS

FA-A conducted molecular and cellular assays, performed data analysis, contributed to study design and wrote the manuscript. CD-L conducted molecular and cellular assays, performed data analysis and contributed to study design and manuscript writing. JGV conducted cellular assays, performed metadata analysis, contributed to study design and critical manuscript revision. FN performed RNA-seq analysis and critical manuscript revision. FG and CF contributed to result discussions, protocol optimization, PDLS imaging and critical manuscript revision. MN, RM, PBL and J-ML were in charge of PDLS imaging by SPIM and mathematical 3D reconstructions. NS, HP-A and RG contributed to result discussions and protocol optimization. EG provided patient clinical data and critical manuscript revision. AL-G provided economic support and clinical data. EC participated in critical revision of the manuscript. DC provided economic support, results discussion, study guidance and critical manuscript revision. CB contributed to result discussion, protocol sharing and critical manuscript revision. PP-G lead the study, provided economic support and wrote the manuscript. All authors have read and approved the manuscript.

COMPETING INTERESTS

MN, RM, PBL and J-ML are employees of Imactiv3D. The rest of the authors declare no conflict of interest.


ADDITIONAL INFORMATION

Supplementary information The online version contains supplementary material available at <https://doi.org/10.1038/s41375-023-01885-1>.

Correspondence and requests for materials should be addressed to Patricia Pérez-Galán.

Reprints and permission information is available at <http://www.nature.com/reprints>.

Publisher's note Springer Nature remains neutral with regard to jurisdictional claims in published maps and institutional affiliations.

 **Open Access** This article is licensed under a Creative Commons Attribution 4.0 International License, which permits use, sharing, adaptation, distribution and reproduction in any medium or format, as long as you give appropriate credit to the original author(s) and the source, provide a link to the Creative Commons license, and indicate if changes were made. The images or other third party material in this article are included in the article's Creative Commons license, unless indicated otherwise in a credit line to the material. If material is not included in the article's Creative Commons license and your intended use is not permitted by statutory regulation or exceeds the permitted use, you will need to obtain permission directly from the copyright holder. To view a copy of this license, visit <http://creativecommons.org/licenses/by/4.0/>.

© The Author(s) 2023

STUDY 2. Patient-Derived Follicular Lymphoma Spheroids recapitulate lymph node signaling and immune profile uncovering galectin-9 as a novel immunotherapeutic target

Dobaño-López C*, Valero JG*, **Araujo-Ayala F**, Nadeu F, Gava F, Faria C, Norlund M, Morin R, Bernes-Lasserre P, Arenas F, Grau M, López C, López-Oreja I, Serrat N, Martínez-Farran A, Hernández L, Playa-Albinyana H, Giménez R, Beà S, Campo E, Lagarde JM, López-Guillermo A, Magnano L, Colomer D, Bezombes C, Pérez-Galán P. Patient-derived follicular lymphoma spheroids recapitulate lymph node signaling and immune profile uncovering galectin-9 as a novel immunotherapeutic target. *Blood Cancer J.* 2024 May 2;14(1):75. doi: 10.1038/s41408-024-01041-7. PMID: 38697976.

*These authors contributed equally to this work

ARTICLE OPEN



Patient-derived follicular lymphoma spheroids recapitulate lymph node signaling and immune profile uncovering galectin-9 as a novel immunotherapeutic target

Cèlia Dobaño-López^{1,2,8}, Juan García Valero^{1,2,8}, Ferran Araujo-Ayala^{1,2}, Ferran Nadeu^{1,2}, Fabien Gava³, Carla Faria³, Marine Norlund⁴, Renaud Morin⁴, Pascale Bernes-Lasserre⁴, Fabian Arenas^{1,2}, Marta Grau¹, Cristina López^{1,2,5}, Irene López-Oreja^{1,2,6}, Neus Serrat¹, Ares Martínez-Farran¹, Lluís Hernández^{1,2}, Heribert Playa-Albinyana^{1,2}, Rubén Giménez^{1,2}, Sílvia Bea^{1,2,5,6}, Elías Campo^{1,2,5,6}, Jean-Michel Lagarde⁴, Armando López-Guillermo^{1,2,5,7}, Laura Magnano^{1,4,5,7}, Dolors Colomer^{1,2,5,6}, Christine Bezombes^{1,2} and Patricia Pérez-Galán^{1,2,8}

© The Author(s) 2024

Follicular lymphoma (FL), the most common indolent non-Hodgkin lymphoma, constitutes a paradigm of immune tumor microenvironment (TME) contribution to disease onset, progression, and heterogenous clinical outcome. Here we present the first FL-Patient Derived Lymphoma Spheroid (FL-PDLS), including fundamental immune actors and features of TME in FL lymph nodes (LNs). FL-PDLS is organized in disc-shaped 3D structures composed of proliferating B and T cells, together with macrophages with an intermediate M1/M2 phenotype. FL-PDLS recapitulates the most relevant B-cell transcriptional pathways present in FL-LN (proliferation, epigenetic regulation, mTOR, adaptive immune system, among others). The T cell compartment in the FL-PDLS preserves CD4 subsets (follicular helper, regulatory, and follicular regulatory), also encompassing the spectrum of activation/exhaustion phenotypes in CD4 and CD8 populations. Moreover, this system is suitable for chemo and immunotherapy testing, recapitulating results obtained in the clinic. FL-PDLS allowed uncovering that soluble galectin-9 limits rituximab, rituximab, plus nivolumab/TIM-3 antitumoral activities. Blocking galectin-9 improves rituximab efficacy, highlighting galectin-9 as a novel immunotherapeutic target in FL. In conclusion, FL-PDLS maintains the crosstalk between malignant B cells and the immune LN-TME and constitutes a robust and multiplexed pre-clinical tool to perform drug screening in a patient-derived system, advancing toward personalized therapeutic approaches.

Blood Cancer Journal (2024) 14:75; <https://doi.org/10.1038/s41408-024-01041-7>

INTRODUCTION

Follicular Lymphoma (FL) is the most common indolent non-Hodgkin's lymphoma (NHL) and is considered a chronic and incurable disease [1]. Despite the high response rates to R-CHOP induction therapy, relapses are a frequent event. The risk of histologic transformation to diffuse large B cell lymphoma (DLBCL) increases over time (2–3% per year) [2], and confers a dismal prognosis [3]. FL arises from the malignant transformation of germinal center (GC) B cells that most frequently (~85%) acquire the t(14;18)(q32;q21) translocation, leading to BCL2 overexpression [4]. In addition, genetic alterations in histone-modifying enzymes are recognized as a central hallmark of FL, being *KMT2D*, *CREBBP*, and *EZH2* [5] the most frequently mutated genes, together with other relevant lesions participating in pathogenic processes (i.e., *MEF2B*, *HVEM*, and *RRAGC*) [6–8]. Moreover, these alterations induce a reshaping in the immune tumor microenvironment (TME), favoring the generation of this disease and its progression [9, 10].

FL represents a paradigm of dependence on the TME [11–13], and current stratification scores include both genetic alterations and immune signatures [14–16]. This TME is composed of an intricate network of cytokines and immune modulators expressed by non-malignant cells present in the normal GC structures of lymph nodes (LN). The main players that support FL cells and maintain the GC structure are CD4⁺ T follicular helpers (T_{FH}) and follicular dendritic cells (FDC), which by means of CD40L, IL-4, and IL-21 cytokine signaling, contribute to tumor survival and proliferation [17–19]. Moreover, FL cells are involved in the recruitment of CD4⁺ T regulatory cells (T_{REG}), in charge of inhibiting anti-tumor immune responses, hampering CD8⁺ granzyme B and perforin release [20]. In addition, these CD8⁺ exhibit an exhaustion profile with high levels of PD-1 and TIM-3 [21]. Nevertheless, the myeloid compartment trans-presents IL-15 which will stimulate NK and CD8⁺ cell activity. Likewise, TAMs encompass several subpopulations with opposing roles in the

¹Fundació de Recerca Clínic Barcelona - Institut d'Investigacions Biomèdiques August Pi i Sunyer, Barcelona, Spain. ²Centro de Investigación Biomédica en Red-Oncología (CIBERONC), Madrid, Spain. ³Université de Toulouse, INSERM, CNRS, Université de Toulouse III-Paul Sabatier, Centre de Recherches en Cancérologie de Toulouse, Toulouse, France. ⁴IMACTIV-3D, Toulouse, France. ⁵University of Barcelona, Medical School, Barcelona, Spain. ⁶Secció Hematopatologia, Servei d'Anatomia Patològica, Hospital Clínic, Barcelona, Spain. ⁷Servei Hematologia, Hospital Clínic, Barcelona, Spain. ⁸These authors contributed equally: Cèlia Dobaño-López, Juan García Valero. ^{*}email: christine.bezombes@inserm.fr; pperez@reerca.clinic.cat

Received: 20 September 2023 Revised: 13 March 2024 Accepted: 20 March 2024
Published online: 02 May 2024

2

TME. Therefore, conflicting prognosis values were obtained using the classical TAM marker CD163 [22]. In this regard, we have demonstrated that the percentage of CSF-1R⁺ macrophages (Mφ) correlates with FL grade and risk of transformation to an aggressive lymphoma [23].

In order to study this complex and heterogeneous network, patient-derived systems that recapitulate microenvironment cues are mandatory. FL cell lines are not representative of FL pathology or its heterogeneity, and patient-derived xenograft (PDX) models fail to recapitulate the human microenvironment. In the last years, there has been an evolution toward patient-derived 3D cultures and organoids in many solid tumors [24], yet lymphomas are scarce [25, 26] and with limited TME [27]. Therefore, there is a need to establish an amenable system recapitulating the main pathogenic pathways delivered to the tumor B-cell in the LN, together with the immune activation/suppression status of T cells and the myeloid compartment. This system would be instrumental in the context of precision medicine. In the same line, we have recently developed a mantle cell lymphoma (MCL) patient-derived 3D model co-culturing MCL primary cells with autologous T cells and monocytes from healthy donors [28].

Here we present the first patient-derived lymphoma spheroids (PDLs) from FL samples (FL-PDLs) that recapitulate the signaling cues of the tumor niche in the GC together with monocytes and autologous T cells, building a system for immunotherapies and cell therapies intervention. In this context, we have uncovered a role for galectin-9 in T-cell responses that may deserve attention in FL immunotherapeutic approaches.

METHODS

FL-PDLs generation

FL samples from LN or peripheral blood (PB) ($n=20$) (Table 1) were thawed in sterile conditions, resuspended in enriched medium [29] (RPMI Glutamax (Gibco, Thermo Fisher Scientific, Waltham, MA, USA); 15% FBS (Gibco, Thermo Fisher Scientific); 1% ITS (Sigma-Aldrich, St. Louis, MO, USA); 1% HEPES (Sigma-Aldrich); 1% Pyruvate (Gibco, Thermo Fisher Scientific); 1% Non-Essential AA (Gibco, Thermo Fisher Scientific); 0.1% 2β-mercaptoethanol (Sigma-Aldrich); 0.5% Gentamicin (Sigma-Aldrich)), and counted using Neubauer chamber system with trypan blue to assess initial cell viability. To assess proliferation, cells were labeled with 0.5 μM carboxyfluorescein succinimidyl ester (CFSE) cell tracker (Thermo Fisher Scientific) following the manufacturer's instructions. CFSE-labeled FL samples were then mixed with monocytes (isolation described in supplemental methods) at 4:1 ratio (FL:monocytes), seeding 50,000 cells/well and 12,500 monocytes/well in a final volume of 200 μL/well in Nunclon™ Sphera™ 96-wells Ultra-Low Attachment (ULA) microplates (Thermo Fisher Scientific) in the enriched medium mentioned above, supplemented with the following cytokines (PDLs medium): 50 ng/mL CD40L-HA tagged (R&D Systems, Minneapolis, MN, USA), 1 μg/mL anti-HA-Tag antibody (R&D Systems), 100 ng/mL IL-21 (Peprotech, Cranbury, NJ, USA), 10 ng/mL IL-4 (Peprotech) and 50 ng/mL IL-15 (R&D Systems). PDLs were maintained at 37 °C 5% CO₂ for up to 10 days. The workflow for FL-PDLs generation is detailed in Fig. 1A.

Drug assays and activation analysis

Six FL-PDLs replicates per experimental condition were cultured in 150 μL/well of PDLs medium + Mn and treated after 72 h (day 3) with 50 μL/well containing the drugs diluted in PDLs medium. The following antibodies and doses were used: 3.75 μg/mL rituximab (provided by Hospital Clinic pharmacy), 10 μg/mL anti-ICOS, 5 μg/mL anti-TIM-3, 2 μg/mL anti-LAG-3, and 10 μg/mL anti-TIGIT, all functional grade antibodies from Thermo Fisher Scientific, 10 μg/mL nivolumab (Selleck Chemicals LLC, Houston, TX, USA) and 2.5 μg/mL anti-galectin9 (Biologend, San Diego, CA, USA). CHOP components, provided by the Hospital Clinic pharmacy, were used at the following concentrations: cyclophosphamide (0.1 μg/mL), doxorubicin hydrochloride (0.5 μg/mL), vincristine sulfate (0.014 μg/mL) and prednisone (1 μg/mL). After 72 h of treatment (day 6), PDLs were mechanically disaggregated to analyze cell viability (LIVE/DEAD Fixable Aqua, Thermo

Table 1. FL patient characteristics.

Study label	Sex/age	Sample type	Disease status	Histological Grade	Stage	FLIP ¹	Treatments ^a	Response to 1st tt ^b	POD24 ^c	Cell count Lympho B (10 ³)	% Lympho B	Code
FL1	F/75	PB	D	2	IVA	H	R-COP/R-mnt	PR	N	76.46	78	●
FL2	F/52	LN	D	1	IV	H	R-CHOP/R-mnt R-ESHAP ASCT R-GENOX Ifosfamide Rx	CR	N	3.13	85	●
FL3a	M/63	PB	Pt	2	IV	M	CAR-T (axicel) R-CHOP/R-mnt GA-Benda + ASCT	CR	N	190.77	95	●
FL3b	M/63	PB	Pt	2	IV	M	Parsadilsib + lbru R-CHOP/R-mnt GA-Benda + ASCT	CR	N	78.05	83	●
FL4	M/27	PB	D	2	IV	M	Parsadilsib + lbru R-CHOP	CR	N	13.75	75	●

Table 1. continued

Study label	Sex/age ^a	Sample type ^a	Disease status ^c	Histological Grade ^a	Stage ^a	FLIPI ^f	Treatments ^g	Response to 1st t ^h	POD24 ⁱ	Cell count Lympho B (10 ³ /L)	% Lympho B ^j	Code
FL7	M/65	LN	R3	2	IV	H	CHOP FCM R-COP	PR	Y	17.58	72	●
FL9	M/25	PB	D	1	IV	M	W&W	–	–	11.69	78	●
FL11	M/37	LN	R1	N/A	N/A	N/A	Chemo-Rx R	N/A	N	N/A	57	○
FL12	M/35	LN and PB	D	2	IV	H	R-CHOP/R-mnt R-Benda/R-mnt	CR	N	1.86	60	●
FL14	M/43	LN and PB	D and R1	1	IV	L	CHOP ESHAP FCM + ASCT Burkinab	SD	Y	14.04	80	●
FL16a	F/51	LN and PB	D	2	IV	H	R-CHOP/R-mnt	CR	N	1.043	64	●
FL16b	F/51	PB	D	2	IV	H	R-CHOP/R-mnt	CR	N	9.64	70	○
FL18	M/56	LN	Pt	2	I	N/A	Rx	CR	N	N/A	55	○
FL21	F/58	PB	R2	1	IV	M	GA-CHOP/GA-mnt R-Benda R2	CR	Y	30.75	78	●
FL23	M/55	Ovary	D	2	IV	M	R-CHOP/R-mnt	CR	N	0.79	40	●
FL25	M/32	LN	R1	3A	I	N/A	Rx R-Rx	CR	N	0.7	40	●
FL29	M/72	PB	R1	2	IV	H	R-COP FCM/PDN	CR	Y	2.31	68	●
FL31	M/58	LN	R1	1	IV	N/A	Rx	CR	N	1.36	80	○
FL32	F	PB	N/A	N/A	N/A	N/A	N/A	N/A	N/A	N/A	92	○
FL34	M/59	PB	R1	3A	IV	H	R-CHOP/R-mnt R-Benda	CR	N	209.21	94	●

^aF: Female; M: Male.

^bPB: Peripheral Blood, LN: Lymph Node.

^cSamples were obtained at: D: diagnosis, R: relapse, Pt: Pretreatment, N/A: Not Available.

^dEvaluated by two independent pathologists.

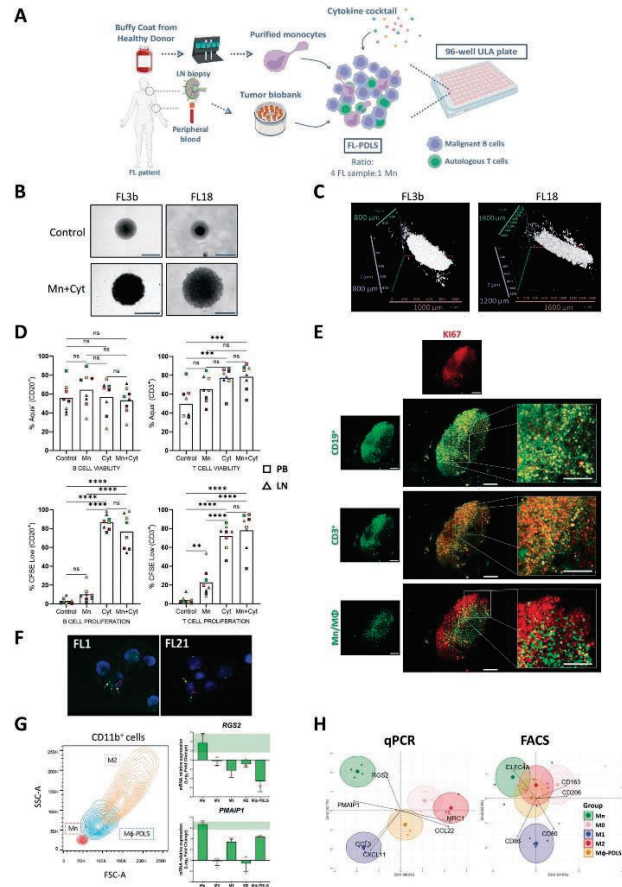
^eAnn Arbor stage.

^fFLIPI: Follicular Lymphoma International Prognostic Index (High (H) ≥ 3, Medium (M), 2: Low (L) 0–1).

^gAll treatments: R: Rituximab, R-mnt: Maintenance Rituximab, R1x: Radiotherapy, GA: Obinutuzumab, Benda: Bendamustine, CHOP: Chemotherapy combination of Cyclophosphamide, Hydroxydaunorubicin, Oncovin and Prednisone, ASCT: Autologous Stem Cell Transplantation, Ibru: Ibrutinib, FCM: Chemotherapy combination of Fludarabine, Cyclophosphamide and Mitoxantrone, W&W: Watch and Wait, CR: Chemotherapy treatment, CR: Complete Response, PR: Partial Response, SD: Stable Disease.

^hPOD24: Response at day 24 post-diagnosis. Y: Yes, N: No, N/A: Not available.

ⁱFrom B-cell panel (CD19, CD20, CD22 and CD79b) in routine diagnosis. Y: Yes, N: No, N/A: Not available.



Fisher Scientific) and cell population proportions (CD20, CD3, CD4, CD8) by flow cytometry (BD LSRFortessa SORP-HTS, BD Biosciences, Franklin Lakes, NJ, USA). To be able to determine cell absolute number of viable cells, disaggregated PDLs were analyzed by reading a fixed volume using a High Throughput Sampler (HTS) integrated in the cytometer. To quantify IFN γ levels after 72 h of treatment, PDLs supernatants were pooled and stored at -80°C . Cytometric Bead Array (CBA) kit was then used following the manufacturer's instructions (BD Biosciences). Data was analyzed using FACS ArrayTM v.3.0 Software (BD Biosciences).

Additional materials and methods, including FL-PDLs imaging, immune profile, immunofluorescence, RNAseq, and metadata analysis, together

with a complete list of antibodies (Table S1), are provided as Supplementary Information.

RESULTS

FL-PDLs generation and characterization

To recreate an ex vivo FL model that recapitulates immune TME signaling in the LN, composed of non-malignant immune cells such as CD4 T_{FH} , T follicular regulatory cells (T_{FR}), and T_{REG} together with CD8 cytotoxic cells and TAMs [13, 30], we have

Fig. 1 FL-PDLS is a novel patient-derived model including an immune microenvironment. **A** Schematic representation of the workflow for FL-PDLS generation. Created with BioRender.com. **B** Brightfield images (Cytation 1) of two representative cases after 7 days of culture showing non-stimulated PDLS (Control) and the PDLS medium with allogeneic monocytes (Mn+Cyt). Magnification 4x and 1000 µm scale. **C** 3D structure obtained by SPIM microscopy of PDLS shown in (B), under complete condition (Mn+Cyt). **D** CD20⁺ and CD3⁺ population viability (upper panel) was determined by the percentage of Aqua⁺ flow cytometry staining, and proliferation (lower panel) was measured by the percentage of CFSE low signal after 7 days of culture in the four experimental scenarios. Patient coding is included in Table 1. One-way ANOVA followed by the Holm-Sidak post hoc test was applied. **E** FL-PDLS immunofluorescence of CD19⁺, CD3⁺, or Mn/Mφ cells (green), merged with Ki-67⁺ (red) to determine the proliferation of each population by signal colocalization (yellow) at day 7 of culture. Captured in confocal Leica TCS SPE microscope. Scale 200 µm. **F** *BCL-2/IGH* rearrangement by FISH using *IGH/BCL2* dual fusion dual color in FL1 and break-apart probe in the case FL21. FL1: the signal constellation illustrates two yellow signals (yellow arrow) corresponding to the *IGH/BCL2* fusion and one red (red arrow), and one green signal (green arrow) for the unrearranged *BCL2* and *IGH*, respectively. Normal cells have two green signals and two red signals. FL21: the signal constellation shows a yellow signal (yellow arrow) for the unrearranged *BCL2* and green and red signals for the rearranged *BCL2* allele. Normal cells display two yellow signals. **G** Side scatter (SSC-A) vs forward scatter (FSC-A) plot of CD11b⁺ cells from Mn, from day 6 Mφ-PDLS, and from M2 macrophages (left). Gene expression of Mn makers (*RG52* and *PMAIP1*) by RT-qPCR in CD11b⁺ cells sorted from day 7 FL-PDLS, compared to Mn, M0, M1, or M2 macrophages. Values are relative to M0 macrophages (mean, *n* = 4) (right). **H** PCA diagrams clustering Mφ-PDLS with in vitro differentiated M0, M1, M2 and non-differentiated Mn, based on CXCL11, CCL5, MRC1, CCL22, *RG52* and *PMAIP1* gene expression levels measured by RT-PCR (left), or based on flow cytometry expression of CD163, CD206, CLEC4A, CD80, and CD86 (right).

established a 3D model using primary FL samples (*n* = 20, Table 1) composed by malignant B FL cells and autologous T cells, together with monocytes (Mn) (1Mn:4FL ratio) purified from healthy donors. We optimized a PDLS medium containing the following cytokines to recapitulate the FL-LN niche: CD40L, IL-21, IL-4, and IL-15 in an enriched medium (described in materials and methods). Several cytokine combinations were tested that maintained B and T cell viability (Figure S1), CD40L clustering and IL-21 were fundamental for B-cell proliferation, while the addition of IL-15, trans-presented by monocytes, promoted T cell proliferation [31].

Either cryopreserved LN biopsies or PB samples were seeded as a multicellular suspension in ULA plates, as shown in the workflow (Fig. 1A), to facilitate cell aggregation and growth. PDLS clustering occurred within the first 12 h (Supplemental Video 1), successfully maintaining a rounded structure for up to 7–10 days of culture, containing darker dense proliferation cores where CFSE staining disappeared (Figs. 1B and S2A). To characterize the real 3D structure, PDLS were imaged by Selective Plane Illumination Microscopy (SPIM, ZEISS Lightsheet Z.7, Imactiv 3D, Toulouse, France), showing self-organized disc-shaped structures with a mean volume of 1.84 mm³ (Fig. 1C and Supplemental Video 2). We then analyzed the viability and proliferation of B and T cells in the PDLS. The culture without cytokines (control) maintained B cell viability (mean: 53.68), and the monocytes moderately improved this effect (mean: 64.45) (Fig. 1D). Cell proliferation, evaluated by accumulative CFSE loss, was prominently engaged when cytokines were added (PDLS medium, Cyt) in B and T cells (mean 86.78 and 71.9 respectively), whereas the co-culture with monocytes alone (Mn) just induced significant proliferation in T cells (mean: 22.68) while the effect on B cells was minor. Likewise, both monocyte co-culture (Mn) and PDLS medium (Cyt) alone enhanced T cell viability (mean: 65.26 and 77.23 respectively), reaching a mean percentage above 78% when both were combined (Fig. 1D). Thus, we decided to combine Cyt (PDLS medium) and Mn to better mimic FL-TME signaling and interactions including the presence of the myeloid compartment. Proliferation was further confirmed by confocal microscopy labelling Ki-67 in CD19⁺, CD3⁺, and macrophages (Fig. 1E). The colocalized signals in yellow validate the expression of Ki67 in B and T cells, whereas in monocytes/macrophages, no double signaling was detected, confirming the low proliferation capacity of human monocytes cultured in vitro [32]. B, T cell and macrophage distribution in the PDLS are shown in Fig. S2B. The cellular composition was evaluated in day 7-PDLS, displaying a mean of 60.11% CD20⁺, 4.62% CD11b⁺, and 35.27% CD3⁺, where CD4⁺/CD8⁺ account for 44%/55% on average (Fig. S2C). Importantly, FL-PDLS maintained the FL hallmark *BCL2* rearrangement as demonstrated by fluorescence in situ hybridization (Fig. 1F). Likewise, we analyzed light chain restriction in the

initial sample and in day 6-PDLS (Fig. S2D), demonstrating that most of B cells maintained the original isotype, with a small portion of cells with a different isotype, indicating some proliferation of existing normal cells in the initial sample. Moreover, tumor cells (CD20⁺CD10⁺ kappa+, in red) were CD43 dim and CD305- at day 0, and this specific FL markers [33] are preserved in the PDLS (shown for FL1, Fig. S2D).

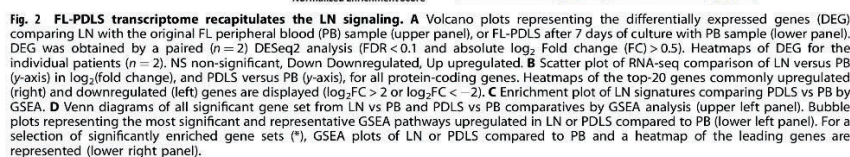
We next analyzed the evolution of monocytes introduced in the FL-PDLS. As shown in Fig. 1G, CD11b⁺ cells in the day 6-PDLS increased size (FSC-A) and complexity (SSC-A) when compared with day 0 CD11b⁺ Mn and downregulated the expression of the monocyte genes *RG52* and *PMAIP1* [34] indicating their differentiation toward macrophages in the FL-PDLS system. We next characterized their phenotype by qPCR (*CXCL11/CCL5* for M1 and *MRC1/CCL22* for M2) and by flow cytometry (CD80/CD86 for M1 and CD163/CD206/CLEC4A for M2) [34]. Most of the M1 and M2-like markers increase with the PDLS condition (Figs. 1H and S2E), indicating that monocytes added in the PDLS culture, after 7 days, partially differentiate into macrophages and polarize within an intermediate state between an activated (M1) and a tumor supportive (M2) phenotype. This phenomenon is clearly displayed in the corresponding PCA diagrams for qPCR and flow cytometry protein markers (Fig. 1H).

In summary, FL-PDLS is organized in a disc-shaped 3D structure composed of proliferating and viable B tumor cells and autologous T cells, together with macrophages with an intermediate M1/M2 phenotype.

FL-PDLS from PB samples recapitulate LN signaling pathways
To determine if FL-PDLS engages a transcriptional program close to that of LN-resident FL cells, we performed RNA-seq analysis on purified B cells from paired PB and LN, together with B cells isolated from the PDLS generated using the same PB sample.

We first performed two differential expression analyses of purified tumor B cells: (1) LN vs PB and (2) PDLS vs PB. A total of 593 genes were upregulated and 227 downregulated in LN compared to PB (Fig. 2A upper panel). This analysis allowed us the generation of LN signatures (Table S2). PDLS vs PB comparison uncovered a significant transcriptome modulation, with 5451 upregulated and 4131 downregulated genes in PDLS (Fig. 2A lower panel). We next analyzed the degree of overlap between these two comparisons as a measurement of how close PDLS were to LN. As shown in Fig. 2B, a significant number of common differentially expressed genes between LN or PDLS compared to PB were identified (199 up, 28 down) (Fig. 2B).

We next proceeded to validate if PDLS summarizes LN signaling pathways. For this purpose, we created two LN signatures including significantly upregulated and downregulated genes



from the LN versus PB comparative (Fig. 2A). Using these signatures, we showed that the expression levels of the genes involved in the LN upregulated signature were also significantly upregulated in the PDLs compared to original PB (NES = 1.78, FDR < 0.001) and moderately downregulated in the case of downregulated signature (NES = 1.48, FDR < 0.001) (Fig. 2C).

To further characterize the FL-PDLs system, we conducted a GSEA analysis in the two previous comparatives (LN vs PB and PDLs vs PB), including all published gene sets in MsigDB (msigdb.v2023.1.Hs.symbols). Noteworthy, 40% of the upregulated gene sets (1084 up) in the LN vs PB comparison were also upregulated in that of PDLs vs PB. This data indicates a remarkably high homology between PDLs and LN samples (Fig. 2D upper panel). A large number of these shared gene sets were related to increased proliferation (E2F, MYC, and cell cycle-related gene sets), survival (mTOR, programmed cell death and apoptosis), metabolic pathways (OXPHOS, glucose and fatty acid metabolism) and epigenetic modifications (DNA methylation). Altogether, these findings reflect that changes that occurred during the generation of the FL-PDLs render initial PB samples to resemble an LN sample rather than the original PB (Fig. 2D lower and left panel, Table 2).

To explore the consequences of growing FL cells in a 3D setup, a parallel comparison was done between PDLs vs 2D culture. First, the principal component analysis (PCA) showed that samples cluster mainly by the patient (Fig. S3A). The changes were moderate and just 29 genes were upregulated and 31 downregulated in PDLs compared to standard 2D culture (Fig. S3B). These genes were related to an increase in fundamental pathways such as cell adhesion, glucose metabolism, and proliferation, while a decrease was observed in pathways related to BCR or TNFα (Fig. S3C).

Another important question was to analyze the effect of co-culturing allogeneic monocytes in comparison with a co-culture with autologous monocytes. The PCA analysis indicated that samples also cluster mainly by the patient (Fig. S4A). Focusing on gene expression analysis, we found that only 39 upregulated genes and 38 downregulated showed a differential expression (Fig. S4B) involving pathways naturally related to allograft rejection (Fig. S4C). This result demonstrates moderate variations in B cell gene expression when using allogeneic monocytes or autologous monocytes.

Altogether, these results support that FL-PDLs represents a robust 3D model recapitulating fundamental biological pathways of FL in secondary lymphoid organs such as the LN.

FL-PDLs exhibit an immune exhaustion profile consistent with FL-LN

Tumor-infiltrating T cells constitute the most abundant non-malignant immune population [35]. Thus, the next step was to characterize to what extent the T cells present in the FL-PDLs represent the T cell subpopulations present in FL-LN. Previous studies have described that this T cell infiltrate is composed of different levels of exhaustion governed by co-expression of specific immune checkpoints (ICs) [36–39]. We first interrogated the expression of a panel of ICs in FL biopsies and tonsils as healthy controls using available bulk RNA-seq data from public repositories. Results confirmed that ICs described in the literature encoding for the exhaustion markers *PDCD1* (PD-1), *HAVCR2* (TIM-3), *LAG-3*, and *TIGIT* were indeed increased in FL biopsies compared with the non-malignant tissue (Fig. 3A). We next validated the expression of these markers by flow cytometry at baseline (FL), and after 3 and 7 days of FL-PDLs in vitro culture. PBMCs from 4 healthy donors were used as controls (Fig. 3B). As expected, PD-1, TIM-3, LAG-3, and TIGIT were expressed in FL-PDLs at higher levels than in healthy controls and increased with culture. Interestingly, TIM-3 and LAG-3 were significantly higher in CD8 than in CD4 T cells (Fig. S4A). The differential expression analysis of FL-LN vs tonsils also highlighted IC activators such as,

TNFRSF9 (4-1BB), *CD28*, and *TNFRSF4* (OX40) (Fig. 3A). Validation of these receptors by flow cytometry showed that 4-1BB expression increased with culture, OX40 was barely expressed, and the co-stimulator CD28 was remarkably high and mostly maintained both in CD4⁺ and CD8⁺ (Fig. 3B and Fig. S5A). The costimulatory molecule ICOS, fundamental in FL-T_H crosstalk, was prominent in CD4⁺ and low in CD8⁺ cells. Finally, the myeloid modulator, CD200, described to be overexpressed in FL-T_H and FL [40], was highly represented in CD4⁺ and CD8⁺ cells and its expression was increased along the culture. In addition, the expression of some of their ligands was assessed in FL cells (CD20⁺) and in the myeloid compartment (CD11b⁺) within the PDLs culture (Fig. S5B). PD-L1 and CD66a (TIM-3 ligand), ICOSL and OX40L were represented in both populations, while 4-1BBL was barely detected neither in CD20⁺ nor CD11b⁺.

To better characterize the immune exhaustion of the T cell compartment in the PDLs, we analyzed the co-expression of PD-1, TIM-3, LAG-3, and ICOS on CD4⁺ and CD8⁺ T cells (day 3-PDLs) using bioinformatics tools to cluster different CD3⁺ phenotypes based on flow cytometry expression (Fig. 3C, D). Eight clusters were identified, divided by a clear polarized expression of the CD8 marker. Within each population (CD3⁺CD8⁺ and CD3⁺CD8⁺), four clusters were identified (C0–C3 and C4–C7, respectively) representing the T cell phenotype spectrum from non-activated or resting populations to terminally differentiated or exhausted (Fig. 3C, D).

Moreover, using CCR7 and CD45RA markers (Fig. 3E), we could confirm that our system recapitulates the whole spectrum of the T cell phenotypic states and the heterogeneity seen in FL scRNA-seq studies [35]. On average and consistent with other NHL studies [41], T effector memory (T_{em}) represented the main subset both in CD4 and CD8 T cells (mean: 48.57 and 49.56, respectively), T naïve (T_n) were also equally represented between CD4 and CD8 (mean: 19.84 and 21.84, respectively). Interestingly T central memory (T_{cm}) cells were more abundant in the CD4 population, while Terminally differentiated T cells (T_{md}) were in CD8 T cells (Fig. S6A).

Finally, considering the remarkable role of CD4⁺ cells in the FL-TME [13, 18], the presence of T_H and the regulatory subsets, T_{REG} and T_{FR}, were confirmed in all PDLs analyzed (Fig. 3F and Fig. S6B), albeit with different abundance depending on the patient material. LN-derived PDLs were significantly enriched in T_H while PB-derived PDLs were, in most cases, enriched with T_{REG}.

In this regard we characterized the evolution of these subpopulations within FL-PDLs (day 3), compared with the unstimulated sample (day 0), together with their ICs. We performed this analysis separately in FL-PDLs generated from PB and LN samples (Fig. S6C). Compared with the corresponding unstimulated samples, T_{REG} increased, and T_H decreased in PB-PDLs, while T_H and T_{FR} increased in LN-PDLs. T_H clearly gains prominence in LN-PDLs, maintaining the expression of PD1 and increasing LAG3 and TIM3, while this observation does not apply to PB-PDLs. T_{FR} constitutes the population with a more immune suppressive profile in both PB and LN-derived PDLs, suggesting a common evolution with the culture conditions, albeit of the origin of the sample.

Altogether we have demonstrated that the T cell compartment in FL-PDLs recapitulates features of the FL-LN microenvironment with different T cell subsets encompassing a spectrum of activation/exhaustion phenotypes and preserving the main T cell subpopulations found in FL-LN.

PDLs represents a suitable system for immunotherapy screening

We next sought to demonstrate that FL-PDLs may be a valuable tool for personalized medicine. In the established workflow (Fig. 4A), treatments were applied to day 3-PDLs, when the spheroid has compacted, and proliferation has been engaged.

Table 2. Gene sets overrepresented in LN vs PB and PDLs vs PB comparatives.

Biological process	# of enriched gene sets	LN vs PB		PDLs vs PB	
		NES (max)	FDR, q value (min)	NES (max)	FDR, q value (min)
Cellular processes					
Apoptosis	6	2.324	0.004	1.996	0.002
Cell Signaling	4	1.860	0.029	1.864	0.002
Cellular response	11	2.407	0.004	2.049	0.002
Enzymatic activity	1	1.819	0.008	1.610	0.002
Proteasome	5	2.221	0.004	1.657	0.003
Protein transport	3	2.231	0.004	2.080	0.002
Senescence	2	2.202	0.004	1.964	0.002
Transcriptional regulation	17	2.374	0.004	1.973	0.002
Epigenetic regulation					
DNA methylation	7	2.339	0.004	1.992	0.002
EZH2	2	1.896	0.035	1.864	0.002
DNA damage					
DNA damage/repair	11	2.245	0.004	1.882	0.002
p53	3	1.995	0.004	1.654	0.003
Immune pathways					
Antigen presentation	1	2.168	0.004	1.688	0.002
Cytokines	35	2.345	0.004	2.056	0.002
Immune response	88	2.402	0.004	2.047	0.002
Complement	1	1.640	0.034	1.554	0.002
Metabolic pathways					
Fatty Acid metabolism	4	2.346	0.004	2.038	0.002
Glucose metabolism	2	1.873	0.035	1.687	0.002
Oxidative phosphorylation (OXPHOS)	5	1.772	0.015	1.724	0.002
Protein metabolism	1	1.799	0.021	1.675	0.002
RNA metabolism	1	1.945	0.013	1.679	0.002
Proliferation					
Cell cycle regulation	91	2.484	0.004	2.051	0.002
Cyclins	2	2.079	0.007	1.903	0.002
DNA replication	20	2.499	0.004	2.085	0.002
Kinase regulation	3	1.838	0.021	1.702	0.002
MYC regulated genes	15	2.265	0.004	1.971	0.002
RAS pathway	3	2.107	0.004	2.022	0.002
Survival pathways					
mTOR	3	2.341	0.004	1.857	0.002
Others					
Angiogenesis	1	2.093	0.004	1.753	0.002
Cytoskeleton	2	1.846	0.006	1.878	0.002
Drug response	4	2.241	0.004	2.034	0.002
Extracellular matrix	1	2.126	0.004	1.954	0.002
Hypoxia	3	2.106	0.004	1.699	0.002
Metastasis	4	2.230	0.004	1.861	0.002
Mitochondrial protein import	1	1.965	0.014	1.617	0.007
Protein folding	4	2.439	0.004	1.563	0.002
Redox balance	1	1.681	0.046	1.599	0.003
Stemness	6	1.927	0.004	1.880	0.002
Telomeres	3	2.325	0.004	1.709	0.002
Unfolded protein response	1	2.022	0.004	1.584	0.003

GSEA was used to test for significant enrichment of defined gene signatures. NES normalized enriched score, FDR false discovery rate. Threshold FDR < 0.05 and NES > 1.5. Gene sets were obtained from the MSigDB v2023.1.Hs (Mar 2023).

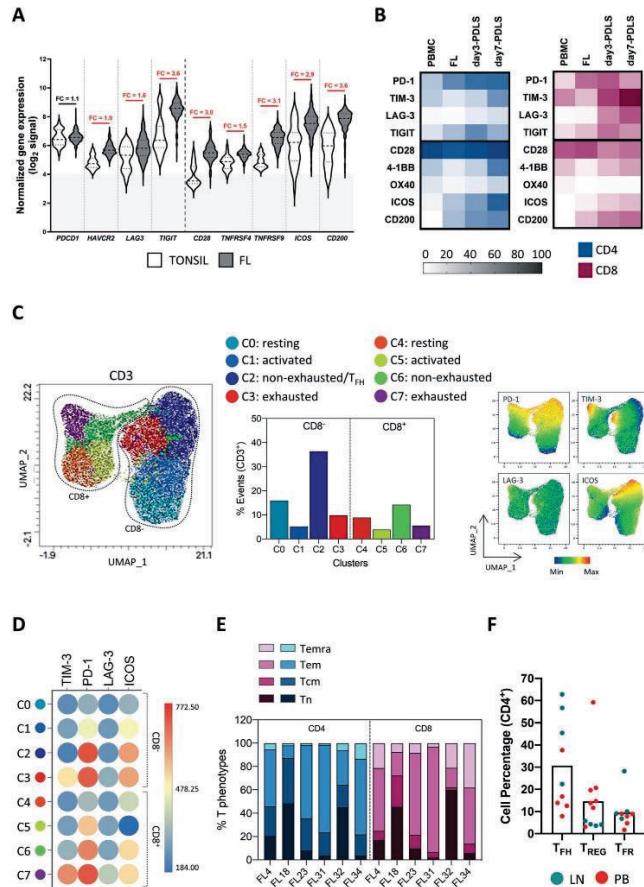


Fig. 3 FL-PDLS immune profile. **A** Differential gene expression analysis from microarray data obtained from public repositories (detailed in supplemental methods) showed up-regulation of several immune regulators in FL-LN (*n* = 427) compared to a normal tonsil (*n* = 30). Fold changes (FC) are indicated and red color means statistical significance (unpaired nonparametric *t* test, Mann-Whitney). **B** Heatmap representing the percentage of positive cells assessed by flow cytometry for the immune regulators on CD4 and CD8 T cells of day 3 and day 7 FL-PDLS (*n* = 3–11). Results were compared with PBMCs from healthy donors (*n* = 4). **C** Uniform Manifold Approximation and Projection (UMAP) plot for day 3-FL-PDLS autologous CD3⁺ cells based on the expression of activation and exhaustion markers assessed by flow cytometry and colored by cluster identity (left panel). Percentage distribution of those clusters (middle panel). UMAP plots show the distribution of PD-1, TIM-3, LAG-3, and ICOS expression (right panel). **D** Average expression levels of each protein represented on CD3⁺ clusters (*n* = 6). **E** Day 3-FL-PDLS autologous CD3⁺ phenotypes based on flow cytometry CCR7 and CD45RA expression. **F** Percentage of T_{FH} (CXCR5⁺ FoxP3⁺), T_{REG} (CXCR5⁺ FoxP3⁺), and T_{FR} (CXCR5⁺ FOXP3⁺) out of CD4⁺ population on day 3-FL-PDLS. Patients are identified by the origin of the FL sample.

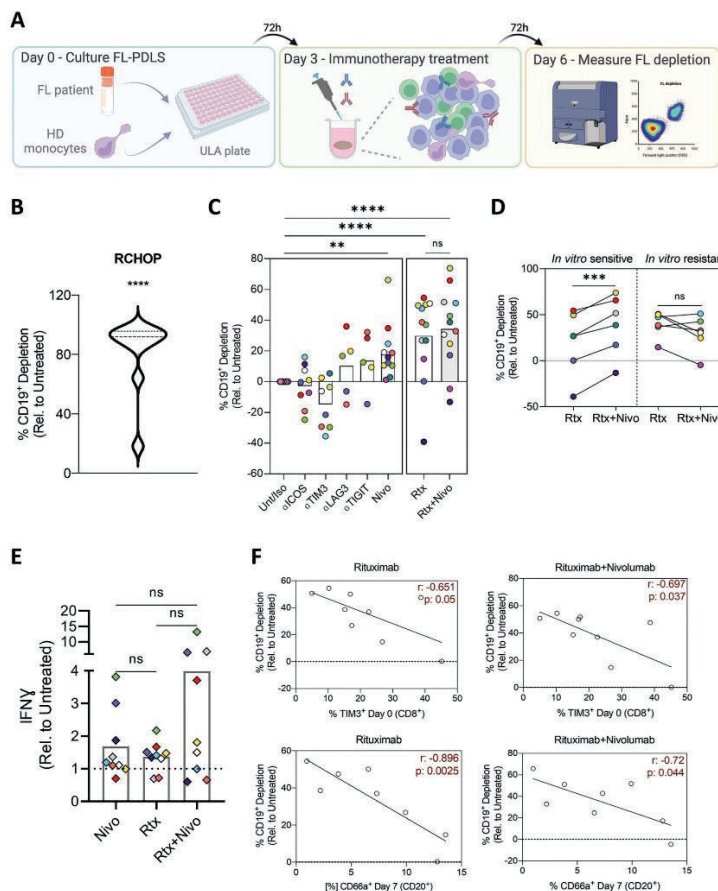


Fig. 4 FL-PDLS represents a suitable system for immunotherapy drug screening. **A** Schematic representation of the workflow used to treat FL-PDLS with immunotherapeutic agents. HD healthy donors. Created with BioRender.com. **B** Percentage of B cell depletion induced by R-CHOP or C a sort of selected monoclonal antibodies (IgG1κ mAbs) against IC of interest, and nivolumab (Nivo) combined with rituximab (Rtx) relative to the untreated/Iso type condition (Unt/Iso). Depletion was assessed by Aqua⁺ cell counting. **D** Percentage of B cell depletion for rituximab (Rtx) and its combination with nivolumab (Rtx+Nivo) of in vitro responder (R) and non-responder (NR) patients. Patients were considered responders when reaching a Response Index[®] superior to the median value of 18%. Patient coding is included in Table 1. **E** IFN γ levels (pg/mL) were measured in the day 6-PDLS supernatants relative to the untreated condition (right panel). Quantification was done using the CBA application. Each supernatant was recovered from 6 replicates per condition and patient. Patient coding is indicated. **F** Correlation plots by simple linear regression of B cell depletion in FL-PDLS treated with rituximab or rituximab + nivolumab and the expression of TIM-3 in CD8⁺ cells at basal levels (day 0) and CD66a in B cells at day 7 of culture. Paired t test–Wilcoxon matched-pairs signed rank test was applied in (B) and (D), and one-way ANOVA followed by Holm–Sidak post hoc test for (C) and (E). *Response index = $\left(\frac{\text{B cell depletion (Rtx + Nivo)} - \text{B cell depletion (Rtx)}}{\text{B cell depletion (Rtx)}} \right) \times 100$.

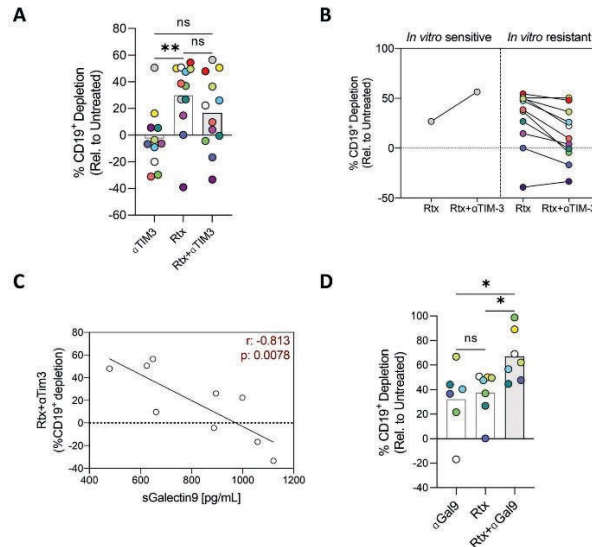


Fig. 5 Galectin-9 blockade improves rituximab-induced depletion in FL-PDLS. **A** B cell depletion induced by mAb anti-TIM-3 (α TIM-3), rituximab (Rtx), or the combination (Rtx + α TIM-3) in all patients and, **B** classified in in vitro responder (R) and non-responder (NR) patients to the combination. Patient coding is included in Table 1. **C** Correlation by simple linear regression between galectin-9 levels (pg/mL) analyzed by ELISA of FL PDLS supernatants at the endpoint (day 6) and the B cell depletion induced by rituximab + anti-TIM-3. **D** B cell depletion induced by mAb anti-galectin-9 (α Gal9), rituximab (Rtx), or the combination. One-way ANOVA followed by Holm-Sidak post hoc test was applied for (**A**) and (**D**).

Treatment efficacy was assessed after 3 days (day 6) by measuring B cell depletion. We first tested the FL first-line treatment R-CHOP, and we observed an induction of tumor cell depletion above 80% in 9 out of 11 FL-PDLS (81%) (Fig. 4B, Figure S7A) that is consistent with the observed response rate in the clinical practice [42].

We next challenged FL-PDLS to several immunotherapeutic agents targeting ICs described before, together with the standard therapy rituximab. Antibodies targeting ICOS, TIM-3, LAG-3, or TIGIT engaged mostly limited and highly heterogeneous responses (Fig. 4C). Anti-PD-1 (nivolumab/Nivo) was the most effective IC inhibitor that also increased rituximab activity in half of the FL-PDLS (6/12) (Fig. 4D). This combination increased the levels of IFN γ in the PDLS supernatants compared to single agents in five out of the nine cases analyzed, albeit without reaching statistical significance (Fig. 4E).

These heterogeneous responses to IC inhibitors are consistent with observations in the clinic and may be explained by the patient-specific composition and activation/exhaustion status of the T cell compartment [43, 44]. In this regard, correlation analyses indicated that depletion induced by rituximab or rituximab combined with nivolumab inversely correlated with the expression of TIM-3 on CD8 T cells and the expression of TIM-3 ligand, CD66a, on B cells (Fig. 4F). It has also been demonstrated that TIM-3 is highly expressed by T_{REG} and promotes T cell dysfunction in several cancers [45]. In our system, we observed that those PDLS with a higher percentage of T_{REG} prior in vitro rituximab treatment responded worse than those with lower proportions (Fig. S7A). In

addition, the percentage of T_{REG} in the PDLS correlated with the expression of TIM-3 in CD4 T cells (Fig. S7B), suggesting a possible relation between TIM-3⁺ T_{REG} and therapy resistance.

In summary, FL-PDLS represents a valuable multiplexed patient-derived system with great potential for personalized immunotherapeutic approaches and for the identification of biomarkers of response and resistance.

Inhibition of galectin-9 but not TIM-3 improves rituximab FL depletion

Based on the possible role of TIM-3 on rituximab activity, it was conceivable that TIM-3 blockade may improve those limited responses. However, combination therapy did not offer any benefit in terms of FL depletion (Fig. 5A). On the contrary, a reduction of rituximab activity was observed in most of the cases analyzed (Fig. 5B). This may be explained by the fact that TIM-3 has multiple ligands: CEACAM1 (CD66a), Phosphatidylserine (PtdSer), High Mobility Group Protein B1 (HMGB1) and galectin-9, which bind to different regions of the receptor [46]. More importantly, it was discovered that antibodies targeting TIM-3 bind to the FG-CC' loops of its extracellular domain but are incapable of blocking the glycan binding site where galectin-9 binds [47] (Fig. S8A). Thus, considering the correlation between therapy resistance and T_{REG} percentages in our cultures, the inactivity of anti-TIM-3 antibodies against galectin-9 interactions, and the growing evidence of galectin-9 role in tumor immune escape [48, 49], we moved to explore galectin-9 as an interesting

target to improve rituximab-induced depletion. We first analyzed soluble galectin-9 (sGalectin-9) in FL-PDLs supernatants, and we observed a negative correlation with rituximab + anti-TIM-3 FL depletion (Fig. 5C). Moreover, high levels of sGalectin-9 also have a negative impact on rituximab and rituximab + nivolumab induced depletion (Fig. 5B). We next demonstrated that anti-galectin-9 mAb was able to induce FL depletion as a single agent and significantly improved rituximab activity (Fig. 5D), frequently decreasing TIM-3 expression in CD4⁺ and CD8⁺ populations (Fig. 5B). Nevertheless, FL depletion negatively correlates with the presence of T_H (Fig. 5B).

Altogether, using our novel FL-PDLs tool, we have uncovered galectin-9 as a new IC with potential interest for FL immunotherapy that may deserve attention to improve standard anti-CD20 immunotherapy or in combination with other IC modulators.

DISCUSSION

Robust patient-derived models constitute one of the fundamental pieces for the successful implementation of personalized medicine. We have previously established 2D cocultures with FDC [50, 51] and Mφ [23] and demonstrated their utility in studying FL-microenvironment crosstalk, therapy testing, and biomarker identification. Yet, 3D models better represent cancer biology, signaling pathways [52], and especially B and T cell activation, as they are influenced by physical forces that are not recapitulated in 2D cultures [53]. We have developed FL 3D models using cell lines alone or in co-culture with immune cells [54–58]. In addition, we have recently made progress in patient-derived FL 3D models, including both tumor cells and the T cell compartment [27]. However, this model does not include myeloid cells also fundamental for lymphoma maintenance and immune suppressive signaling. For these reasons, we endeavored to generate the first immunocompetent patient-derived FL 3D model, including B, T, and myeloid compartments. Future perspectives we are approaching to improve and complexify this system include the integration of FDC cells and ECM, together with the inclusion of these tumoroids in a microvascularized system.

The FL-PDLs model we present here is an affordable and robust system for the following reasons:

First, using PBMCs from PB or LN samples of FL patients, we optimized a cytokine cocktail to mimic the underlying interactions between FL-T_H (CD40/CD40L, IL-4, and IL-21) [17–19]. The addition of IL-15 together with the monocytes completes the main immunological actors. IL-15 activates both NK and T cells, while the presence of monocytes/macrophages, together with CD40/CD40L engagement, can activate B cells [31]. Due to the low number of monocytes in the original FL-PB sample and as macrophages are not recovered with the LN mechanical dissociation performed in the clinical routine, we decided to introduce monocytes from healthy donors in a conservative ratio since they represent an elemental compartment that constitutes a source of immunosuppressive signal [23]. Because of the proliferation engaged by B and T cells in the FL-PDLs, the monocyte ratio decreases after several days (mean population distribution in day 7-FL-PDLs: 60.11% CD20⁺, 35.27% CD3⁺, and 4.62% CD11b⁺). It is noteworthy that in the FL-PDLs system, monocytes started a process of differentiation and polarization in the absence of specific differentiation factors, with some limitations due to the absence of ECM that enables their adhesion. We have previously reported that FL cells secrete M-CSF that facilitates Mφ differentiation. In the FL-PDLs, the presence of IL-4 (in the PDLs medium) and IL-10 generated by FL-Mφ crosstalk [23] may contribute to the acquisition of a phenotype with some markers of immunosuppressive M2-Mφ, as seen in FL-LN biopsies [22], while CD40L signaling would enhance the expression of M1 markers.

Second, we have demonstrated that B cells in the FL-PDLs recapitulate fundamental transcriptional pathways in FL-LN. To do

so, we have performed a 3-way transcriptomic comparison of B cells isolated from paired LN, PB, and PB-derived FL-PDLs. With this approach we have demonstrated that B cells in FL-PDLs are committed to a LN transcriptomic program through the enrichment of LN signatures and the activation of pathways overrepresented in LN compared to paired PB. These pathways include proliferation, mTOR pathway, epigenetic regulation, diverse metabolic pathways and housekeeping processes, overall reflecting that FL-PDLs is a living and dynamic system. Moreover, RNA-seq analysis highlighted the activation of immune pathways in the FL-PDLs as seen in the LN (antigen presentation, IFNγ, TGFβ, IL-2, and IL-10 signaling). Altogether, our results are in agreement with previous scRNA-seq studies showing common gene set enrichments in B cells from FL-LN compared to normal B cells [59].

Third, FL-PDLs recapitulates the immune exhaustion profile of FL-LN. We have demonstrated the previously acknowledged high expression of immune regulators such as TIM-3, LAG-3, TIGIT, ICOS, or CD200. More importantly, the analysis of the IC co-expression, together with the activation phenotype (T_H, T_{EM}, T_{CM}, T_{EMRA}), allowed us to confirm that FL-PDLs fairly recapitulates the spectrum of CD8 clusters recently acknowledged in FL studies and the interpatient variability [35]. This feature is mandatory to use FL-PDLs as a system for immunotherapies testing.

Thus, we decided to challenge FL-PDLs with rituximab + anti-PD-1 combination as this regimen has demonstrated favorable efficacy (ORR; 67%; CR:50%) and safety profile in relapsed/refractory FL [60]. In the FL-PDLs system, 50% of the cases benefit from the combination, and resistance was related to CD8 exhaustion, a feature also acknowledged in the correlative analysis of the above-mentioned clinical trial. In our FL-PDLs system, we observed that the TIM-3 axis may have a role in this CD8 exhaustion since its expression in CD8 and the expression of its ligand CD66a in B cells correlated with reduced responses to rituximab or rituximab + nivolumab combination. However, when we challenged FL-PDLs with rituximab + mAb anti-TIM-3 combination, we obtained unforeseen results with a general decrease in antitumor activity. TIM-3 has multiple ligands, among them, galectin-9 is gaining relevance in cancer [61]. Galectins are a family of endogenous glycan-binding proteins that reprogram tumor, vascular, and immune landscapes in the tumor microenvironment [62, 63]. Moreover, galectins dampen antitumor immune responses by targeting both lymphoid and myeloid cells. In the precise case of galectin-9, expression can be up or downregulated in association with neoplastic transformation depending on the specific tumor type [61]. Galectin-9 is increased in several hematologic neoplasia, including chronic lymphocytic leukemia [64], cutaneous T cell lymphoma, and acute myeloid leukemia (AML) [65]. In this latter, TIM-3/Gal-9 constitutes an autocrine stimulatory loop that regulates the self-renewal of leukemic cells [66]. Importantly, anti-TIM-3 mAbs are incapable of blocking the binding site where galectin-9 binds, and a specific mAb is required. In this regard, two clinical trials with the mAb anti-Gal9 (LYT-200) are currently ongoing for AML (NCT05829226) and advanced solid tumors (NCT04666688). In FL-PDLs, we have demonstrated that sGalectin-9 is related to reduced responses to rituximab or rituximab + nivolumab, and to the lack of activity observed in rituximab + mAb anti-TIM-3 combination. Finally, mAb blocking galectin-9 offered a therapeutic benefit in combination with rituximab in all cases analyzed. Additionally, those patients with limited responses to rituximab + anti-galectin-9 combination showed a higher proportion of T_H, known to overexpress PD-1. These observations suggest that co-blockade of galectin-9 and PD-1 could benefit rituximab combinations in those patients with high numbers of T_H.

In summary, we have set up a robust patient-derived system, recapitulating LN signaling in FL cells, the spectrum of T cell phenotypes, and the presence of main T cell subpopulations. We have demonstrated that FL-PDLs represents a novel tool for the

discovery of immunotherapeutic targets, such as galectin-9. FL-PDLs may serve as a platform to perform preclinical screening in a robust, 96-well format system and may also constitute a complementary in vitro tool for phase 1/2 trials to help identify biomarkers of response and mechanisms of resistance.

DATA AVAILABILITY

RNA sequencing data generated and analyzed during the current study are available in the European Genome-phenome Archive (<http://ebi.ac.uk/ega/>) under accession number EGAS50000000233. The datasets generated and/or analyzed during the current study are available from the corresponding authors upon reasonable request.

REFERENCES

1. Swerdlow SH, Campo E, Pileri SA, Lee Harris N, Stein H, Siebert R, et al. The 2016 revision of the World Health Organization classification of lymphoid neoplasms. *Blood*. 2016;127:2375–90.
2. Link BK, Maurer MJ, Nowakowski GS, Ansell SM, MacOn WR, Syrbu SI, et al. Rates and outcomes of follicular lymphoma transformation in the immunochemotherapy era: a report from the University of Iowa/Mayo Clinic specialized program of research excellence molecular epidemiology resource. *J Clin Oncol*. 2013;31:3272–8.
3. Jacobsen E. Follicular lymphoma: 2023 update on diagnosis and management. *Am J Hematol*. 2022;97:1638–51.
4. Carbone A, Roulland S, Ghoghini A, Younes A, von Kneudell G, López-Guillermo A, et al. Follicular lymphoma. *Nat Rev Dis Prim*. 2019;5:83.
5. Araf S, Okosun J, Koniall L, Fitzgibbon J, Heward J. Epigenetic dysregulation in follicular lymphoma. *Epigenomics*. 2016;8:77–84.
6. Okosun J, Wolfson RL, Wang J, Araf S, Wilkins L, Castellano BM, et al. Recurrent mTORC1-activating RAS mutations in follicular lymphoma. *Nat Genet*. 2016;48:183–8.
7. Huet S, Sjobert P, Salles G. From genetics to the clinic: a translational perspective on follicular lymphoma. *Nat Rev Cancer*. 2018;18:224–39.
8. Boice M, Saloum D, Mourcin F, Sanghi V, Amin R, Oricchio E, et al. Loss of the HVEF tumor suppressor in lymphoma and restoration by modified CAR-T cells. *Cell*. 2016;167:405–18.e13.
9. Green MR, Gentles AJ, Nair RV, Irish JM, Khira S, Liu CL, et al. Hierarchy in somatic mutations arising during genomic evolution and progression of follicular lymphoma. *Blood*. 2013;121:1604–11.
10. Béguin W, Teater M, Meydan C, Hoehn KB, Phillip JM, Soshnev AA, et al. Mutant EZH2 induces a pre-malignant lymphoma niche by reprogramming the immune response. *Cancer Cell*. 2020;37:655–73.e11.
11. Dobaño-López C, Araujo-ayala F, Serrat N, Valero JG, Pérez-galan P. Follicular lymphoma microenvironment: an intricate network ready for therapeutic intervention. *Cancers (Basel)*. 2021;13:1–22.
12. Scott DW, Gascoyne RD. The tumour microenvironment in B cell lymphomas. *Nat Rev Cancer*. 2014;14:517–34.
13. Amé-Thomas P, Tarte K. The yin and the yang of follicular lymphoma cell niches: Role of microenvironment heterogeneity and plasticity. *Semin Cancer Biol*. 2014;24:23–32.
14. Bolen CR, McCord R, Huet S, Frampton GM, Bourgon R, Jardin F, et al. Mutation load and an effector T-cell gene signature may distinguish immunologically distinct and clinically relevant lymphoma subsets. *Blood Adv*. 2017;1:1884–90.
15. Huet S, Tesson B, Jais JP, Feldman AL, Magnano L, Thomas E, et al. A gene-expression profiling score for prediction of outcome in patients with follicular lymphoma: a retrospective training and validation analysis in three international cohorts. *Lancet Oncol*. 2018;19:549–61.
16. Dave SS, Wright G, Ph D, Tan B, Rosenwald A, Gascoyne RD, et al. Prediction of survival in follicular lymphoma based on molecular features of tumor-infiltrating immune cells. *N Engl J Med*. 2004;351:2159–69.
17. Wood B, Sildar S, Choi SJ, Virk S, Alhejaily A, Baetz T, et al. Abundant expression of interleukin-21 receptor in follicular lymphoma cells is associated with more aggressive disease. *Leuk Lymphoma*. 2013;54:1212–20.
18. Amé-Thomas P, Le Priol J, Yssel H, Caron G, Pangault C, Jean R, et al. Characterization of intratumoral follicular helper T cells in follicular lymphoma: Role in the survival of malignant B cells. *Leukemia*. 2012;26:1053–63.
19. Pandey S, Mourcin F, Marchand T, Nayar S, Guiricé M, Pangault C, et al. IL-4/CXCL12 loop is a key regulator of lymphoid stroma function in follicular lymphoma. *Blood*. 2017;129:2507–18.
20. Yang ZZ, Novak AJ, Ziesmer SC, Witzig TE, Ansell SM. Attenuation of CD8–T cell function by CD4–CD25+ regulatory T cells in B-cell non-Hodgkin's lymphoma. *Cancer Res*. 2006;66:10145–52.

C. Dobaño-López et al.

13

21. Yang ZZ, Grote DM, Ziesmer SC, Niki T, Hirashima M, Novak AJ, et al. IL-12 upregulates TIM-3 expression and induces T cell exhaustion in patients with follicular B cell non-Hodgkin lymphoma. *J Clin Invest*. 2012;122:1271–82.
22. Kridel R, Xerri L, Gelas-Dore B, Tan K, Feugier P, Vawda A, et al. The prognostic impact of CD163-positive macrophages in follicular lymphoma: a study from the BC cancer agency and the lymphoma study association. *Clin Cancer Res*. 2015;21:3428–35.
23. Valero JG, Matas-Céspedes A, Arenas F, Rodríguez V, Carreras J, Serrat N, et al. The receptor of the colony-stimulating factor-1 (CSF-1R) is a novel prognostic factor and therapeutic target in follicular lymphoma. *Leukemia*. 2021;35:2635–49.
24. Schutgens F, Clevers H. Human organoids: tools for understanding biology and treating diseases. *Annu Rev Pathol*. 2020;15:211–34.
25. Maura R, Francesco A, Simona R, Elena S, Claudio A. Three-dimensional models: a novel approach for lymphoma research. *J Cancer Res Clin Oncol*. 2022;148:753–65.
26. Lamaison C, Latour S, Hélaine N, Le Morvan V, Saint-Vanne J, Mahouche I, et al. A novel 3D culture model recapitulates primary FL B-cell features and promotes their survival. *Blood Adv*. 2021;5:5372–86.
27. Faria C, Gava F, Gravelle P, Valero JG, Dobaño-López C, Van Acker N, et al. Patient-derived lymphoma spheroids integrating immune tumor microenvironment as preclinical follicular lymphoma models for personalized medicine. *J Immunother Cancer*. 2023;11:7156.
28. Araujo-ayala F, Dobaño-López C, Valero JG, Nadeu F, Gava F, Faria C, et al. A novel patient-derived 3D model recapitulates mantle cell lymphoma lymph node signaling, immune profile and in vivo ibrutinib responses. *Leukemia*. 2023;37:1311–23.
29. Mongini PKA, Imman JK, Han H, Kalled SL, Fattah RJ, McCormick S. Innate immunity and human B cell clonal expansion: effects on the recirculating B2 subpopulation. *J Immunol*. 2005;175:6143–54.
30. Yang ZZ, Ansell SM. The tumor microenvironment in follicular lymphoma. *Clin Adv Hematol Oncol*. 2012;10:810–8.
31. Epron G, Amé-Thomas P, Le Priol J, Pangault C, Dulong J, Lamy T, et al. Monocytes and T cells cooperate to favor normal and follicular lymphoma B-cell growth: role of IL-15 and CD40L signaling. *Leukemia*. 2012;26:139–48.
32. Van Furth R, Raeburn JA, van Zwet TL. Characteristics of human mononuclear phagocytes. *Blood*. 1979;54:485–500.
33. Bottcher S, Engelmann R, Grigore G, Fernandez P, Caetano J, Flores-Montero J, et al. Expert-independent classification of mature B-cell neoplasms using standardized flow cytometry: a multicentric study. *Blood Adv*. 2022;6:976–92.
34. Martinez FO, Gordon S, Locati M, Mantovani A. Transcriptional profiling of the human monocyte-to-macrophage differentiation and polarization: new molecules and patterns of gene expression. *J Immunol*. 2006;177:7303–11.
35. Han G, Deng Q, Marques-Piubelli ML, Dai E, Dang M, Chun M, et al. Follicular lymphoma microenvironment characteristics associated with tumor cell mutations and MHC class II expression. *Blood Cancer Discov*. 2022;3:428–43.
36. Yang Z, Kim H, Villasboas JC, Price-Troska T, Jalali S, Novak AJ, et al. Expression of Lag-3 defines exhaustion of intratumoral PD-1+ T cells and correlates with poor outcome in follicular lymphoma. *Hematol Oncol*. 2017;35:260–1.
37. Yang ZZ, Kim HJ, Wu H, Jalali S, Tang X, Krull JE, et al. TIGIT expression is associated with T-cell suppression and exhaustion and predicts clinical outcome and anti-PD-1 response in follicular lymphoma. *Clin Cancer Res*. 2020;26:5217–31.
38. Josefsson SE, Beiske K, Blaker YN, Førsund MS, Holte H, Stenstad B, et al. TIGIT and PD-1 mark intratumoral T cells with reduced effector function in B-cell non-Hodgkin lymphoma. *Cancer Immunol Res*. 2019;7:355–62.
39. Josefsson SE, Huse K, Kolstad A, Beiske K, Pende D, Steen CB, et al. T cells expressing checkpoint receptor TIGIT are enriched in follicular lymphoma tumors and characterized by reversible suppression of T-cell receptor signaling. *Clin Cancer Res*. 2018;24:870–81.
40. Pangault C, Amé-Thomas P, Rossille D, Dulong J, Caron G, Nonn C, et al. Integrative analysis of cell crosstalk within follicular lymphoma cell niches towards a definition of the FL supportive synapse. *Cancers (Basel)*. 2020;12:3865.
41. Anagnostou T, Yang ZZ, Jalali S, Kim HJ, Larson DP, Tang X, et al. Characterization of immune exhaustion and suppression in the tumor microenvironment of splenic marginal zone lymphoma. *Leukemia*. 2023;37:1485–98.
42. Federico M, Luminari S, Dondi A, Tucci A, Vitolo U, Rigacci L, et al. R-CVP versus R-CHOP versus R-FM for the initial treatment of patients with advanced-stage follicular lymphoma: results of the FOLL05 Trial Conducted by the Fondazione Italiana Linfomi. *J Clin Oncol*. 2013;31:1506–13.
43. Lesokhin AM, Ansell SM, Armand P, Scott EC, Halwani A, Gutierrez M, et al. Nivolumab in patients with relapsed or refractory hematologic malignancy: preliminary results of a phase Ib study. *J Clin Oncol*. 2016;34:2698–704.
44. Voilán P, de Bruijn M, Roelofs LM, Hendriks SH, Brokamp S, van den Braber M, et al. An ex vivo tumor fragment platform to dissect response to PD-1 blockade in cancer. *Nat Med*. 2021;27:1250–61.

45. Saluishi K, Ngiew SF, Sullivan JM, Teng MWL, Kuchroo K, Smyth MJ, et al. Promoters of T-cell dysfunction in cancer TIM3 – FOXP3 – regulatory T cells are tissue-specific promoters of T-cell dysfunction in cancer. *Oncoimmunology*. 2013;2:e23849.
46. Wolf Y, Anderson AC, Kuchroo VK. TIM3 comes of age as an inhibitory receptor. *Nat Rev Immunol*. 2020;20:173–85.
47. Sabatos-peyton CA, Nevin J, Brock A, Venable JD, Tan DJ, Kassam N, et al. Blockade of Tim-3 binding to phosphatidylserine and CEACAM1 is a shared feature of anti-Tim-3 antibodies that have functional efficacy. *Oncoimmunology*. 2018;7:1–9.
48. Qi Y, Chang Y, Wang Z, Chen L, Kong Y, Zhang P, et al. Tumor-associated macrophages expressing galectin-9 identify immunoevasive subtype muscle-invasive bladder cancer with poor prognosis but favorable adjuvant chemotherapeutic response. *American Joint Committee on Cancer. Cancer Immunol Immunother*. 2019;68:2067–80.
49. Zhang LI, Tian S, Pei M, Zhao M, Wang LI, Jiang Y, et al. Crosstalk between histone modification and DNA methylation orchestrates the epigenetic regulation of the costimulatory factors, Tim-3 and galectin-9, in cervical cancer. *Oncol Rep*. 2019;42:2655–69.
50. Matas-Céspedes A, Rodríguez V, Kalko SG, Vidal-Crespo A, Rosich L, Casserras T, et al. Disruption of follicular dendritic cells–follicular lymphoma cross-talk by the Pan-Pi3K inhibitor BKM120 (Buparlisib). *Clin Cancer Res*. 2014;20:3458–71.
51. Serrat N, Guerrero-Hernández M, Matas-Céspedes A, Yahiaoui A, Valero JG, Nadeu F, et al. PI3Kd inhibition reshapes follicular lymphoma–immune microenvironment cross talk and unleashes the activity of venetoclax. *Blood Adv*. 2020;4:4217–31.
52. Gravelle P, Jean C, Familades J, Decaup E, Blanc A, Bezombes-Cagnac C, et al. Cell growth in aggregates determines gene expression, proliferation, survival, chemoresistance, and sensitivity to immune effectors in follicular lymphoma. *Am J Pathol*. 2014;184:282–95.
53. Apoorva F, Loiben AM, Shah SB, Purwada A, Fontan L, Goldstein R, et al. How biophysical forces regulate human B cell lymphomas. *Cell Rep*. 2018;23:499–511.
54. Vidal-Crespo A, Matas-Céspedes A, Rodríguez V, Rossi C, Valero JG, Serrat N, et al. Daratumumab displays in vitro and in vivo anti-tumor activity in models of B-cell non-Hodgkin lymphoma and improves responses to standard chemotherapy regimens. *Haematologica*. 2020;105:1032–41.
55. Gava F, Faria C, Gravelle P, Valero JG, Dobaño-López C, Morin R, et al. 3D model characterization by 2D and 3D imaging in t(14;18)-positive B-NHL: perspectives for in vitro drug screens in follicular lymphoma. *Cancers (Basel)*. 2021;13:1490.
56. Decaup E, Jean C, Laurent C, Gravelle P, Fruchon S, Capilla F, et al. Anti-tumor activity of obinutuzumab and rituximab in a follicular lymphoma 3D model. *Blood Cancer J*. 2013;3:131.
57. Rossi C, Gravelle P, Decaup E, Bordenave J, Pouput M, Tosolini M, et al. Boosting γδ T cell-mediated antibody-dependent cellular cytotoxicity by PD-1 blockade in follicular lymphoma. *Oncoimmunology*. 2019;8:1554175.
58. Decaup E, Rossi C, Gravelle P, Laurent C, Bordenave J, Tosolini M, et al. A tridimensional model for NK cell-mediated ADCC of follicular lymphoma modelization of NK-mediated ADCC in follicular lymphoma. *Front Immunol*. 2019;10:1943.
59. Andor N, Simonds EF, Czerwinski DK, Chen J, Grimes SM, Wood-Bowens C, et al. Single-cell RNA-Seq of follicular lymphoma reveals malignant B-cell types and coexpression of T-cell immune checkpoints. *Blood*. 2019;133:1119–29.
60. Nastoupil LJ, Chin CK, Westin JR, Fowler NH, Samaniego F, Cheng X, et al. Safety and activity of pembrolizumab in combination with rituximab in relapsed or refractory follicular lymphoma. *Blood Adv*. 2022;6:1143–51.
61. Lv Y, Ma X, Ma Y, Du Y, Feng J. A new emerging target in cancer immunotherapy: Galectin-9 (LGALS9). *Genes Dis*. 2022;10:2366–82.
62. Mariño KV, Gagnoni AJ, Croci DO, Rabinovich GA. Targeting galectin-driven regulatory circuits in cancer and fibrosis. *Nat Rev Drug Discov*. 2023;22:295–316.
63. Mantuano R. Tumor-associated carbohydrates and immunomodulatory lectins as targets for cancer immunotherapy. *J Immunother Cancer*. 2020;8:1222.
64. Pang N, Alimi X, Chen R, Mufasni M, Ma J, Chen G, et al. Activated Galectin-9/TIM3 promotes Treg and suppresses Th1 effector function in chronic lymphocytic leukemia. *FASEB J*. 2021;35:e21556.
65. Kocibalova Z, Guzyova M, Borovska I, Messingerova L, Copakova L, Sulova Z, et al. Development of Multidrug Resistance in Acute Myeloid Leukemia Is Associated with Alterations of the LPHN1/GAL-9/TIM-3 Signaling Pathway. *Cancers*. 2021;13:3629.
66. Kikushige Y, Miyamoto T, Yuda J, Takenaka K, Iwasaki H, Correspondence KA. A TIM-3/Gal-9 autocrine stimulatory loop drives self-renewal of human myeloid leukemia stem cells and leukemic progression. *Cell Stem Cell*. 2015;17:341–52.

ACKNOWLEDGEMENTS

We thank Ariadna Giró for their technical assistance, the IDIBAPS genomics facility for gene expression data generation, and the IDIBAPS Flow Cytometry and Cell Sorting

Core facility. The authors would also like to thank Dr. Martina Seifert from DKFZ for her support and critical reading of the article. We are indebted to the HCB-IDIBAPS Biobank, integrated into the Spanish National Biobanks Network, for the biological human samples and data procurement. This work was carried out at the Esther Koplowitz Center, Barcelona. Grants that contributed to this work included: This work was part of an Interreg POCTEFA program (IMUNFO EFA281/16). Spanish Ministry of Economy and Competitiveness & European Regional Development Fund (ERDF) "Una manera de hacer Europa" for SAF2017/88275R and to PP-G. PID2021-1248940B-I00 funded by MICIU/AEI/ 10.13039/501100011033 and by ERDF/EU to PPG. CD-L was supported by a personal FPI fellowship from the Ministry of Economy and Competitiveness (PRE2018-083797) associated with the project SAF2017-88275-R. Additional grants are CIBERONC (CB16/12/00334 to DC and CB16/12/00225 to ECI), Fundació la Marató TV3 (TAIFOL project, ref 201993-30) to PP-G, and finally Generalitat de Catalunya support for AGAUR 2021SGR01294 to PP-G and to 2017SGR1009 DC.

AUTHOR CONTRIBUTIONS

CD-L conducted molecular and cellular assays, performed data analysis, contributed to the study design and wrote the paper. JGV conducted molecular assays, performed data analysis, and contributed to study design and paper writing. FA-A conducted cellular assays, and contributed to the study design and critical paper revision. FN performed RNAseq analysis and critical paper revision. FG and CF contributed to result discussions, protocol optimization, PDLs imaging and critical paper revision. MN, RM, PB-L, and J-ML performed PDLs imaging by SPIIM and mathematical 3D reconstructions. FA contributed to confocal imaging and critical paper revision. MG, CL, and SB conducted the FISH assay and contributed to critical paper revision. ILQ provided technical advice and performed data analysis. NS, HP-A, and RG contributed to result discussions, protocol optimization and critical paper revision. AMF and LM provided patient clinical data and critical paper revision. LH contributed to result discussions and critical paper revision. EC participated in the critical revision of the paper. AL-G provided economic support and clinical data. DC provided economic support, results discussion, study guidance and critical paper revision. CB co-supervised the study, discussed the experiments, and critically revised the paper. PP-G led the study, provided economic support, and wrote the paper. All authors have read and approved the paper.

COMPETING INTERESTS

MN, RM, PB-L, and J-ML are employees of Imactiv3D. The rest of the authors declare no conflict of interest.


ADDITIONAL INFORMATION

Supplementary information The online version contains supplementary material available at <https://doi.org/10.1038/s41408-024-01041-7>.

Correspondence and requests for materials should be addressed to Christine Bezombes or Patricia Pérez-Galán.

Reprints and permission information is available at <http://www.nature.com/reprints>

Publisher's note Springer Nature remains neutral with regard to jurisdictional claims in published maps and institutional affiliations.

 **Open Access** This article is licensed under a Creative Commons Attribution 4.0 International License, which permits use, sharing, adaptation, distribution and reproduction in any medium or format, as long as you give appropriate credit to the original author(s) and the source, provide a link to the Creative Commons licence, and indicate if changes were made. The images or other third party material in this article are included in the article's Creative Commons licence, unless indicated otherwise in a credit line to the material. If material is not included in the article's Creative Commons licence and your intended use is not permitted by statutory regulation or exceeds the permitted use, you will need to obtain permission directly from the copyright holder. To view a copy of this licence, visit <http://creativecommons.org/licenses/by/4.0/>.

© The Author(s) 2024

CHAPTER 2. IDENTIFICATION OF TAILORED IMMUNOTHERAPIES IN FOLLICULAR LYMPHOMA

The second chapter of this dissertation is based on a manuscript in preparation (**Study 3**) which identified *CD70* as an up-regulated gene in follicular patients that relapse. This finding led to the development of a novel dual CAR-T targeting CD19 and CD70.

STUDY 3. CD70 deregulation in follicular lymphoma at diagnosis is associated with relapse and opens new avenues for dual CD19-CD70 CAR-T therapy

Ferran Araujo-Ayala, Maria Ros, Mireia Bachiller, Raluca Alexandru, Pablo Mozas, Salut Colell, María Villalba-Esparza, Judith Mateos-Jaimez, Ferran Nadeu, Andrea Rivero, Cèlia Dobaño-López, Juan G. Valero, Neus Serrat, Marta Giménez-Alejandre, Ariadna Giró, Daniel Hodson, Armando López-Guillermo, Elias Campo, Dolors Colomer, Alba Maiques, Jose Ignacio Martin-Subero, Silvia Beà, Laura Magnano, Sonia Guedan, Carlos E. De Andrea and Patricia Pérez-Galán

Manuscript in preparation

CD70 deregulation in follicular lymphoma at diagnosis is associated with relapse and opens new avenues for dual CD19-CD70 CAR-T therapy

Ferran Araujo-Ayala^{1,2}, Maria Ros^{1,2}, Mireia Bachiller¹, Raluca Alexandru⁴, Pablo Mozas³, Salut Colell¹, Maria Villalba-Esparza⁴, Judith Mateos-Jaimez¹, Ferran Nadeu^{1,2}, Andrea Rivero³, Cèlia Dobaño-López^{1,2}, Juan G. Valero^{1,2}, Neus Serrat¹, Marta Giménez-Alejandre¹, Ariadna Giró¹, Daniel Hodson⁵, Armando López-Guillermo^{1,3,7}, Elías Campo^{1,2,6,7}, Dolors Colomer^{1,2,6}, Alba Maiques¹, Jose Ignacio Martin-Subero^{1,7,8}, Silvia Beà^{1,2}, Laura Magnano³, Sonia Guedan¹, Carlos E. De Andrea^{2,4} and Patricia Pérez-Galán^{1,2}

¹Department of Hematology-Oncology, IDIBAPS, Barcelona, Spain

²Centro de Investigación Biomédica en Red-Oncología (CIBERONC), Madrid, Spain

³Department of Hematology, Hospital Clínic de Barcelona, Barcelona, Spain

⁴Clínica Universidad de Navarra, Pamplona, Spain

⁵Wellcome MRC Cambridge Stem Cell Institute, University of Cambridge, Cambridge, UK

⁶Department of Pathology, Hospital Clínic de Barcelona, Barcelona, Spain

⁷Faculty of Medicine, University of Barcelona, Barcelona, Spain

⁸Institució Catalana de Recerca i Estudis Avançats (ICREA), Barcelona, Spain

Running title: CD70 deregulation in follicular lymphoma at diagnosis is associated with relapse and opens new avenues for dual CD19-CD70 CAR-T therapy

Keywords: Follicular lymphoma, immune profile, CD70, CD27, multiplex immunofluorescence, CRISPR/Cas9, CAR-T

Corresponding author information

Patricia Pérez-Galán, PhD. Department of Hemato-Oncology, Institut d'investigacions Biomèdiques August Pi i Sunyer (IDIBAPS). Rosselló 149-153. 08036 Barcelona, Spain. Email: pperez@recerca.clinic.cat

MATERIAL, METHODS AND RESULTS

27 ABSTRACT

28 Despite most follicular lymphoma (FL) patients achieve a complete response to first-line treatment,
29 an important fraction of them relapse, which may worsen the prognosis. Here, we have assessed the
30 immune profile in FFPE-derived biopsies in a series of FL patients at diagnosis, homogenously treated
31 with immunochemotherapy regimen, and followed-up for more than 11 years. By comparing patients
32 who experienced relapse (Rel, n=20) with those who did not (NR, n=12), we have found 25 up-
33 regulated genes in the relapse group. Among them, we validated the over-expression in relapse group
34 of CD70 at protein level by multiplex immunofluorescence, which highly correlates with inferior PFS.
35 Intriguingly, a fraction of T cells from the tumor microenvironment also expresses CD70, and higher
36 levels were detected in both CD4+ and CD8+ T cells in the relapse group. CD27, the ligand of CD70,
37 was also increased in the B cell population in patients who eventually relapse and in TFH cells, while
38 it was down-regulated in CD8+ and CD4+ T helper non-follicular cells. To investigate the role of CD70
39 in FL pathogenesis we generated two CD70 KO cell lines and FL patient derived cells (n=4) using
40 CRISPR/Cas9 technique. By co-culturing healthy donors' T cells with CD70+ or CD70- FL cells, we
41 observed CD70+ tumor cells promote CD70 expression in T cells. In primary samples, we have
42 demonstrated that CD70-KO B cells exhibit reduced response to proliferative stimuli. Finally, to
43 advance towards personalized therapies for this high-risk patient, we have generated a dual CD19-
44 CD70 CAR-T combining an approved academic product, ARI-0001, and a truncated CD27 protein.

45 INTRODUCTION

46 Follicular lymphoma (FL) represents the second most common B-cell non-Hodgkin lymphoma (B-NHL),
 47 accounting for 20% of cases, with an incidence of 4-5 cases / 100,000 people / year.(1) FL is considered
 48 an indolent lymphoma and, after the introduction of anti-CD20 rituximab treatment, median survival
 49 time has significantly increased, with a 10-year OS of approximately 80%.(2) Nevertheless, even
 50 though most patients achieve a complete response to immunochemotherapy treatment, a high
 51 proportion of them eventually relapse to first-line therapy, which worsens the prognosis, especially if
 52 the relapse occurs within the first 2 years after treatment initiation (POD24).(3) Moreover, around 2%
 53 of individuals per year suffer a histological transformation to an aggressive lymphoma, mainly, diffuse-
 54 large B-cell lymphoma (DLBCL), which represents a high-risk subset of FL patients.(4) (5) (6)
 55 Importantly, there is a lack of prognostic factors that predict whether a patient will relapse or not to
 56 standard treatment. Follicular Lymphoma International Prognosis Index (FLIPI) was developed in the
 57 pre-rituximab era but is still widely used in clinical routine.(7) Although several attempts have been
 58 made to develop new predictive models, their impact on treatment has been very limited.(8)
 59 Intriguingly, a gene expression-based predictor that stratified FL patients according to the high or low
 60 risk of survival ascertained that the genes which determined a favorable or unfavorable prognosis
 61 were expressed in the tumor microenvironment (TME).(9)
 62 In fact, follicular lymphoma is considered a paradigm of the support given by the TME in the germinal
 63 center of the lymph nodes, in which participate different subsets of T cells (including CD8+ cells, T
 64 follicular helper (TFH) cells, T regulatory cells (Treg) and T follicular regulatory (TFR) cells), tumor-
 65 associated macrophages (TAMs), follicular dendritic cells (FDCs) and other stromal cells with
 66 mesenchymal origin.(10) (11)
 67 CD70 is a protein belonging to the tumor necrosis factor (TNF) superfamily.(12) (13) Even though it
 68 was initially described as the ligand of CD27, it was later demonstrated that a reverse signaling also
 69 occurred.(14) (15) (16) (17) Furthermore, CD70 can induce CD27 cleavage from the membrane which,
 70 in soluble state (sCD27), maintains capacity to bind CD70 protein.(18) (19) Despite CD70 expression is

MATERIAL, METHODS AND RESULTS

71 limited to activated lymphocytes (B, T or NK cells) in physiological conditions, it is frequently
72 deregulated in many cancers, acting as a pro-oncogenic gene in both solid and hematologic
73 tumors.(20) Furthermore, there are evidences that CD70 is over-expressed in many B-cell neoplasms,
74 in which it contributes to the tumor – TME crosstalk.(21) (22) (23)
75 In this work, we aimed to better characterize the immune genes profile in FL-LN biopsies from follicular
76 patients at diagnose using a homogeneously treated cohort with an extensive follow-up. Our results
77 demonstrated a differential immune pattern in pre-treated patients with different clinical responses
78 and uncovered CD70 is up-regulated in patients that eventually relapse. This observation may not only
79 be useful in predicting response to standard treatment, but also supports the development CD70-
80 targeting therapies, including the development of dual CD19-CD70 CAR-Ts for relapsed follicular
81 lymphoma.
82

83 METHODS

84 FL patients cohort

85 Thirty-eight FL patients grade 1-3A diagnosed at Hospital Clínic de Barcelona between 1997 and 2015
 86 who met prespecified criteria were selected. All patients were treated with immunochemotherapy
 87 (ICT), either with R-CHOP or GA-CHOP and with or without autologous stem cell transplant (ASCT),
 88 and achieved at least a partial response (PR). Exclusion criteria included grade 3B FL, primary
 89 gastrointestinal or cutaneous FL, composite (FL/DLBCL) histology, histological transformation (HT)
 90 during follow-up and primary refractoriness to first-line treatment. Nineteen patients did not relapse
 91 (NR) for at least 10 years of follow-up (range, 11.5-17.8 years). Nineteen patients relapsed after
 92 responding to ICT, with a median of time of 4.1 years (range, 0.7 – 7.0 years). All patients had an
 93 available lymphoid tissue biopsy from the time of diagnosis. The diagnosis of grade 1-3A FL, underwent
 94 histological review and assessment of BCL2 rearrangement have been previously published in (24).
 95 The study was designed in line with the Declaration of Helsinki and informed consent was obtained
 96 according to the Institutional Review Board of Hospital Clínic de Barcelona.

97 DNA and RNA extraction

98 DNA and RNA from 38 formalin-fixed, paraffin-embedded (FFPE) samples were extracted using the
 99 AllPrep DNA/RNA FFPE Kit (Qiagen, Germany). The mutational status of recurrently mutated genes
 100 was examined using a custom targeted NGS panel and sequenced in a MiSeq instrument (Illumina).
 101 Complete mutational profile is published in Mozas *et al.*(24) The bioinformatic analysis was performed
 102 using an updated version of our in-house pipeline.(25) (26)

103 Nanostring® nCounter PanCancer Immune Profile

104 Targeted transcriptomic analysis of 730 immune-related genes was performed using Nanostring®
 105 PanCancer Immune Profile(27) (NanoString Technologies, Inc, Seattle, WA, USA) with 150 ng of RNA
 106 extracted from FFPE samples. Samples with lower amount of RNA were not included. Quality and
 107 quantity of RNA was analyzed using NanoDrop 1000 spectrophotometer. Quality control and
 108 normalization were performed following manufacturer's recommendations and samples with a high

MATERIAL, METHODS AND RESULTS

109 normalization factor were removed for further analysis. Out of 30 genes defined as housekeeping (HK)
110 in the panel, we selected the following 6 based on their expression and the coefficient of variance:
111 *CNOT4*, *DHX16*, *ERCC3*, *GUSB*, *HDAC3*, *SAP130* and *ZNF143*.

112 Differential expression analysis between relapse and non-relapse groups was performed with 32
113 samples that passed quality and normalization controls using a negative binomial model within the
114 advanced analysis options from nSolver™ analysis software (NanoString Technologies). Gene filtering
115 was applied to genes <20 normalized counts. False discovery rate (FDR) was calculated from obtained
116 p-values using Benjamini-Hochberg method using R software. Cut-off for genes differentially
117 expressed were FDR < 0.05 and absolute fold change (FC) > 1.5 (log2FC > 0.58).

118 Pathway analysis

119 Gene-set enrichment analyses (GSEAs) were conducted with GSEA software (version 4.3.2)(28) using
120 the pre-ranked mode based on log2FC results obtained from nSolver analysis. Hallmark gene sets, the
121 C2 curated gene sets and the C5 gene ontology gene sets (Molecular Signature Database v7.5) were
122 used. Pathways with an absolute normalized enrichment score (NES) > 1.5, p-value < 0.05 and FDR <
123 0.25 were selected.

124 Additionally, genes that were significantly more expressed in each group and genes that significantly
125 correlated with *CD70*, were interrogated for a significantly increased overlap using the “Investigate
126 Human Gene Sets” tool available at <https://www.gsea-msigdb.org>. Again, Hallmarks, C2 and C5 gene
127 sets were used. A threshold of FDR q value < 0.05 was used for filtering.

128 FL mutational status

129 Mutational status of recurrently altered genes in FL was examined in 37 out of 38 patients by next-
130 generation sequencing (NGS) using a custom targeted NGS panel. Libraries were generated from 150
131 ng of DNA, using molecular-barcoded library adapters (ThruPLEX Tagseq kit; Takara) coupled with a
132 custom hybridization capture-based method (SureSelectXT Target Enrichment System Capture
133 strategy, Agilent Technologies). The quality of the libraries was determined using the Bioanalyzer high
134 sensitivity DNA kit (Agilent) and quantified by PCR using the KAPA library quantification kit (KAPA

Biosystems). Finally, the libraries were pooled and sequenced 2x130 bp in the MiSeq instrument (Illumina). The bioinformatic analysis was performed using an updated version of our in-house pipeline, described in previous publications. (25) (26)

Multiplex immunofluorescence

Multiplex immunofluorescence staining and analysis was performed as previously described on a Bond RX autostainer (PMID: 36169332, PMID: 32591586). Four-microns-thick FFPE tissue sections were deparaffinized (Bond DeWax, Leica Biosystems) and rehydrated per standard protocols. Antigen retrieval was performed with Bond Epitope Retrieval Solution 1 (ER1, Leica Biosystems) or 2 (ER2, Leica Biosystems, product number AR9640), followed by sequential cycles of staining with each cycle including a 30-minute combined block and primary antibody incubation (Akoya antibody diluent/block), followed by a secondary HRP-conjugated polymer. Signal amplification was achieved with TSA-Opal fluorophores. Between cycles of staining, tissue sections underwent heat-induced epitope retrieval to remove the primary/secondary-HRP antibody complexes before staining with the next antibody.

Three complementary multiplex immunolabelling panels to simultaneously evaluate the lymphocytic contexture were established.

The primary antibodies and corresponding fluorophores included:

Panel 1: anti-CD20 (IgG2 α , mouse monoclonal, clone: L26, ready-to-use; Agilent) in Opal 520, and anti-CD27 (IgG, rabbit monoclonal, clone: EPR8569, 1:500; Abcam) in Opal 570.

Panel 2: anti-CD20 (IgG2 α , mouse monoclonal, clone: L26, ready-to-use; Agilent) in Opal 520, and anti-CD70 (IgG, rabbit monoclonal, clone: E3Q1A, 1:100; Cell Signaling) in Opal 690.

Panel 3: anti-CD8 (mouse monoclonal, clone C8/144B, ready-to-use, Agilent, product number GA62361-2) in Opal 480, anti-CD4 (mouse monoclonal, clone 4B12, ready-to-use; Agilent) in Opal 620, anti-FOXP3 (mouse monoclonal, clone 236A/E7, 1:300; Abcam), anti-CD27 (IgG, rabbit monoclonal, clone: EPR8569, 1:100; Abcam) in Opal 570, anti-CD70 (IgG, rabbit monoclonal, clone: E3Q1A, 1:100;

MATERIAL, METHODS AND RESULTS

160 Cell Signaling) in Opal 690, and anti-CXCR5 (IgG2b, rabbit monoclonal, clone: 51505, 1:100; Bio-
161 Techne) in Opal 520.

162 We counterstained nuclei with Spectral DAPI (Akoya Biosciences, FP1490) and mounted the stained
163 tissues with ProLong Diamond Antifade mounting medium (Thermo Fisher Scientific). The stained
164 slides were scanned using the PhenolImager™ HT Automated Quantitative Pathology Imaging System
165 (Akoya Biosciences). After image acquisition, unmixing of the spectral libraries was performed with
166 inForm software (Akoya Biosciences). Unmixed images were then imported into the open source
167 digital pathology software QuPath version 0.4.4 for stitching, cell segmentation and cell phenotyping.
168 Whole tumor regions from each slide were analyzed. Marker expression was used to identify immune
169 cell subpopulations by fluorescent colocalization within CD4+ cells: T helper non-follicular
170 (CD4+CXCR5-FOXP3-), T follicular helper (CD4+CXCR5+FOXP3-), T regulatory (CD4+FOXP3+) and T
171 follicular regulatory (CD4+CXCR5+FOXP3+). Densities of each cell population were quantified and
172 expressed as number of cells per mm².

173 **Survival and correlations analysis**

174 Survival analysis were performed using progression-free survival data from time of first treatment to
175 first relapse. Patients that did not relapse were censored according to the time of follow-up after the
176 first treatment. Expression data from Nanostring® nCounter and multiplex immunofluorescence were
177 classified into high or low expression for CD70 or CD27 using maxstat library in R software. This
178 classification was used to perform Kaplan-Meier analysis with GraphPad Prism v.9.5.

179 Expression data from Nanostring® nCounter and multiplex immunofluorescence were used to perform
180 correlation analysis tests. Shapiro-wilk test was used to check whether the populations followed a
181 Gaussian distribution. Correlation coefficient and p-values were calculated with Spearman correlation
182 test in R software.

183 **CAR construction and lentivirus production**

184 Single-targeting 41BBz-based CAR targeting CD19 (ARI-0001)(29) has been previously described.
185 CD27-ECD CAR-T was designed using the full sequence of nucleotides of the extracellular domain of

MATERIAL, METHODS AND RESULTS

186 CD27 together with CD8 hinge and transmembrane domain, as in ARI-0001. Truncated CD27 – ECD
187 (trCD27-ECD) had the same structure of CD27-ECD but was shortened, as described in Leick *et al.*(30)
188 For the scFv-based anti-CD70 CAR-T, the construct was adapted from Sauer *et al.*(31)
189 All CAR sequences were cloned into the pCCL third-generation lentiviral vector with EF1a promoter.
190 The plasmid coding for GFP-ffLuc was kindly provided by Dr. Amer Najjar. Lentiviral vectors were
191 produced by 293FT transfection and tittered in CD27⁺ T-cell line Jurkat following previously described
192 methods.(32) Briefly, 293FT were transfected with pCCL transfer plasmid, and a packaging mix (pREV,
193 pRRE and pVSV) using PEI (Polysciences). The supernatant was harvested at 48 and 72h and
194 concentrated with LentiX following manufacturer's protocol (Clontech).

195 Isolation, transduction and primary T-cell Expansion

196 Human T cells were isolated from healthy donor buffy-coats obtained from Banc de Sang i Teixits,
197 Barcelona, following approved Institutional Review Board protocols. CAR-T cells were generated and
198 expanded as previously described.(33) Briefly, CD4⁺ and CD8⁺ T cells were isolated from peripheral
199 blood using RosetteSep Kits (Stem Cell Technologies). T cells were stimulated for 72h with anti-
200 CD3/CD28 magnetic beads (Invitrogen) and transduced by LVs at indicated MOIs. T cells were cultured
201 in RPMI-1640 supplemented with 10% of FBS, 100 mg/mL of Penicillin/streptomycin (P/S) 10 mM
202 Glutamax and 10 mM Hepes.
203 IL-7 and IL-15 (Miltenyi) were added to a final concentration of 10 ng/mL. CAR-T cell products were
204 mixed to a final 1:1 (CD4⁺:CD8⁺) ratio and normalized for CAR expression at day 10 before
205 cryopreservation.

206 *In vitro* killing and proliferation assays with cell lines

207 WSU-FSCCL and WSU-NHL tumor cell lines were acquired from the Leibniz Institute DSMZ, while RL
208 cell line was obtained from the American Tissue Culture Collection (ATCC). CD19 and/or CD70-
209 expressing K562 were generated through lentiviral transduction of parental K562 cells. Cell lines
210 were cultured in RPMI-1640 supplemented with 10% FBS (except for RL, supplemented with 20% FBS)

MATERIAL, METHODS AND RESULTS

211 and 100mg/ml P/S. Cell lines were maintained at 37°C with 5% CO₂ and were regularly validated to
212 be Mycoplasma free.

213 For bioluminescence-based killing assays, CAR-T cells were co-cultured with luciferase-expressing
214 target cells (K562) at indicated ratios and run in triplicates. Luciferase signal, indicative of surviving
215 cells, was determined between 24 to 48h of co-culture using a Tecan multireader (Tecan Life Sciences)
216 within 20 min after the addition of D-luciferin (20mg/mL; Perkin Elmer). Percent specific lysis was
217 calculated as follows: % Specific lysis = $[1 - (\text{BLI signal in treated wells} / \text{BLI signal in untreated wells})] \times$
218 100%.

219 For long-term assays, effector and target cells (lymphoma tumor cells) were co-cultured at indicated
220 ratios for 7 days. We harvested the culture and calculated the total number of T cells and tumor cells
221 by flow cytometry (BD LSRFortessa 5L) using CountBright beads (Thermo Fisher). T-cell and tumor cell
222 proliferation were calculated as the fold change compared to initial co-culture. Singlets were selected
223 and dead cells were excluded by Fixable Viability Dye eFluor 450 staining (ThermoFisher). Tumor cells
224 were identified by CD10 expression and T cells were stained with a CD3 antibody.

225 CRISPR/Cas9 genetic editing

226 WSU-FSCCL and SC-1 cell lines or FL primary samples in growing conditions were electroporated with
227 the conditions described in (34). Briefly, a complex formed by gRNA:tracrRNA was mixed with Cas9
228 enzyme (IDT technologies) and electroporation enhancer (IDT technologies) for 20' RT. In parallel, 1
229 M cells / condition were centrifuged and resuspended in a specific buffer for electroporation (Thermo
230 Fisher). Electroporation was performed using Neon Transfection System (Thermo Fisher) in sterile
231 conditions.

232 After 7 days, cell lines were stained with CD70-APC antibody (Miltenyi) and sorted out (BD Aria II, BD
233 Biosciences) selecting viable cells (Live/Dead Fixable Aqua, ThermoFisher) and +/- CD70. Cells were
234 incubated, expanded and cryopreserved.

235 For primary samples, cells were thawed in Mongini media and co-cultured with irradiated YK6-CD40L-
236 IL21(35) in a ratio FL:YK6 of 2:1 and supplemented with IL-4 and IL-15, reproducing the stimuli

published in (36). After 4 days, cells were electroporated and seeded in a new YK6 layer. CD70 down-regulation was confirmed 4 days post-electroporation by CD70 staining and flow cytometry analysis, calculating the median fluorescence intensity (MFI).

FL – T cell co-culture

Isolated human T cells were obtained from buffy coats (Banc de Sang i Teixits) using RosetteSep™ Human T Cell Enrichment Cocktail (Stemcell technologies) and sequential Ficoll gradient separation. T cells were cryopreserved (FBS + 10% DMSO) and thawed for the experiment. After thawing, T cells were activated with CD3/CD28 Dynabeads (Thermo Fisher) at a ratio of 1 bead per T cell and cultured +/- FL cells expressing or not CD70 (ratio 1 : 1), in previously described culture media supplemented with 1% Hepes buffer. Cells were seeded in 96-wells plates in triplicate. After 72h, cells were harvested and analyzed by flow cytometry (BD LSRFortessa 4L).

Proliferation assay

EdU reagent (Thermo Fisher) was added in FL primary samples co-cultured with YK6-CD40L-IL21 cells, at a final concentration of 10 µM. Cells were incubated for 2h at 37°C and then harvested for flow cytometry analysis (BD LSRFortessa 4L). Briefly, cells were stained for extracellular antibodies and viability dye (Live/Dead Fixable Aqua), fixed, permeabilized and stained with Click-iT™ EdU, using an AF488 conjugated dye. Tumor cells were identified by CD20 and CD19 expression, as well as CD3 exclusion.

ELISA

IL-2 was used as a readout of CAR-T cell proliferation and was analyzed in supernatants from K562 cells (WT or overexpressing CD19 and/or CD70) co-cultured with CAR-T cells in a E:T ratio of 3:1 for 24h. Determination of IL-2 concentration was performed using ELISA MAX™ Deluxe Set Human IL-2 (BioLegend).

Soluble CD27 (sCD27) was analyzed in CAR-T cells after 10 days of expansion, in FL primary samples after 4 days of electroporation, and in FL cell lines, in standard culture conditions or co-cultured with

MATERIAL, METHODS AND RESULTS

262 T cells from healthy donors. Determination of sCD27 was performed using Human CD27/TNFRSF7
263 DuoSet ELISA kit (R&D systems).

264 **Statistical analysis**

265 Apart from Nanostring analysis, data comparing two groups were analyzed using Prism Software v9.5
266 (GraphPad Software, San Diego, CA, USA). Depending on the assay and based on Shapiro-Wilk
267 normality test, t test or Mann-Whitney U test were used. Analysis in which was compared two
268 conditions on the same donors/patients a paired t-test was applied. In analysis comparing multiple
269 groups, an ANOVA test and a Holm-Sidak post hoc test for multiple comparisons were applied. Data
270 were represented as the mean +/- sd values of the patients. Differences between the results of
271 comparative tests were considered significant if the two-sided P value was less than 0.05. The
272 statistical significance convention used along the manuscript was as follows: * p<0.05, **p<0.01,
273 ***p<0.001 and ****p<0.0001.

274

275

276 RESULTS

277 FL-LN transcriptomic profile unravels differences at diagnosis in patients that relapse

278 Follicular lymphoma lymph nodes are characterized by a high percentage of non-malignant cells that
 279 cooperate with tumor B cells in the development of the disease. As genetic mutations hardly
 280 discriminate between patients with different clinical responses to first-line treatment, we
 281 hypothesized differences could be in the immune profile of the patients. Therefore, we analyzed the
 282 transcriptome of 730 immune-related genes within the Nanostring® nCounter PanCancer Immune
 283 Profile panel in a patients cohort described in **Table 1** and **Table S1**. This FL series represents a single-
 284 center, homogenic cohort, as all the patients have been treated with immunochemotherapy (mostly,
 285 R-CHOP). In our analysis, we compared patients that did not relapse (n=20) with an extensive follow-
 286 up of more than ten years or patients that eventually relapsed during the follow-up (n=12).
 287 By applying a negative binomial model, we found 31 genes differentially expressed (FDR < 0.05 and
 288 an absolute fold change > 1.5 ($\log_2FC > 0.58$), and 25 of them were up-regulated in the Relapse group
 289 (Rel), while only 6 were increased in the Non-relapse (NR) group. (**Figure 1A**) Thus, we could
 290 demonstrate patients with different clinical responses to immunochemotherapy exhibit a different
 291 transcriptomic profile, although intra-group differences regarding gene expression are still very high.
 292 (**Figure 1B**)

293 A gene-set enrichment analysis (GSEA) using genes up-regulated in each condition showed the relapse
 294 group had an over-representation of genes related to B-cell proliferation, B and T-cell activation,
 295 cytokine regulation, extracellular matrix and cell adhesion, as well as different pro-oncogenic
 296 pathways (PI3K/Akt, IL6/JAK-STAT, IL4), among others. (**Figure 1C**) On the other hand, negative
 297 regulation of cell-cell adhesion, immunoglobulin production and BCR signaling pathways were
 298 significantly over-represented in genes enriched in NR patients. (**Figure 1D**).
 299 Furthermore, we performed a pre-ranked GSEA using all the genes included in the Immune Profile
 300 panel, which confirmed a decrease in BCR pathway in non-relapse patients, accompanied by
 301 interferon I signaling, T cytotoxicity pathway and Fcγ mediated phagocytosis, which could indicate a

MATERIAL, METHODS AND RESULTS

302 higher rituximab benefit that prolongs response to anti-CD20 treatment. On relapse group, we also
303 confirmed a higher cytokine activity (**Figure S1A**). Some of the most representatives GSEA plots are
304 represented in **Figure S1B**, including the down-regulation of BCR and phagocytosis (NES -1.77 and -
305 1.61 respectively) and the increase in cytokines (NES = 1.60) and a possible role of dendritic cells (NES
306 = 1.51). Overall, we assessed patients that relapse or do not relapse have a previous differential
307 immune profile at diagnosis.

308

309 **CD70 is up-regulated in relapse group and is associated to a lower mutational burden**

310 Deciphering a differential immune profile between patients that relapse or not may be useful, not
311 only to improve the FL prognosis, but also to better understand the biology of the disease and design
312 new therapies for patients who repeatedly relapse, worsening their prognosis. Among the genes up-
313 regulated in patients who relapse, we further focus on *CD70*, as it has been defined as an oncogenic
314 factor in many cancers, including B-cell lymphoma(20)(21)(37) and it is expressed in the cell
315 membrane, making it easily targetable.

316 Interestingly, *CD70* is not only increased in the Relapse group (FC = 1.88, p-value = 3.39×10^{-3} ,
317 FDR = 4.08×10^{-2}) (**Figure 1E**), but it is also associated with shorter progression-free survival (PFS) time,
318 closely to significance (p = 0.067) (**Figure 1F**). *CD70* is the only known ligand of *CD27*, and can be
319 mutually activated;(17) thus, we also analyzed *CD27* RNA levels. Interestingly, *CD27* is widely
320 expressed in FL-LN but we did not find differences between patients (FC = 0.96, p = 0.83). (**Figure S1C**).
321 Moreover, we investigated whether *CD70* expression was correlated with other genes. Among the
322 730 genes included in the Nanostring® Immune Profile panel, *CD70* significantly correlates with 30
323 genes, and inversely with only 5 genes. (**Figure S1D**). Notably, some of the most represented genes
324 that directly correlate with *CD70* are cytokines and chemokines, as it is corroborated by GSEA
325 enrichment analysis (**Figures S1D, S1F**). Among them, we highlight the Th17/Treg chemoattractant
326 *CCL20*(38) (R = 0.64), *CCL22* (R = 0.49), a relevant cytokine in FL-TME(39), and *IRF4* (R = 0.48), related
327 to FL transformation into DLBCL.(4) (**Figure S1D**)

Finally, other enriched pathways include cell to cell adhesion, monocyte chemotaxis, oncogenic pathways (MAPK, JAK-STAT and NFkB) and positive regulation of cellular processes (gene expression, metabolism and protein modification and phosphorylation). (Figure S1F)

The mutational profile from the patients used in our series has also been published by Mozas *et al.*(24)

Intriguingly, we found a tendency of a lower mutational burden in patients with higher CD70 RNA levels. (Figure S2A) In patients harboring less than 8 mutations (median value of the total patients, among the 28 most frequently genes that have been examined), CD70 counts were significantly higher than in patients with at least 8 mutations. (Figure S2B) These differences can be also visualized in Figure S2C, in which the number of accumulated mutations in CD70^{low} (n=15) or CD70^{high} (n=15) patients is represented. CD70^{high} curve rises more rapidly compared to CD70 low curve, as patients belonging to this group usually harbor less mutations. This observation is also reflected in a superior area under curve (AUC) in CD70^{high} group, 38% higher than in CD70^{low} group. (Figure S2D).

When analyzing individual mutations, we found significant differences in CD70 expression in *CARD11*, *CIITA* and *TNFSRSF14*, also known as *HVEM*. In all of them, patients with alterations in these genes have lower CD70 levels. (Figure S2E). In single-cell data, CD70 has been associated to wild-type state of *EZH2*, one of the most frequently mutated genes in FL.(40) In our data, we found the same tendency, although it did not reach significance (p = 0.21).

345

CD70 and CD27 protein expression is increased in FL cells from Relapse patients

In order to validate our results at protein level, we performed multiplex immunofluorescence (mIF) staining the FFPE samples from FL-LN patients of our cohort who had available material (n=21, of which 13 relapsed and 8 did not relapse). In physiological conditions, CD70 is found in activated lymphocytes, meaning it is transitory expressed. However, in other B-cell lymphoid neoplasias, its aberrant expression in tumor cells has been described. For this reason, we stained samples with both CD20 (yellow) and CD70 (red) and confirmed CD70 is up-regulated in tumor cells from patients who eventually relapse. (Figure 2A) Remarkably, the relapse patients have a superior, non-overlapping

MATERIAL, METHODS AND RESULTS

range compared to NR patients (38-95% in relapse group vs 3-32% in NR group) (**Figure 2B**), which is reflected in a high difference in the survival analysis based on PFS ($p<0.0001$). (**Figure 2C**). These data led us to anticipate an over-activation of the CD27/CD70 axis. Even though we did not find differences in CD27 RNA levels, FL-LN is very heterogeneous and there are evidences that, in FL, it is also related to increased risk of transformation.(41)(42) When looking at protein expression in CD20+ population, we found an increase in terms of positivity in the Relapse group. (mean=44.2% in Rel and 24.3% in NR) (**Figure 2D, 2E**), and CD27^{high} patients have a shorter PFS (**Figure 2F**).

CD70 is also expressed in T cells from FL-TME, and display higher levels in Relapse patients

Furthermore, given the fact CD70 role has also been highlighted in FL-TME, we used mIF technique to decipher CD70 expression among T cells. To obtain a full and accurate picture of CD70 and CD27 expression across the different subtypes of T cells, we built a six-color panel including CD4, CD8, FOXP3, CXCR5, CD27 and CD70. (**Figure 3A, S3A**) As expected, CD4+ cells are more abundant in FL-LN than CD8+ cells. Moreover, we found a tendency of lower numbers of CD8+ cells in Relapse patients, indicating a lower cytotoxic response, while no differences were observed in CD4+ cells (data not shown). Remarkably, a higher protein expression of CD70 in both populations has been observed in the relapse group. (**Figure 3B**) In any case, CD70 expression in T cells is manifestly lower compared to B cells, as may be observed in **Figure S3B**.

Within CD4+ cells, we are able to distinguish T follicular helper (TFH) cells, characterized by CXCR5+FOXP3- cells, as well as T regulatory (Treg) cells, defined by expression of the transcription factor FOXP3, including the subset of T follicular regulatory (TFR) cells (double positive for CXCR5 and FOXP3). Notably, TFH, Treg and T helper non-follicular (Th non-follicular, CXCR5-FOXP3-) cells in relapse patients have higher expression of CD70, being TFH the population with a more pronounced rise. (**Figures 3B, S3B, S3C**) As for TFR, it was the only population analyzed which maintained low levels in both groups of patients. (**Figure S3C**) In the same line, CD70^{high} expression in all T-cell populations were related to a lower PFS except for TFR. (**Figures 3C, S3C**)

MATERIAL, METHODS AND RESULTS

380 To complete our analysis, we described CD27 expression in the different T-cell populations across FL-
381 LN. CD27 is known to be a costimulatory molecule and a naïve T-cell marker, which is lost after antigen
382 contact.(43) As expected, and according to RNA data, CD27 is expressed at high levels in T cells, but
383 its expression is very variable among subpopulations. (Figure S3B) In CD8+ cells, Relapse patients had
384 a lower percentage of CD27+ cells and high levels significantly correlate with good prognosis, thus
385 indicating cytotoxic T cells (CTL) with lower CD27 could have less proliferative capacity. On the other
386 hand, we did not appreciate differences within CD4+ cells. (Figure 3B, 3C)
387 As done for CD70, we analyzed CD27 expression in the different CD4+ subpopulations. While TFH cells
388 in relapse group have higher CD27 protein levels and CD27^{high} patients have a remarkably shorter PFS,
389 its expression is diminished in Th non-follicular cells and patients with CD27^{low} have a worse survival.
390 (Figures 3B, 3C and S3D) The different pattern of expression could be explained by the different role
391 of each population. Differences in CD27 expression were not detected in Treg neither TFR cells, but
392 we could confirm Treg cells in FL-LN express high levels of CD27. (Figures 3B, 3C and S3D)
393 Overall, we could assess an up-regulation of CD70 in both B and T cells, while CD27 is also increased
394 in B cells but has a heterogeneous pattern in T cells. (Figure S3B) Although in this analysis we have
395 represented the percentage of positive cells for each marker, we also examined the density of positive
396 cells and similar results were found in both CD70 and CD27. (Figure S3E, S3F) Finally, as in RNA analysis
397 we described a correlation of *CD70* with cytokines described as Treg chemoattractant (CCL20, CCL22)
398 (Figure S1D, S1E), we investigated a link between CD70 and Treg in FFPE samples. Intriguingly,
399 CD4+FOXP3+ cells are more abundant in patients who relapse ($p = 0.12$, data not shown). Besides, the
400 density of CD20+CD70+ cells correlates with Treg density, with a promising coefficient of correlation
401 ($R = 0.44$) and close to statistical significance ($p = 0.059$). (Figure S3G)

402

403 CD70 expression in B cells induce higher levels of CD70 in T cells

404 Using multiplex immunofluorescence we could determine CD70 expression occurs mainly in B cells.
405 (Figure S3B) Therefore, we further focused on the effect of this aberrant expression in the malignant

MATERIAL, METHODS AND RESULTS

cells. First, we analyzed the correlation scores between CD70+ in B cells with CD70 or CD27 in the different populations analyzed. **(Figure S4A)** The percentage of CD70+ cells within tumor population significantly correlates with CD70+ in CD8+ cells ($R = 0.51$) and CD4+ cells ($R = 0.51$), including TFH cells ($R = 0.58$) **(Figure S4B)**, but the higher scores were found in the correlation with CD27+ in CD20+ cells ($R = 0.68$) and in TFH cells ($R = 0.68$). **(Figure S4C)** Strikingly, a negative correlation between CD70+ in CD20+ cells and CD27+ in CD4+ Th non-follicular was found ($R = -0.46$) **(Figure S4C)** and, in lower levels, to CD8+ cells ($R = -0.32$).

Willing to confirm the results observed in FFPE samples, we generated by CRISPR/Cas9 technology two FL-derived cell lines CD70-KO, WSU-FSCCL and SC-1, which are highly positive for CD70. **(Figure S5A)** WSU-FSCCL and SC-1 were transfected by electroporation with either a non-targeting control guide (gCtrl) or a guide targeting CD70 (gCD70). A complex between each guide with a tracrRNA conjugated with ATTO-550 fluorochrome was used as a positive control of electroporation. **(Figure S5B)** 7 days after electroporation, almost all gCD70 cells had lost CD70 expression, while gCtrl did not alter the protein compared to untransfected (UNT) condition. **(Figure 4A)** Then, cells were sorted out to get a CD70+ cell line (from gCtrl) and a CD70-KO cell line (from gCD70). After cryopreservation and posterior thawing, we demonstrated we have achieved CD70- stable cell lines at both cell membrane **(Figure 4B)** and intracellular compartments. **(Figure S5C)**

Despite both cell lines are mainly negative for CD27 expression, after CD70 knocking-out in SC-1 cells, CD27 could be detected and increased over time. **(Figure S5D, S5F)** Thus, the CD70-KO cell line we generated has a notable expression of CD27, with around half of the cells expressing CD27. On the contrary, this phenomenon was not observed in WSU-FSCCL, which remained CD27 negative. **(Figure 4B)** As CD27 is easily cleaved from the cell membrane, we checked supernatant concentrations in wild-type cells and detected a remarkably higher soluble CD27 (sCD27) in SC-1 than in WSU-FSCCL, indicating SC-1 cell line express CD27 but is not maintained in the cell membrane. **(Figure S5E)**

After co-culturing T cells from healthy donors' PBMCs with CD70+ or CD70- FL cell lines, we analyzed CD27 and CD70 levels in T cells. Importantly, T cells were activated with anti-CD3/CD28 stimuli, so a

fraction of them express CD70 without the addition of tumor cells (**Figure 4C**, condition “none”). Remarkably, when they are co-cultured with a CD70+ cell line, the expression of CD70 in both CD4+ and CD8+ T cells is highly up-regulated, as it has been observed in patient samples. On the opposite, when the FL cell do not express CD70, these increased does not occur, indicating a CD70-specific effect. (**Figure 4C**) Regarding CD27, after the activation, T cells maintained a high percentage of positivity. This expression was dampened when T cells are cultured with CD70+ FL cells but not with CD70- FL cells. (**Figure 4D**) A plausible explanation is that CD70, when binds CD27, can cause its cleavage from the membrane. To check this hypothesis, we analyzed sCD27 protein in the supernatant and found they are diminished when the co-culture is done with the CD70- FL cell line. (**Figure S5G**) Overall, we could recapitulate the increase of CD70 and decrease of CD27 expression observed by multiplex immunofluorescence in CD8+ and CD4+ Th non-follicular cells. Finally, we assessed CD70 and CD27 expression in B cells to check CD70-KO cells maintained the null expression of CD70 along the culture, while CD27 was found in SC-1 CD70-KO cells but also decreased after co-culture with T cells. (**Figure S5H**)

446

CD70 expression is related to B cell proliferation in primary FL samples

CRISPR/Cas9 electroporation-based assay was also applied to primary FL samples, as previously it has been demonstrated to be useful in other B-cell malignancies, including chronic lymphocytic leukemia (CLL) and mantle cell lymphoma (MCL).(34)

After stimulating during 4 days primary FL samples using the follicular dendritic cell line YK6 expressing CD40L and IL21 (YK6-CD40L-IL21) and supplemented with IL-4 and IL-15 cytokines, reproducing proliferation conditions previously described,(36) we analyzed CD70 expression and proliferation. Interestingly, CD70+ cells had a higher percentage of cells in S phase (EdU+) than CD70- population. (**Figure 5E**)

Then, four days after electroporation, CD70 expression in B cells was effectively knocked-down, even though, as expected, this decrease was patient-dependent. (**Figure 4E, S5I**) CD70 also diminished in T

MATERIAL, METHODS AND RESULTS

cells, while CD27 expression was slightly increased. (Figure 55I) Intriguingly, genetically-edited FL samples showed a lower percentage of proliferation in B-cell population and a lower B-cell count. Furthermore, soluble CD27 levels were also reduced. (Figures 4G and 55J) In conclusion, this experimental validation supports an oncogenic role of CD70 in FL biology and reinforces its therapeutic intervention.

463

A truncated ligand-based CAR-T targeting CD70 has a high anti-lymphoma efficacy and may be combined with CD19 CAR-T to obtain a novel dual CAR-T

Anti-CD19 chimeric antigen receptor (CAR) T cells have revolutionized the treatment of B-cell lymphoma. Nevertheless, a fraction of patients does not have durable responses and a fraction of them experience CD19 loss-of-antigen relapse.(44) As we demonstrated that CD70 is highly expressed in tumor cells in patients that relapse, we hypothesized CD70 could represent a promising target for CAR-T therapy in follicular lymphoma, especially in the context of a dual CD19-CD70 CAR-T.

First, we investigated which construct, as a single anti-CD70 CAR-T, performed better against follicular lymphoma cells. In our approach, we have designed two ligand-based CAR-T using its natural ligand, CD27, and a single-chain variable fragment (scFv) based construct. About the ligand-based CAR-Ts, one of them had the sequence to encode the complete extracellular domain (ECD) of CD27 (CD27-ECD), while the other represented a truncated version (trCD27-ECD). Finally, an approved, academic anti-CD19 CAR-T product (ARI-0001) was included in the comparison. (Figure 5A)

T cells from healthy donors' PBMCs were activated and transduced with the corresponding lentiviral vectors and expanded for ten days. After that period, population doublings were calculated, and only scFv-based CAR-Ts but not ligand-based CAR-Ts had a lower T-cell expansion compared to untransduced (UTD) cells. In addition, CD70-scFv had a poorer expansion compared to ARI-0001. (Figure 5B)

ARI-0001 and CD70-scFv were successfully detected by flow cytometry using recombinant human proteins; however, ligand-based CAR-Ts represents a limitation as T cells also express CD27 protein in

MATERIAL, METHODS AND RESULTS

484 abundance. An arbitrary gate of “CD27^{high}” was determined by using CD27 expression in UTD cells, and
485 results indicate trCD27 had a superior expression of CD27 in membrane compared to CD27-ECD.
486 (Figure S6A) As CD27 is easily cleaved from the membrane, we checked sCD27 levels in supernatants
487 of CAR-Ts at the end of the expansion, and assessed CD27-ECD, but not trCD27-ECD was released at
488 high quantity. (Figure S6B)

489 Then, cytotoxicity experiments were performed using the single CAR-Ts. First, short-term, luciferine-
490 based assays at 24h using K562 cell line, which in wild-type condition is negative for CD19 and CD70,
491 was used. In addition, K562 was transduced with luciferase and was modified to over-express CD19
492 and/or CD70, to be used as an artificial antigen presenting cell. CAR-Ts were co-cultured with the four
493 different versions of K562 (WT, CD19, CD70, CD19-CD70) at different effector to target (E:T) ratios
494 (3:1, 1:1, 1:3). (Figures 5C and S6C) While in K562-WT cells we did not detect a significant killing by
495 any CAR-T, ARI-0001 could efficiently deplete K562-CD19 cells, and the different anti-CD70 CAR-Ts had
496 a cytotoxic effect on K562-CD70 cells. (Figure S6C) Importantly, trCD27-ECD had a superior activity on
497 both K562-CD70 and K562-CD19-CD70 cells than the other anti-CD70 CAR-Ts, showing a similar
498 efficacy than ARI-0001 when co-cultured with K562 expressing both antigens. (Figures 5C and S6C)

499 Moreover, IL-2 concentration was analyzed in supernatants after 24h of culture at 3:1 ratio, and
500 trCD27-ECD released higher cytokine levels than CD70-scFv and CD27-ECD; however, in a lower
501 amount than ARI-001. (Figure 5D)

502 Then, long-term assays were performed by co-culturing CD19+CD70+ FL cell lines with low E:T ratios
503 of CAR-T cells. WSU-FSCCL was found to be the most sensitive one to CAR-T therapy; thus, a 1:8 ratio
504 was performed. A high specific killing was found with ARI-0001, but also with trCD27-ECD and CD70-
505 scFv constructs, while it was lower in CD27-ECD. However, T-cell proliferation was higher in trCD27
506 than other CD70-targeting CAR-Ts, which was also reflected in a cell proportion (tumor B cells vs CAR-
507 T cells) completely polarized to CD3+ cells. (Figure 5E) Similar results were found in other two cell
508 lines: SC-1 and WSU-NHL, in 1:4 ratios. In SC-1 cells, ARI-0001 completely depleted B cells, while
509 trCD27-ECD was quite close, while the other anti-CD70 CAR-T failed to control tumor cells. (Figure S6E,

MATERIAL, METHODS AND RESULTS

upper and middle panels) Finally, WSU-NHL cells were more resistant to CAR-T cells, including to ARI-0001. As shown in other cell lines, trCD27-ECD had inferior results than ARI-0001 but were superior than CD27-ECD and CD70-scFv. (Figure S6E, lower panel) Overall, we considered that trCD27-ECD was the construct that performed better, so it has been further utilized to achieve a dual CD19-CD70 CAR-T.

To optimize a cotransduction (cotrans)-based dual CAR-T product, different ARI-0001 : trCD27 ratios have been used. As also observed in ARI-0003, a cotrans-based dual CAR-T containing ARI-0001(45) ARI-0001 expression was dampened when it was cotransduced with trCD27-ECD. On the opposite, CD27 expression was quite maintained in cotrans compared to single CAR-T. By maintaining a fixed MOI 2 at ARI-0001, in which we achieve a 50% of CAR-T expression, we added trCD27-ECD at different 1:2 dilutions, from MOI 0.125 to MOI 4. Importantly, presence of trCD27 lentivirus, including the lower ratios, led to a lower ARI-0001 expression. Altogether, we determined MOI of trCD27-ECD at 0.5 maintains ARI-0001 positivity at reasonable levels and could be used to develop a dual CAR-T product. (Figure 5F)

DISCUSSION

B-cell non-Hodgkin lymphoma are a group of lymphoid malignancies that develop from mature B cells within the secondary lymphoid organs, mainly the lymph nodes. The introduction of rituximab, the first-in-class anti-CD20 antibody, revolutionized B-NHL treatment and, although there are some differences in the treatment of the different entities, standard treatment is mostly based on combination of rituximab and chemotherapy, known as immunochemotherapy.(2) In the recent years, the advances on identifying the genomic and molecular features of each lymphoma enabled the development of targeted therapies that have broaden the therapeutical repertoire (e.g.: anti-EZH2 tazemetostat in follicular lymphoma).(46)(47) Finally, we have to highlight the introduction of CAR-T cell therapies, which induce high rates of overall response.(44)

In our work, we focused on follicular lymphoma, which represents the most common indolent B-NHL subtype. FL development is a long process in which B cells resistant to apoptosis (due to the overexpression of BCL-2 protein caused by translocation t(14;18) in the bone marrow) acquire additional genetic mutations in the germinal center of the lymph nodes.(48) Nevertheless, there is the need of a permissive tumoral microenvironment that supports FL growth.(10) In this frame, FL-TME is very heterogeneous and include immune and non-immune cells;(11) thus, the study of both tumor cells and TME is necessary to compile FL complexity.

First, we analyzed RNA expression of >700 immune-related genes in full lysates FFPE biopsies from FL patients at diagnose from a homogeneous cohort. Despite the fact that a single-center series could have limitations and may require validation in other cohorts, there are also some advantages: i) patients were diagnosed following the same clinico-pathological criteria, ii) all patients were homogeneously treated with ICT (100% patients received CHOP as a 1st-line chemotherapy), and iii) during the follow-up period patients that suffered a histological transformation were excluded. Our analysis assessed a differential immune pattern between a group of patients that relapse and a group that never relapsed, with a very prolonged follow-up time. These differences revealed 31 differentially

MATERIAL, METHODS AND RESULTS

551 expressed genes (representing a 4.2% of studied genes) and a differential enrichment of biological
552 pathways (**Figure 1A-D**). One of the up-regulated genes in the relapse group is *CD70*, which was also
553 associated, close to statistical significance, to a shorter progression-free survival (**Figure 1C, 1D**).
554 Moreover, we have depicted that patients with high *CD70* RNA levels use to have a lower number of
555 mutations (**Figure S2**). Therefore, CD70 could constitute a pro-oncogenic mechanism that bypasses
556 the need of B lymphocytes to acquire additional mutations in order to develop an overt disease.
557 Lately, CD70 has drawn attention on the context of cancer. In solid cancers, there are evidences that
558 is deregulated in pancreatic, renal, lung or colon, among others. In a recent study by Nilsson *et al*, an
559 interesting association to epithelial to mesenchymal transition was described.(49) In hematologic
560 tumors, it has been deeply studied in acute myeloblastic leukemia (AML) as leukemia stem cells highly
561 express CD70. Besides, a pro-oncogenic role has been assessed in B-cell malignancies(50) including FL,
562 (51) (52) DLBCL (319), MCL (37) and CLL (18) (53). Moreover, CD27/CD70 axis has been linked to
563 diverse mechanisms of TME modulation in lymphoma. (21) (54) (23)
564 Our results clearly indicate that CD70 is more prevalent in the tumor fraction and abundantly
565 expressed on patients that relapse. Importantly, its association with survival is more pronounced than
566 in whole lysate RNA, thus having a more prognostic significance (**Figures 2, S3B**). CD70 from the tumor
567 could bind to CD27-expressing cells, including T regulatory cells, which are highly positive for
568 CD27.(55) (56) Furthermore, it was previously described that CD70+ B-NHL cells induce FOXP3
569 expression. (21) Gene expression analysis also correlated CD70 expression with cytokines responsible
570 for Treg chemoattraction (CCL20, CCL22)(38) (39) and IRF4, linked to a higher risk of transformation.(4)
571 (**Figure S1D, F**). Finally, a positive correlation was found between the density of CD20+CD70+ cells
572 with the abundance of Treg in FL-LN biopsies. (**Figure S3G**)
573 The diminished CD27 in CD8+ and CD4+ T helper non-follicular cells may be related to a lower T-cell
574 anti-tumoral response (317) and induced by a CD70-dependent cleavage. *In vitro* experiments using
575 FL CD70-KO cells point out to this phenomenon (**Figure 4 C,D**). Furthermore, the up-regulation of CD27
576 in B cells, usually linked to a memory-like phenotype suggest CD70+ and CD27+ tumor cells mutually

577 interact. Historically, FL cells have been defined to be frozen in a GC state; however, single-cell analysis
 578 revealed distinct cell states co-exist(57) and memory-like features have been linked to a higher risk of
 579 transformation.(41)(42)

580 While most of the studies focus on the significance of CD70 over-expression on the tumor fraction,
 581 we also interrogated its expression in the T cells from the FL-TME. Intriguingly, all T-cell populations
 582 analyzed except TFR cells showed higher CD70 protein levels in patients that relapse. We validated
 583 the co-culture of T cells with CD70+ FL cell lines, but not CD70 knocked out cells, induced higher CD70
 584 levels (**Figure 4C**), pointing out to a CD70-dependent regulation. CD27 down-stream signaling
 585 activates NF- κ B and JNK, and CD70 promoter is enriched in binding sites for NF- κ B and c-Jun
 586 transcription factors.(58) Whether this positive feedback mechanism could also happen between
 587 tumor cells remains to be confirmed.

588 Tumor CD70+ cells not only are capable to induce tumor-promoting effects in other B cells or T cells
 589 from the TME, but also receive signals from CD27+ cells or soluble CD27. Notably, activation of CD70
 590 leads to MEK and Akt phosphorylation.(17) Overall, the pathogenic mechanisms in which CD70
 591 participates are complex and diverse, and include tumor and non-tumor cells. In this work, we adapted
 592 a CRISPR/Cas9 protocol developed to genetically modify B-cell lymphoid malignancies(34) by using
 593 FDC-derived YK6 cells mimicking germinal center stimuli(35) (36) and achieve a significant reduction
 594 of CD70 protein levels, which was related to lower B-cell proliferation. (**Figure 4 F,G**)

595 After validating CD70 as an increased protein in FL patients that relapse, together with a biological
 596 validation of the target, we proposed the generation of a dual CAR-T cell that can target CD19 and
 597 CD70. Although anti-CD19 CAR-Ts have improved the management of high-risk lymphoma patients,
 598 still a relevant portion of them have limited, non-durable responses.(44) Moreover, CD19-CAR-T
 599 relapse has been described, indicating antigen loss as a mechanism of evasion.(44) (59) For this
 600 reason, dual CAR-T cells have been proposed as a therapeutic strategy to avoid antigen escape or to
 601 treat relapsed CAR-T patients that lost CD19 expression. To date, only single anti-CD70 CAR-Ts or CAR-

MATERIAL, METHODS AND RESULTS

602 NK have been explored (NCT04429438) (NCT04502446), apart from the coadministration of a CD19
603 and a CD70 CAR-T.(60) (NCT04429438)

604 We first investigated the best construct to deplete CD70+ lymphoma cells as a single CAR-T. Two
605 ligand-based and a scFv-based CAR-T were used and compared to ARI-0001, an approved academic
606 product from our institution.(61) We validated ligand-based CAR-Ts using CD27 expanded better.
607 However, CD27-ECD lost expression on the membrane and was released into the supernatant, which
608 did not occur in trCD27-ECD as described in Leick *et al.*(30) (**Figure 5 A,B**) Although it has been
609 envisioned that ligand-based could have benefits compared to scFv-based CAR-Ts,(62) this cleavage
610 issue has also been described in (334). Despite having pros and cons regarding the use of ligand-based
611 CAR-Ts, cytotoxicity experiments demonstrated trCD27 was the most effective anti-CD70 CAR-T.
612 (**Figures 5C,E S6C,E**) and released higher IL-2 cytokine. (**Figures 5D, S6D**) In conclusion, trCD27-ECD is
613 a promising anti-CD70 CAR-T with high anti-lymphoma effect.

614 In addition, we generated a dual CD19-CD70 CAR-T using a co-transduction strategy, as done with ARI-
615 0003, a dual CAR-T combining CD19 (ARI-0001) and BCMA (ARI-0002).(45) Importantly, the
616 combination of both viruses led to a lower ARI-0001 expression compared to the single
617 transduction, while CD27 remained stable. (**Figure 5F**) Therefore, we optimized the ARI-0001 : trCD27
618 ratio, and determined a MOI 2 for ARI-0001 and MOI 0.5 for trCD27-ECD as the optimal.

619 Nevertheless, the fact that T cells can also express CD70, although in low levels, could constitute a
620 limitation on anti-CD70 CAR-T therapies. Although we did not find a diminished T-cell expansion during
621 CAR-T generation, we observed loss of CD70 expression (data not shown). Some recent works
622 knocked-out CD70 expression in T cells during CAR-T expansion, including clinical trials with a
623 genetically modified, allogenic anti-CD70 CAR-T, with published results in clear-cell renal
624 carcinoma.(63) Probably, by applying this strategy to our construct, a higher T-cell proliferation and
625 improved long-term cytotoxicity efficacy could be achieved.

626 To sum up, we found that FL patients that relapse have at the diagnose higher CD70 expression, at
627 both RNA and protein level. CD70 is mainly expressed in tumor B cells, but is also up-regulated in T

628 cells from the TME. These findings reinforce the development of CD70-targeting CAR-T cells and
629 anticipate a high anti-lymphoma activity of a dual CD19-CD70 CAR-T.

630

631 **ACKNOWLEDGEMENTS**

632 We thank the IDIBAPS genomics facility for gene expression data generation and the IDIBAPS Flow
633 Cytometry and Cell Sorting Core facility. We are indebted to the HCB-IDIBAPS Biobank, integrated in
634 the Spanish National Biobanks Network, for the biological human samples and data procurement. This
635 work was carried out at the Esther Koplowitz Center, Barcelona.

636 This work was part of Fundació la Marató TV3- (TAIFOL project , ref 201933-30) to PP-G and the
637 Follicular Lymphoma Foundation. Grants that contributed to this work included: CIBERONC
638 (CB16/12/00334 to DC and CB16/12/00225 to EC and finally Generalitat de Catalunya support for
639 AGAUR 2021-SGR-01294 to PP-G.

640

641

642

643

644

645

646

647

MATERIAL, METHODS AND RESULTS

648 BIBLIOGRAPHY

- 649 1. Rosenquist R, Beà S, Du MQ, Nadel B, Pan-Hammarström Q. Genetic landscape and
650 deregulated pathways in B-cell lymphoid malignancies. *J Intern Med.* 2017;282(5):371–94.
- 651 2. Sarkozy C, Maurer MJ, Link BK, Ghesquieres H, Nicolas E, Thompson CA, et al. Cause of death
652 in follicular lymphoma in the first decade of the rituximab era: A pooled analysis of French and
653 US cohorts. *Journal of Clinical Oncology.* 2019;37(2):144–52.
- 654 3. Casulo C, Dixon JG, Le-Rademacher J, Hoster E, Hochster HS, Hiddemann W, et al. Validation of
655 POD24 as a robust early clinical end point of poor survival in FL from 5225 patients on 13 clinical
656 trials. *Blood.* 2022;139(11):1684–93.
- 657 4. Kridel R, Mottok A, Farinha P, Ben-Neriah S, Ennishi D, Zheng Y, et al. Cell of origin of
658 transformed follicular lymphoma. *Blood [Internet].* 2015;126(18):2118–27. Available from:
659 <http://ashpublications.org/blood/article-pdf/126/18/2118/1389627/2118.pdf>
- 660 5. Federico M, Caballero Barrigón MD, Marcheselli L, Tarantino V, Manni M, Sarkozy C, et al.
661 Rituximab and the risk of transformation of follicular lymphoma: a retrospective pooled
662 analysis. *Lancet Haematol.* 2018 Aug;5(8):e359–67.
- 663 6. Kumar E, Pickard L, Okosun J. Pathogenesis of follicular lymphoma: genetics to the
664 microenvironment to clinical translation. Vol. 194, *British Journal of Haematology.* John Wiley
665 and Sons Inc; 2021. p. 810–21.
- 666 7. Gordon MJ, Smith MR, Nastoupil LJ. Follicular lymphoma: The long and winding road leading
667 to your cure? Vol. 57, *Blood Reviews.* Churchill Livingstone; 2023.
- 668 8. Qu X, Li H, Braziel RM, Passerini V, Rimsza LM, Hsi ED, et al. Genomic alterations important for
669 the prognosis in patients with follicular lymphoma treated in SWOG study S0016. *Blood*
670 *[Internet].* 2019 Jan 3;133(1):81–93. Available from:
671 <http://www.ncbi.nlm.nih.gov/pubmed/30446494>
- 672 9. Dave SS, Wright G, Tan B, Rosenwald A, Gascoyne RD, Chan WC, et al. Prediction of Survival in
673 Follicular Lymphoma Based on Molecular Features of Tumor-Infiltrating Immune Cells. *New*

- 674 England Journal of Medicine [Internet]. 2004 Nov 18;351(21):2159–69. Available from:
675 <http://www.nejm.org/doi/abs/10.1056/NEJMoa041869>
- 676 10. Laurent C, Dietrich S, Tarte K. Cell cross talk within the lymphoma tumor microenvironment:
677 follicular lymphoma as a paradigm. *Blood*. 2024 Mar 21;143(12):1080–90.
- 678 11. Dobaño-lópez C, Araujo-ayala F, Serrat N, Valero JG, Pérez-galán P. Follicular lymphoma
679 microenvironment: An intricate network ready for therapeutic intervention. *Cancers (Basel)*.
680 2021;13(4):1–22.
- 681 12. Goodwin RG, Alderson MR, Smith CA, Armitage RJ, VandenBos T, Jerzy R, et al. Molecular and
682 biological characterization of a ligand for CD27 defines a new family of cytokines with
683 homology to tumor necrosis factor. *Cell*. 1993 May 7;73(3):447–56.
- 684 13. Bowman MR, Crimmins MA, Yetz-Aldape J, Kriz R, Kelleher K, Herrmann S. The cloning of CD70
685 and its identification as the ligand for CD27. *J Immunol*. 1994 Feb 15;152(4):1756–61.
- 686 14. Hintzen RQ, Lens SM, Lammers K, Kuiper H, Beckmann MP, van Lier RA. Engagement of CD27
687 with its ligand CD70 provides a second signal for T cell activation. *J Immunol*. 1995 Mar
688 15;154(6):2612–23.
- 689 15. Hendriks J, Gravestein LA, Tesselaar K, van Lier RA, Schumacher TN, Borst J. CD27 is required
690 for generation and long-term maintenance of T cell immunity. *Nat Immunol [Internet]*. 2000
691 Nov;1(5):433–40. Available from: <http://www.ncbi.nlm.nih.gov/pubmed/11062504>
- 692 16. Arens R, Tesselaar K, Baars PA, van Schijndel GM, Hendriks J, Pals ST, et al. Constitutive
693 CD27/CD70 interaction induces expansion of effector-type T cells and results in IFNgamma-
694 mediated B cell depletion. *Immunity [Internet]*. 2001 Nov;15(5):801–12. Available from:
695 <http://www.ncbi.nlm.nih.gov/pubmed/11728341>
- 696 17. Arens R, Nolte MA, Tesselaar K, Heemskerk B, Reedquist KA, van Lier RAW, et al. Signaling
697 through CD70 Regulates B Cell Activation and IgG Production. *The Journal of Immunology*.
698 2004;173(6):3901–8.

MATERIAL, METHODS AND RESULTS

- 699 18. Ranheim EA, Cantwell MJ, Kipps TJ. Expression of CD27 and its ligand, CD70, on chronic
700 lymphocytic leukemia B cells. *Blood* [Internet]. 1995 Jun 15;85(12):3556–65. Available from:
701 <http://www.ncbi.nlm.nih.gov/pubmed/7540066>
- 702 19. Zhou Y, Liu X, Xu L, Tseng H, Cao Y, Jiang J, et al. Matrix metalloproteinase-8 is overexpressed
703 in Waldenström's macroglobulinemia cells, and specific inhibition of this metalloproteinase
704 blocks release of soluble CD27. *Clin Lymphoma Myeloma Leuk*. 2011 Feb;11(1):172–5.
- 705 20. Flieswasser T, Van den Eynde A, Van Audenaerde J, De Waele J, Lardon F, Riether C, et al. The
706 CD70-CD27 axis in oncology: the new kids on the block. *Journal of Experimental and Clinical*
707 *Cancer Research* [Internet]. 2022;41(1):1–15. Available from: [https://doi.org/10.1186/s13046-](https://doi.org/10.1186/s13046-021-02215-y)
708 [021-02215-y](https://doi.org/10.1186/s13046-021-02215-y)
- 709 21. Yang ZZ, Novak AJ, Ziesmer SC, Witzig TE, Ansell SM. CD70+ non-Hodgkin lymphoma B cells
710 induce Foxp3 expression and regulatory function in intratumoral CD4+CD25- T cells. *Blood*.
711 2007;110(7):2537–44.
- 712 22. Yang ZZ, Novak AJ, Ziesmer SC, Witzig TE, Ansell SM. Malignant B cells skew the balance of
713 regulatory T cells and T H17 cells in B-cell non-Hodgkin's lymphoma. *Cancer Res*.
714 2009;69(13):5522–30.
- 715 23. Yang ZZ, Grote DM, Xiu B, Ziesmer SC, Price-Troska TL, Hodge LS, et al. TGF- β upregulates CD70
716 expression and induces exhaustion of effector memory T cells in B-cell non-Hodgkin's
717 lymphoma. *Leukemia*. 2014;28(9):1872–84.
- 718 24. Mozas P, López C, Grau M, Nadeu F, Clot G, Valle S, et al. Genomic landscape of follicular
719 lymphoma across a wide spectrum of clinical behaviors. *Hematol Oncol*. 2023 Oct 1;41(4):631–
720 43.
- 721 25. Nadeu F, Delgado J, Royo C, Baumann T, Stankovic T, Pinyol M, et al. Clinical impact of clonal
722 and subclonal TP53, SF3B1, BIRC3, NOTCH1, and ATM mutations in chronic lymphocytic
723 leukemia. *Blood* [Internet]. 2016;127(17):2122–30. Available from: <https://www>.

26. Rivas-Delgado A, Nadeu F, Enjuanes A, Casanueva-Eliceiry S, Mozas P, Magnano L, et al. Mutational landscape and tumor burden assessed by cell-free DNA in diffuse large B-cell lymphoma in a population-based study. *Clinical Cancer Research*. 2021 Jan 15;27(2):513–21.
27. Cesano A. nCounter® PanCancer Immune Profiling Panel (NanoString Technologies, Inc., Seattle, WA). *J Immunother Cancer*. 2015 Dec 15;3(1).
28. Subramanian A, Tamayo P, Mootha VK, Mukherjee S, Ebert BL, Gillette MA, et al. Gene set enrichment analysis: A knowledge-based approach for interpreting genome-wide expression profiles. *Proc Natl Acad Sci U S A*. 2005;102(43):15545–50.
29. Castella M, Boronat A, Martín-Ibáñez R, Rodríguez V, Suñé G, Caballero M, et al. Development of a Novel Anti-CD19 Chimeric Antigen Receptor: A Paradigm for an Affordable CAR T Cell Production at Academic Institutions. *Mol Ther Methods Clin Dev*. 2019 Mar 15;12:134–44.
30. Leick MB, Silva H, Scarfò I, Larson R, Choi BD, Bouffard AA, et al. Non-cleavable hinge enhances avidity and expansion of CAR-T cells for acute myeloid leukemia. *Cancer Cell*. 2022 May 9;40(5):494–508.e5.
31. Sauer T, Parikh K, Sharma S, Omer B, Sedloev D, Chen Q, et al. CD70-specific CAR T cells have potent activity against acute myeloid leukemia without HSC toxicity. *Blood*. 2021;138(4):318–30.
32. Guedan S, Chen X, Madar A, Carpenito C, McGettigan SE, Frigault MJ, et al. ICOS-based chimeric antigen receptors program bipolar TH17/ TH1 cells. *Blood*. 2014 Aug 14;124(7):1070–80.
33. Calderon H, Mamonkin M, Guedan S. Analysis of CAR-Mediated Tonic Signaling. *Methods Mol Biol* [Internet]. 2020;2086:223–36. Available from: <http://www.ncbi.nlm.nih.gov/pubmed/31707680>
34. Mateos-Jaimez J, Mangolini M, Vidal A, Kulis M, Colomer D, Campo E, et al. Robust CRISPR-Cas9 Genetic Editing of Primary Chronic Lymphocytic Leukemia and Mantle Cell Lymphoma Cells. Vol. 7, *HemaSphere*. Wolters Kluwer Health; 2023. p. E909.

MATERIAL, METHODS AND RESULTS

- 749 35. Caesar R, Di Re M, Krupka JA, Gao J, Lara-Chica M, Dias JML, et al. Genetic modification of
750 primary human B cells to model high-grade lymphoma. *Nat Commun* [Internet]. 2019;10(1):1–
751 16. Available from: <http://dx.doi.org/10.1038/s41467-019-12494-x>
- 752 36. Dobaño-Lopez C, Valero JG, Araujo-Ayala F, Nadeu F, Gava F, Bezombes C, et al. Patient-derived
753 follicular lymphoma spheroids recapitulate lymph node signaling and immune profile
754 uncovering galectin-9 as a novel immunotherapeutic target. *Blood Cancer J*. 2024;
- 755 37. Balsas P, Veloza L, Clot G, Sureda-Gómez M, Rodríguez ML, Masaoutis C, et al. SOX11, CD70,
756 and Treg cells configure the tumor-immune microenvironment of aggressive mantle cell
757 lymphoma. *Blood*. 2021;138(22):2202–15.
- 758 38. Korbecki J, Kojder K, Simińska D, Bohatyrewicz R, Gutowska I, Chlubek D, et al. Cc chemokines
759 in a tumor: A review of pro-cancer and anti-cancer properties of the ligands of receptors ccr1,
760 ccr2, ccr3, and ccr4. *Int J Mol Sci*. 2020;21(21):1–29.
- 761 39. Rawal S, Chu F, Zhang M, Park HJ, Nattamai D, Kannan S, et al. Cross Talk between Follicular Th
762 Cells and Tumor Cells in Human Follicular Lymphoma Promotes Immune Evasion in the Tumor
763 Microenvironment. *The Journal of Immunology*. 2013;190(12):6681–93.
- 764 40. Han G, Deng Q, Marques-Piubelli ML, Dai E, Dang M, Ma MCJ, et al. Follicular Lymphoma
765 Microenvironment Characteristics Associated with Tumor Cell Mutations and MHC Class II
766 Expression. *Blood Cancer Discov*. 2022 Sep 1;3(5):428–43.
- 767 41. Wang X, Nissen M, Gracias D, Kusakabe M, Simkin G, Jiang A, et al. Single-cell profiling reveals
768 a memory B cell-like subtype of follicular lymphoma with increased transformation risk. *Nat*
769 *Commun*. 2022 Dec 1;13(1).
- 770 42. Perrett M, Pickard L, Kumar E, Palladino G, Khan F, Edmondson C, et al. Longitudinal Single Cell
771 Analyses Reveal the Co-Evolutionary Dynamics of the Tumor and Microenvironment
772 Accompanying Follicular Lymphoma Transformation. *Blood*. 2022 Nov 15;140(Supplement
773 1):748–9.

- 774 43. Buchan SL, Rogel A, Al-Shamkhani A. The immunobiology of CD27 and OX40 and their potential
775 as targets for cancer immunotherapy. *Blood*. 2018;131(1):39–48.
- 776 44. Hirayama A V, Gauthier J, Hay KA, Voutsinas JM, Wu Q, Pender BS, et al. Brief Report High rate
777 of durable complete remission in follicular lymphoma after CD19 CAR-T cell immunotherapy
778 [Internet]. 2019. Available from: [http://ashpublications.org/blood/article-](http://ashpublications.org/blood/article-pdf/134/7/636/1554299/bloodbld2019000905.pdf)
779 [pdf/134/7/636/1554299/bloodbld2019000905.pdf](http://ashpublications.org/blood/article-pdf/134/7/636/1554299/bloodbld2019000905.pdf)
- 780 45. Bachiller M, Dobaño-López C, Rodríguez-García A, Castellsagué J, Gimenez-Alejandro M,
781 Antónana-Vildosola A, et al. Co-Transduced CD19/BCMA Dual-Targeting CAR-T Cells for the
782 Treatment of Non-Hodgkin Lymphoma. *Blood*. 2022 Nov 15;140(Supplement 1):7386–7.
- 783 46. Italiano A, Soria JC, Toulmonde M, Michot JM, Lucchesi C, Varga A, et al. Tazemetostat, an EZH2
784 inhibitor, in relapsed or refractory B-cell non-Hodgkin lymphoma and advanced solid tumours:
785 a first-in-human, open-label, phase 1 study. *Lancet Oncol* [Internet]. 2018;19(5):649–59.
786 Available from: [http://dx.doi.org/10.1016/S1470-2045\(18\)30145-1](http://dx.doi.org/10.1016/S1470-2045(18)30145-1)
- 787 47. Morschhauser F, Tilly H, Chaidos A, McKay P, Phillips T, Assouline S, et al. Tazemetostat for
788 patients with relapsed or refractory follicular lymphoma: an open-label, single-arm,
789 multicentre, phase 2 trial. *Lancet Oncol*. 2020;21(11):1433–42.
- 790 48. Huet S, Sujobert P, Salles G. From genetics to the clinic: A translational perspective on follicular
791 lymphoma [Internet]. Vol. 18, *Nature Reviews Cancer*. Nature Publishing Group; 2018. p. 224–
792 39. Available from: <http://dx.doi.org/10.1038/nrc.2017.127>
- 793 49. Nilsson MB, Yang Y, Heeke S, Patel SA, Poteete A, Udagawa H, et al. CD70 is a therapeutic target
794 upregulated in EMT-associated EGFR tyrosine kinase inhibitor resistance. *Cancer Cell*. 2023 Feb
795 13;41(2):340-355.e6.
- 796 50. Lens SMA, Drillenburger P, Den Drijver BFA, Van Schijndel G, Pals ST, Van Lier RAW, et al. Aberrant
797 expression and reverse signalling of CD70 on malignant B cells. *Br J Haematol*.
798 1999;106(2):491–503.

MATERIAL, METHODS AND RESULTS

- 799 51. Yang ZZ, Kim HJ, Villasboas JC, Price-Troska T, Jalali S, Wu H, et al. Mass Cytometry Analysis
800 Reveals that Specific Intratumoral CD4 + T Cell Subsets Correlate with Patient Survival in
801 Follicular Lymphoma. *Cell Rep.* 2019 Feb 19;26(8):2178-2193.e3.
- 802 52. Mondello P, Fama A, Larson MC, Feldman AL, Villasboas JC, Yang ZZ, et al. Lack of intrafollicular
803 memory CD4 + T cells is predictive of early clinical failure in newly diagnosed follicular
804 lymphoma. *Blood Cancer J* [Internet]. 2021;11(7). Available from:
805 <http://dx.doi.org/10.1038/s41408-021-00521-4>
- 806 53. Goto N, Tsurumi H, Takemura M, Kanemura N, Kasahara S, Hara T, et al. Serum soluble CD27
807 level is associated with outcome in patients with diffuse large B-cell lymphoma treated with
808 rituximab, cyclophosphamide, doxorubicin, vincristine and prednisolone. *Leuk Lymphoma.*
809 2012 Aug;53(8):1494–500.
- 810 54. Yang ZZ, Novak AJ, Ziesmer SC, Witzig TE, Ansell SM. Malignant B cells skew the balance of
811 regulatory T cells and T H17 cells in B-cell non-Hodgkin's lymphoma. *Cancer Res.*
812 2009;69(13):5522–30.
- 813 55. Muth S, Klaric A, Radsak M, Schild H, Probst HC. CD27 expression on Treg cells limits immune
814 responses against tumors. *J Mol Med.* 2022 Mar 1;100(3):439–49.
- 815 56. Bowakim-Anta N, Acolty V, Azouz A, Yagita H, Leo O, Goriely S, et al. Chronic CD27-CD70
816 costimulation promotes type 1-specific polarization of effector Tregs. *Front Immunol.* 2023;14.
- 817 57. Milpied P, Cervera-Marzal I, Mollichella ML, Tesson B, Brisou G, Traverse-Glehen A, et al.
818 Human germinal center transcriptional programs are de-synchronized in B cell lymphoma. *Nat*
819 *Immunol* [Internet]. 2018;19(9):1013–24. Available from: [http://dx.doi.org/10.1038/s41590-](http://dx.doi.org/10.1038/s41590-018-0181-4)
820 018-0181-4
- 821 58. Yamamoto H, Kishimoto T, Minamoto S. NF-kappaB activation in CD27 signaling: involvement
822 of TNF receptor-associated factors in its signaling and identification of functional region of
823 CD27. *J Immunol.* 1998 Nov 1;161(9):4753–9.

- 824 59. Branella GM, Spencer HT. Natural receptor-and ligand-based chimeric antigen receptors:
825 Strategies using natural ligands and receptors for targeted cell killing. Vol. 11, Cells. MDPI;
826 2022.
- 827 60. Tu S, Zhou X, Guo Z, Huang R, Yue C, He Y, et al. CD19 and CD70 Dual-Target Chimeric Antigen
828 Receptor T-Cell Therapy for the Treatment of Relapsed and Refractory Primary Central Nervous
829 System Diffuse Large B-Cell Lymphoma. Front Oncol. 2019 Dec 4;9.
- 830 61. Ortíz-Maldonado V, Rives S, Castellà M, Alonso-Saladrigues A, Benítez-Ribas D, Caballero-
831 Baños M, et al. CART19-BE-01: A Multicenter Trial of ARI-0001 Cell Therapy in Patients with
832 CD19+ Relapsed/Refractory Malignancies. Molecular Therapy. 2021 Feb 3;29(2):636–44.
- 833 62. Ramírez-Chacón A, Betriu-Méndez S, Bartoló-Ibars A, González A, Martí M, Juan M. Ligand-
834 based CAR-T cell: Different strategies to drive T cells in future new treatments. Vol. 13,
835 Frontiers in Immunology. Frontiers Media S.A.; 2022.
- 836 63. Pal SK, Tran B, Haanen JBAG, Hurwitz ME, Sacher A, Tannir NM, et al. CD70-Targeted Allogeneic
837 CAR T-Cell Therapy for Advanced Clear Cell Renal Cell Carcinoma. Cancer Discov [Internet].
838 2024;OF1–14. Available from: <http://www.ncbi.nlm.nih.gov/pubmed/38583184>
- 839
- 840

MATERIAL, METHODS AND RESULTS

841 TABLES
842

	Total (n=32)	NR (n=12)	Rel (n=20)
Female sex, n (%)	20 (62.5)	7 (58.3)	13 (65.0)
Median age (range)	52.5 (26-78)	54 (26-74)	52 (26-78)
B-cell symptoms, n (%)	5 (15.6)	2 (16.7)	3 (15.0)
ECOG PS 2 or more, n (%)	1 (3.1)	0 (0.0)	1 (5.0)
Ann-Arbor stage III-IV, n (%)	23 (71.9)	6 (50.0)	17 (85.0)
High-risk FLIPI score (3-5), n (%)	9 (30.0)	1 (9.1)	8 (42.1)
Frontline treatment with R-CHOP, n (%)	31 (96.9)	12 (100.0)	19 (95.0)
CR rate, n (%)	28 (87.5)	12 (100.0)	16 (80.0)
Hb < 120 g/L	7 (21.9)	4 (33.3)	3 (15.0)
B2M high	14 (53.8)	2 (18.2)	12 (80.0)
LDH high	23 (82.1)	10 (90.9)	13 (76.5)

843

844 **Table 1. Summary of patients characteristics.** Clinical parameters applied in our FL cohort globally
845 (total, n=32) or by group. NR = non-relapse; Rel = relapse; ECOG = Eastern Cooperative Oncology
846 Group; FLIPI = Follicular Lymphoma International Prognostic Index; CR = complete response; Hb =
847 hemoglobin; B2M = beta-2-microglobulin; LDH = lactate dehydrogenase

848

849 FIGURE LEGENDS

850 **Figure 1. Differential immune profile between patients that will or will not relapse (A)** Volcano plot
 851 representing differentially expressed genes between relapse (Rel) and non-relapse (NR) patients. **(B)**
 852 Heatmap of differentially expressed genes between both groups, showing z-scores for each gene in
 853 individual patients. **(C and D)** Biological pathways over-represented by GSEA in the relapse **(C)** and
 854 non-relapse **(D)** group. **(E)** Box-plot representation of mRNA expression levels of *CD70* in each group,
 855 expressed in log2 from Nanostring counts, each patient is represented by a single dot. **(F)** Kaplan-
 856 meier analysis and representation of the progression-free survival (PFS) in patients classified according
 857 *CD70* status. Low and high *CD70* was determined using maxstat library in R software.

858

859 **Figure 2. CD70 and CD27 expression in FL cells (A)** multiplexed immunofluorescence (mIF)
 860 representative image from a NR and a Rel patient stained with Panel 1: CD20 in yellow, CD70 in red
 861 and DAPI (nuclei) in blue. **(B)** Percentage of CD70+ cells within CD20+ population in both groups (mean
 862 +/- sd); each patient is represented with a single dot. **(C)** Kaplan-meier survival analysis representing
 863 PFS in patients classified as CD70 low and CD70 high. **(D)** mIF representative image from a NR and a
 864 Rel patient stained with Panel 2: CD20 in yellow, CD27 in red and DAPI in blue. **(E)** Percentage of CD27+
 865 cells within CD20+ population in both groups (mean +/- sd). **(F)** Kaplan-meier survival analysis
 866 representing PFS in patients classified as CD27 low and CD27 high. T-test or Mann-Whitney U test
 867 were applied for B and E.

868

869 **Figure 3. CD70 and CD27 expression in T cells from the FL-TME (A)** multiplexed immunofluorescence
 870 (mIF) representative image from a NR and a Rel patient stained with Panel 3: CD8 in red, CD4 in yellow,
 871 FOXP3 in pink, CXCR5 in grey, CD27 in sky blue, CD70 in green and DAPI (nuclei) in blue. **(B)**
 872 Percentage of CD70+ cells (upper panels) and CD27+ cells (lower panels) within CD8+, CD4+, T follicular
 873 helper (TFH) and T regulatory (Treg) populations. T-test or Mann-Whitney U test were applied.

MATERIAL, METHODS AND RESULTS

874 (C) Kaplan-meier survival analysis representing PFS in patients classified as CD70 low and CD70 high
875 (upper panels) or CD27 low and CD27 high (lower panels) in CD8+, CD4+, TFH and Treg populations.

876

877 **Figure 4. Galectin-9 blockade improves rituximab-induced depletion in FL-PDLS. (A)** Generation of
878 CD70-KO FL cell lines WSU-FSCCL (left panel) and SC-1 (right panel). Histogram representation of CD70
879 protein after 7 days of electroporation. Cells were untransfected (UNT, grey) or transfected with a
880 non-targeting control (gCtrl, red) or with a CD70-targeting guide (gCD70, blue). **(B)** CD70 and CD27
881 protein expression in stable CD70+ (gCtrl, red) or CD70- (gCD70, blue) FL cell lines WSU-FSCCL (left
882 panel) and SC-1 (right panel). **(C)** Percentage of CD70+ cells in CD4+ (left panel) and CD8+ (right panel)
883 T cells activated with CD3/CD8 stimuli (none) and co-cultured with CD70+ or CD70- FL cell lines **(D)**
884 Percentage of CD27+ cells in CD4+ (left panel) and CD8+ (right panel) T cells activated with CD3/CD8
885 stimuli (none) and co-cultured with CD70+ or CD70- FL cell lines. **(E)** Percentage of CD20+ proliferating
886 cells (EdU+) within CD70+ or CD70- cells in FL primary samples co-cultured with 4 days with YK6-
887 CD40L-IL21 cells. Represented as mean +/- sd. **(F)** MFI ratio of CD70 expression in cells electroporated
888 with a gCtrl or a gCD70, after 4 days of electroporation. **(G)** Percentage of CD20+ proliferating cells
889 (EdU+) in FL electroporated with a gCtrl or a gCD70, after 4 days of electroporation (left panel) and
890 soluble CD27 (sCD27) levels after 4 days of electroporation. Paired t-test was applied in E, F and G.

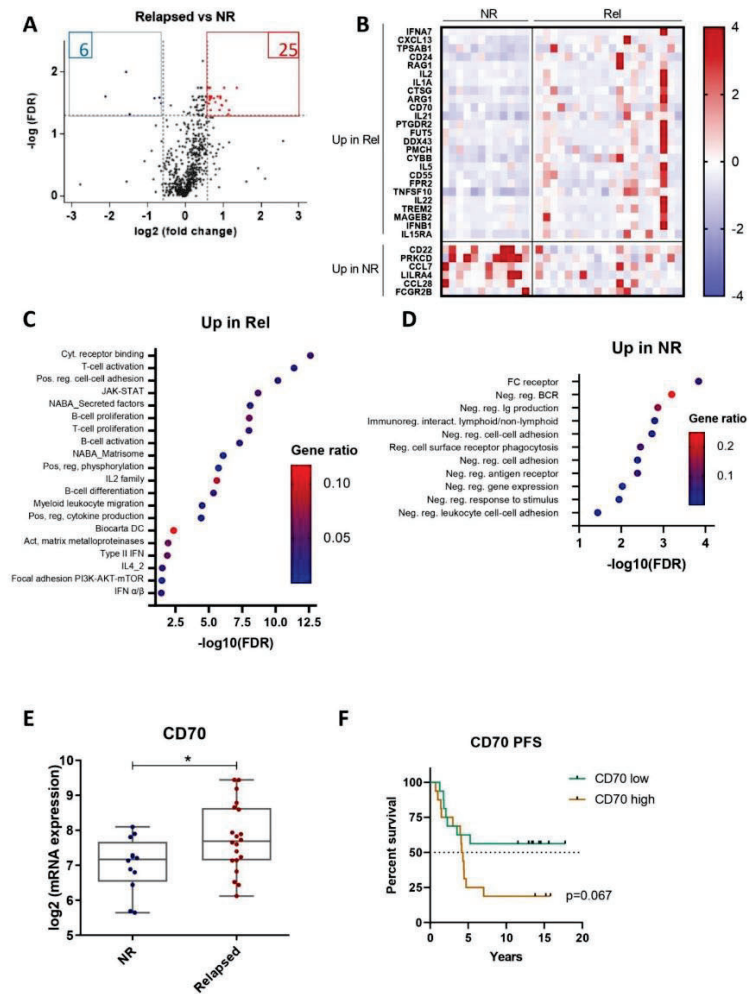
891

892 **Figure 5. Generation of a dual CD19-CD27 CAR-T for the treatment of FL (A)** CAR-T constructs used:
893 ARI-0001 (anti-CD19, blue), CD27-ECD (light green), truncated CD27-ECD (trCD27-ECD, dark green)
894 and CD70-scFv (red). All of the constructs had the same hinge, transmembrane and costimulatory
895 domains. **(B)** T-cell expansion of the different constructs after 10 days of stimulation. Represented as
896 population doublings (mean +/- sd) from 3 different donors. **(C)** Percentage of specific lysis,
897 represented as mean +/- sd of bioluminescence lose in K562 cells transduced with CD19 and CD70
898 (K562-CD19-CD70), compared to cells without CAR-T, after 24h of co-culture (n=3). 3 different effector
899 to target (E:T) ratios (3:1, 1:1, 1:3) were used. **(D)** IL-2 levels in supernatants of K562-CD19-CD70 cells

MATERIAL, METHODS AND RESULTS

900 co-cultured for 24h with CAR-T, in a E:T ratio of 3:1 **(E)** Specific killing (left panel), T-cell proliferation
901 (middle panel) and B/T cell proportion (right panel) of WSU-FSCCL cells co-cultured for six days with
902 CAR-T in a E:T ratio of 1:8. Specific killing was calculated as the depletion compared to untransduced
903 (UTD) cells. T-cell proliferation was calculated as the fold change comparing the number of CD3+ cells
904 at endpoint. (n=3) **(F)** Percentage of ARI-0001 CAR-T expression in single CAR-T (blue) and in co-
905 transduction with CD27 (purple) (left panel). Expression of ARI-0001 is represented in lower panel.
906 Expression of CD27 protein (MFI) in single or in co-transduction is represented in the right panel.
907 Anova test and Holm-Sidak test for multiple group comparisons was applied in B and E.
908

Figure 1



909

Figure 2

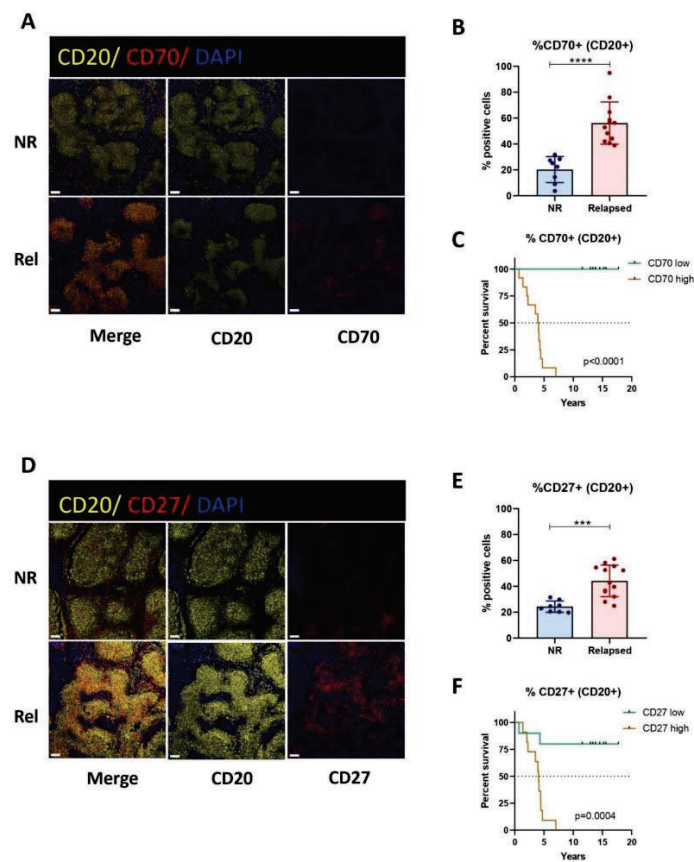
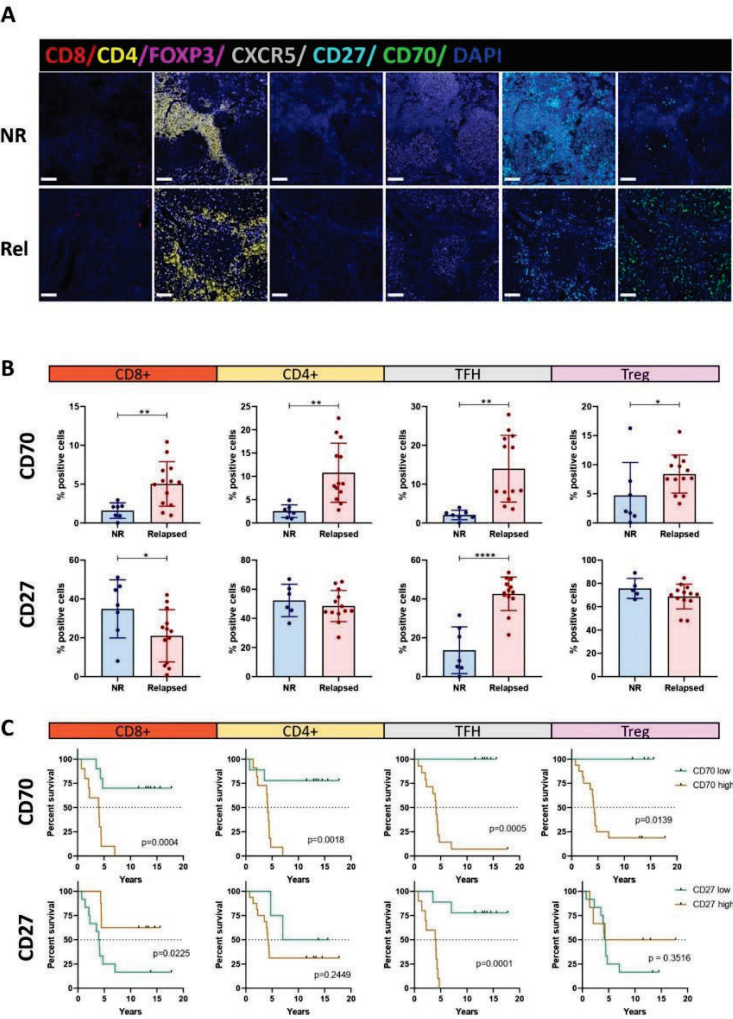
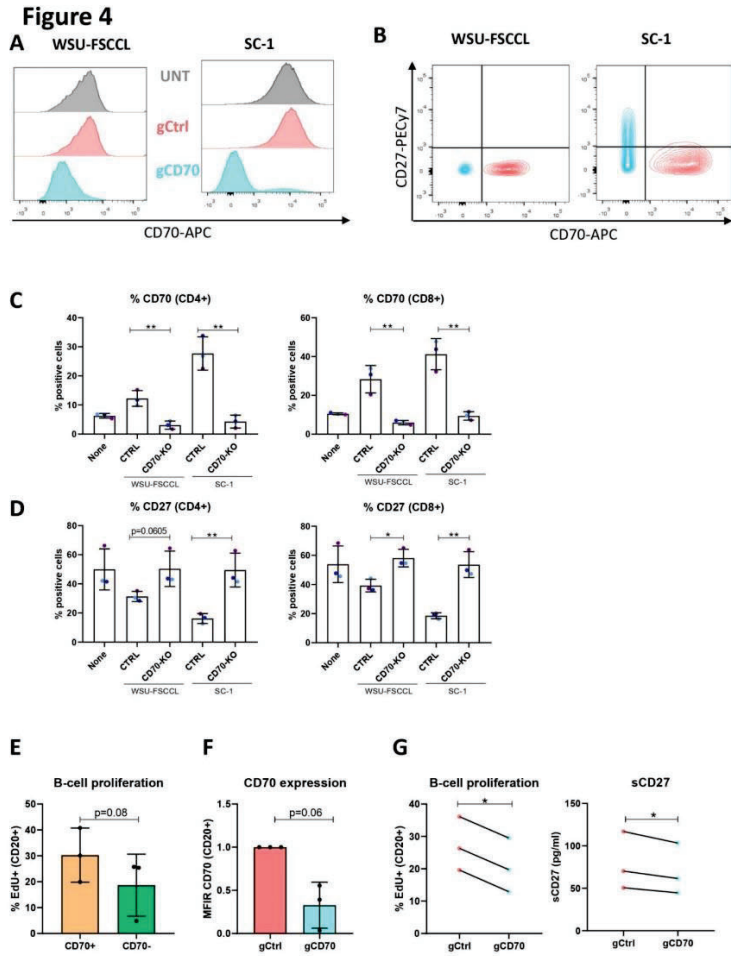


Figure 3



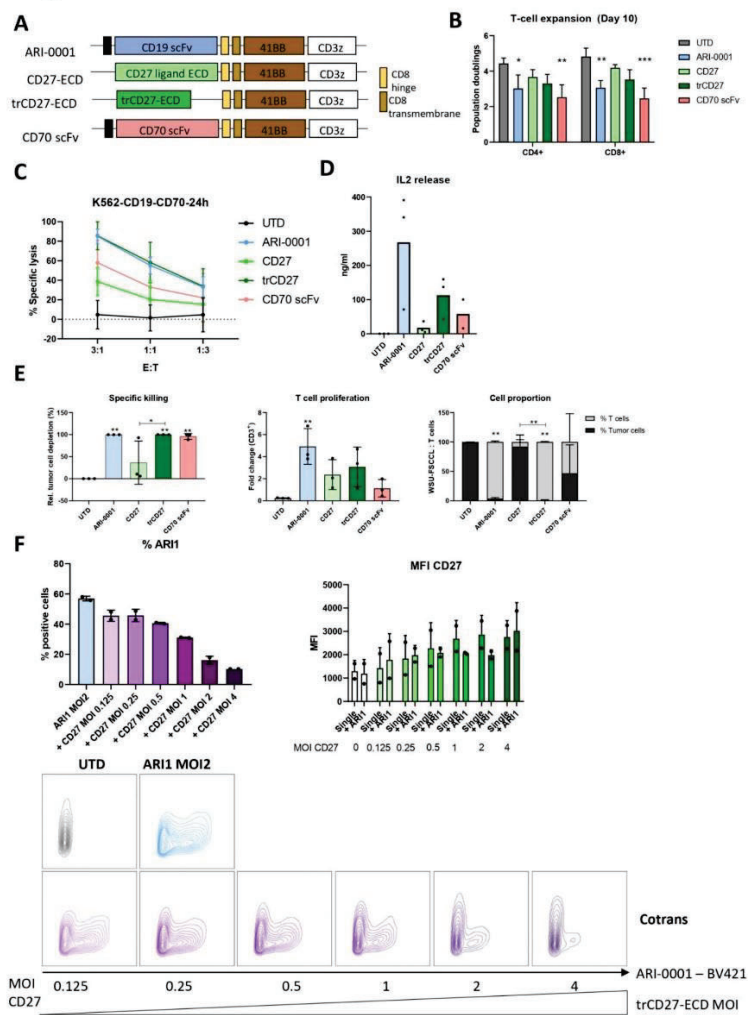
911



912

913

Figure 5



AUTHOR CONTRIBUTIONS

Ferran Araujo Ayala has contributed to the two papers indicated below with the following tasks:

1. Study 1: A novel Patient-Derived 3D Model Recapitulates Mantle Cell Lymphoma Lymph Node Signaling, Immune Profile and *in vivo* Ibrutinib Responses

Authors: *Ferran Araujo-Ayala**, *Cèlia Dobaño-López**, *Juan García Valero*, *Ferran Nadeu*, *Fabien Gava*, *Carla Faria*, *Marine Norlund*, *Renaud Morin*, *Pascale Bernes-Lasserre*, *Neus Serrat*, *Heribert Playa-Albinyana*, *Rubén Giménez*, *Eliás Campo*, *Jean-Michel Lagarde*, *Armando López-Guillermo*, *Eva Gine*, *Dolors Colomer*, *Christine Bezombes*, and *Patricia Pérez-Galán*. *co-first authors.

Published in *Leukemia* 2023 Jun;37(6):1311-1323. doi: [10.1038/s41375-023-01885-1](https://doi.org/10.1038/s41375-023-01885-1)
IF: 11.4. Ranked in D1 of Hematology.

In this first study Ferran Araujo Ayala has contributed to the experimental design, he has conducted most of the molecular and cellular assays and performed the corresponding data analysis. He wrote a draft of the manuscript and together with his supervisor introduced coauthor corrections and suggestions. Finally, he also performed the necessary experiments requested by the reviewers of *Leukemia* journal.

2. Study 2: Patient-Derived Follicular Lymphoma Spheroids recapitulate lymph node signaling and immune profile uncovering galectin-9 as a novel immunotherapeutic target

Authors: *Cèlia Dobaño-López**, *Juan García Valero**, *Ferran Araujo-Ayala*, *Ferran Nadeu*, *Fabien Gava*, *Carla Faria*, *Marine Norlund*, *Renaud Morin*, *Pascale Bernes-Lasserre*, *Fabian Arenas*, *Marta Grau*, *Cristina López*, *Irene López-Oreja*, *Neus Serrat*, *Ares Martínez-Farran*, *Lluís Hernández*, *Heribert Playa-Albinyana*, *Rubén Giménez*, *Silvia Beà*, *Eliás Campo*, *Jean-Michel Lagarde*, *Armando López-Guillermo*, *Laura Magnano*, *Dolors Colomer*, *Christine Bezombes* and *Patricia Pérez-Galán*. *co-first authors

Published in *Blood Cancer Journal J.* 2024 May 2;14(1):75. doi: [10.1038/s41408-024-01041-7](https://doi.org/10.1038/s41408-024-01041-7)
IF : 12.8. Ranked in D1 of Hematology.

In this second study Ferran Araujo Ayala has conducted cellular assays, has contributed to study design and to critical manuscript revision. He also participated in the execution and analysis of the experiments requested by the reviewers of *Blood Cancer Journal*.

Barcelona, 2nd May 2024

Patricia
Perez
Galan

Digitally signed
by Patricia Perez
Galan
Date: 2024.05.03
09:33:54 +02'00'

Thesis director: Patricia Pérez Galán

SUMMARY OF THE RESULTS

In **Chapter 1**, we generated 3D models (PDLS) to mimic the mantle cell lymphoma (**Study 1**) and follicular lymphoma (**Study 2**) lymph nodes. To achieve that, we cultured primary cells from lymphoma patients, mainly from peripheral blood in the MCL project and from lymph node or peripheral blood in FL. Lymphoma cells were enriched with a lymphoma-specific cytokine cocktail and monocytes from healthy donors' peripheral blood were added. In both cases, we achieved a high viability after 7 days of *ex vivo* culture, and an enhanced proliferation, which was superior in FL than in MCL.

RNA-seq was performed in order to analyze the transcriptomic profile from our PDLS and compare to patients' samples. FL and MCL-PDLS are enriched with pathways related to the pathological lymph nodes. In MCL, gene signatures from Saba *et al* and Rosenwald *et al* were highly recapitulated. On the other hand, we developed a FL-LN signature in our work by comparing LN and PB samples to assess FL-PDLS also reassembles to the original LN sample.

Importantly, our samples contain not only tumor B cells, but also T cells from the tumor microenvironment. In this project, we characterized these T lymphocytes and demonstrated that express increased levels of immune checkpoints (ICP) as well as other immune regulator proteins up-regulated in the pathological lymph nodes compared to normal tonsils. Moreover, T-cell phenotype was depicted in FL-PDLS, showing we have a notable proportion of TFH and Treg cells.

Furthermore, our PDLS models may be used to test different types of drugs, including standard-of-care immunochemotherapy (R-CHOP), targeted therapy (Ibrutinib) or other immunotherapies (Nivolumab, anti-galectin9).

Remarkably, MCL-PDLS recapitulated ibrutinib responses, thus indicating our models could be used as a predictive tool to test therapies and advance in the personalized medicine era.

In **Chapter 2 (Study 3)** we performed an RNA analysis of several immune-related genes in cancer context using a well-established FL patients cohort from our institution. Using samples at diagnose, we found *CD70* was increased at transcriptomic level in patients that eventually relapse compared to those that did not. Moreover, higher expression of *CD70* was associated to a lower mutational burden.

Moreover, we validated CD70 over-expression at protein level using multiplex immunofluorescence techniques. Interestingly, CD70 is increased, not only in tumor B cells, in which there is a clear association to a shorter progression-free survival (PFS), but also in T cells from the TME, although in a lower percentage of expression. CD70 ligand, CD27, was also investigated, and while tumor cells in relapse patients are also increased, in T cells the differential expression was dependent on the population. In CD8+ and CD4+ T helper non-follicular cells patients which experienced relapse had lower CD27 expression but it was higher in TFH.

Using CRISPR/Cas9 techniques to knock-out CD70, we were able to experimentally validate our findings and assessed a higher CD70 expression in tumor cells induce increased CD70 levels in T cells while dampened CD27. Besides, in primary cells, CD70-KO samples had a lower proliferation than those transfected with a non-targeting control.

Our results motivated the generation of a novel dual CD19-CD70 CAR-T therapy. We compared ligand-based and scFv-based constructs and

MATERIAL, METHODS AND RESULTS

concluded ligand-based CAR-Ts had a better *in vitro* expansion. Furthermore, a truncated CD27-ECD (trCD27-ECD) construct, which avoids cleavage from the membrane, had a superior cytotoxicity activity and cytokine release. By co-transducing trCD27-ECD with an approved, academic CD19 CAR-T (ARI-0001), we achieved the generation of a dual CAR-T that may be used to treat high-risk FL patients.

DISCUSSION

DISCUSSION

PDLS as a 3D system to culture NHL samples mimicking the lymph node

Culture of primary samples from non-Hodgkin lymphoma has historically represented a major limitation in the research of the field. *In vivo*, B lymphocytes grow within the lymph nodes, where they are supported by the surrounding microenvironment^{26 88}. However, LN samples are usually scarce, while in some B-cell malignancies, including MCL and FL, peripheral blood samples are more likely to be available. Importantly, PB samples change the transcriptomic profile, losing proliferation capacity and the activation of many pathways involved in lymphoma pathogenesis.^{25 280 281} In our work (**Studies 1 and 2**), we demonstrated PB are a suitable source of biological material to study lymphoma.

In a parallel PDLS development for FL and MCL, we cultured primary samples with monocytes purified from healthy donors and a lymphoma-specific cytokine cocktail, in ultra-low attachment plates to achieve the formation of 3D structures. Nowadays, it is commonly accepted that 3D models better represent cancer biology, signaling pathways and lymphocyte activation as they are subjected to mechanical forces.^{201 282 283}

First, we analyzed viability and proliferation after 7 days of culture. In both PDLS, we achieve a high viability B-cell and T-cell viability, with an expected interpatient variability. Curiously, although in both cases we used the same media²⁸⁴, MCL cells without stimuli were barely alive (**Study 1**), while FL cells showed better viability and was not increased after addition of cytokines

DISCUSSION

(**Study 2**). Regarding proliferation, both models had a significant enhanced proliferation compared to non-stimulated control; however, B-cell proliferation in FL was much higher than in MCL.

Importantly, both cytokine cocktails contain common factors (CD40L, IL4), but also other specific for each lymphoma, which may explained these differences. CD40L ligand represents an important survival stimulus provided by TFH cells in both FL and MCL.^{43 119} TFH are also responsible for the secretion of IL-4, which enhances JAK-STAT pathway by binding to IL-4R in B cells,^{42 99} but also is responsible for TME remodeling.¹²⁰ While in MCL we added BAFF, secreted by stromal cells and described to activate NFkB,²⁷ in FL we used IL-21 and IL-15. IL-15 is trans-presented by macrophages and synergies with CD40L to induce B-cell proliferation in FL.²⁸⁵ Finally, IL-21 induces proliferation in germinal center cells¹⁹³ and has been correlated with aggressivity in FL.²⁸⁶ Probably, the differential use of IL-21 makes a difference in the induction of proliferation. IL-21 was also used in a recently published 3D model to culture CLL primary samples. This model is also characterized by a high proliferation, but the authors also used CpG as a toll-like receptor (TLR) stimulation, which is a potent stimulator for CLL cells.^{287 288} Thus, it is difficult to discriminate whether IL-21 had a beneficial effect on B cells. Importantly, IL-21 has been described to induce apoptosis in MCL.²⁸⁶ Altogether, we decided not to include this cytokine in MCL cocktail at the expense of having lower proliferation levels. Indeed, proliferation is also very heterogeneous in the 2D model described in Chiron *et al*, in which MCL cells were co-cultured with CD40L-expressing stromal cells and soluble BAFF was also added, among other cytokines.¹⁸⁶

Interestingly, PDLS transcriptome strongly recapitulates the pathological LN. RNA-seq analysis in FL included LN and PB original samples, as well as PDLS derived from PB. Paired analysis on LN – PB samples allowed the generation of a FL-LN signature. After comparing the PDLS with the original PB sample, we assessed this LN signature was highly up-regulated in our PDLS. In MCL, opposite as FL, we did not have paired LN-PB samples; however, we benefited from previous studies which defined a proliferation signature²⁸⁹ and a MCL-LN signature, as well as identified an up-regulation of NFkB, NIK and BCR pathways due to LN TME.²⁵ All of these pathways were enriched in MCL-PDLS compared to the original PB, while a MCL-PB signature was down-regulated. Furthermore, in both cases, gene-set enrichment analysis showed our PDLS recapitulate pathways related to proliferation and lymphomagenesis, such as metabolic pathways including OXPHOS²⁹⁰, MYC and different cytokines such as IL-10 or IFN γ .

In order to investigate the effects of culturing our cells in three dimensions, we included our PB-NHL cells cultured with the same stimuli as the PDLS but in a regular, flat 96-wells plate. Despite the number of differential expressed genes was lower, we found that, in MCL, 3D culture better recapitulates MCL-specific signatures, as well as there was an increase in MYC, angiogenesis and extracellular matrix / collagen pathways. Involvement of cell adhesion pathways was also confirmed in FL, together with an increase of glucose metabolism and E2F targets in the PDLS.

The pro-survival effects by adding myeloid cells in lymphoma cultures have been demonstrated in both FL and MCL.¹⁴⁶¹⁸⁸ Nevertheless, single-cell suspensions from LN do not recover adherent cells, and PB samples from leukemic patients usually have very low numbers of monocytes. In order to

DISCUSSION

include the myeloid compartment, we added allogenic monocytes from healthy donors. In the case of follicular lymphoma, we were able to compare the expression of tumor cells co-cultured with autologous or allogenic monocytes. PCA analysis determined samples are clustered according the patient, while we found 77 differentially expressed genes and an increase in pathways related to allograft rejection. On the contrary, in MCL we did not have the biological material to perform this comparison; however, it has been previously determined both autologous and allogenic monocytes support MCL viability.¹⁸⁸

Regarding the phenotype these monocytes acquire within the PDLS, we could detect significant changes. In both models, but more pronounced in MCL, monocytes grew and gained complexity, suggesting a differentiation process into macrophages. When investigating whether they polarized into M1 or M2 macrophages by qPCR analysis of previously reported genes,^{291 292} in MCL we found they clearly had an M2-like phenotype, with high expression of *MRC1* and *CCL22*, while *CCL5* and *CXCL11* were decreased as M2 macrophages differentiated with M-CSF. In FL, we did not find a fixed pattern, and PCA analysis determined macrophages were in a separated group between M1 and M2, suggesting an intermediate phenotype.

Overall, we developed two spheroid models that maintain viability and proliferate *in vitro*, as well as recapitulate the pathogenesis of malignant lymph nodes and incorporates myeloid cells to recapitulate the tumor microenvironment.

Drug testing in PDLS recapitulate *in vivo* responses and may be used for immunotherapeutic treatment

One of the major applications of spheroids development is the possibility of a drug-testing platform.²⁹³ Some of the advantages of our PDLS models include they are scaffold-free models, allowing an easy manipulation to assess a reliable cellular count by flow cytometry, multiplexed (96-well format) and proliferative, allowing the use of drugs with impact on this aspect.

To demonstrate our models are suitable for drug testing, we used approved drugs for the treatment of lymphoma. R-CHOP, the combination of anti-CD20 rituximab and chemotherapy, is widely used as a 1st line therapy in follicular lymphoma, but also in other B-cell lymphoma including MCL. In our project, we focused R-CHOP in the context of FL (**Study 2**), and found that almost all patients responded. These results are similar as the clinical response, in which almost 90% of patients achieve at least a PR.²⁹⁴

In **Study 1**, we focused on the use of BTK inhibitors for the treatment of relapsed MCL. Ibrutinib is a first-in-class covalent inhibitor and its used has been extended as 2nd-line therapy, although recent data from clinical trials suggest a beneficial effect if used in front-line therapy.^{70 57 295}

Nevertheless, more than 30% of patients do not achieve an objective response to ibrutinib,⁶⁶ which leads to a rapid relapse and a poor prognosis. Thus, it is mandatory to develop novel systems to assess the response prior to its clinical use. In our study, we used 8 samples from patients that had or not achieved at least a PR *in vivo*. Remarkably, in all of the PDLS coming from

DISCUSSION

resistant samples (n=3) we did not observe a B-cell depletion, while ibrutinib efficiently depleted tumor cells in sensitive samples (n=5). Altogether, the use of a 3D system that recapitulates clinical responses to BTK inhibitors is a promising tool; however, extended series of patients are needed to confirm its use to anticipate clinical decisions.

Importantly, our lymphoma samples contain a variable fraction of non-tumoral T-cells. Therefore, in a second part of the drug testing in our PDLS, we investigated whether they may be used as a platform for immunotherapy testing.

First, we characterized the immune regulators expression in T cells. By bioinformatics analysis from public databases (gene expression omnibus, GEO), we compared the expression of these genes between the pathologic non-purified lymph nodes and the normal tonsil. In both diseases, we found an increase on the immune checkpoints (ICP) *TIGIT* and *HAVCR2* (TIM-3). PD-1 was not up-regulated, but PD-L1 was increased in MCL; moreover, PD-1 was highly expressed in FL. Besides, anti-PD1 inhibitors have revolutionized the treatment of some cancers, including lung cancer,²⁹⁶ melanoma²⁹⁷ or Hodgkin lymphoma.²⁹⁸

Along the PDLS culture, we found an increase of most of the immune regulators analyze, recapitulating an exhausted immune phenotype. The ligands of the main immune checkpoints were also characterized in both the tumor cells and the macrophages. In FL, as the proportion of tumor cells was lower, we were able to deeper characterize the T-cell population, and different levels of immune exhaustion were found. Finally, we also showed that FL samples maintain a notable proportion of TFH, Treg and TFR cells,

reassembling the pathological lymph nodes. Overall, we had evidences that PDLS are a suitable tool for immunotherapeutic testing.

Contrary to other tumors, responses to nivolumab as monotherapy in B-NHL have not been that successful.²⁹⁹ However, its combination with ibrutinib has been investigated in a clinical trial (NCT02329847) in FL, DLBCL and CLL, but not in mantle cell lymphoma. Interestingly, ORR superior to 60% was found in CLL and Richter transformation.³⁰⁰ In MCL-PDLS, the combination of ibrutinib and anti-PD1 resulted in an increase in B-cell depletion but only in patients with lower responses to ibrutinib as monotherapy. Remarkably, among the patients that benefit with the combination we found the three ibrutinib-resistant cases in the clinics. Besides, we found an enhanced release of cytokines (IFN γ and granzyme B, the last only in patients that responded to the combination), indicating that PDLS can be used as an immunocompetent system.

Anti-PD1 therapy has also been combined with anti-CD20 in FL patients, with responses superior to 60% of patients including ~50% of CR.^{301 302} In our study, we observed a trend of higher B-cell depletion compared to rituximab alone. Nevertheless, there was a high interpatient variability. Intriguingly, we found a significant negative correlation between the expression of TIM-3 or one of its ligands, CD66a (*CEACAM1*),³⁰³ and the response to either anti-CD20 or anti-CD20 + anti-PD1. This observation provides a rational therapeutic intervention in TIM-3. However, anti-TIM3 antibody did not result in an improvement in B-cell depletion. This may be explained because TIM-3 is able to bind to different ligands, including the mentioned CD66a, but also galectin-9 and phosphatidylserine.³⁰⁴ Besides, it has been reported that anti-TIM3 antibodies are unable to block the galectin-9 binding site.³⁰⁵ As galectin-9 it is

DISCUSSION

presented as a soluble TIM-3 ligand,³⁰⁴ we analyzed the supernatants from our PDLS treated with the combination of rituximab and anti-TIM3, and found a noteworthy correlation, with higher levels of soluble galectin-9 related to lower response to the combination, but also we found correlations in the same direction with rituximab as monotherapy and rituximab + nivolumab.

Finally, we demonstrated that the combination of rituximab and anti-galectin9 had an improved tumor depletion in our PDLS, being significantly higher compared to both antibodies as single agents. Due to the role of galectin-9 as an immune escape molecule,^{306 307} it has recently gained attention as an immunotherapeutic target for cancer therapy.^{308 309} Nevertheless, in B-cell neoplasms data is scarce, and only has been described as an up-regulated protein in Treg and Th1 T cells in CLL and was related to increased IL-10 levels³¹⁰ In conclusion, our results showed galectin-9 would also have a key immunosuppressive role in FL and be used as a novel therapeutic target.

CD70 is up-regulated in FL-LN in patients that will relapse

The introduction of rituximab, the first-in-class anti-CD20 antibody, revolutionized follicular lymphoma treatment. Nowadays, standard treatment is mostly based on combination of rituximab and chemotherapy, known as immunochemotherapy.¹⁵³ In the recent years, the advances on identifying the genomic and molecular features of each lymphoma enabled the development of targeted therapies that have broaden the therapeutical repertoire; in the case of FL, we must highlight anti-EZH2 tazemetostat.^{168 169}

Finally, ultimate advances based on immunotherapeutic drugs, mainly T-cell engagers^{171 172} and anti-CD19 CAR-T.²⁵⁴

In our work (**Study 3**), we focused on the role of the tumor microenvironment in follicular lymphoma, necessary to develop an overt disease.³¹¹ FL-TME is very heterogeneous and include immune and non-immune cells;⁸⁸ thus, the study of both tumor cells and TME is necessary to compile FL complexity.

First, we analyzed RNA expression of more than 700 immune-related genes in full lysates FFPE biopsies from FL patients at diagnose from a homogeneous cohort. Despite the fact that a single-center series could have limitations and may require validation in other cohorts, there are also some advantages: i) patients were diagnosed following the same clinico-pathological criteria, ii) all patients were homogeneously treated with ICT (100% patients received CHOP as a 1st-line chemotherapy), and iii) during the follow-up period patients that suffered a histological transformation were excluded. Our analysis assessed a differential immune pattern between a group of patients that relapse and a group that never relapsed, with a very prolonged follow-up time. These differences revealed 31 differentially expressed genes (representing a 4.2% of studied genes) and a differential enrichment of biological pathways, including cytokine-associated pathways, oncogenic pathways (JAK-STAT³¹² and PI3K/Akt³¹³) and those related to cell adhesion and extracellular matrix (ECM). In the last years, the role of the ECM in FL pathogenesis has gained attention as single-cell studies have confirmed a high expression of ECM genes³¹⁴ in LN stromal cells,³¹⁵ which may be related to early relapse.³¹⁶

Among the 25 up-regulated genes in the relapse group, we found *CD70*, which was also associated, close to statistical significance, to a shorter progression-

DISCUSSION

free survival. Moreover, we have depicted that patients with high *CD70* RNA levels use to have a lower number of mutations. Therefore, *CD70* could constitute a pro-oncogenic mechanism that bypasses the need of B lymphocytes to acquire additional mutations in order to achieve FL progression.

Lately, *CD70* has drawn attention on the context of cancer. In solid cancers, there are evidences that is deregulated in pancreatic, renal, lung or colon, among others. In a recent study by Nilsson *et al*, an interesting association to epithelial to mesenchymal transition was described.²⁷⁶ In hematologic tumors, it has been deeply studied in acute myeloblastic leukemia (AML) as leukemia stem cells highly express *CD70*. Besides, an aberrant expression and a potential pro-oncogenic role has been described in B-cell lymphoma²¹¹ including FL,^{317 318} DLBCL,³¹⁹ MCL⁴⁸ and CLL.^{320 227} Moreover, *CD27/CD70* axis has been linked to diverse mechanisms of TME modulation in lymphoma.^{321 322 323}

Our results clearly indicate that *CD70* is more prevalent in the tumor fraction and abundantly expressed on patients that relapse. Importantly, its association with survival is more pronounced than in whole lysate RNA, thus having a more prognostic significance. *CD70* from the tumor could bind to *CD27*-expressing cells, including T regulatory cells, which are highly positive for *CD27*.^{324 325} Furthermore, it was previously described that *CD70*+ B-NHL cells induce *FOXP3* expression.³²¹ Gene expression analysis also correlated *CD70* expression with cytokines responsible for Treg chemoattraction (*CCL20*, *CCL22*)^{326, 120} and *IRF4*, linked to a higher risk of transformation.¹⁷³ Finally, a positive correlation was found between the density of *CD20*+*CD70*+ cells with the abundance of Treg in FL-LN biopsies.

The diminished CD27 in CD8+ and CD4+ T helper non-follicular cells may be related to a lower T-cell anti-tumoral response³¹⁷ and induced by a CD70-dependent cleavage. Soluble CD27 (sCD27) has not been deeply studied in lymphoma, but its levels are increased in CLL³²⁰ and it has been related to bad prognosis in DLBCL.³²⁷ *In vitro* experiments we have performed using FL CD70-KO cells point out to this phenomenon. Furthermore, the up-regulation of CD27 in B cells, usually linked to a memory-like phenotype suggest CD70+ and CD27+ tumor cells mutually interact. Historically, FL cells have been defined to be frozen in a GC state; however, single-cell analysis revealed distinct cell states co-exist³²⁸ and memory-like features have been linked to a higher risk of transformation.³²⁹³³⁰

While most of the studies focus on the significance of CD70 over-expression on the tumor fraction, we also interrogated its expression in the T cells from the FL-TME. Intriguingly, all T-cell populations analyzed except TFR cells showed higher CD70 protein levels in patients that relapse. We validated the co-culture of T cells with CD70+ FL cell lines, but not CD70 knocked out cells, induced higher CD70 levels, pointing out to a CD70-dependent regulation. CD27 downstream signaling activates NF- κ B and JNK, and CD70 promoter is enriched in binding sites for NF- κ B and c-Jun transcription factors.³³¹ Whether this positive feedback mechanism could also happen between tumor cells remains to be confirmed.

Tumor CD70+ cells not only are capable to induce tumor-promoting effects in other B cells or T cells from the TME, but also receive signals from CD27+ cells or soluble CD27. Notably, activation of CD70 leads to MEK and Akt phosphorylation.²¹⁷ Overall, the pathogenic mechanisms in which CD70 participates are complex and diverse, and include tumor and non-tumor cells.

DISCUSSION

In this work, we adapted a CRISPR/Cas9 protocol developed to genetically modify B-cell lymphoid malignancies³³² by using FDC-derived YK6 cells mimicking germinal center stimuli^{193 333} and adding IL-4 and IL-15 to use the same factors as in **Study 2**. Remarkably, we achieved a significant reduction of CD70 protein levels, which was associated to lower B-cell proliferation and diminished sCD27 levels.

To sum up, we found that FL patients that relapse have at the diagnose higher *CD70* expression, at both RNA and protein level. CD70 is mainly expressed in tumor B cells, but is also up-regulated in T cells from the TME. These findings reinforce the oncogenic role of CD27/CD70 axis in FL as well as its therapeutic intervention.

CD70 as a target for CAR-T cells in B-cell lymphoma

After validating CD70 as an increased protein in FL patients that relapse, together with a biological validation of the target, we proposed the generation of a dual CAR-T cell that can target CD19 and CD70. Although anti-CD19 CAR-Ts have improved the management of high-risk lymphoma patients, still a relevant portion of them have limited, non-durable responses.²⁵⁴ Moreover, CD19-CAR-T relapse has been described, indicating antigen loss as a mechanism of evasion^{254 247} For this reason, dual CAR-T cells have been proposed as a therapeutic strategy to avoid antigen escape or to treat relapsed CAR-T patients that lost CD19 expression. To date, only single anti-CD70 CAR-Ts have been explored (NCT04429438) (NCT04502446), apart from the coadministration of a CD19 and a CD70 CAR-T.²⁶⁶ (NCT04429438)

We first investigated the best construct to deplete CD70+ lymphoma cells as a single CAR-T. Two ligand-based and a scFv-based CAR-T were used and compared to ARI-0001, an approved academic product from our institution.^{250 251} We validated ligand-based CAR-Ts using CD27 expanded better. However, CD27-ECD lost expression on the membrane and was released into the supernatant, which did not occur in trCD27-ECD as described in Leick *et al.*²⁷³ Although it has been envisioned that ligand-based could have benefits compared to scFv-based CAR-Ts,²⁴⁶ this cleavage issue has also been described in a CAR-T targeting thrombopoietin.³³⁴

Despite having pros and cons regarding the use of ligand-based CAR-Ts, cytotoxicity experiments demonstrated trCD27 was the most effective anti-CD70 CAR-T and released higher IL-2 cytokine. This enhanced anti-tumoral effect has been assessed in both artificial antigen presenting cells (K562 cells transduced with CD19 and/or CD70) at short-term (24h) and at long-term (6 days) using FL-derived cell lines at low ratios. Compared to ARI-0001, cytotoxicity at 24h was very similar, but IL-2 levels were inferior than those induced by CD19 CAR-T. This inferior cytokine release was reflected in a lower T-cell proliferation in long-term assays compared to ARI-0001. In conclusion, we selected trCD27-ECD as the most promising anti-CD70 construct.

In addition, we generated a dual CD19-CD70 CAR-T using a co-transduction strategy, as done with ARI-0003, a dual CAR-T combining CD19 (ARI-0001) and BCMA (hARI-0002).²⁵⁸ Importantly, the combination of both viruses led to a lower ARI-0001 expression compared to the single transduction, while CD27 remained stable. Therefore, we optimized the ARI-0001 : trCD27 ratio, and determined a MOI 2 for ARI-0001 and MOI 0.5 for trCD27-ECD as the optimal.

DISCUSSION

Nevertheless, the fact that T cells can also express CD70, although in low levels, could constitute a limitation on anti-CD70 CAR-T therapies. Although we did not find a diminished T-cell expansion during CAR-T generation, we observed a loss of CD70 expression in conditions carrying trCD27-ECD construct (data not shown), suggesting fratricide. Aiming to avoid this process, we investigated the use of dasatinib during the T-cell expansions, a tyrosine kinase inhibitor that reversibly switch off the CAR-T cytotoxic effects.³³⁵ By using this drug, we restored CD70 expression but, when CAR-T cells were co-cultured with primary FL / MCL samples using PDLs methodology (**Studies 1 and 2**) fratricide was present. Even so, preliminary data suggested a higher tumor killing in two patients exhibiting a CD70^{high} CD19^{dim} phenotype (data not shown).

Some published studies knocked-out CD70 expression in T cells during CAR-T expansion,^{279 277} including clinical trials with a genetically modified, allogenic anti-CD70 CAR-T, which results in clear-cell renal carcinoma were recently published.³³⁴ Probably, by applying this strategy to our construct, a higher T-cell proliferation and improved long-term cytotoxicity efficacy could be achieved.

In conclusion, after validating CD70 as a promising target in follicular lymphoma, we developed a dual CD19-CD70 CAR-T combining an academic, approved CD19 (ARI-0001) and a ligand-based (trCD27-ECD) construct. However, this novel product still needs to be improved by knocking-out CD70 expression and a further preclinical testing is needed. While CAR-T testing has usually based on non-immunocompetent *in vitro* (cell lines) and *in vivo* (xenografts using NSG mice) systems, the PDLs models we developed during this thesis also proved to be useful for CAR-T testing.²⁵⁸ Among the

advantages of PDLS for cellular therapies we envision the following: i) they are immunocompetent models, ii) recapitulate inter-patient heterogeneity, iii) CD70 expression is close to the observed in the patients' lymph nodes, and iv) reflect intra-tumor heterogeneity, with subpopulations with different CD19/CD70 levels in our case.

CONCLUSIONS

CONCLUSIONS

The general conclusions derived from this thesis are as follows:

1. PDLS represent dynamic and alive 3D structures that contain proliferating tumor B cells, autologous T cells and myeloid cells.
2. Monocytes differentiate into macrophages within the PDLS, and polarized into M2-like macrophages in MCL while present an intermediate M1-M2 phenotype in FL.
3. PDLS created from PB samples transcriptionally reassemble to the pathogenic LN and recapitulate fundamental lymphoma signatures.
4. MCL-PDLS faithfully reproduce clinical responses to ibrutinib and FL-PDLS respond to standard R-CHOP treatment.
5. Autologous T cells from PDLS up-regulate specific immunoregulators that are increased at RNA level in the FL and MCL LN.
6. FL-PDLS contain a high number of TFH and Treg cells, recapitulating the T-cell heterogeneity found in the FL-LN.
7. Combination of ibrutinib and anti-PD1 overcomes ibrutinib resistance in MCL-PDLS, together with an activation of the anti-tumoral immune response,

CONCLUSIONS

8. Galectin-9 represents a novel immunosuppressor target in FL as it dampens anti-CD20 activity. Its therapeutical intervention improves rituximab efficacy.
9. *CD70* is increased at RNA level in the LN of FL patients at diagnose that eventually relapse.
10. At protein level, CD70 up-regulation is validated in both tumor cells and T cells from the TME, but expression levels are higher in B cells.
11. CD70 is associated with a lower progression-free survival in both RNA and protein levels; however, the prognostic value is higher in protein.
12. CD27 is over-expressed in FL patients that relapse in the tumor fraction, but diminished in CD8+ and CD4+ T helper non-follicular cells.
13. CRISPR/Cas9 experiments demonstrated CD70 in tumor cells induce higher CD70 levels in T cells. In primary cells, we observed a decrease in B-cell proliferation in CD70-KO cells.
14. CD70 represents a promising target for CAR-T cell therapy. In the context of lymphoma, a dual CD19-CD70 CAR-T could constitute a reliable alternative in the clinics.
15. Fratricide due to CD70 expression in T cells represents a limitation but might be overcome by knocking-out CD70 expression during CAR-T expansion.

REFERENCES

REFERENCES

1. Thandra KC, Barsouk A, Saginala K, Padala SA, Barsouk A, Rawla P. Epidemiology of Non-Hodgkin's Lymphoma. *Med Sci (Basel)*. 2021;9(1). doi:10.3390/medsci9010005
2. Swerdlow SH, Campo E, Pileri SA, et al. The 2016 revision of the World Health Organization classification of lymphoid neoplasms. *Blood*. 2016;127(20):2375-2390. doi:10.1182/blood-2016-01-643569
3. Shankland KR, Armitage JO, Hancock BW. Non-Hodgkin lymphoma. *The Lancet*. 2012;380(9844):848-857. doi:10.1016/S0140-6736(12)60605-9
4. Riether C, Schürch CM, Ochsenbein AF. Regulation of hematopoietic and leukemic stem cells by the immune system. *Cell Death Differ*. 2015;22(2):187-198. doi:10.1038/cdd.2014.89
5. Gatto D, Brink R. The germinal center reaction. *Journal of Allergy and Clinical Immunology*. 2010;126(5):898-907. doi:10.1016/j.jaci.2010.09.007
6. Ruddle NH, Akirav EM. Secondary Lymphoid Organs: Responding to Genetic and Environmental Cues in Ontogeny and the Immune Response. *The Journal of Immunology*. 2009;183(4):2205-2212. doi:10.4049/jimmunol.0804324
7. Van Krieken JHJM, Thierry H, Molina Editor J. *Encyclopedia of Pathology Series Editor*. <http://www.springer.com/series/14876>
8. Basso K, Dalla-Favera R. Germinal centres and B cell lymphomagenesis. *Nat Rev Immunol*. 2015;15(3):172-184. doi:10.1038/nri3814
9. Allen CDC, Okada T, Cyster JG. Germinal-Center Organization and Cellular Dynamics. *Immunity*. 2007;27(2):190-202. doi:10.1016/j.immuni.2007.07.009
10. Pasqualucci L. Molecular pathogenesis of germinal center-derived B cell lymphomas. *Immunol Rev*. 2019;288(1):240-261. doi:10.1111/imr.12745
11. Young C, Brink R. The unique biology of germinal center B cells. *Immunity*. 2021;54(8):1652-1664. doi:10.1016/j.immuni.2021.07.015
12. Mlynarczyk C, Fontán L, Melnick A. Germinal center-derived lymphomas: The darkest side of humoral immunity. *Immunol Rev*. 2019;288(1):214-239. doi:10.1111/imr.12755

REFERENCES

13. Rosenquist R, Beà S, Du MQ, Nadel B, Pan-Hammarström Q. Genetic landscape and deregulated pathways in B-cell lymphoid malignancies. *J Intern Med.* 2017;282(5):371-394. doi:10.1111/joim.12633
14. Efremov DG, Turkalj S, Laurenti L. Mechanisms of b cell receptor activation and responses to b cell receptor inhibitors in b cell malignancies. *Cancers (Basel).* 2020;12(6). doi:10.3390/cancers12061396
15. Weisenburger DD, Kim H, Rappaport H. Mantle-zone lymphoma: A follicular variant of intermediate lymphocytic lymphoma. *Cancer.* 1982;49(7):1429-1438. doi:10.1002/1097-0142(19820401)49:7<1429::AID-CNCR2820490720>3.0.CO;2-5
16. Teras LR, DeSantis CE, Cerhan JR, Morton LM, Jemal A, Flowers CR. 2016 US lymphoid malignancy statistics by World Health Organization subtypes. *CA Cancer J Clin.* 2016;66(6):443-459. doi:10.3322/caac.21357
17. Vose JM. Mantle cell lymphoma: 2017 update on diagnosis, risk-stratification, and clinical management. *Am J Hematol.* 2017;92(8):806-813. doi:10.1002/ajh.24797
18. Welzel N, Le T, Marculescu R, et al. *Templated Nucleotide Addition and Immunoglobulin JH-Gene Utilization in t(11;14) Junctions: Implications for the Mechanism of Translocation and the Origin of Mantle Cell Lymphoma.* Vol 15.; 2001.
19. Jares P, Colomer D, Campo E. Molecular pathogenesis of mantle cell lymphoma. *Journal of Clinical Investigation.* 2012;122(10):3416-3423. doi:10.1172/JCI61272
20. Jain P, Wang M. Mantle cell lymphoma: 2019 update on the diagnosis, pathogenesis, prognostication, and management. *Am J Hematol.* 2019;94(6):710-725. doi:10.1002/ajh.25487
21. Salaverria I, Royo C, Carvajal-Cuenca A, et al. CCND2 rearrangements are the most frequent genetic events in cyclin D1 - mantle cell lymphoma. *Blood.* 2013;121(8):1394-1402. doi:10.1182/blood-2012-08-452284
22. Beà S, Valdés-Mas R, Navarro A, et al. Landscape of somatic mutations and clonal evolution in mantle cell lymphoma. *Proc Natl Acad Sci U S A.* 2013;110(45):18250-18255. doi:10.1073/pnas.1314608110
23. Kotlov N, Bagaev A, Revuelta M V., et al. Clinical and Biological Subtypes of B-cell Lymphoma Revealed by Microenvironmental Signatures. *Cancer Discov.* 2021;11(6):1468-1489. doi:10.1158/2159-8290.CD-20-0839

24. Jain P, Nomie K, Kotlov N, et al. Immune-depleted tumor microenvironment is associated with poor outcomes and BTK inhibitor resistance in mantle cell lymphoma. *Blood Cancer J.* 2023;13(1). doi:10.1038/s41408-023-00927-2
25. Saba NS, Liu D, Herman SEM, et al. Pathogenic role of B-cell receptor signaling and canonical NF- κ B activation in mantle cell lymphoma. *Blood.* 2016;128(1):82-92. doi:10.1182/blood-2015-11-681460
26. Burger JA, Ford RJ. The microenvironment in mantle cell lymphoma: Cellular and molecular pathways and emerging targeted therapies. *Semin Cancer Biol.* 2011;21(5):308-312. doi:10.1016/j.semcancer.2011.09.006
27. Medina DJ, Goodell L, Glod J, G  linas C, Rabson AB, Strair RK. Mesenchymal stromal cells protect mantle cell lymphoma cells from spontaneous and drug-induced apoptosis through secretion of B-cell activating factor and activation of the canonical and non-canonical nuclear factor κ B pathways. *Haematologica.* 2012;97(8):1255-1263. doi:10.3324/haematol.2011.040659
28. Springer TA. Traffic signals for lymphocyte recirculation and leukocyte emigration: The multistep paradigm. *Cell.* 1994;76(2):301-314. doi:10.1016/0092-8674(94)90337-9
29. Trentin L, Cabrelle A, Facco M, et al. Homeostatic chemokines drive migration of malignant B cells in patients with non-Hodgkin lymphomas. *Blood.* 2004;104(2):502-508. doi:10.1182/blood-2003-09-3103
30. Corcione A, Arduino N, Ferretti E, et al. *CCL19 and CXCL12 Trigger in Vitro Chemotaxis of Human Mantle Cell Lymphoma B Cells.* <http://aacrjournals.org/clincancerres/article-pdf/10/3/964/1955896/zdf00304000964.pdf>
31. Balsas P, Palomero J, Eguileor   , et al. SOX11 promotes tumor protective microenvironment interactions through CXCR4 and FAK regulation in mantle cell lymphoma. *Blood.* 2017;130(4):501-513. doi:10.1182/blood-2017-04-776740
32. Kurtova A V, Balakrishnan K, Chen R, et al. LYMPHOID NEOPLASIA Diverse marrow stromal cells protect CLL cells from spontaneous and drug-induced apoptosis: development of a reliable and reproducible system to assess stromal cell adhesion-mediated drug resistance. Published online 2009. doi:10.1182/blood-2009-07
33. Schrader C, Meusers P, Brittinger G, et al. Growth pattern and distribution of follicular dendritic cells in mantle cell lymphoma: A clinicopathological

REFERENCES

- study of 96 patients. *Virchows Archiv*. 2006;448(2):151-159.
doi:10.1007/s00428-005-0049-5
34. Hou W, Wei P, Xie J, Zheng Y, Zhang Y, Zhou X. The degree of overlap between the follicular dendritic cell meshwork and tumor cells in mantle cell lymphoma is associated with prognosis. *Pathol Res Pract*. 2018;214(4):513-520. doi:10.1016/j.prp.2018.02.015
35. Pollard JW. Trophic macrophages in development and disease. *Nat Rev Immunol*. 2009;9(4):259-270. doi:10.1038/nri2528
36. Sánchez-Martín L, Estechea A, Samaniego R, Sánchez-Ramón S, Vega MÁ, Sánchez-Mateos P. The chemokine CXCL12 regulates monocyte-macrophage differentiation and RUNX3 expression. *Blood*. 2011;117(1):88-97. doi:10.1182/blood-2009-12-258186
37. Mantovani A, Allavena P, Marchesi F, Garlanda C. Macrophages as tools and targets in cancer therapy. *Nat Rev Drug Discov*. 2022;21(11):799-820. doi:10.1038/s41573-022-00520-5
38. Pham L V., Pogue E, Ford RJ. The role of macrophage/B-cell interactions in the pathophysiology of B-cell lymphomas. *Front Oncol*. 2018;8(MAY). doi:10.3389/fonc.2018.00147
39. Le K, Sun J, Khawaja H, et al. Mantle cell lymphoma polarizes tumor-associated macrophages into M2-like macrophages, which in turn promote tumorigenesis. *Blood Adv*. 2021;5(14):2863-2878. doi:10.1182/BLOODADVANCES.2020003871
40. Papin A, Tessoulin B, Bellanger C, et al. CSF1R and BTK inhibitions as novel strategies to disrupt the dialog between mantle cell lymphoma and macrophages. *Leukemia*. 2019;33(10):2442-2453. doi:10.1038/s41375-019-0463-3
41. Decombis S, Papin A, Bellanger C, et al. The IL32/BAFF axis supports prosurvival dialogs in the lymphoma ecosystem and is disrupted by NIK inhibition. *Haematologica*. 2022;107(12):2905-2917. doi:10.3324/haematol.2021.279800
42. Castillo R, Mascarenhas J, Telford W, Chadburn A, Friedman SM, Schattner EJ. *Proliferative Response of Mantle Cell Lymphoma Cells Stimulated by CD40 Ligation and IL-4*. Vol 14.; 2000. www.nature.com/leu
43. Andersen NS, Larsen JK, Christiansen J, et al. Soluble CD40 ligand induces selective proliferation of lymphoma cells in primary mantle cell lymphoma

- cell cultures. *Blood*. 2000;96(6):2219-2225.
<http://www.ncbi.nlm.nih.gov/pubmed/10979969>
44. Nygren L, Wasik AM, Baumgartner-Wennerholm S, et al. T-cell levels are prognostic in mantle cell lymphoma. *Clinical Cancer Research*. 2014;20(23):6096-6104. doi:10.1158/1078-0432.CCR-14-0889
 45. Zhang XY, Xu J, Zhu HY, et al. Negative prognostic impact of low absolute CD4+ T cell counts in peripheral blood in mantle cell lymphoma. *Cancer Sci*. 2016;107(10):1471-1476. doi:10.1111/cas.13020
 46. Zhang S, Jiang VC, Han G, et al. Longitudinal single-cell profiling reveals molecular heterogeneity and tumor-immune evolution in refractory mantle cell lymphoma. *Nat Commun*. 2021;12(1). doi:10.1038/s41467-021-22872-z
 47. Yang ZZ, Novak AJ, Stenson MJ, Witzig TE, Ansell SM. Intratumoral CD4+CD25+ regulatory T-cell-mediated suppression of infiltrating CD4+ T cells in B-cell non-Hodgkin lymphoma. *Blood*. 2006;107(9):3639-3646. doi:10.1182/blood-2005-08-3376
 48. Balsas P, Veloza L, Clot G, et al. SOX11, CD70, and Treg cells configure the tumor-immune microenvironment of aggressive mantle cell lymphoma. *Blood*. 2021;138(22):2202-2215. doi:10.1182/blood.2020010527
 49. Assis-Mendonça GR, Fattori A, Rocha RM, et al. Single nucleotide variants in immune-response genes and the tumor microenvironment composition predict progression of mantle cell lymphoma. *BMC Cancer*. 2021;21(1):1-13. doi:10.1186/s12885-021-07891-9
 50. Hummel M, Tamaru JI, Kalvelage B, Stein H. Mantle cell (previously centrocytic) lymphomas express VH genes with no or very little somatic mutations like the physiologic cells of the follicle mantle. *Blood*. 1994;84(2):403-407. doi:10.1182/blood.v84.2.403.bloodjournal842403
 51. Orchard J, Garand R, Davis Z, et al. A subset of t(11;14) lymphoma with mantle cell features displays mutated IgVH genes and includes patients with good prognosis, nonnodal disease. *Blood*. 2003;101(12):4975-4981. doi:10.1182/blood-2002-06-1864
 52. Fernández V, Salamero O, Espinet B, et al. Genomic and gene expression profiling defines indolent forms of mantle cell lymphoma. *Cancer Res*. 2010;70(4):1408-1418. doi:10.1158/0008-5472.CAN-09-3419

REFERENCES

53. Royo C, Navarro A, Clot G, et al. Non-nodal type of mantle cell lymphoma is a specific biological and clinical subgroup of the disease. *Leukemia*. 2012;26(8):1895-1898. doi:10.1038/leu.2012.72
54. Navarro A, Clot G, Prieto M, et al. MicroRNA expression profiles identify subtypes of mantle cell lymphoma with different clinicobiological characteristics. *Clinical Cancer Research*. 2013;19(12):3121-3129. doi:10.1158/1078-0432.CCR-12-3077
55. Swerdlow SH, Campo E, Pileri SA, et al. The 2016 revision of the World Health Organization classification of lymphoid neoplasms. *Blood*. 2016;127(20):2375-2390. doi:10.1182/blood-2016-01-643569
56. Queirós AC, Beekman R, Vilarresa-Blasi R, et al. Decoding the DNA Methyome of Mantle Cell Lymphoma in the Light of the Entire B Cell Lineage. *Cancer Cell*. 2016;30(5):806-821. doi:10.1016/j.ccell.2016.09.014
57. Jain P, Wang M. Mantle cell lymphoma: 2019 update on the diagnosis, pathogenesis, prognostication, and management. *Am J Hematol*. 2019;94(6):710-725. doi:10.1002/ajh.25487
58. Armitage JO, Longo DL. Mantle-Cell Lymphoma. Hardin CC, ed. *New England Journal of Medicine*. 2022;386(26):2495-2506. doi:10.1056/NEJMra2202672
59. Dreyling M, Klapper W, Rule S. Blastoid and pleomorphic mantle cell lymphoma: Still a diagnostic and therapeutic challenge! *Blood*. 2018;132(26):2722-2729. doi:10.1182/blood-2017-08-737502
60. International Non-Hodgkin's Lymphoma Prognostic Factors Project. A Predictive Model for Aggressive Non-Hodgkin's Lymphoma. *New England Journal of Medicine*. 1993;329(14):987-994. doi:10.1056/NEJM199309303291402
61. Hoster E. The FLIPI nowadays: validation and modification. *Blood*. 2018;132(1):3-4. doi:10.1182/blood-2018-05-847558
62. Martin P, Chadburn A, Christos P, et al. Outcome of deferred initial therapy in mantle-cell lymphoma. *Journal of Clinical Oncology*. 2009;27(8):1209-1213. doi:10.1200/JCO.2008.19.6121
63. Abrisqueta P, Scott DW, Slack GW, et al. Observation as the initial management strategy in patients with mantle cell lymphoma. *Annals of Oncology*. 2017;28(10):2489-2495. doi:10.1093/annonc/mdx333

64. Vidal L, Gafter-Gvili A, Dreyling M, et al. Maintenance treatment for patients with mantle cell lymphoma: A systematic review and meta-analysis of randomized trials. *Hemasphere*. 2018;2(4):1-6. doi:10.1097/HS9.000000000000136
65. Buggy JJ, Elias L. Bruton tyrosine kinase (BTK) and its role in B-cell malignancy. *Int Rev Immunol*. 2012;31(2):119-132. doi:10.3109/08830185.2012.664797
66. Wang ML, Rule S, Martin P, et al. Targeting BTK with Ibrutinib in Relapsed or Refractory Mantle-Cell Lymphoma. *New England Journal of Medicine*. 2013;369(6):507-516. doi:10.1056/nejmoa1306220
67. Byrd JC, Furman RR, Coutre SE, et al. Targeting BTK with Ibrutinib in Relapsed Chronic Lymphocytic Leukemia. *New England Journal of Medicine*. 2013;369(1):32-42. doi:10.1056/nejmoa1215637
68. Hershkovitz-Rokah O, Pulver D, Lenz G, Shpilberg O. Ibrutinib resistance in mantle cell lymphoma: clinical, molecular and treatment aspects. *Br J Haematol*. 2018;181(3):306-319. doi:10.1111/bjh.15108
69. Zhao X, Lwin T, Silva A, et al. Unification of de novo and acquired ibrutinib resistance in mantle cell lymphoma. *Nat Commun*. 2017;8:1-15. doi:10.1038/ncomms14920
70. Giné E, de la Cruz F, Jiménez Ubieto A, et al. Ibrutinib in Combination With Rituximab for Indolent Clinical Forms of Mantle Cell Lymphoma (IMCL-2015): A Multicenter, Open-Label, Single-Arm, Phase II Trial. *J Clin Oncol*. 2022;40(11):1196-1205. doi:10.1200/JCO.21.02321
71. Jain P, Zhao S, Hun ;, et al. Ibrutinib With Rituximab in First-Line Treatment of Older Patients With Mantle Cell Lymphoma. *J Clin Oncol*. 2021;40:202-212. doi:10.1200/JCO.21
72. Bentz M, Plesch A, Bullinger L, et al. t(11;14)-positive mantle cell lymphomas exhibit complex karyotypes and share similarities with B-cell chronic lymphocytic leukemia. *Genes Chromosomes Cancer*. 2000;27(3):285-294. doi:10.1002/(SICI)1098-2264(200003)27:3<285::AID-GCC9>3.0.CO;2-M
73. Davids MS, Roberts AW, Seymour JF, et al. Phase i first-in-human study of venetoclax in patients with relapsed or refractory non-hodgkin lymphoma. In: *Journal of Clinical Oncology*. Vol 35. American Society of Clinical Oncology; 2017:826-833. doi:10.1200/JCO.2016.70.4320

REFERENCES

74. Jain N, Mamgain M, Chowdhury SM, et al. Beyond Bruton's tyrosine kinase inhibitors in mantle cell lymphoma: bispecific antibodies, antibody–drug conjugates, CAR T-cells, and novel agents. *J Hematol Oncol*. 2023;16(1). doi:10.1186/s13045-023-01496-4
75. Friedberg JW. Update on follicular lymphoma. *Hematol Oncol*. 2023;41(S1):43-47. doi:10.1002/hon.3138
76. Freedman A, Jacobsen E. Follicular lymphoma: 2020 update on diagnosis and management. *Am J Hematol*. 2020;95(3):316-327. doi:10.1002/ajh.25696
77. Nakajima R, Moskowitz AJ, Michaud L, et al. Baseline FDG-PET/CT detects bone marrow involvement in follicular lymphoma and provides relevant prognostic information. *Blood Adv*. 2020;4(8):1812-1823. doi:10.1182/bloodadvances.2020001579
78. Carreras J. The pathobiology of follicular lymphoma. *Journal of Clinical and Experimental Hematopathology*. 2023;63(3):152-163. doi:10.3960/jslrt.23014
79. Sarkozy C, Baseggio L, Feugier P, et al. Peripheral blood involvement in patients with follicular lymphoma: A rare disease manifestation associated with poor prognosis. *Br J Haematol*. 2014;164(5):659-667. doi:10.1111/bjh.12675
80. Huet S, Sujobert P, Salles G. From genetics to the clinic: A translational perspective on follicular lymphoma. *Nat Rev Cancer*. 2018;18(4):224-239. doi:10.1038/nrc.2017.127
81. Tsujimoto Y, Gorham J, Cossman J, Jaffe E, Croce CM. The t(14;18) Chromosome Translocations Involved in B-Cell Neoplasms Result from Mistakes in VDJ Joining. *Science (1979)*. 1985;229(4720):1390-1393. doi:10.1126/science.3929382
82. Limpens J, Stad R, Vos C, et al. *Lymphoma-Associated Translocation t(14; 18) in Blood B Cells of Normal Individuals*.
83. Roulland S, Kelly RS, Morgado E, et al. t(14;18) translocation: A predictive blood biomarker for follicular lymphoma. *Journal of Clinical Oncology*. 2014;32(13):1347-1355. doi:10.1200/JCO.2013.52.8190
84. Salaverria I, Weigert O, Quintanilla-Martinez L. The clinical and molecular taxonomy of t(14;18)-negative follicular lymphomas. *Blood Adv*. 2023;7(18):5258-5271. doi:10.1182/bloodadvances.2022009456

85. Sungalee S, Mamessier E, Morgado E, et al. Germinal center reentries of BCL2-overexpressing B cells drive follicular lymphoma progression. *Journal of Clinical Investigation*. 2014;124(12):5337-5351. doi:10.1172/JCI72415
86. Roulland S, Faroudi M, Mamessier E, Sungalee S, Salles G, Nadel B. Early Steps of Follicular Lymphoma Pathogenesis. In: *Advances in Immunology*. Vol 111. Academic Press Inc.; 2011:1-46. doi:10.1016/B978-0-12-385991-4.00001-5
87. Korfi K, Ali S, Heward JA, Fitzgibbon J. Follicular lymphoma, a B cell malignancy addicted to epigenetic mutations. *Epigenetics*. 2017;12(5):370-377. doi:10.1080/15592294.2017.1282587
88. Dobaño-lópez C, Araujo-ayala F, Serrat N, Valero JG, Pérez-galán P. Follicular lymphoma microenvironment: An intricate network ready for therapeutic intervention. *Cancers (Basel)*. 2021;13(4):1-22. doi:10.3390/cancers13040641
89. Morin RD, Mendez-Lago M, Mungall AJ, et al. Frequent mutation of histone-modifying genes in non-Hodgkin lymphoma. *Nature*. 2011;476(7360):298-303. doi:10.1038/nature10351
90. Okosun J, Bödör C, Wang J, Araf S, Yang C yuan. Europe PMC Funders Group Integrated genomic analysis identifies recurrent mutations and evolution patterns driving the initiation and progression of follicular lymphoma. 2014;46(2):176-181. doi:10.1038/ng.2856.Integrated
91. Pasqualucci L, Khiabanian H, Fangazio M, et al. Genetics of Follicular Lymphoma Transformation. *Cell Rep*. 2014;6(1):130-140. doi:10.1016/j.celrep.2013.12.027
92. Pastore A, Jurinovic V, Kridel R, et al. Integration of gene mutations in risk prognostication for patients receiving first-line immunochemotherapy for follicular lymphoma: A retrospective analysis of a prospective clinical trial and validation in a population-based registry. *Lancet Oncol*. 2015;16(9):1111-1122. doi:10.1016/S1470-2045(15)00169-2
93. Pasqualucci L, Dominguez-Sola D, Chiarenza A, et al. Inactivating mutations of acetyltransferase genes in B-cell lymphoma. *Nature*. 2011;471(7337):189-196. doi:10.1038/nature09730
94. Green MR, Kihira S, Liu CL, et al. Mutations in early follicular lymphoma progenitors are associated with suppressed antigen presentation. *Proc Natl Acad Sci U S A*. 2015;112(10):E1116-E1125. doi:10.1073/pnas.1501199112

REFERENCES

95. Krysiak K, Gomez F, White BS, et al. Recurrent somatic mutations affecting B-cell receptor signaling pathway genes in follicular lymphoma. *Blood*. 2017;129(4):473-483. doi:10.1182/blood-2016-07-729954
96. Bödör C, Grossmann V, Popov N, et al. EZH2 mutations are frequent and represent an early event in follicular lymphoma. *Blood*. 2013;122(18):3165-3168. doi:10.1182/blood-2013-04-496893
97. Béguelin W, Teater M, Meydan C, et al. Mutant EZH2 Induces a Pre-malignant Lymphoma Niche by Reprogramming the Immune Response. *Cancer Cell*. 2020;37(5):655-673.e11. doi:10.1016/j.ccell.2020.04.004
98. Cheung KJJ, Johnson NA, Affleck JG, et al. Acquired TNFRSF14 mutations in follicular lymphoma are associated with worse prognosis. *Cancer Res*. 2010;70(22):9166-9174. doi:10.1158/0008-5472.CAN-10-2460
99. Yildiz M, Li H, Bernard D, et al. Activating STAT6 mutations in follicular lymphoma. Published online 2015. doi:10.1182/blood-2014
100. Okosun J, Wolfson RL, Wang J, et al. Recurrent mTORC1-activating RRAGC mutations in follicular lymphoma. *Nat Genet*. 2016;48(2):183-188. doi:10.1038/ng.3473
101. Ying ZX, Jin M, Peterson LF, et al. Recurrent mutations in the MTOR regulator RRAGC in follicular lymphoma. In: *Clinical Cancer Research*. Vol 22. American Association for Cancer Research Inc.; 2016:5383-5393. doi:10.1158/1078-0432.CCR-16-0609
102. Ortega-Molina A, Deleyto-Seldas N, Carreras J, et al. Oncogenic Rag GTPase signalling enhances B cell activation and drives follicular lymphoma sensitive to pharmacological inhibition of mTOR. *Nat Metab*. 2019;1(8):775-789. doi:10.1038/s42255-019-0098-8
103. Verdière L, Mourcin F, Tarte K. Microenvironment signaling driving lymphomagenesis. *Curr Opin Hematol*. 2018;25(4):335-345. doi:10.1097/MOH.0000000000000440
104. Sugimoto T, Watanabe T. Follicular Lymphoma: The Role of the Tumor Microenvironment in Prognosis. *J Clin Exp Hematop*. 2016;56(1):1-19. doi:10.3960/jslrt.56.1
105. Dave SS, Wright G, Tan B, et al. Prediction of Survival in Follicular Lymphoma Based on Molecular Features of Tumor-Infiltrating Immune Cells. *New England Journal of Medicine*. 2004;351(21):2159-2169. doi:10.1056/NEJMoa041869

106. Amé-thomas P, Tarte K. The yin and the yang of follicular lymphoma cell niches: Role of microenvironment heterogeneity and plasticity. *Semin Cancer Biol.* 2014;24:23-32. doi:10.1016/j.semcancer.2013.08.001
107. Han G, Deng Q, Marques-Piubelli ML, et al. Follicular Lymphoma Microenvironment Characteristics Associated with Tumor Cell Mutations and MHC Class II Expression. *Blood Cancer Discov.* 2022;3(5):428-443. doi:10.1158/2643-3230.BCD-21-0075
108. Umetsu DT, Esserman L, Donlon TA, DeKruyff RH, Levy R. Induction of proliferation of human follicular (B type) lymphoma cells by cognate interaction with CD4+ T cell clones. *J Immunol.* 1990;144(7):2550-2557. <http://www.ncbi.nlm.nih.gov/pubmed/1969451>
109. Álvaro-Naranjo T, Lejeune M, Salvadó MT, et al. Immunohistochemical patterns of reactive microenvironment are associated with clinicobiologic behavior in follicular lymphoma patients. *Journal of Clinical Oncology.* 2006;24(34):5350-5357. doi:10.1200/JCO.2006.06.4766
110. Philip M, Schietinger A. CD8+ T cell differentiation and dysfunction in cancer. *Nat Rev Immunol.* 2022;22(4):209-223. doi:10.1038/s41577-021-00574-3
111. Gravelle P, Do C, Franchet C, et al. Impaired functional responses in follicular lymphoma CD8+TIM-3+ T lymphocytes following TCR engagement. *Oncoimmunology.* 2016;5(10). doi:10.1080/2162402X.2016.1224044
112. Yang ZZ, Kim HJ, Villasboas JC, et al. Expression of LAG-3 defines exhaustion of intratumoral PD-1+ T cells and correlates with poor outcome in follicular lymphoma. *Oncotarget.* 2017;8(37):61425-61439. doi:10.18632/oncotarget.18251
113. Yang ZZ, Kim HJ, Wu H, et al. TIGIT Expression Is Associated with T-cell Suppression and Exhaustion and Predicts Clinical Outcome and Anti-PD-1 Response in Follicular Lymphoma. *Clinical Cancer Research.* 2020;26(19):5217-5231. doi:10.1158/1078-0432.CCR-20-0558
114. Yang ZZ, Grote DM, Ziesmer SC, et al. IL-12 upregulates TIM-3 expression and induces T cell exhaustion in patients with follicular B cell non-Hodgkin lymphoma. *Journal of Clinical Investigation.* 2012;122(4):1271-1282. doi:10.1172/JCI59806

REFERENCES

115. Tay C, Tanaka A, Sakaguchi S. Tumor-infiltrating regulatory T cells as targets of cancer immunotherapy. *Cancer Cell*. 2023;41(3):450-465. doi:10.1016/j.ccell.2023.02.014
116. Farinha P, Al-Tourah A, Gill K, Klasa R, Connors JM, Gascoyne RD. The architectural pattern of FOXP3-positive T cells in follicular lymphoma is an independent predictor of survival and histologic transformation. *Blood*. 2010;115(2):289-295. doi:10.1182/blood-2009-07-235598
117. Yang ZZ, Novak AJ, Stenson MJ, Witzig TE, Ansell SM. Intratumoral CD4+CD25+ regulatory T-cell-mediated suppression of infiltrating CD4+ T cells in B-cell non-Hodgkin lymphoma. *Blood*. 2006;107(9):3639-3646. doi:10.1182/blood-2005-08-3376
118. Crotty S. Revealing T follicular helper cells with BCL6. *Nat Rev Immunol*. 2021;21(10):616-617. doi:10.1038/s41577-021-00591-2
119. Amé-Thomas P, Le Priol J, Yssel H, et al. Characterization of intratumoral follicular helper T cells in follicular lymphoma: Role in the survival of malignant B cells. *Leukemia*. 2012;26(5):1053-1063. doi:10.1038/leu.2011.301
120. Rawal S, Chu F, Zhang M, et al. Cross Talk between Follicular Th Cells and Tumor Cells in Human Follicular Lymphoma Promotes Immune Evasion in the Tumor Microenvironment. *The Journal of Immunology*. 2013;190(12):6681-6693. doi:10.4049/jimmunol.1201363
121. Chung Y, Tanaka S, Chu F, et al. Follicular regulatory T cells expressing Foxp3 and Bcl-6 suppress germinal center reactions. *Nat Med*. 2011;17(8):983-988. doi:10.1038/nm.2426
122. Aloulou M, Carr EJ, Gador M, et al. Follicular regulatory T cells can be specific for the immunizing antigen and derive from naive T cells. *Nat Commun*. 2016;7:1-10. doi:10.1038/ncomms10579
123. Wollenberg I, Agua-Doce A, Hernández A, et al. Regulation of the Germinal Center Reaction by Foxp3+ Follicular Regulatory T Cells. *The Journal of Immunology*. 2011;187(9):4553-4560. doi:10.4049/jimmunol.1101328
124. Linterman MA, Pierson W, Lee SK, et al. Foxp3+ follicular regulatory T cells control the germinal center response. *Nat Med*. 2011;17(8):975-982. doi:10.1038/nm.2425

125. Laidlaw BJ, Lu Y, Amezquita RA, et al. Interleukin-10 from CD4+ follicular regulatory T cells promotes the germinal center response. *Sci Immunol*. 2017;2(16):1-10. doi:10.1126/sciimmunol.aan4767
126. Xie MM, Dent AL. Unexpected Help: Follicular Regulatory T Cells in the Germinal Center. *Front Immunol*. 2018;9(July):1-9. doi:10.3389/fimmu.2018.01536
127. Carreras J, Lopez-Guillermo A, Fox BC, et al. High numbers of tumor-infiltrating FOXP3-positive regulatory T cells are associated with improved overall survival in follicular lymphoma. *Blood*. 2006;108(9):2957-2964. doi:10.1182/blood-2006-04-018218
128. Mourcin F, Pangault C, Amin-Ali R, Amé-Thomas P, Tarte K. Stromal cell contribution to human follicular lymphoma pathogenesis. *Front Immunol*. 2012;3(SEP):1-7. doi:10.3389/fimmu.2012.00280
129. Park CS, Choi YS. How do follicular dendritic cells interact intimately with B cells in the germinal centre? *Immunology*. 2005;114(1):2-10. doi:10.1111/j.1365-2567.2004.02075.x
130. Roozendaal R, Mebius RE. Stromal cell-immune cell interactions. *Annu Rev Immunol*. 2011;29:23-43. doi:10.1146/annurev-immunol-031210-101357
131. Boice M, Salloum D, Mourcin F, et al. Loss of the HVEM Tumor Suppressor in Lymphoma and Restoration by Modified CAR-T Cells. *Cell*. 2016;167(2):405-418.e13. doi:10.1016/j.cell.2016.08.032
132. Wang X, Cho B, Suzuki K, et al. Follicular dendritic cells help establish follicle identity and promote B cell retention in germinal centers. *Journal of Experimental Medicine*. 2011;208(12):2497-2510. doi:10.1084/jem.20111449
133. Pandey S, Mourcin F, Marchand T, et al. IL-4/CXCL12 loop is a key regulator of lymphoid stroma function in follicular lymphoma. *Blood*. 2017;129(18):2507-2518. doi:10.1182/blood-2016-08
134. Mourcin F, Verdière L, Roulois D, et al. Follicular lymphoma triggers phenotypic and functional remodeling of the human lymphoid stromal cell landscape. *Immunity*. 2021;54(8):1788-1806.e7. doi:10.1016/j.immuni.2021.05.019
135. Fletcher AL, Acton SE, Knoblich K. Lymph node fibroblastic reticular cells in health and disease. *Nat Rev Immunol*. 2015;15(6):350-361. doi:10.1038/nri3846

REFERENCES

136. Dubey LK, Ludewig B, Luther SA, Harris NL. IL-4R α -Expressing B Cells Are Required for CXCL13 Production by Fibroblastic Reticular Cells. *Cell Rep*. 2019;27(8):2442-2458.e5. doi:10.1016/j.celrep.2019.04.079
137. Amé -Thomas P, Ne H, Hajjami ME, et al. Human mesenchymal stem cells isolated from bone marrow and lymphoid organs support tumor B-cell growth: role of stromal cells in follicular lymphoma pathogenesis. Published online 2007. doi:10.1182/blood-2006-05
138. Guilloton F, Caron G, Ménard C, et al. Mesenchymal stromal cells orchestrate follicular lymphoma cell niche through the CCL2-dependent recruitment and polarization of monocytes. *Blood*. 2012;119(11):2556-2567. doi:10.1182/blood-2011-08-370908
139. Grégoire M, Guilloton F, Pangault C, et al. Neutrophils trigger a NF-KB dependent polarization of tumorsupportive stromal cells in germinal center B-cell lymphomas. *Oncotarget*. 2015;6(18):16471-16487. doi:10.18632/oncotarget.4106
140. Safi W, Kuehnl A, Nüssler A, Eckstein HH, Pelisek J. Differentiation of human CD14+ monocytes: an experimental investigation of the optimal culture medium and evidence of a lack of differentiation along the endothelial line. *Exp Mol Med*. 2016;48(4). doi:10.1038/EMM.2016.11
141. Ugel S, Canegrave S, De Sanctis F, Bronte V. Monocytes in the Tumor Microenvironment. *Annual Review of Pathology: Mechanisms of Disease*. 2021;16:93-122. doi:10.1146/annurev-pathmechdis-012418-013058
142. Farinha P, Masoudi H, Skinnider BF, et al. Analysis of multiple biomarkers shows that lymphoma-associated macrophage (LAM) content is an independent predictor of survival in follicular lymphoma (FL). *Blood*. 2005;106(6):2169-2174. doi:10.1182/blood-2005-04-1565
143. Canioni D, Salles G, Mounier N, et al. High numbers of tumor-associated macrophages have an adverse prognostic value that can be circumvented by rituximab in patients with follicular lymphoma enrolled onto the GELA-GOELAMS FL-2000 trial. *Journal of Clinical Oncology*. 2008;26(3):440-446. doi:10.1200/JCO.2007.12.8298
144. Clear AJ, Lee AM, Calaminici M, et al. Increased angiogenic sprouting in poor prognosis FL is associated with elevated numbers of CD163+ macrophages within the immediate sprouting microenvironment. *Blood*. 2010;115(24):5053-5056. doi:10.1182/blood-2009-11-253260

145. Kridel R, Xerri L, Gelas-Dore B, et al. The Prognostic Impact of CD163-Positive Macrophages in Follicular Lymphoma: A Study from the BC Cancer Agency and the Lymphoma Study Association. *Clin Cancer Res*. 2015;21(15):3428-3435. doi:10.1158/1078-0432.CCR-14-3253
146. Valero JG, Matas-Céspedes A, Arenas F, et al. The receptor of the colony-stimulating factor-1 (CSF-1R) is a novel prognostic factor and therapeutic target in follicular lymphoma. *Leukemia*. 2021;35(9):2635-2649. doi:10.1038/s41375-021-01201-9
147. Epron G, Ame-Thomas P, Le Priol J, et al. Monocytes and T cells cooperate to favor normal and follicular lymphoma B-cell growth: role of IL-15 and CD40L signaling. *Leukemia*. 2012;26(1):139-148. doi:10.1038/leu.2011.179
148. Amin R, Mourcin F, Uhel F, et al. DC-SIGN-expressing macrophages trigger activation of mannosylated IgM B-cell receptor in follicular lymphoma. *Blood*. 2015;126(16):1911-1920. doi:10.1182/blood-2015-04
149. Mantovani A, Allavena P, Marchesi F, Garlanda C. Macrophages as tools and targets in cancer therapy. *Nat Rev Drug Discov*. 2022;21(11):799-820. doi:10.1038/s41573-022-00520-5
150. Chen YP, Kim HJ, Wu H, et al. SIRP α expression delineates subsets of intratumoral monocyte/macrophages with different functional and prognostic impact in follicular lymphoma. *Blood Cancer J*. 2019;9(10). doi:10.1038/s41408-019-0246-0
151. Blaker YN, Spetalen S, Brodtkorb M, et al. The tumour microenvironment influences survival and time to transformation in follicular lymphoma in the rituximab era. *Br J Haematol*. 2016;175(1):102-114. doi:10.1111/bjh.14201
152. Dreyling M, Ghielmini M, Rule S, et al. Newly diagnosed and relapsed follicular lymphoma: ESMO Clinical Practice Guidelines for diagnosis, treatment and follow-up. *Annals of Oncology*. 2021;32(3):298-308. doi:10.1016/j.annonc.2020.11.008
153. Sarkozy C, Maurer MJ, Link BK, et al. Cause of death in follicular lymphoma in the first decade of the rituximab era: A pooled analysis of French and US cohorts. *Journal of Clinical Oncology*. 2019;37(2):144-152. doi:10.1200/JCO.18.00400
154. Gordon MJ, Smith MR, Nastoupil LJ. Follicular lymphoma: The long and winding road leading to your cure? *Blood Rev*. 2023;57. doi:10.1016/j.blre.2022.100992

REFERENCES

155. Solal-Céligny P, Roy P, Colombat P, et al. Follicular lymphoma international prognostic index. *Blood*. 2004;104(5):1258-1265. doi:10.1182/blood-2003-12-4434
156. Federico M, Bellei M, Marcheselli L, et al. Follicular lymphoma international prognostic index 2: A new prognostic index for follicular lymphoma developed by the international follicular lymphoma prognostic factor project. *Journal of Clinical Oncology*. 2009;27(27):4555-4562. doi:10.1200/JCO.2008.21.3991
157. Casulo C, Byrtek M, Dawson KL, et al. Early relapse of follicular lymphoma after rituximab plus cyclophosphamide, doxorubicin, vincristine, and prednisone defines patients at high risk for death: An analysis from the National LymphoCare Study. *Journal of Clinical Oncology*. 2015;33(23):2516-2522. doi:10.1200/JCO.2014.59.7534
158. Casulo C, Dixon JG, Le-Rademacher J, et al. Validation of POD24 as a robust early clinical end point of poor survival in FL from 5225 patients on 13 clinical trials. *Blood*. 2022;139(11):1684-1693. doi:10.1182/blood.2020010263
159. Hübel K, Ghielmini M, Ladetto M, Gopal AK. Controversies in the treatment of follicular lymphoma. *Hemasphere*. 2020;4(1). doi:10.1097/HS9.0000000000000317
160. Herfarth K, Borchmann P, Schnaidt S, et al. Rituximab with Involved Field Irradiation for Early-stage Nodal Follicular Lymphoma: Results of the MIR Study. *Hemasphere*. 2018;2(6). doi:10.1097/HS9.0000000000000160
161. Ardeschna KM, Smith P, Norton A, et al. Long-term effect of a watch and wait policy versus immediate systemic treatment for asymptomatic advanced-stage non-Hodgkin lymphoma: A randomised controlled trial. *Lancet*. 2003;362(9383):516-522. doi:10.1016/S0140-6736(03)14110-4
162. Ardeschna KM, Qian W, Smith P, et al. Rituximab versus a watch-and-wait approach in patients with advanced-stage, asymptomatic, non-bulky follicular lymphoma: An open-label randomised phase 3 trial. *Lancet Oncol*. 2014;15(4):424-435. doi:10.1016/S1470-2045(14)70027-0
163. Mössner E, Brünker P, Moser S, et al. Increasing the efficacy of CD20 antibody therapy through the engineering of a new type II anti-CD20 antibody with enhanced direct and immune effector cell - mediated B-cell cytotoxicity. *Blood*. 2010;115(22):4393-4402. doi:10.1182/blood-2009-06-225979

164. Luminari S, Ferrari A, Manni M, et al. Long-Term results of the FOLL05 trial comparing R-CVP Versus R-CHOP versus R-FM for the initial treatment of patients with advanced-stage symptomatic follicular lymphoma. *Journal of Clinical Oncology*. 2018;36(7):689-696. doi:10.1200/JCO.2017.74.1652
165. Bachy E, Seymour JF, Feugier P, et al. Sustained progression-free survival benefit of rituximab maintenance in patients with follicular lymphoma: Long-term results of the PRIMA study. *Journal of Clinical Oncology*. 2019;37(31):2815-2824. doi:10.1200/JCO.19.01073
166. Fowler NH, Davis RE, Rawal S, et al. Safety, activity, and immune effects of lenalidomide and rituximab in untreated indolent lymphoma. *Lancet Oncol*. 2014;15(12):1311-1318. doi:10.1016/S1470-2045(14)70455-3.Safety
167. Gopal AK, Kahl BS, de Vos S, et al. PI3K δ Inhibition by Idelalisib in Patients with Relapsed Indolent Lymphoma. *New England Journal of Medicine*. 2014;370(11):1008-1018. doi:10.1056/nejmoa1314583
168. Italiano A, Soria JC, Toulmonde M, et al. Tazemetostat, an EZH2 inhibitor, in relapsed or refractory B-cell non-Hodgkin lymphoma and advanced solid tumours: a first-in-human, open-label, phase 1 study. *Lancet Oncol*. 2018;19(5):649-659. doi:10.1016/S1470-2045(18)30145-1
169. Morschhauser F, Tilly H, Chaidos A, et al. Tazemetostat for patients with relapsed or refractory follicular lymphoma: an open-label, single-arm, multicentre, phase 2 trial. *Lancet Oncol*. 2020;21(11):1433-1442. doi:10.1016/S1470-2045(20)30441-1
170. Schuster SJ, Svoboda J, Chong EA, et al. Chimeric Antigen Receptor T Cells in Refractory B-Cell Lymphomas. *New England Journal of Medicine*. 2017;377(26):2545-2554. doi:10.1056/nejmoa1708566
171. Falchi L, Vardhana SA, Salles GA. Bispecific antibodies for the treatment of B-cell lymphoma: promises, unknowns, and opportunities. *Blood*. 2023;141(5):467-480. doi:10.1182/blood.2021011994
172. Budde LE, Sehn LH, Matasar M, et al. Safety and efficacy of mosunetuzumab, a bispecific antibody, in patients with relapsed or refractory follicular lymphoma: a single-arm, multicentre, phase 2 study. *Lancet Oncol*. 2022;23(8):1055-1065. doi:10.1016/S1470-2045(22)00335-7
173. Kridel R, Mottok A, Farinha P, et al. Cell of origin of transformed follicular lymphoma. *Blood*. 2015;126(18):2118-2127. doi:10.1182/blood-2015-06

REFERENCES

174. Link BK, Maurer MJ, Nowakowski GS, et al. Rates and outcomes of follicular lymphoma transformation in the immunochemotherapy era: A report from the university of Iowa/mayo clinic specialized program of research excellence molecular epidemiology resource. In: *Journal of Clinical Oncology*. Vol 31. American Society of Clinical Oncology; 2013:3272-3278. doi:10.1200/JCO.2012.48.3990
175. Federico M, Caballero Barrigón MD, Marcheselli L, et al. Rituximab and the risk of transformation of follicular lymphoma: a retrospective pooled analysis. *Lancet Haematol*. 2018;5(8):e359-e367. doi:10.1016/S2352-3026(18)30090-5
176. Kumar E, Pickard L, Okosun J. Pathogenesis of follicular lymphoma: genetics to the microenvironment to clinical translation. *Br J Haematol*. 2021;194(5):810-821. doi:10.1111/bjh.17383
177. Lossos IS, Gascoyne RD. Transformation of follicular lymphoma. *Best Pract Res Clin Haematol*. 2011;24(2):147-163. doi:10.1016/j.beha.2011.02.006
178. Maeshima AM, Taniguchi H, Fukuhara S, et al. Clinicopathological prognostic indicators in 107 patients with diffuse large B-cell lymphoma transformed from follicular lymphoma. *Cancer Sci*. 2013;104(7):952-957. doi:10.1111/cas.12158
179. Bouska A, McKeithan TW, Deffenbacher KE, et al. Genome-wide copy-number analyses reveal genomic abnormalities involved in transformation of follicular lymphoma. *Blood*. 2014;123(11):1681-1690. doi:10.1182/blood-2013-05-500595
180. Kaur G, Dufour JM. Cell lines. *Spermatogenesis*. 2012;2(1):1-5. doi:10.4161/spmg.19885
181. Maesako Y, Uchiyama T, Ohno H. Comparison of gene expression profiles of lymphoma cell lines from transformed follicular lymphoma, Burkitt's lymphoma and de novo diffuse large B-cell lymphoma. *Cancer Sci*. 2003;94(9):774-781. doi:10.1111/j.1349-7006.2003.tb01518.x
182. Olson B, Li Y, Lin Y, Liu ET, Patnaik A. Mouse models for cancer immunotherapy research. *Cancer Discov*. 2018;8(11):1358-1365. doi:10.1158/2159-8290.CD-18-0044
183. Byrne AT, Alférez DG, Amant F, et al. Interrogating open issues in cancer precision medicine with patient-derived xenografts. *Nat Rev Cancer*. 2017;17(4):254-268. doi:10.1038/nrc.2016.140

184. Zhang L, Nomie K, Zhang H, et al. B-Cell Lymphoma Patient-Derived Xenograft Models Enable Drug Discovery and Are a Platform for Personalized Therapy. *Clinical Cancer Research*. 2017;23(15):4212-4223. doi:10.1158/1078-0432.CCR-16-2703
185. Pasqualucci L, Klein U. Mouse models in the study of mature B-cell malignancies. *Cold Spring Harb Perspect Med*. 2021;11(4). doi:10.1101/cshperspect.a034827
186. Chiron D, Bellanger C, Papin A, et al. Rational targeted therapies to overcome microenvironment-dependent expansion of mantle cell lymphoma. *Blood*. 2016;128(24):2808-2818. doi:10.1182/blood-2016-06-720490
187. Rudelius M, Rosenfeldt MT, Leich E, et al. Inhibition of focal adhesion kinase overcomes resistance of mantle cell lymphoma to ibrutinib in the bone marrow microenvironment. *Haematologica*. 2018;103(1):116-125. doi:10.3324/haematol.2017.177162
188. Papin A, Tessoulin B, Bellanger C, et al. CSF1R and BTK inhibitions as novel strategies to disrupt the dialog between mantle cell lymphoma and macrophages. *Leukemia*. 2019;33(10):2442-2453. doi:10.1038/s41375-019-0463-3
189. Kim HS, Zhang X, Choi YS. Activation and proliferation of follicular dendritic cell-like cells by activated T lymphocytes. *The Journal of Immunology*. 1994;153(7):2951-2961. doi:10.4049/jimmunol.153.7.2951
190. Li L, Zhang X, Kovacic S, et al. Identification of a human follicular dendritic cell molecule that stimulates germinal center B cell growth. *Journal of Experimental Medicine*. 2000;191(6):1077-1083. doi:10.1084/jem.191.6.1077
191. Park CS, Yoon SO, Armitage RJ, Choi YS. Follicular Dendritic Cells Produce IL-15 That Enhances Germinal Center B Cell Proliferation in Membrane-Bound Form. *The Journal of Immunology*. 2004;173(11):6676-6683. doi:10.4049/jimmunol.173.11.6676
192. Serrat N, Guerrero-Hernández M, Matas-Céspedes A, et al. PI3Kd inhibition reshapes follicular lymphoma-immune microenvironment cross talk and unleashes the activity of venetoclax. *Blood Adv*. 2020;4(17):4217-4231. doi:10.1182/BLOODADVANCES.2020001584

REFERENCES

193. Caesar R, Di Re M, Krupka JA, et al. Genetic modification of primary human B cells to model high-grade lymphoma. *Nat Commun.* 2019;10(1):1-16. doi:10.1038/s41467-019-12494-x
194. Lamaison C, Latour S, Hélaine N, et al. A novel 3D culture model recapitulates primary FL B-cell features and promotes their survival. *Blood Adv.* 2021;5(23):5372-5386. doi:10.1182/bloodadvances.2020003949
195. Faria C, Gava F, Gravelle P, et al. Patient-derived lymphoma spheroids integrating immune tumor microenvironment as preclinical follicular lymphoma models for personalized medicine. *J Immunother Cancer.* 2023;11(10). doi:10.1136/jitc-2023-007156
196. Zanoni M, Cortesi M, Zamagni A, Arienti C, Pignatta S, Tesei A. Modeling neoplastic disease with spheroids and organoids. *J Hematol Oncol.* 2020;13(1). doi:10.1186/s13045-020-00931-0
197. Sant S, Johnston PA. The production of 3D tumor spheroids for cancer drug discovery. *Drug Discov Today Technol.* 2017;23:27-36. doi:10.1016/j.ddtec.2017.03.002
198. Pozzi S, Scomparin A, Israeli Dangoor S, et al. Meet me halfway: Are in vitro 3D cancer models on the way to replace in vivo models for nanomedicine development? *Adv Drug Deliv Rev.* 2021;175:113760. doi:10.1016/j.addr.2021.04.001
199. Vinci M, Gowan S, Boxall F, et al. Advances in establishment and analysis of three-dimensional tumor spheroid-based functional assays for target validation and drug evaluation. *BMC Biol.* 2012;10. doi:10.1186/1741-7007-10-29
200. Park SE, Georgescu A, Huh D. Organoids-on-a-chip. *Science (1979).* 2019;364(6444):960-965. doi:10.1126/science.aaw7894
201. Decaup E, Jean C, Laurent C, et al. Anti-tumor activity of obinutuzumab and rituximab in a follicular lymphoma 3D model. *Blood Cancer J.* 2013;3(8):e131. doi:10.1038/bcj.2013.32
202. Vidal-Crespo A, Matas-Céspedes A, Rodriguez V, et al. Daratumumab displays in vitro and in vivo anti-tumor activity in models of B-cell non-Hodgkin lymphoma and improves responses to standard chemo-immunotherapy regimens. *Haematologica.* 2020;105(4):1032-1041. doi:10.3324/haematol.2018.211904

203. Gava F, Faria C, Gravelle P, et al. 3d model characterization by 2d and 3d imaging in t(14;18)-positive b-nhl: Perspectives for in vitro drug screens in follicular lymphoma. *Cancers (Basel)*. 2021;13(7). doi:10.3390/cancers13071490
204. Haselager M V., Van Driel BF, Perelaer E, et al. In Vitro 3D Spheroid Culture System Displays Sustained T Cell-dependent CLL Proliferation and Survival. *Hemasphere*. 2023;7(9):E938. doi:10.1097/HS9.0000000000000938
205. Sbrana FV, Pinos R, Barbaglio F, et al. 3D Bioprinting Allows the Establishment of Long-Term 3D Culture Model for Chronic Lymphocytic Leukemia Cells. *Front Immunol*. 2021;12(May):1-15. doi:10.3389/fimmu.2021.639572
206. Foxall R, Narang P, Glaysher B, et al. Developing a 3D B Cell Lymphoma Culture System to Model Antibody Therapy. *Front Immunol*. 2021;11(February):1-20. doi:10.3389/fimmu.2020.605231
207. Mannino RG, Santiago-Miranda AN, Pradhan P, et al. 3D microvascular model recapitulates the diffuse large B-cell lymphoma tumor microenvironment in vitro. *Lab Chip*. 2017;17(3):407-414. doi:10.1039/c6lc01204c
208. Goodwin RG, Alderson MR, Smith CA, et al. Molecular and biological characterization of a ligand for CD27 defines a new family of cytokines with homology to tumor necrosis factor. *Cell*. 1993;73(3):447-456. doi:10.1016/0092-8674(93)90133-b
209. Bowman MR, Crimmins MA, Yetz-Aldape J, Kriz R, Kelleher K, Herrmann S. The cloning of CD70 and its identification as the ligand for CD27. *J Immunol*. 1994;152(4):1756-1761.
210. Tesselaar K, Gravestien LA, van Schijndel GM, Borst J, van Lier RA. Characterization of murine CD70, the ligand of the TNF receptor family member CD27. *J Immunol*. 1997;159(10):4959-4965.
211. Lens SMA, Drillenburger P, Den Drijver BFA, et al. Aberrant expression and reverse signalling of CD70 on malignant B cells. *Br J Haematol*. 1999;106(2):491-503. doi:10.1046/j.1365-2141.1999.01573.x
212. Flieswasser T, Van den Eynde A, Van Audenaerde J, et al. The CD70-CD27 axis in oncology: the new kids on the block. *Journal of Experimental and Clinical Cancer Research*. 2022;41(1):1-15. doi:10.1186/s13046-021-02215-y

REFERENCES

213. Hintzen RQ, Lens SM, Lammers K, Kuiper H, Beckmann MP, van Lier RA. Engagement of CD27 with its ligand CD70 provides a second signal for T cell activation. *J Immunol.* 1995;154(6):2612-2623.
214. Hendriks J, Gravestein LA, Tesselaar K, van Lier RA, Schumacher TN, Borst J. CD27 is required for generation and long-term maintenance of T cell immunity. *Nat Immunol.* 2000;1(5):433-440. doi:10.1038/80877
215. Arens R, Tesselaar K, Baars PA, et al. Constitutive CD27/CD70 interaction induces expansion of effector-type T cells and results in IFNgamma-mediated B cell depletion. *Immunity.* 2001;15(5):801-812. doi:10.1016/s1074-7613(01)00236-9
216. Kobata T, Jacquot S, Kozlowski S, Agematsu K, Schlossman SF, Morimoto C. *CD27-CD70 Interactions Regulate B-Cell Activation by T Cells (Tumor Necrosis Factor Receptor Family/Immunoregulation)*. Vol 92.; 1995. <https://www.pnas.org>
217. Arens R, Nolte MA, Tesselaar K, et al. Signaling through CD70 Regulates B Cell Activation and IgG Production. *The Journal of Immunology.* 2004;173(6):3901-3908. doi:10.4049/jimmunol.173.6.3901
218. Oshima H, Nakano H, Nohara C, et al. Characterization of murine CD70 by molecular cloning and mAb. *Int Immunol.* 1998;10(4):517-526. doi:10.1093/intimm/10.4.517
219. Jacobs J, Deschoolmeester V, Zwaenepoel K, et al. CD70: An emerging target in cancer immunotherapy. *Pharmacol Ther.* 2015;155:1-10. doi:10.1016/j.pharmthera.2015.07.007
220. Perna F, Berman SH, Soni RK, et al. Integrating Proteomics and Transcriptomics for Systematic Combinatorial Chimeric Antigen Receptor Therapy of AML. *Cancer Cell.* 2017;32(4):506-519.e5. doi:10.1016/j.ccell.2017.09.004
221. Silence K, Dreier T, Moshir M, et al. ARGX-110, a highly potent antibody targeting CD70, eliminates tumors via both enhanced ADCC and immune checkpoint blockade. *MAbs.* 2014;6(2):523-532. doi:10.4161/mabs.27398
222. Riether C, Pabst T, Höpner S, et al. Targeting CD70 with cusatuzumab eliminates acute myeloid leukemia stem cells in patients treated with hypomethylating agents. *Nat Med.* 2020;26(9):1459-1467. doi:10.1038/s41591-020-0910-8

223. Pabst T, Vey N, Adès L, et al. Results from a phase I/II trial of cusatuzumab combined with azacitidine in patients with newly diagnosed acute myeloid leukemia who are ineligible for intensive chemotherapy. *Haematologica*. 2023;108(7):1793-1802. doi:10.3324/haematol.2022.281563
224. Ikezoe T, Usuki K, Aida K, Hatayama T, Shirahase T, Yamauchi T. Cusatuzumab plus azacitidine in Japanese patients with newly diagnosed acute myeloid leukemia ineligible for intensive treatment. *Cancer Sci*. 2023;114(3):1037-1044. doi:10.1111/cas.15663
225. Aftimos P, Rolfo C, Rottey S, et al. Phase I dose-escalation study of the anti-CD70 antibody ARGX-110 in advanced malignancies. *Clinical Cancer Research*. 2017;23(21):6411-6420. doi:10.1158/1078-0432.CCR-17-0613
226. Leupin N, Zinzani PL, Morschhauser F, et al. Cusatuzumab for treatment of CD70-positive relapsed or refractory cutaneous T-cell lymphoma. *Cancer*. 2022;128(5):1004-1014. doi:10.1002/cncr.34005
227. Chen SS, Yan XJ, Van Rompaey L, Zabrocki P, Chiorazzi N. Anti-CD70 Monoclonal Antibodies Show Efficacy in Preclinical Models for Chronic Lymphoblastic Leukemia. *Blood*. 2022;140(Supplement 1):1803-1804. doi:10.1182/blood-2022-159016
228. Phillips T, Barr PM, Park SI, et al. A phase 1 trial of SGN-CD70A in patients with CD70-positive diffuse large B cell lymphoma and mantle cell lymphoma. *Invest New Drugs*. 2019;37(2):297-306. doi:10.1007/s10637-018-0655-0
229. Wang H, Horbinski C, Wu H, et al. NanoStringDiff: A novel statistical method for differential expression analysis based on NanoString nCounter data. *Nucleic Acids Res*. 2016;44(20):e151. doi:10.1093/nar/gkw677
230. Owonikoko TK, Hussain A, Stadler WM, et al. First-in-human multicenter phase i study of BMS-936561 (MDX-1203), an antibody-drug conjugate targeting CD70. *Cancer Chemother Pharmacol*. 2016;77(1):155-162. doi:10.1007/s00280-015-2909-2
231. Vitale LA, He LZ, Thomas LJ, et al. Development of a human monoclonal antibody for potential therapy of CD27-expressing lymphoma and leukemia. *Clinical Cancer Research*. 2012;18(14):3812-3821. doi:10.1158/1078-0432.CCR-11-3308
232. Ramakrishna V, Sundarapandiyan K, Zhao B, Bylesjo M, Marsh HC, Keler T. Characterization of the human T cell response to in vitro CD27 costimulation

REFERENCES

- with varlilumab. *J Immunother Cancer*. 2015;3(1). doi:10.1186/s40425-015-0080-2
233. Wasiuk A, Testa J, Weidlick J, et al. CD27-Mediated Regulatory T Cell Depletion and Effector T Cell Costimulation Both Contribute to Antitumor Efficacy. *The Journal of Immunology*. 2017;199(12):4110-4123. doi:10.4049/jimmunol.1700606
 234. Buchan SL, Fallatah M, Thirdborough SM, et al. Pd-1 blockade and cd27 stimulation activate distinct transcriptional programs that synergize for CD8 β T-cell-driven antitumor immunity. *Clinical Cancer Research*. 2018;24(10):2383-2394. doi:10.1158/1078-0432.CCR-17-3057
 235. Burris HA, Infante JR, Ansell SM, et al. JOURNAL OF CLINICAL ONCOLOGY Safety and Activity of Varlilumab, a Novel and First-in-Class Agonist Anti-CD27 Antibody, in Patients With Advanced Solid Tumors. *J Clin Oncol*. 2017;35:2028-2036. doi:10.1200/JCO
 236. Sanborn RE, Pishvaian MJ, Callahan MK, et al. Safety, tolerability and efficacy of agonist anti-CD27 antibody (varlilumab) administered in combination with anti-PD-1 (nivolumab) in advanced solid tumors. In: *Journal for ImmunoTherapy of Cancer*. Vol 10. BMJ Publishing Group; 2022. doi:10.1136/jitc-2022-005147
 237. Ansell SM, Flinn I, Taylor MH, et al. Safety and activity of varlilumab, a novel and first-in-class agonist anti-CD27 antibody, for hematologic malignancies. *Blood Adv*. 2020;4(9):1917-1926. doi:10.1182/bloodadvances.2019001079
 238. Singh AK, McGuirk JP. CAR T cells: continuation in a revolution of immunotherapy. *Lancet Oncol*. 2020;21(3):e168-e178. doi:10.1016/S1470-2045(19)30823-X
 239. June CH, Sadelain M. Chimeric Antigen Receptor Therapy. *New England Journal of Medicine*. 2018;379(1):64-73. doi:10.1056/NEJMra1706169
 240. Krause A, Guo HF, Latouche JB, Tan C, Cheung NK V, Sadelain M. *Antigen-Dependent CD28 Signaling Selectively Enhances Survival and Proliferation in Genetically Modified Activated Human Primary T Lymphocytes*. Vol 188.; 1998. <http://www.jem.org>
 241. Maher J, Brentjens RJ, Gunset G, Rivière I, Sadelain M. *Human T-Lymphocyte Cytotoxicity and Proliferation Directed by a Single Chimeric TCR ζ /CD28 Receptor*.; 2002. <http://biotech.nature.com>

242. Imai C, Ross C, Reid G, et al. Expression of the adaptor protein BLNK/SLP-65 in children acute lymphoblastic leukemia. *Leukemia*. 2004;18(5):922-925. doi:10.1038/sj.leu.2403349
243. Chmielewski M, Abken H. TRUCKs: The fourth generation of CARs. *Expert Opin Biol Ther*. 2015;15(8):1145-1154. doi:10.1517/14712598.2015.1046430
244. Huang R, Li X, He Y, et al. Recent advances in CAR-T cell engineering. *J Hematol Oncol*. 2020;13(1). doi:10.1186/s13045-020-00910-5
245. Jhunjhunwala S, Hammer C, Delamarre L. Antigen presentation in cancer: insights into tumour immunogenicity and immune evasion. *Nat Rev Cancer*. 2021;21(5):298-312. doi:10.1038/s41568-021-00339-z
246. Ramírez-Chacón A, Betriu-Méndez S, Bartoló-Ibars A, González A, Martí M, Juan M. Ligand-based CAR-T cell: Different strategies to drive T cells in future new treatments. *Front Immunol*. 2022;13. doi:10.3389/fimmu.2022.932559
247. Branella GM, Spencer HT. Natural receptor-and ligand-based chimeric antigen receptors: Strategies using natural ligands and receptors for targeted cell killing. *Cells*. 2022;11(1). doi:10.3390/cells11010021
248. Rafiq S, Hackett CS, Brentjens RJ. Engineering strategies to overcome the current roadblocks in CAR T cell therapy. *Nat Rev Clin Oncol*. 2020;17(3):147-167. doi:10.1038/s41571-019-0297-y
249. Ruella M, Kalos M. Adoptive immunotherapy for cancer. *Immunol Rev*. 2014;257(1):14-38. doi:10.1111/imr.12136
250. Ortiz-Maldonado V, Rives S, Castellà M, et al. CART19-BE-01: A Multicenter Trial of ARI-0001 Cell Therapy in Patients with CD19+ Relapsed/Refractory Malignancies. *Molecular Therapy*. 2021;29(2):636-644. doi:10.1016/j.ymthe.2020.09.027
251. Juan M, Delgado J, Calvo G, Trias E, Urbano-Ispizua Á. Is Hospital Exemption an Alternative or a Bridge to European Medicines Agency for Developing Academic Chimeric Antigen Receptor T-Cell in Europe? Our Experience with ARI-0001. *Hum Gene Ther*. 2021;32(19-20):1004-1007. doi:10.1089/hum.2021.168
252. Ortiz-Maldonado V, Frigola G, Español-Rego M, et al. Results of ARI-0001 CART19 Cells in Patients With Chronic Lymphocytic Leukemia and Richter's Transformation. *Front Oncol*. 2022;12. doi:10.3389/fonc.2022.828471

REFERENCES

253. Mozas P, Sorigué M, López-Guillermo A. Follicular lymphoma: an update on diagnosis, prognosis, and management. *Med Clin (Barc)*. 2021;157(9):440-448. doi:10.1016/j.medcli.2021.03.041
254. Hirayama A V, Gauthier J, Hay KA, et al. *Brief Report High Rate of Durable Complete Remission in Follicular Lymphoma after CD19 CAR-T Cell Immunotherapy.*; 2019. <http://ashpublications.org/blood/article-pdf/134/7/636/1554299/bloodbld2019000905.pdf>
255. Cappell KM, Kochenderfer JN. Long-term outcomes following CAR T cell therapy: what we know so far. *Nat Rev Clin Oncol*. 2023;20(6):359-371. doi:10.1038/s41571-023-00754-1
256. Cappell KM, Sherry RM, Yang JC, et al. Long-Term Follow-Up of Anti-CD19 Chimeric Antigen Receptor T-Cell Therapy. *J Clin Oncol*. 2020;38:3805-3815. doi:10.1200/JCO.20
257. Oliver-Caldés A, González-Calle V, Cabañas V, et al. Fractionated initial infusion and booster dose of ARI0002h, a humanised, BCMA-directed CAR T-cell therapy, for patients with relapsed or refractory multiple myeloma (CARTBCMA-HCB-01): a single-arm, multicentre, academic pilot study. *Lancet Oncol*. 2023;24(8):913-924. doi:10.1016/S1470-2045(23)00222-X
258. Bachiller M, Dobaño-López C, Rodríguez-García A, et al. Co-Transduced CD19/BCMA Dual-Targeting CAR-T Cells for the Treatment of Non-Hodgkin Lymphoma. *Blood*. 2022;140(Supplement 1):7386-7387. doi:10.1182/blood-2022-168651
259. Qin H, Ramakrishna S, Nguyen S, et al. Preclinical Development of Bivalent Chimeric Antigen Receptors Targeting Both CD19 and CD22. *Mol Ther Oncolytics*. 2018;11:127-137. doi:10.1016/j.omto.2018.10.006
260. Huang C, Zhang HC, Ho JY, et al. Dual specific CD19/CD22-targeted chimeric antigen receptor T-cell therapy for refractory diffuse large B-cell lymphoma: A case report. *Oncol Lett*. 2020;20(4):21. doi:10.3892/ol.2020.11882
261. Wei G, Zhang Y, Zhao H, et al. CD19/CD22 dual-targeted car t-cell therapy for relapsed/refractory aggressive b-cell lymphoma: A safety and efficacy study. *Cancer Immunol Res*. 2021;9(9):1061-1070. doi:10.1158/2326-6066.CIR-20-0675
262. Roddie C, Lekakis LJ, Marzolini MA V, et al. *Dual Targeting of CD19 and CD22 with Bicistronic CAR-T Cells in Patients with Relapsed/Refractory Large B-Cell*

- Lymphoma*. http://ashpublications.org/blood/article-pdf/141/20/2470/2051702/blood_bld-2022-018598-main.pdf
263. Spiegel JY, Patel S, Muffly L, et al. CAR T cells with dual targeting of CD19 and CD22 in adult patients with recurrent or refractory B cell malignancies: a phase 1 trial. *Nat Med*. 2021;27(8):1419-1431. doi:10.1038/s41591-021-01436-0
 264. Roddie C, Lekakis LJ, Marzolini MAV, et al. Dual targeting of CD19 and CD22 with bicistronic CAR-T cells in patients with relapsed/refractory large B-cell lymphoma. *Blood*. 2023;141(20):2470-2482. doi:10.1182/blood.2022018598
 265. Deng W, Chen P, Lei W, et al. CD70-targeting CAR-T cells have potential activity against CD19-negative B-cell Lymphoma. *Cancer Commun*. 2021;41(9):925-929. doi:10.1002/cac2.12201
 266. Tu S, Zhou X, Guo Z, et al. CD19 and CD70 Dual-Target Chimeric Antigen Receptor T-Cell Therapy for the Treatment of Relapsed and Refractory Primary Central Nervous System Diffuse Large B-Cell Lymphoma. *Front Oncol*. 2019;9. doi:10.3389/fonc.2019.01350
 267. Park YP, Jin L, Bennett KB, et al. CD70 as a target for chimeric antigen receptor T cells in head and neck squamous cell carcinoma. *Oral Oncol*. 2018;78:145-150. doi:10.1016/j.oraloncology.2018.01.024
 268. Jin L, Ge H, Long Y, et al. CD70, a novel target of CAR T-cell therapy for gliomas. *Neuro Oncol*. 2018;20(1):55-65. doi:10.1093/neuonc/nox116
 269. Shaffer DR, Savoldo B, Yi Z, et al. T cells redirected against CD70 for the immunotherapy of CD70-positive malignancies. *Blood*. 2011;117(16):4304-4314. doi:10.1182/blood-2010-04-278218
 270. Wang QJ, Yu Z, Hanada KI, et al. Preclinical evaluation of chimeric antigen receptors targeting CD70-expressing cancers. *Clinical Cancer Research*. 2017;23(9):2267-2276. doi:10.1158/1078-0432.CCR-16-1421
 271. Zhu G, Zhang J, Zhang Q, et al. Enhancement of CD70-specific CAR T treatment by IFN- γ released from oHSV-1-infected glioblastoma. *Cancer Immunology, Immunotherapy*. 2022;71(10):2433-2448. doi:10.1007/s00262-022-03172-x
 272. Sauer T, Parikh K, Sharma S, et al. CD70-specific CAR T cells have potent activity against acute myeloid leukemia without HSC toxicity. *Blood*. 2021;138(4):318-330. doi:10.1182/blood.2020008221

REFERENCES

273. Leick MB, Silva H, Scarfò I, et al. Non-cleavable hinge enhances avidity and expansion of CAR-T cells for acute myeloid leukemia. *Cancer Cell*. 2022;40(5):494-508.e5. doi:10.1016/j.ccell.2022.04.001
274. Seyfrid M, Maich WT, Shaikh VM, et al. CD70 as an actionable immunotherapeutic target in recurrent glioblastoma and its microenvironment. *J Immunother Cancer*. 2022;10(1):1-20. doi:10.1136/jitc-2021-003289
275. Wu G, Guo S, Luo Q, et al. Preclinical evaluation of CD70-specific CAR T cells targeting acute myeloid leukemia. *Front Immunol*. 2023;14. doi:10.3389/fimmu.2023.1093750
276. Nilsson MB, Yang Y, Heeke S, et al. CD70 is a therapeutic target upregulated in EMT-associated EGFR tyrosine kinase inhibitor resistance. *Cancer Cell*. 2023;41(2):340-355.e6. doi:10.1016/j.ccell.2023.01.007
277. Cheng J, Ge T, Zhu X, et al. Preclinical development and evaluation of nanobody-based CD70-specific CAR T cells for the treatment of acute myeloid leukemia. *Cancer Immunology, Immunotherapy*. 2023;72(7):2331-2346. doi:10.1007/s00262-023-03422-6
278. Cooper ML, Choi J, Staser K, et al. An “off-the-shelf” fratricide-resistant CAR-T for the treatment of T cell hematologic malignancies. *Leukemia*. 2018;32(9):1970-1983. doi:10.1038/s41375-018-0065-5
279. Panowski SH, Srinivasan S, Tan N, et al. Preclinical Development and Evaluation of Allogeneic CAR T Cells Targeting CD70 for the Treatment of Renal Cell Carcinoma. *Cancer Res*. 2022;82(14):2610-2624. doi:10.1158/0008-5472.CAN-21-2931
280. Herishanu Y, Pérez-Galán P, Liu D, et al. The lymph node microenvironment promotes B-cell receptor signaling, NF- κ B activation, and tumor proliferation in chronic lymphocytic leukemia. *Blood*. 2011;117(2):563-574. doi:10.1182/blood-2010-05-284984
281. Herndon TM, Chen SS, Saba NS, et al. Direct in vivo evidence for increased proliferation of CLL cells in lymph nodes compared to bone marrow and peripheral blood. *Leukemia*. 2017;31(6):1340-1347. doi:10.1038/leu.2017.11
282. Riedl A, Schleder M, Pudalko K, et al. Comparison of cancer cells in 2D vs 3D culture reveals differences in AKT-mTOR-S6K signaling and drug responses. *J Cell Sci*. 2017;130(1):203-218. doi:10.1242/jcs.188102

283. Apoorva F, Loiben AM, Shah SB, et al. How Biophysical Forces Regulate Human B Cell Lymphomas. *Cell Rep.* 2018;23(2):499-511. doi:10.1016/j.celrep.2018.03.069
284. Mongini PKA, Gupta R, Boyle E, et al. TLR-9 and IL-15 Synergy Promotes the In Vitro Clonal Expansion of Chronic Lymphocytic Leukemia B Cells. *The Journal of Immunology.* 2015;195(3):901-923. doi:10.4049/jimmunol.1403189
285. Epron G, Ame-Thomas P, Le Priol J, et al. Monocytes and T cells cooperate to favor normal and follicular lymphoma B-cell growth: role of IL-15 and CD40L signaling. *Leukemia.* 2012;26(1):139-148. doi:10.1038/leu.2011.179
286. Gelebart P, Zak Z, Anand M, Dien-Bard J, Amin HM, Lai R. Interleukin-21 effectively induces apoptosis in mantle cell lymphoma through a STAT1-dependent mechanism. *Leukemia.* 2009;23(10):1836-1846. doi:10.1038/leu.2009.100
287. Leadbetter EA, Rifkin IR, Hohlbaum AM, Beaudette BC, Shlomchik MJ, Marshak-Rothstein A. *Chromatin-IgG Complexes Activate B Cells by Dual Engagement of IgM and Toll-like Receptors.*; 2002. www.nature.com
288. Muzio M, Bertilaccio MTS, Simonetti G, Frenquelli M, Caligaris-Cappio F. The role of Toll-like receptors in chronic B cell malignancies. *Leuk Lymphoma.* 2009;50(10):1573-1580. doi:10.1080/10428190903115410
289. Rosenwald A, Wright G, Wiestner A, et al. The proliferation gene expression signature is a quantitative integrator of oncogenic events that predicts survival in mantle cell lymphoma. *Cancer Cell.* 2003;3(2):185-197. doi:10.1016/S1535-6108(03)00028-X
290. Fuhr V, Heidenreich S, Srivastava M, et al. CD52 and OXPHOS-potential targets in ibrutinib-treated mantle cell lymphoma. *Cell Death Discov.* 2022;8(1):505. doi:10.1038/s41420-022-01289-7
291. Martinez FO, Gordon S, Locati M, Mantovani A. Transcriptional profiling of the human monocyte-to-macrophage differentiation and polarization: new molecules and patterns of gene expression. *J Immunol.* 2006;177(10):7303-7311. doi:10.4049/jimmunol.177.10.7303
292. Jaguin M, Houlbert N, Fardel O, Lecureur V. Polarization profiles of human M-CSF-generated macrophages and comparison of M1-markers in classically activated macrophages from GM-CSF and M-CSF origin. *Cell Immunol.* 2013;281(1):51-61. doi:10.1016/j.cellimm.2013.01.010

REFERENCES

293. Imamura Y, Mukohara T, Shimono Y, et al. Comparison of 2D- and 3D-culture models as drug-testing platforms in breast cancer. *Oncol Rep.* 2015;33(4):1837-1843. doi:10.3892/or.2015.3767
294. Nizzoli ME, Manni M, Ghiggi C, et al. Impact of immunochemotherapy with R-bendamustine or R-CHOP for treatment naïve advanced-stage follicular lymphoma: A subset analysis of the FOLL12 trial by Fondazione Italiana Linfomi. *Hematol Oncol.* 2023;41(4):655-662. doi:10.1002/hon.3184
295. Wang ML, Jurczak W, Jerkeman M, et al. Ibrutinib plus Bendamustine and Rituximab in Untreated Mantle-Cell Lymphoma. *New England Journal of Medicine.* 2022;386(26):2482-2494. doi:10.1056/nejmoa2201817
296. Provencio M, Nadal E, González-Larriba JL, et al. Perioperative Nivolumab and Chemotherapy in Stage III Non–Small-Cell Lung Cancer. *New England Journal of Medicine.* 2023;389(6):504-513. doi:10.1056/nejmoa2215530
297. Ralli M, Botticelli A, Visconti IC, et al. Immunotherapy in the Treatment of Metastatic Melanoma: Current Knowledge and Future Directions. *J Immunol Res.* 2020;2020. doi:10.1155/2020/9235638
298. Armand P, Shipp MA, Ribrag V, et al. Programmed death-1 blockade with pembrolizumab in patients with classical hodgkin lymphoma after brentuximab vedotin failure. In: *Journal of Clinical Oncology.* Vol 34. American Society of Clinical Oncology; 2016:3733-3739. doi:10.1200/JCO.2016.67.3467
299. Lesokhin AM, Ansell SM, Armand P, et al. Nivolumab in patients with relapsed or refractory hematologic malignancy: Preliminary results of a phase ib study. *Journal of Clinical Oncology.* 2016;34(23):2698-2704. doi:10.1200/JCO.2015.65.9789
300. Younes A, Brody J, Carpio C, et al. Safety and activity of ibrutinib in combination with nivolumab in patients with relapsed non-Hodgkin lymphoma or chronic lymphocytic leukaemia: a phase 1/2a study. *Lancet Haematol.* 2019;6(2):e67-e78. doi:10.1016/S2352-3026(18)30217-5
301. Westin JR, Chu F, Zhang M, et al. Safety and activity of PD1 blockade by pidilizumab in combination with rituximab in patients with relapsed follicular lymphoma: a single group, open-label, phase 2 trial. *Lancet Oncol.* 2014;15(1):69-77. doi:10.1016/S1470-2045(13)70551-5

302. Nastoupil LJ, Chin CK, Westin JR, et al. Safety and activity of pembrolizumab in combination with rituximab in relapsed or refractory follicular lymphoma. *Blood Adv.* 2022;6(4):1143-1151. doi:10.1182/bloodadvances.2021006240
303. Huang YH, Zhu C, Kondo Y, et al. CEACAM1 regulates TIM-3-mediated tolerance and exhaustion. *Nature.* 2015;517(7534):386-390. doi:10.1038/nature13848
304. Wolf Y, Anderson AC, Kuchroo VK. TIM3 comes of age as an inhibitory receptor. *Nat Rev Immunol.* 2020;20(3):173-185. doi:10.1038/s41577-019-0224-6
305. Sabatos-Peyton CA, Nevin J, Brock A, et al. Blockade of Tim-3 binding to phosphatidylserine and CEACAM1 is a shared feature of anti-Tim-3 antibodies that have functional efficacy. *Oncoimmunology.* 2018;7(2). doi:10.1080/2162402X.2017.1385690
306. Yang R, Sun L, Li CF, et al. Galectin-9 interacts with PD-1 and TIM-3 to regulate T cell death and is a target for cancer immunotherapy. *Nat Commun.* 2021;12(1). doi:10.1038/s41467-021-21099-2
307. Schlichtner S, Yasinska IM, Lall GS, et al. T lymphocytes induce human cancer cells derived from solid malignant tumors to secrete galectin-9 which facilitates immunosuppression in cooperation with other immune checkpoint proteins. *J Immunother Cancer.* 2023;11(1). doi:10.1136/jitc-2022-005714
308. Mantuano NR, Natoli M, Zippelius A, Läubli H. Tumor-associated carbohydrates and immunomodulatory lectins as targets for cancer immunotherapy. *J Immunother Cancer.* 2020;8(2). doi:10.1136/jitc-2020-001222
309. Mariño K V., Cagnoni AJ, Croci DO, Rabinovich GA. Targeting galectin-driven regulatory circuits in cancer and fibrosis. *Nat Rev Drug Discov.* 2023;22(4):295-316. doi:10.1038/s41573-023-00636-2
310. Pang N, Alimu X, Chen R, et al. Activated Galectin-9/Tim3 promotes Treg and suppresses Th1 effector function in chronic lymphocytic leukemia. *FASEB Journal.* 2021;35(7). doi:10.1096/fj.202100013R
311. Laurent C, Dietrich S, Tarte K. Cell cross talk within the lymphoma tumor microenvironment: follicular lymphoma as a paradigm. *Blood.* 2024;143(12):1080-1090. doi:10.1182/blood.2023021000

REFERENCES

312. Karpathiou G, Papoudou-Bai A, Ferrand E, Dumollard JM, Peoc'h M. STAT6: A review of a signaling pathway implicated in various diseases with a special emphasis in its usefulness in pathology. *Pathol Res Pract*. 2021;223. doi:10.1016/j.prp.2021.153477
313. Fruman DA, Rommel C. PI3K and cancer: Lessons, challenges and opportunities. *Nat Rev Drug Discov*. 2014;13(2):140-156. doi:10.1038/nrd4204
314. Naba A, Clauser KR, Hoersch S, Liu H, Carr SA, Hynes RO. The matrisome: In silico definition and in vivo characterization by proteomics of normal and tumor extracellular matrices. *Molecular and Cellular Proteomics*. 2012;11(4). doi:10.1074/mcp.M111.014647
315. Abe Y, Sakata-Yanagimoto M, Fujisawa M, et al. A single-cell atlas of non-haematopoietic cells in human lymph nodes and lymphoma reveals a landscape of stromal remodelling. *Nat Cell Biol*. 2022;24(4):565-578. doi:10.1038/s41556-022-00866-3
316. Radtke AJ, Postovalova E, Varlamova A, et al. Multi-omic profiling of follicular lymphoma reveals changes in tissue architecture and enhanced stromal remodeling in high-risk patients. *Cancer Cell*. 2024;42(3):444-463.e10. doi:10.1016/j.ccell.2024.02.001
317. Yang ZZ, Kim HJ, Villasboas JC, et al. Mass Cytometry Analysis Reveals that Specific Intratumoral CD4 + T Cell Subsets Correlate with Patient Survival in Follicular Lymphoma. *Cell Rep*. 2019;26(8):2178-2193.e3. doi:10.1016/j.celrep.2019.01.085
318. Mondello P, Fama A, Larson MC, et al. Lack of intrafollicular memory CD4 + T cells is predictive of early clinical failure in newly diagnosed follicular lymphoma. *Blood Cancer J*. 2021;11(7). doi:10.1038/s41408-021-00521-4
319. Ye X, Wang L, Nie M, et al. A single-cell atlas of diffuse large B cell lymphoma. *Cell Rep*. 2022;39(3). doi:10.1016/j.celrep.2022.110713
320. Ranheim EA, Cantwell MJ, Kipps TJ. Expression of CD27 and its ligand, CD70, on chronic lymphocytic leukemia B cells. *Blood*. 1995;85(12):3556-3565. <http://www.ncbi.nlm.nih.gov/pubmed/7540066>
321. Yang ZZ, Novak AJ, Ziesmer SC, Witzig TE, Ansell SM. CD70+ non-Hodgkin lymphoma B cells induce Foxp3 expression and regulatory function in intratumoral CD4+CD25- T cells. *Blood*. 2007;110(7):2537-2544. doi:10.1182/blood-2007-03-082578

322. Yang ZZ, Novak AJ, Ziesmer SC, Witzig TE, Ansell SM. Malignant B cells skew the balance of regulatory T cells and T H17 cells in B-cell non-Hodgkin's lymphoma. *Cancer Res.* 2009;69(13):5522-5530. doi:10.1158/0008-5472.CAN-09-0266
323. Yang ZZ, Grote DM, Xiu B, et al. TGF- β upregulates CD70 expression and induces exhaustion of effector memory T cells in B-cell non-Hodgkin's lymphoma. *Leukemia.* 2014;28(9):1872-1884. doi:10.1038/leu.2014.84
324. Muth S, Klaric A, Radsak M, Schild H, Probst HC. CD27 expression on Treg cells limits immune responses against tumors. *J Mol Med.* 2022;100(3):439-449. doi:10.1007/s00109-021-02116-9
325. Bowakim-Anta N, Acolty V, Azouz A, et al. Chronic CD27-CD70 costimulation promotes type 1-specific polarization of effector Tregs. *Front Immunol.* 2023;14. doi:10.3389/fimmu.2023.1023064
326. Korbecki J, Kojder K, Simińska D, et al. Cc chemokines in a tumor: A review of pro-cancer and anti-cancer properties of the ligands of receptors ccr1, ccr2, ccr3, and ccr4. *Int J Mol Sci.* 2020;21(21):1-29. doi:10.3390/ijms21218412
327. Goto N, Tsurumi H, Takemura M, et al. Serum soluble CD27 level is associated with outcome in patients with diffuse large B-cell lymphoma treated with rituximab, cyclophosphamide, doxorubicin, vincristine and prednisolone. *Leuk Lymphoma.* 2012;53(8):1494-1500. doi:10.3109/10428194.2012.660627
328. Milpied P, Cervera-Marzal I, Mollicella ML, et al. Human germinal center transcriptional programs are de-synchronized in B cell lymphoma. *Nat Immunol.* 2018;19(9):1013-1024. doi:10.1038/s41590-018-0181-4
329. Wang X, Nissen M, Gracias D, et al. Single-cell profiling reveals a memory B cell-like subtype of follicular lymphoma with increased transformation risk. *Nat Commun.* 2022;13(1). doi:10.1038/s41467-022-34408-0
330. Perrett M, Pickard L, Kumar E, et al. Longitudinal Single Cell Analyses Reveal the Co-Evolutionary Dynamics of the Tumor and Microenvironment Accompanying Follicular Lymphoma Transformation. *Blood.* 2022;140(Supplement 1):748-749. doi:10.1182/blood-2022-159995
331. Yamamoto H, Kishimoto T, Minamoto S. NF-kappaB activation in CD27 signaling: involvement of TNF receptor-associated factors in its signaling and

REFERENCES

- identification of functional region of CD27. *J Immunol.* 1998;161(9):4753-4759.
332. Mateos-Jaimez J, Mangolini M, Vidal A, et al. Robust CRISPR-Cas9 Genetic Editing of Primary Chronic Lymphocytic Leukemia and Mantle Cell Lymphoma Cells. *Hemasphere.* 2023;7(6):E909. doi:10.1097/HS9.0000000000000909
333. Caesar R, Gao J, Di Re M, Gong C, Hodson DJ. Genetic manipulation and immortalized culture of ex vivo primary human germinal center B cells. *Nat Protoc.* 2021;16(5):2499-2519. doi:10.1038/s41596-021-00506-4
334. Pal SK, Tran B, Haanen JBAG, et al. CD70-Targeted Allogeneic CAR T-Cell Therapy for Advanced Clear Cell Renal Cell Carcinoma. *Cancer Discov.* Published online 2024:OF1-OF14. doi:10.1158/2159-8290.CD-24-0102
335. Ruella M, Korell F, Porazzi P, Maus M V. Mechanisms of resistance to chimeric antigen receptor-T cells in haematological malignancies. *Nat Rev Drug Discov.* 2023;22(12):976-995. doi:10.1038/s41573-023-00807-1

ANNEXES

ANNEXES

SUPPLEMENTAL MATERIAL STUDY 1

SUPPLEMENTAL METHODS

Patient samples and healthy donor peripheral blood mononuclear cells

MCL primary samples used in this study belong to Hematopathology collection, registered in the Biobank of IDIBAPS-Hospital Clínic, Barcelona (R121004-094) and in the National Registry of Biobanks-ISCIII (C.0000397), according to *Real Decreto 1716/2011*. This collection corresponds to biological material remaining from the samples used for the diagnosis, according to the World Health Organization (WHO), in the Hematopathology Unit of Hospital Clínic de Barcelona (HCB, Barcelona, Spain). Informed consent has been obtained from each patient in accordance with the Institutional Ethics Committee of the HCB and the Declaration of Helsinki.

Peripheral blood mononuclear cells (PBMCs) were obtained from healthy donor buffy coats provided by Banc de Sang i Teixits (Barcelona, Spain) after Ficoll-Paque gradient separation (GE Healthcare, Chicago, IL, USA). Monocytes were purified using CD14⁺ magnetic beads and LS columns (Miltenyi Biotec, Bergisch Gladbach, Germany) and purity >98% was verified by flow cytometry (FACS Fortessa (BD Biosciences, Franklin Lakes, NJ, USA)). Monocytes were cryopreserved with 10% DMSO (Sigma-Aldrich, St. Louis, MO, USA) and stored in liquid nitrogen until use at IDIBAPS Biobank.

MCL-PDLS imaging

PDLS formation and growth were monitored by brightfield illumination on the automated digital microscope Cytation 1 (Biotek, Agilent, Santa Clara, CA, USA) under temperature (37°C) and CO₂/O₂ gas control. Z-stacking function (n=5) was always performed to account for the third dimension. Image analysis and Z-projection were done with manufacturer's software Gen 5 (Biotek).

PDLS were also characterized by Selective Plane Illumination Microscopy (SPIM). Day 7 PDLS were fixed in 4% paraformaldehyde (PFA) for 12h, then PFA was diluted to 0.5% with PBS after several rinse cycles, and finally replaced by blocking/permeabilization buffer (PBS + 2% FBS + 2% BSA + 0.6% Triton + 0.01% Azide) and incubated overnight (ON) with agitation at room temperature (RT). PDLS were then labeled with 10 µg/mL propidium iodide (Thermo Fisher Scientific) and incubated for 4h at RT with agitation, washed and included in agarose.

Then, PDLS included in agarose were cleared using methanol and Benzyl Alcohol/Benzyl Benzoate (BABB) reagent. Finally, PDLS included were imaged by SPIM microscope (ZEISS Lightsheet Z.7, Imactiv 3D, Toulouse) and image-processing algorithms were developed in MATLAB.

Monocyte-Macrophage differentiation and polarization analysis

ANNEXES

To assess MCL induced monocyte-macrophage differentiation /polarization, CD11b⁺ Far Red⁺ cells were recovered by cells sorting (FACS Aria, BD) from PDLS (day 7), and RNA isolated with TRIzol following manufacturer's protocol (Thermo Fisher Scientific). cDNA was synthesized using Preamp RT Master Mix (Fluidigm, San Francisco, CA, USA). Next, cDNA was pre-amplified for the following genes: *CXCL11*, *CCL5*, *MRC1*, *CCL22*, *PMAIP1*, *RSG2*, *GUSB*, *ACTB*, *B2M* using pre-designed TaqMan probes (Thermo Scientific) and PreAmp Master Mix (Fluidigm).

Quantitative real-time PCR (qPCR) was then performed on a StepOne Real-Time PCR System (Thermo Fisher Scientific) using the same probes as the preamplification. Samples were analyzed in duplicate and expression was normalized using the mean of the three endogenous genes: *GUSB*, *ACTB*, *B2M*.

To evaluate the degree of M1/M2 polarization MCL-macrophages were compared with M1 or M2-polarized macrophages generated as follows: monocytes obtained from PBMCs as previously described were seeded in 6-wells plates at 0.5×10^6 cells/mL in enriched medium supplemented with macrophage colony stimulating factor (M-CSF) (ThermoFisher Scientific) at 100 ng/mL. After 6 days, additional stimuli were provided to obtain M1-polarized macrophages ((20ng/mL IFN γ (Gibco, Thermo Fisher Scientific) + 100ng/mL LPS (Sigma-Aldrich)) or M2-polarized macrophages (20ng/mL IL-4 (PeproTech, Rocky Hill, NJ)) for 24h.

MCL-PDLS immune profile and activation

MCL-PDLS (day 3 and day 7) immune profile were both characterized with several panels for B (CD20+) cells, T (CD4+ and CD8+) cells and monocytes/macrophages (CD11b+) using the following antibodies PD1, TIGIT, TIM-3, CD27, CD70, CD66a, CD112, CD155, PD-L1, CD47, SIRP α followed by flow cytometry analysis. PBMCs from healthy donors were used as controls. A complete list of antibodies is provided in supplemental table S1.

Granzyme B and interferon (IFN)- γ were used as read-out of T cell activation and were analyzed in cell culture supernatants using Cytometric Bead Array (CBA) kits and FACS Fortessa (BD Biosciences) following manufacturer's instructions. Data was analyzed using FCAP ArrayTM v.3.0 Software (BD Biosciences).

RNA-seq and data analysis

Day 7 PDLS was disaggregated, labelled with LIVE/DEAD Aqua, CD20 - eIF450 (Thermo Fisher Scientific) and CD3-FITC (BD Biosciences). CD20⁺, CD3⁺ Aqua⁺ cells were recovered using a BD FACSAria II sorter (Cytometry and cell sorting facility, IDIBAPS) and RNA extracted as before. Likewise, CD20⁺, CD3⁻ Aqua⁻ cells isolated from the original MCL sample at thawing (day 0) were used as a comparator for RNA-seq studies.

RNA was assayed for quantity and quality using Qubit RNA HS Assay (Life Technologies) and RNA 6000 Nano Assay on a Bioanalyzer 2100. Stranded RNA-seq libraries were performed for 150 ng of mRNA using the TruSeq library kit (Illumina, San Diego, CA, USA). Libraries were sequenced on a NextSeq2000 (Illumina) in a 2x50bp length with a coverage of >40 million paired-reads per sample.

Sequencing reads were trimmed using trimmomatic (version 0.38),¹ and ribosomal RNA reads were filtered out using SortMeRNA (version 2.1b).² Gene-level counts (GRCh38.p13; Ensembl release 100) were calculated using kallisto (version 0.46.1)³ and tximport (version 1.6.0).⁴ Differential expression was conducted using DESeq2 (version 1.18.1).⁵ Shrinkage of effect size was performed using the apeglm method.⁶ Adjusted *P* value (*Q*) <0.10 and absolute log2-transformed fold change >0.5 were used to identify differentially expressed genes (DEGs).

Gene-set enrichment analyses (GSEAs) were conducted with GSEA software (version 4.2.3),⁷ using the pre-ranked modality and log2FC results obtained from DESeq2 as input data. Hallmark gene sets, the C2 curated gene sets, the C3 motif gene sets, the C5 gene ontology gene sets (Molecular Signature Database v7.5), and custom gene sets^{8,9} were used. Heatmaps of selected genes were generated using GraphPad software. RNA-seq data have been deposited at the European Genome-phenome Archive (accession number EGAS00001006964) and will be publicly accessible at the time of publication.

Metadata comparative analysis

mRNA relative expression levels of selected immune checkpoints in whole lysates of Mantle Cell Lymphoma lymph nodes (MCL-LN, n=199) was compared with normal tonsils (TONSIL n=30) according to GEP public databases (GSE21452, GSE93291, GSE70910, GSE70927, GSE132929, GSE3526, GSE7307, GSE39503, GSE43346, GSE65135, GSE65136 and GSE71810). These selected data were all generated with Affymetrix Human Genome U133 Plus 2.0. Briefly, CEL files were normalized using the Expression Console™ Software v1.4.1.46 (Affymetrix). To take in consideration the batch effect, join data were normalized using the Limma package included in Transcriptome Analysis console (Applied Biosystems).

Statistical analysis

Data were analyzed using Prism Software 8.0 (GraphPad Software, San Diego, CA, USA). Depending on the assay and based on Shapiro-Wilk normality test, paired *t* test or Wilcoxon test were used. Data were represented as the mean values of the patients. Differences between the results of comparative tests were

considered significant if the two-sided P value was less than 0.05. The statistical significance convention used along the manuscript was as follows: * $p < 0.05$, ** $p < 0.01$, *** $p < 0.001$ and **** $p < 0.0001$.

Bibliography

- 1 Bolger AM, Lohse M, Usadel B. Trimmomatic: a flexible trimmer for Illumina sequence data. *Bioinformatics* 2014; **30**: 2114–2120.
- 2 Kopylova E, Noé L, Touzet H. SortMeRNA: fast and accurate filtering of ribosomal RNAs in metatranscriptomic data. *Bioinformatics* 2012; **28**: 3211–3217.
- 3 Bray NL, Pimentel H, Melsted P, Pachter L. Near-optimal probabilistic RNA-seq quantification. *Nat Biotechnol* 2016; **34**: 525–527.
- 4 Soneson C, Love MI, Robinson MD. Differential analyses for RNA-seq: transcript-level estimates improve gene-level inferences. *F1000Research* 2015; **4**: 1521.
- 5 Love MI, Huber W, Anders S. Moderated estimation of fold change and dispersion for RNA-seq data with DESeq2. *Genome Biol* 2014; **15**: 550.
- 6 Zhu A, Ibrahim JG, Love MI. Heavy-tailed prior distributions for sequence count data: removing the noise and preserving large differences. *Bioinformatics* 2019; **35**: 2084–2092.
- 7 Subramanian A, Kuehn H, Gould J, Tamayo P, Mesirov JP. GSEA-P: a desktop application for Gene Set Enrichment Analysis. *Bioinformatics* 2007; **23**: 3251–3253.
- 8 Saba NS, Liu D, Herman SEMM, Underbayev C, Tian X, Behrend D *et al*. Pathogenic role of B-cell receptor signaling and canonical NF- κ B activation in mantle cell lymphoma. *Blood* 2016; **128**: 82–92.
- 9 Rosenwald A, Wright G, Wiestner A, Chan WC, Connors JM, Campo E *et al*. The proliferation gene expression signature is a quantitative integrator of oncogenic events that predicts survival in mantle cell lymphoma. *Cancer Cell* 2003; **3**: 185–197.

SUPPLEMENTARY FIGURES

Figure S1

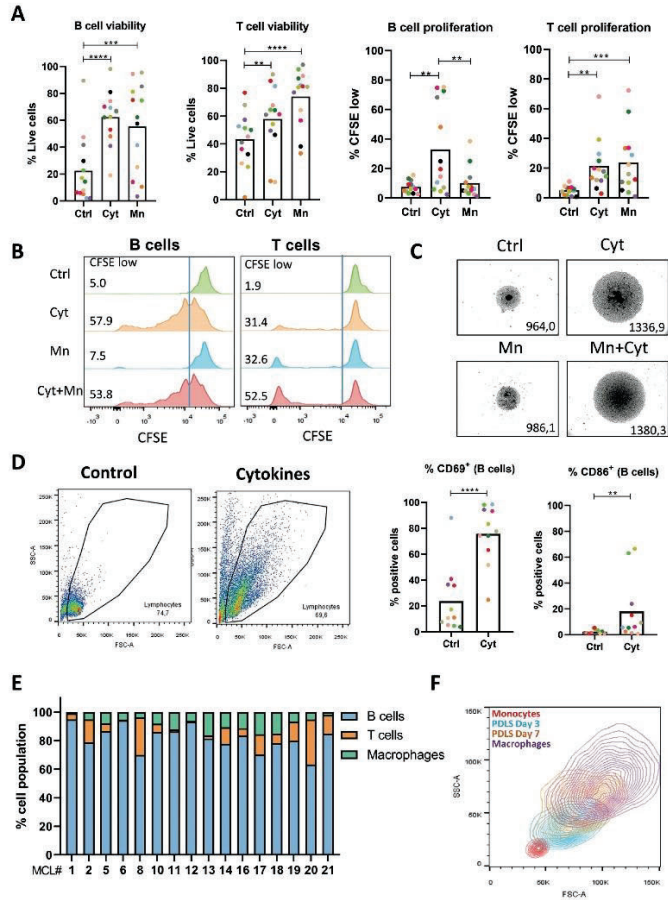


Figure S1. Effect of cytokines and/or monocytes on PDLS culture. (A) B/T cell viability and proliferation (%CFSE low) of MCL-PDLS cultured during 7 days with cytokines (Cyt) or monocytes (Mn) compared to the control (Ctrl) condition of non-stimulated PDLS. **(B)** Representative CFSE histogram (MCL10) plot showing B- and T cell proliferation when adding cytokines and/or monocytes. Percentage of CFSE low cells is indicated. **(C)** PDLS (MCL13) brightfield imaging (Cytation 1, x40 magnification) with cytokines (Cyt) and/or monocytes (Mn) stimuli compared to control (Ctrl) condition. Size in μm is indicated. **(D)** Density plots illustrate the increase in cell growth (FSC-A) and cell complexity (SSC-A) of PDLS cultured with only cytokines for 7 days. B cell activation was assessed by the percentage of CD69 and CD86 positive cells. **(E)** B, T and monocyte distribution after 7 days with cytokines and monocytes. **(F)** Evolution in size (FSC-A) and complexity (SSC-A) of CD11b⁺ isolated from the PDLS (MCL13) after 3 or 7 days in PDLS media, compared to monocytes or to macrophages differentiated in 2D with M-CSF.

Figure S2

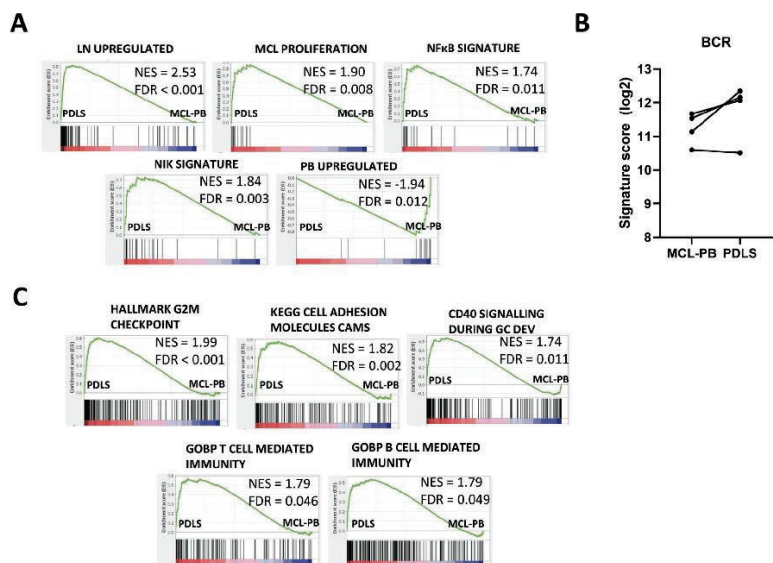


Figure S2. MCL-PDLS GSEA analysis. (A) GSEA enrichment plots representing relevant pathways in MCL pathogenesis, with significant increase or decrease in the signature score (Figure 2C). (B) BCR signature score calculated as explained in Figure 2C, detailed by each individual patient. (C) GSEA enrichment plots representing up-regulated pathways in the PDLS, related to cell cycle, adhesion and immune system.

Figure S3

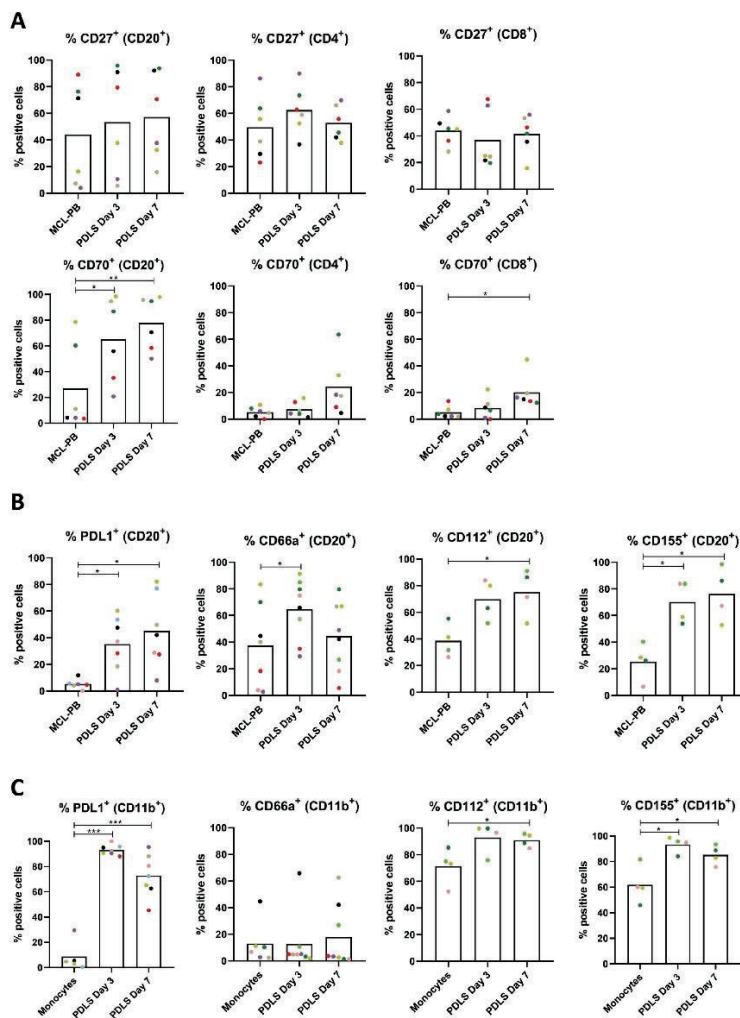
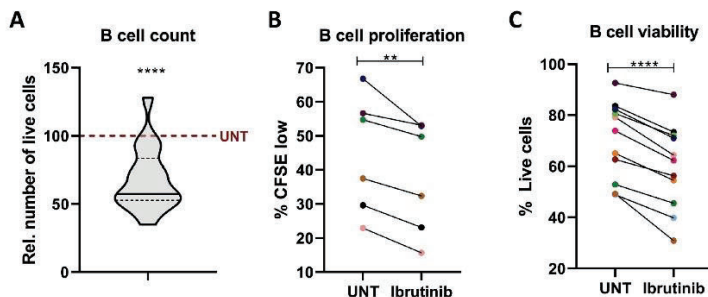


Figure S3. Up-regulation of immune modulators markers in MCL-PDLS. (A) Percentage of positive cells for CD70 and CD27 in B cells and CD4/CD8 T cells from MCL-PDLS (n=6). **(B)** Percentage of positive cells of PDL1, CD66a, CD112 and CD155 in tumor B cell population in the PB sample and from MCL-PDLS at day 3 or day 7 of culture (n=4-8). **(C)** Percentage of positive cells of ICP ligands in monocytes and macrophages from PDLS after 3 or 7 days of culture (n=4-8).

Figure S4**Figure**

S4. Ibrutinib is active in MCL-PDLS. MCL-PDLS were treated at day 3 with ibrutinib. B cell count ($n=17$) (**A**), B cell proliferation quantified by the percentage of CFSE low (**B**) and B cell viability measured by percentage of negative LIVE/DEAD (**C**) were assessed after 72h of ibrutinib treatment compared to untreated (UNT) samples.

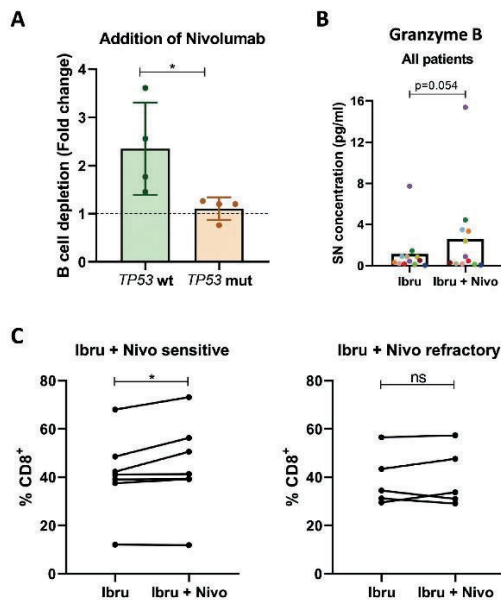
Figure S5

Figure S5. Ibrutinib and nivolumab combination in MCL-PDLS. (**A**) Effect of adding nivolumab to ibrutinib treatment in patients with *TP53* gene mutated (mut) or non-mutated (wild-type (wt)), represented as the fold change of B cell depletion. (**B**) Granzyme B concentration by CBA comparing ibrutinib monotherapy or in combination with nivolumab. (**C**) Percentage of CD8⁺ T cells (CD3⁺-gated) after ibrutinib or ibrutinib +nivolumab in sensitive or resistant MCL-PDLS to the combination.

SUPPLEMENTARY TABLES

Table S1. Antibodies used in flow cytometry

Target	Conjugate	Clone	Dilution
CD112	PE	R2.525	1/40
CD155	BV605	SKII.4	1/100
CD19	PE	SJ25C1	1/200
CD20	eFluor 450	2H7	1/50
CD27	PE-Cy7	LG.7F9	1/100
CD3	PE-Cy5	UCHT1	1.5/100
CD4	SB600	RPA-T4	1.5/100
CD47	PE-Cy7	B6H12	1/20
CD66a	AF488	283340	1/50
CD70	APC	REA292	1/20
CD8	APC-H7	SK1	1/100
PD-1	PE-Cy7	EH12.1	1/50
PD-L1	PE	MIH1	1/200
SIRP α	APC	15-414	1/200
TIGIT	APC	MBSA43	1/50
TIM-3	PE	F38-2E2	1/50

ANNEXES

Table S2. Leading edge genes of specific signatures from Figure 2C

LN	CENPA	KIF20A	PBK	PB
ANLN	CENPE	KIF23	PLK4	CKAP4
ASPM	CENPF	KIF2C	POLQ	KLF2
AURKA	CENPM	KIFC1	PTPN7	KLF9
AURKB	CEP55	LTBP1	RRM2	MXI1
BID	CLSPN	MCM10	SIRPA	PCGF5
BUB1	CTNNAL1	MELK	SKA3	RIN3
BUB1B	DLGAP5	MKI67	SMC2	SEMA4B
CCL22	DTL	MND1	SPAG5	UCKL1
CDC20	E2F8	MRPS14	TOP2A	
CDC25A	ESCO2	NCAPG	TOX	
CDC45	ESPL1	NCAPG2	TPX2	NFKB
CDC6	EXO1	NCAPH	TYMS	BCL2A1
CDCA3	FAM72A	NEIL3	UBE2C	CCL3
CDCA5	FEN1	NEK2	UBE2T	CCL4
CDCA8	FOXM1	NEURL1B	UHRF1	DUSP2
CDK1	HJURP	NLRP3		EBI3
CDKN3	IPCEF1	NME1		ID2
	KIF14	NUF2		IL12B
				LTA
				NFKBIE
				RGS1
				TNF
MCL Prol	H2AZ1	ODC1	SET	
AIMP2	HDAC2	PCNA	SF3B3	
AP3S1	HDGF	POLD2	SLC25A3	
APEX1	HNRNPA1	POLE3		
C1QBP	HNRNPA2B1	PPIA	SNRPA	
CBX3	HNRNPA3	PPM1G	SNRPA1	
CCT2	HNRNPC	PRDX4	SNRBP2	
CCT3	HNRNPD	PRPF31	SNRPD1	
CCT4	HNRNPR	PSMA1	SNRPD2	
CCT5	HNRNPU	PSMA2	SNRPG	
CCT7	HPRT1	PSMA4	SRM	
CDC20	HSP90AB1	PSMA6	SRSF2	
CDC45	HSPD1	PSMA7	SRSF3	
CDK4	HSPE1	PSMB2	SRSF7	
CLNS1A	IARS1	PSMB3	SSB	
CNBP	IFRD1	PSMC4	SSBP1	
COPS5	ILF2	PSMC6	SYNCRIP	
COX5A	KARS1	PSMD1	TARDBP	
CTPS1	KPNA2	PSMD14	TCP1	
DEK	LDHA	PSMD3	TOMM70	
EEF1B2	LSM7	PSMD7	TRA2B	
EIF1AX	MAD2L1	PTGES3	TRIM28	
EIF2S1	MCM2	PWP1	TUFM	
EIF2S2	MCM4	RAN	TXNL4A	
EIF3B	MCM6	RANBP1	UBE2L3	
EIF4A1	MCM7	RFC4	USP1	
EIF4E	MRPL23	RPL18	VBP1	
ERH	MRPL9	RPL34	XRCC6	
EXOSC7	MRPS18B	RPL6	YWHAE	
FBL	NDUFAB1	RPS2		
GLO1	NHP2	RPS5		
GNL3	NME1	RRM1		
GOT2	NOLC1	RRP9		
GSPT1	NOP16	RUVEL2		
	NPM1	SERBP1		

Table S3. Gene sets (by biological process) overrepresented in MCL-PDLs compared to unstimulated (MCL-PB) controls

Biological process	# of enriched gene sets	NES (max)	FDR, q value (min)
Proliferation			
Cell cycle regulation	18	2,31	<0,001
DNA replication	31	2	<0,001
MYC regulated genes	1	1.64	0.008
KRAS pathway	1	1.51	0.024
Immune pathways			
Chemokines	5	2,11	<0,001
Allograft reaction	3	2,02	<0,001
Immune checkpoint control	1	1,97	0.002
Antigen presentation	9	1,91	0,013
Interleukins	3	1,84	0,007
Cytokines	2	1,75	0,035
Immune response	22	1,75	0.020
CD40-CD40L signalling	1	1,74	0,011
Survival pathways			
NFκB	8	1,94	0,001
TNF	3	1,75	0,037
Cellular processes			
Protein synthesis	10	3,01	0,001
RNA synthesis	4	1,87	0,006
Cell adhesion	2	1,82	0,002
Proteasome	2	1,71	0,011
Metabolic pathways			
Oxidative phosphorylation (OXPHOS)	13	1,96	0,002
Glucose metabolism	6	1,72	0,023
Fatty acid metabolism	4	1,72	0,023
Aminoacid metabolism	3	1,69	0,028
DNA damage			
DNA damage/repair	7	1,94	0,002
p53	1	1,65	0,04
Others			
Telomeres	2	1,77	0,016
Redox balance	4	1,73	0,017

GSEA was used to test for significant enrichment of defined gene signatures. NES indicates Normalized Enriched Score; FDR, False Discovery Rate. Threshold FDR<0.05 and NES>1.5. Custom genes set were experimentally derived and downloaded from <http://lymphochip.nih.gov/signaturedb/index.html>. C2CP, C3, C5 and H gene sets were obtained from the Molecular Signature Database (v2.5).

Table S4. Complete GSEA results of MCL-PDLs compared to unstimulated (MCL-PB) controls

GENESET	SIZE	NES	FDR q-val
Allograft reaction			
KEGG_GRAFT_VERSUS_HOST_DISEASE	39	2.02	0.000
KEGG_ALLOGRAFT_REJECTION	37	1.94	0.000
HALLMARK_ALLOGRAFT_REJECTION	195	1.77	0.002
Aminoacids Metabolism			
KEGG_VALINE_LEUCINE_AND_ISOLEUCINE_DEGRADATION	44	1.64	0.023
KEGG_TRYPTOPHAN_METABOLISM	40	1.63	0.025
REACTOME_SELENOAMINO_ACID_METABOLISM	118	1.69	0.028
Angiogenesis			
HALLMARK_ANGIOGENESIS	33	1.61	0.010
Antigen presentation			
GOBP_ANTIGEN_PROCESSING_AND_PRESENTATION	107	1.91	0.013
REACTOME_ANTIGEN_PROCESSING_CROSS_PRESENTATION	106	1.86	0.006
GOBP_ANTIGEN_PROCESSING_AND_PRESENTATION_OF_ENDOGENOUS_ANTIGEN	26	1.84	0.032
GOBP_ANTIGEN_PROCESSING_AND_PRESENTATION_OF_EXOGENOUS_ANTIGEN	47	1.82	0.034
GOBP_PEPTIDE_ANTIGEN_ASSEMBLY_WITH_MHC_CLASS_II_PROTEIN_COMPLEX	16	1.83	0.036
GOBP_PEPTIDE_ANTIGEN_ASSEMBLY_WITH_MHC_PROTEIN_COMPLEX	20	1.82	0.034
MHC CLASS I	7	1.50	0.096
KEGG_ANTIGEN_PROCESSING_AND_PRESENTATION	73	1.76	0.006
REACTOME_CROSS_PRESENTATION_OF_SOLUBLE_EXOGENOUS_ANTIGENS_ENDOSOMES	50	1.8	0.012
CD40-CD40L signalling			
CD40_SIGNALLING_DURING_GC_DEV	150	1.74	0.011
Cell Adhesion			
HALLMARK_APICAL_JUNCTION	197	1.55	0.018
KEGG_CELL_ADHESION_MOLECULES_CAMS	131	1.82	0.002
Cell cycle regulation			
HALLMARK_E2F_TARGETS	200	2.31	0.000
HALLMARK_G2M_CHECKPOINT	199	1.99	0.000
HALLMARK_MITOTIC_SPINDLE	199	1.59	0.013
KEGG_CELL_CYCLE	124	1.65	0.023
REACTOME_POLO_LIKE_KINASE_MEDIATED_EVENTS	16	1.73	0.021
REACTOME_APC_C_MEDIATED_DEGRADATION_OF_CELL_CYCLE_PROTEINS	88	1.94	0.002
REACTOME_CELL_CYCLE_CHECKPOINTS	289	1.92	0.003
REACTOME_G2_M_CHECKPOINTS	165	1.87	0.006
REACTOME_S_PHASE	162	1.84	0.007
REACTOME_G1_S_SPECIFIC_TRANSCRIPTION	29	1.82	0.011
REACTOME_MITOTIC_G1_PHASE_AND_G1_S_TRANSITION	149	1.81	0.012
REACTOME_CYCLIN_A_B1_B2_ASSOCIATED_EVENTS_DURING_G2_M_TRANSITION	25	1.72	0.023
REACTOME_TP53_REGULATES_TRANSCRIPTION_OF_GENES_INVOLVED_IN_G2_CELL_CYCLE_ARREST	18	1.71	0.023
REACTOME_MITOTIC_METAPHASE_AND_ANAPHASE	236	1.64	0.045
GOBP_REGULATION_OF_CHROMOSOME_SEPARATION	69	1.97	0.010
GOBP_MICROTUBULE_CYTOSKELETON_ORGANIZATION_INVOLVED_IN_MITOSIS	153	1.83	0.036
GOBP_MITOTIC_NUCLEAR_DIVISION	291	1.82	0.035
GOBP_MITOTIC_SPINDLE_ORGANIZATION	126	1.79	0.044
Chemokines			
REACTOME_CHEMOKINE_RECEPTORS_BIND_CHEMOKINES	53	1.86	0.006
GOMF_CCR_CHEMOKINE_RECEPTOR_BINDING	34	2.11	0.000
GOMF_CHEMOKINE_RECEPTOR_BINDING	54	2.08	0.000
GOMF_CHEMOKINE_ACTIVITY	40	2.07	0.000
GOMF_CHEMOATTRACTANT_ACTIVITY	29	1.73	0.047
Cytokines			
KEGG_CYTOKINE_CYTOKINE_RECEPTOR_INTERACTION	240	1.57	0.041
GOMF_CYTOKINE_ACTIVITY	205	1.75	0.035
DNA damage/repair			
KEGG_MISMATCH_REPAIR	23	1.77	0.005
KEGG_BASE_EXCISION_REPAIR	34	1.67	0.016
KEGG_NUCLEOTIDE_EXCISION_REPAIR	44	1.58	0.040
REACTOME_ACTIVATION_OF_ATR_IN_RESPONSE_TO_REPLICATION_STRESS	37	1.94	0.002
REACTOME_BASE_EXCISION_REPAIR	86	1.7	0.024
REACTOME_DNA_DOUBLE_STRAND_BREAK_REPAIR	164	1.63	0.046
REACTOME_MISMATCH_REPAIR	15	1.62	0.050
DNA replication			
KEGG_DNA_REPLICATION	36	2.00	0.000
REACTOME_DNA_STRAND_ELONGATION	32	2.02	0.001

REACTOME_SYNTHESIS_OF_DNA	120	2.01	0.000
REACTOME_CHROMOSOME_MAINTENANCE	135	1.97	0.002
REACTOME_DNA_REPLICATION	186	1.96	0.002
REACTOME_DEPOSITION_OF_NEW_CENPA_CONTAINING_NUCLEOSOMES_AT_THE_CENTROMERE	68	1.91	0.003
REACTOME_ACTIVATION_OF_THE_PRE_REPLICATIVE_COMPLEX	33	1.9	0.003
REACTOME_DNA_REPLICATION_PRE_INITIATION	143	1.88	0.005
REACTOME_MITOTIC_SPINDLE_CHECKPOINT	111	1.84	0.007
REACTOME_SEPARATION_OF_SISTER_CHROMATIDS	191	1.72	0.023
REACTOME_RESOLUTION_OF_SISTER_CHROMATID_COHESION	126	1.72	0.023
REACTOME_CONDENSATION_OF_PROPHASE_CHROMOSOMES	69	1.67	0.034
REACTOME_MITOTIC_PROMETAPHASE	203	1.67	0.035
GOBP_MONOCYTE_CHEMOTAXIS	62	2.08	0.000
GOBP_MITOTIC_SISTER_CHROMATID_SEGREGATION	171	1.98	0.012
GOBP_METAPHASE_ANAPHASE_TRANSITION_OF_CELL_CYCLE	63	1.96	0.009
GOBP_REGULATION_OF_CHROMOSOME_SEGREGATION	86	1.96	0.008
GOBP_SISTER_CHROMATID_SEGREGATION	203	1.96	0.007
GOBP_CENTROMERE_COMPLEX_ASSEMBLY	31	1.94	0.008
GOBP_KINETOCHORE_ORGANIZATION	23	1.93	0.010
GOBP_REGULATION_OF_MITOTIC_SISTER_CHROMATID_SEGREGATION	45	1.92	0.011
GOBP_CHROMOSOME_SEPARATION	94	1.91	0.013
GOBP_CHROMOSOME_SEGREGATION	343	1.89	0.017
GOBP_NUCLEAR_CHROMOSOME_SEGREGATION	284	1.89	0.016
GOBP_NEGATIVE_REGULATION_OF_METAPHASE_ANAPHASE_TRANSITION_OF_CELL_CYCLE	41	1.86	0.026
GOBP_DNA_REPLICATION_INITIATION	38	1.81	0.037
GOCC_NUCLEAR_REPLICATION_FORK	28	1.85	0.007
GOCC_REPLICATION_FORK	60	1.84	0.007
GOCC_CONDENSED_CHROMOSOME_CENTROMERIC_REGION	166	1.83	0.006
GOCC_CHROMOSOME_CENTROMERIC_REGION	226	1.76	0.014
GOCC_REPLISOME	15	1.69	0.023
Fatty Acid metabolism			
KEGG_BIOSYNTHESIS_OF_UNSATURATED_FATTY_ACIDS	22	1.60	0.037
KEGG_FATTY_ACID_METABOLISM	42	1.59	0.042
REACTOME_FATTY_ACID_METABOLISM	177	1.72	0.023
REACTOME_MITOCHONDRIAL_FATTY_ACID_BETA_OXIDATION	37	1.64	0.044
Glucose metabolism			
HALLMARK_GLYCOLYSIS	199	1.57	0.015
KEGG_GLYCOLYSIS_GLUONEOGENESIS	61	1.56	0.046
KEGG_ONE_CARBON_POOL_BY_FOLATE	17	1.55	0.050
KEGG_PENTOSE_PHOSPHATE_PATHWAY	26	1.54	0.050
REACTOME_GLUONEOGENESIS	33	1.72	0.023
KEGG_PYRUVATE_METABOLISM	40	1.58	0.041
Immune checkpoint control			
REACTOME_PD_1_SIGNALING	23	1.97	0.002
Immune response			
REACTOME_IMMUNOREGULATORY_INTERACTIONS_BETWEEN_A_LYMPHOID_AND_A_NON_LYMPHOID_CELL	184	1.75	0.020
REACTOME_INTERFERON_GAMMA_SIGNALING	92	1.74	0.021
GOBP_ANTIGEN_PROCESSING_AND_PRESENTATION	107	1.91	0.013
GOBP_ANTIGEN_PROCESSING_AND_PRESENTATION_OF_ENDOGENOUS_ANTIGEN	26	1.84	0.032
GOBP_LYMPHOCYTE_MEDIATED_IMMUNITY	351	1.83	0.034
GOBP_PEPTIDE_ANTIGEN_ASSEMBLY_WITH_MHC_CLASS_II_PROTEIN_COMPLEX	16	1.83	0.036
GOBP_PEPTIDE_ANTIGEN_ASSEMBLY_WITH_MHC_PROTEIN_COMPLEX	20	1.82	0.034
EPTORS_BUILT_FROM_IMMUNOGLOBULIN_SUPERFAMILY_DOMAINS	357	1.82	0.034
GOBP_ANTIGEN_PROCESSING_AND_PRESENTATION_OF_EXOGENOUS_ANTIGEN	47	1.82	0.034
GOBP_MACROPHAGE_MIGRATION	53	1.80	0.042
GOBP_CELLULAR_RESPONSE_TO_INTERFERON_GAMMA	113	1.80	0.043
GOBP_T_CELL_MEDIATED_IMMUNITY	111	1.79	0.046
GOBP_B_CELL_MEDIATED_IMMUNITY	208	1.79	0.049
GOCC_MHC_PROTEIN_COMPLEX	26	1.91	0.003
GOCC_IMMUNOGLOBULIN_COMPLEX_CIRCULATING	67	1.85	0.007
GOCC_T_CELL_RECEPTOR_COMPLEX	39	1.84	0.006
GOCC_MHC_CLASS_II_PROTEIN_COMPLEX	17	1.78	0.011
GOCC_IMMUNOGLOBULIN_COMPLEX	146	1.76	0.014
GOMF_ANTIGEN_BINDING	156	1.87	0.012
GOMF_MHC_PROTEIN_COMPLEX_BINDING	36	1.83	0.022
GOMF_MHC_CLASS_II_PROTEIN_COMPLEX_BINDING	27	1.80	0.027
GOMF_IMMUNOGLOBULIN_RECEPTOR_BINDING	70	1.78	0.031

ANNEXES

Interleukins			
IL17PATHWAY	14	1.64	0.031
REACTOME_INTERLEUKIN_10_SIGNALING	46	1.84	0.007
REACTOME_INTERLEUKIN_4_AND_INTERLEUKIN_13_SIGNALING	110	1.63	0.048
KRAS pathway			
HALLMARK_KRAS_SIGNALING_UP	195	1.51	0.024
MYC regulates genes			
HALLMARK_MYC_TARGETS_V1	200	1.64	0.008
NFkB			
NFKB_TARGET_GENES	23	1.98	0.000
NFKB_DLBCL_NATURE_2009_COMPAGNO	109	1.94	0.001
NFKB_ALL_OCILY3_LY10	57	1.87	0.003
NIK_SIGNATURE	26	1.84	0.003
NFKB_PATHWAY_MODULATED_BY_IBRUTINIB	39	1.83	0.004
NFKB_BOTHOCILY3ANDLY10	33	1.76	0.010
NFKB_SIGNATURE	18	1.74	0.011
REACTOME_DECTIN_1_MEDIATED_NONCANONICAL_NF_KB_SIGNALING	62	1.81	0.011
Oxidative phosphorylation			
HALLMARK_OXIDATIVE_PHOSPHORYLATION	200	1.86	0.001
KEGG_OXIDATIVE_PHOSPHORYLATION	129	1.71	0.011
REACTOME_MITOCHONDRIAL_TRANSLATION	94	1.96	0.002
REACTOME_RESPIRATORY_ELECTRON_TRANSPORT	103	1.73	0.022
GOBP_MITOCHONDRIAL_RESPIRATORY_CHAIN_COMPLEX_ASSEMBLY	94	1.86	0.025
GOBP_OXIDATIVE_PHOSPHORYLATION	136	1.84	0.034
GOBP_ELECTRON_TRANSPORT_CHAIN	165	1.78	0.049
GOCC_MITOCHONDRIAL_PROTEIN_CONTAINING_COMPLEX	279	1.93	0.002
GOCC_INNER_MITOCHONDRIAL_MEMBRANE_PROTEIN_COMPLEX	153	1.81	0.008
GOCC_PROTON_TRANSPORTING_ATP_SYNTHASE_COMPLEX	21	1.73	0.017
GOCC_RESPIRASOME	100	1.71	0.018
GOCC_NADH_DEHYDROGENASE_COMPLEX	49	1.62	0.044
GOMF_ELECTRON_TRANSFER_ACTIVITY	124	1.77	0.030
p53			
REACTOME_STABILIZATION_OF_P53	57	1.65	0.040
Proliferation			
MCL_PROLIFERATION_SIGNATURE	14	1.90	0.002
Proteasome			
KEGG_PROTEASOME	44	1.71	0.011
GOCC_PROTEASOME_CORE_COMPLEX	20	1.70	0.022
Protein synthesis			
KEGG_RIBOSOME	88	1.82	0.002
GOCC_RIBOSOMAL_SUBUNIT	177	2.01	0.001
GOCC_ORGANELLAR_RIBOSOME	81	1.99	0.000
GOCC_LARGE_RIBOSOMAL_SUBUNIT	111	1.96	0.001
GOCC_MITOCHONDRIAL_LARGE_RIBOSOMAL_SUBUNIT	54	1.90	0.003
GOCC_RIBOSOME	208	1.83	0.007
GOCC_SMALL_RIBOSOMAL_SUBUNIT	69	1.74	0.015
GOCC_CYTOSOLIC_RIBOSOME	101	1.71	0.019
GOCC_CYTOSOLIC_LARGE_RIBOSOMAL_SUBUNIT	57	1.69	0.023
REACTOME_EUKARYOTIC_TRANSLATION_INITIATION	120	1.65	0.040
Redox balance			
KEGG_PEROXISOME	78	1.59	0.040
REACTOME_DETOXIFICATION_OF_REACTIVE_OXYGEN_SPECIES	36	1.64	0.042
GOCC_OXIDOREDUCTASE_COMPLEX	120	1.73	0.017
AS_ACCEPTOR	57	1.73	0.046
RNA synthesis			
REACTOME_LAGGING_STRAND_SYNTHESIS	20	1.87	0.006
REACTOME_EUKARYOTIC_TRANSLATION_ELONGATION	94	1.86	0.006
REACTOME_TELOMERE_C_STRAND_LAGGING_STRAND_SYNTHESIS	34	1.82	0.010
REACTOME_TRANSLATION	293	1.8	0.013
Telomeres			
REACTOME_EXTENSION_OF_TELOMERES	51	1.77	0.016
REACTOME_TELOMERE_MAINTENANCE	108	1.75	0.018
TNF			
REACTOME_TNFS_BIND_THEIR_PHYSIOLOGICAL_RECEPTORS	29	1.69	0.027
REACTOME_TNFR2_NON_CANONICAL_NF_KB_PATHWAY	101	1.67	0.033
GOMF_TUMOR_NECROSIS_FACTOR_RECEPTOR_BINDING	31	1.75	0.037

Table S5. Complete GSEA results of MCL-PDLs compared to MCL-2D co-cultures

GENE SET	SIZE	NES	FDR q-val	CLASS
REACTOME_CROSS_PRESENTATION_OF_SOLUBLE_EXOGENOUS_ANTIGENS_ENDOSOMES	50	1.88	0.048	Ag presentation
HALLMARK_ANGIOGENESIS	33	1.72	0.042	Angiogenesis
REACTOME_ADHERENS_JUNCTIONS_INTERACTIONS	33	1.91	0.028	Cell adhesion
REACTOME_SCF_SKP2_MEDIATED_DEGRADATION_OF_P27_P21	60	1.87	0.044	Cell cycle
REACTOME_CDT1_ASSOCIATION_WITH_THE_CDC6_ORC_ORIGIN_COMPLEX	59	1.90	0.032	DNA replication
REACTOME_EXTRACELLULAR_MATRIX_ORGANIZATION	295	1.98	0.003	Extracellular matrix
REACTOME_ACTIVATION_OF_MATRIX_METALLOPROTEINASES	31	1.89	0.038	Extracellular matrix
GOCC_COLLAGEN_CONTAINING_EXTRACELLULAR_MATRIX	413	2.03	<0.001	Extracellular matrix
GOCC_COLLAGEN_TRIMER	84	1.94	0.009	Extracellular matrix
GOMF_EXTRACELLULAR_MATRIX_STRUCTURAL_CONSTITUENT	165	2.08	<0.001	Extracellular matrix
GOMF_COLLAGEN_BINDING	65	2.01	0.002	Extracellular matrix
REACTOME_DECTIN_2_FAMILY	26	1.89	0.039	Immune response
HALLMARK_EPITHELIAL_MESENCHYMAL_TRANSITION	198	1.72	0.034	Metastasis
BIOCARTA_RACC_PATHWAY	15	1.90	0.048	Ion channel activity
GOMF_EXTRACELLULAR_LIGAND_GATED_ION_CHANNEL_ACTIVITY	73	1.93	0.023	Ion channel activity
GOMF_LIGAND_GATED_ION_CHANNEL_ACTIVITY	144	1.90	0.044	Ion channel activity
GOCC_ION_CHANNEL_COMPLEX	286	1.93	0.009	Ion channel activity
HALLMARK_KRAS_SIGNALING_UP	195	1.84	0.015	KRAS
HALLMARK_MYC_TARGETS_V1	200	1.83	0.010	MYC
REACTOME_NEGATIVE_REGULATION_OF_NOTCH4_SIGNALING	54	1.88	0.042	Notch pathway
E47_O2	249	1.72	0.014	Stemness
KEGG_PROTEASOME	44	1.97	0.004	Proteasome
REACTOME_DISEASES_ASSOCIATED_WITH_O_GLYCOSYLATION_OF_PROTEINS	68	1.98	0.003	Protein glycosylation
REACTOME_O_GLYCOSYLATION_OF_TSR_DOMAIN_CONTAINING_PROTEINS	39	1.94	0.012	Protein glycosylation
REACTOME_DEFECTIVE_GALNT3_CAUSES_HFTC	16	1.92	0.026	Protein glycosylation
REACTOME_TERMINATION_OF_O_GLYCAN_BIOSYNTHESIS	23	1.91	0.028	Protein glycosylation
REACTOME_DEFECTIVE_C1GALT1C1_CAUSES_TNPS	17	1.87	0.046	Protein glycosylation

GSEA was used to test for significant enrichment of defined gene signatures. NES indicates Normalized Enriched Score; FDR, False Discovery Rate. Threshold FDR<0.05 and NES>1.5. Custom genes set were experimentally derived and downloaded from <http://lymphochip.nih.gov/signaturedb/index.html>. C2CP, C3, C5 and H gene sets were obtained from the Molecular Signature Database (v2.5).

ANNEXES

Table S6. Leading edge genes of specific signatures from Figure 3E

Myc			
AIMP2	H2AZ1	NOP16	RRM1
AP3S1	HDAC2	NPM1	RRP9
APEX1	HDGF	ODC1	RUVBL2
C1QBP	HNRNPA1	PCNA	SERBP1
CBX3	HNRNPA2B1	POLD2	SET
CCT2	HNRNPA3	POLE3	SF3B3
CCT3	HNRNPC	PPIA	SLC25A3
CCT4	HNRNPD	PPM1G	SNRPA
CCT5	HNRNPR	PRDX4	SNRPA1
CCT7	HNRNPU	PRPF31	SNRPB2
CDC20	HPRT1	PSMA1	SNRPD1
CDC45	HSP90AB1	PSMA2	SNRPD2
CDK4	HSPD1	PSMA4	SNRPG
CLNS1A	HSPE1	PSMA6	SRM
CNBP	IARS1	PSMA7	SRSF2
COPS5	IFRD1	PSMB2	SRSF3
COX5A	ILF2	PSMB3	SRSF7
CTPS1	KARS1	PSMC4	SSB
DEK	KPNA2	PSMC6	SSBP1
EEF1B2	LDHA	PSMD1	SYNCRIP
EIF1AX	LSM7	PSMD14	TARDBP
EIF2S1	MAD2L1	PSMD3	TCP1
EIF2S2	MCM2	PSMD7	TOMM70
EIF3B	MCM4	PTGES3	TRA2B
EIF4A1	MCM6	PWP1	TRIM28
EIF4E	MCM7	RAN	TUFM
ERH	MRPL23	RANBP1	TXNL4A
EXOSC7	MRPL9	RFC4	UBE2L3
FBL	MRPS18B	RPL18	USP1
GLO1	NDUFAB1	RPL34	VPB1
GNL3	NHP2	RPL6	XRCC6
GOT2	NME1	RPS2	YWHAE
GSPT1	NOLC1	RPS5	
Collagen			
	COL7A1	LGALS9	TNC
	CRELD1	LTBP3	USH2A
C1QB	CTSL	MMP9	VWF
C1QC	EGFLAM	PTPRZ1	WNT5B
CCDC80	FRAS1	S100A4	ZP3
COL12A1	HSP90B1	SEMA3B	
COL6A3	ITIH4	THBS1	
ECM org			
	E47_02		
COL12A1	GABRE		
COL22A1	COL22A1		
COL6A3	MMP16		
COL7A1	DOC2B		
CTSL	BTBD3		
LRP4	CASKIN2		
MMP16	FGF13		
MMP19	ELP5		
MMP9	ERBB3		
NRXN1	SNAP25		
SPP1	TPI1		
THBS1			
TNC			
VWF			

SUPPLEMENTAL MATERIAL STUDY 2

SUPPLEMENTAL METHODS

Patient samples and healthy donor peripheral blood monocytes isolation

FL primary samples, diagnosed according to the World Health Organization classification criteria in the Hematopathology Unit of Hospital Clinic of Barcelona (HCB, Barcelona, Spain), were isolated from peripheral blood (PB) and tumor lymph nodes (LN) biopsies. These samples belong to Hematopathology collection, registered in the Biobank of IDIBAPS-Hospital Clinic, Barcelona (R121004-094) and in the National Registry of Biobanks-ISCIII (C.0000397). Patients had signed an informed consent approved by the Ethics Committee of HCB and the Declaration of Helsinki. Patient clinical features are summarized in Table 1. Monocytes from healthy donors were isolated from peripheral blood mononuclear cells (PBMCs) of buffy coats provided by Banc de Sang i Teixits (Barcelona, Spain). After Ficoll-Paque gradient separation (GE Health Care, Chicago, IL, USA), monocytes were purified using CD14⁺ human magnetic beads and LS columns (Miltenyi Biotec, Bergisch Gladbach, Germany). Purity >96% was verified by flow cytometry (FACS Fortessa (BD Biosciences)) before cryopreservation with 10% DMSO (Sigma-Aldrich, St. Louis, MO, USA).

FL-PDLS immune profile

The immune profile of FL samples after thawing (day 0), at day 3 (day 3-PDLS) and day 7 (day 7-PDLS) was characterized using flow cytometry panels for B (CD20⁺) cells, T (CD4⁺ and CD8⁺) cells and monocytes/macrophages (CD11b⁺) including the following antibodies against: TIM-3, PD-1, TIGIT, ICOS, LAG-3, CD28, 41BB, OX40, CD200, ICOSL, CD66a, PD-L1, OX40L, 41BBL, CD200R. PBMCs (n=4) from healthy donors were used as controls. T cell phenotype was characterized by the expression of CCR7 and CD45RA. FoxP3 intracellular staining together with CXCR5 were used to characterize T_{FH}, T_{REG} and T follicular regulatory cells (T_{FR}) subsets. The study of CD3⁺ clusters (C0-C7) based on the expression of CD8, PD-1, TIM-3, LAG-3 and ICOS was assessed using FlowJo (BD Biosciences, Franklin Lanes, NJ, USA) plugins using data from 6 patients. Cluster Explorer after dimensionality reduction (UMAP) (1) and hierarchical clustering (FlowSOM) (2) creates an interactive cluster profile graph and heatmaps.

Additionally, frozen supernatants from day 6-PDLS samples were used to quantify soluble galectin-9 concentration by ELISA (Thermo Fisher) following the manufacturer's instructions. Data was collected using the colorimetric microplate reader Infinite® 200 PRO (Tecan, Männedorf, Switzerland).

FL-PDLS imaging

PDLS formation has been tracked by brightfield illumination on the automated digital microscope Cytation 1 Cell Imaging Multi-Mode Readers (BioTek, Agilent, Santa Clara, CA, USA) and analyzed with Gen5 software (Biotek). Captures were performed under 37°C temperature and 5% CO₂ using Z-stacking function (n=3).

3D captures and analysis were performed with SPIM (ZEISS Lightsheet Z.7, Imactiv 3D) and image-processing algorithms were developed in MATLAB. Day 7-PDLS were fixed in 4% paraformaldehyde (PFA (Electron Microscopy Sciences, Hatfield, PA, USA)) overnight (ON) at 4°C. Then, after three rinses, PFA was diluted to 0.5% with PBS and labeled with 10 µg/mL Propidium Iodide (Thermo Fisher Scientific) for 4h at room temperature (RT) with agitation. After the incubation, PDLS were washed three times with PBS, included in 1.5% agarose and cleared using methanol and Benzyl Alcohol/Benzyl Benzoate (BABB) reagent.

Immunofluorescence

PDLS populations had been captured using confocal microscopy (LEICA TCS SPE, Wetzlar, Germany) and analyzed with ImageJ software (NIH, Bethesda, MD, USA). After fixation and several rinse cycles, PBS was finally replaced by permeabilization/blocking (P/B) buffer (PBS + 2% FBS + 2% BSA + 0.6% Triton + 0.01% Azide) and incubated ON with agitation at RT. PDLS were then labeled with 1:100 CD19 (Invitrogen), 1:100 CD3 (Bioss Antibodies, Woburn, MA, USA) and 1:100 Ki-67 (Dako Omnis, Santa Clara, CA, USA) anti-human antibodies under agitation at RT ON. Monocytes were stained before being cultured, with Far Red CellTrace (Thermo Fisher Scientific) to be localized in the spheroid. After 3 washes with P/B buffer, PDLS were labeled with a mixture of 1:500 anti-Rat + 1:500 anti-Rabbit + 1:500 anti-Mouse secondary antibodies (Thermo Fisher Scientific) ON at RT under agitation. After the incubation, PDLS were washed three times with PBS, included in 1.5% agarose and cleared using methanol and Benzyl Alcohol/Benzyl Benzoate (BABB) reagent.

BCL2 rearrangement was assessed by Fluorescence in situ hybridization (FISH) using *BCL2* break-apart and/or *IGH/BCL2* dual-color dual-fusion commercial probes (Metasystems, Altlußheim, Germany). The hybridization was performed according to the manufacturer's protocols. At least 100 nuclei were examined for each probe whenever possible. Digital image acquisition, processing, and evaluation were performed using ISIS digital image analysis version 5.0 (MetaSystems Barcelona, Spain).

Monocyte-Macrophage differentiation and polarization analysis

To assess differentiation and polarization of the myeloid compartment included in the day 7-PDLS, CD11b⁺ Far Red⁺ cells were purified (over 96.0%) and recovered by cell sorting (FACS Aria, BD Biosciences (Cytometry and cell sorting facility, IDIBAPS, Barcelona, Spain)) and RNA was isolated with TRIzol following manufacturer's protocol (Thermo Fisher Scientific). cDNA was synthesized using Preamp RT Master Mix (Fluidigm, San Francisco, CA, USA). Next, cDNA was pre-amplified for the following genes: *CXCL11*, *CCL5*, *MRC1*, *CCL22*, *PMAIP1*, *RSG2*, *GUSB*, using pre-designed TaqMan probes (Thermo Fisher Scientific) and PreAmp Master Mix (Fluidigm).

Quantitative real-time PCR (qPCR) was then performed on a StepOne Real-Time PCR System (Thermo Fisher Scientific) using the same probes as the preamplification. Samples were analyzed in duplicate, and expression was normalized using the housekeeping gene *GUSB*. To evaluate the degree of M1/M2 polarization FL-macrophages were compared with M1 or M2-polarized macrophages generated as follows: monocytes obtained from PBMCs as previously described were seeded in 6-wells plates at 0.5×10^6 cells/mL in enriched medium (EM) supplemented with macrophage colony stimulating factor (M-CSF) (Thermo Fisher Scientific) at 100 ng/mL to differentiate them to macrophages (M0). After 6 days, additional stimuli were provided to obtain M1-polarized macrophages (20 ng/mL IFN γ (Gibco, Thermo Fisher Scientific) + 100 ng/mL LPS (Sigma-Aldrich)) or M2-polarized macrophages (20 ng/mL IL-4 (PeproTech, Rocky Hill, NJ)) for 24h.

RNA-seq and data analysis

Day 7-PB-PDLs were disaggregated, labeled with LIVE/DEAD Aqua, CD20 (Thermo Fisher Scientific) and CD3 (BD Biosciences). FL-B cells (CD20⁺ CD3⁻ FR⁻ Aqua⁻) were recovered using a BD FACSAria II sorter (Cytometry and cell sorting facility, IDIBAPS) and RNA extracted as previously mentioned. Likewise, FL-B cells (CD20⁺ CD3⁻ FR⁻ Aqua⁻) isolated from the original paired FL-PB and FL-LN sample from the same patient at thawing (day 0) were used as a comparator for RNA-seq studies. Purity was over 95%.

RNA was assayed for quantity and quality using Qubit RNA HS Assay (Thermo Fisher Scientific) and RNA 6000 Nano Assay on a Bioanalyzer 2100 (Agilent). Stranded RNA-seq libraries were performed for 150 ng of mRNA using the TruSeq library kit (Illumina, San Diego, CA, USA). Libraries were sequenced on a NextSeq2000 (Illumina) in a 2x50bp length with a coverage of >40 million paired-reads per sample.

Sequencing reads were trimmed using trimmomatic (version 0.38) (3) and ribosomal RNA reads were filtered out using SortMeRNA (version 2.1b) (4). Gene-level counts (GRCh38.p13; Ensembl release 100) were calculated using kallisto (version 0.46.1) (5) and tximport (version 1.6.0) (6). Paired differential expression analyses were conducted using DESeq2 (version 1.18.1) (7). All samples were used to estimate size factors and dispersions. Shrinkage of effect size was performed using the ash method (8). Adjusted *P* value (*Q*) <0.10 and absolute log₂-transformed fold change >0.5 were used to identify differentially expressed genes (DEGs).

Gene-set enrichment analyses (GSEAs) were conducted with GSEA software (version 4.3.2) (9) using the pre-ranked modality and log₂FC results obtained from DESeq2 as input data. All Human collections of MSigDB gene sets were used (Human MSigDB v2023.1.Hs updated March 2023). Heatmaps of selected genes were generated using R and Morpheus software.

Metadata comparative analysis

mRNA relative expression levels of selected immune checkpoints in whole lysates of follicular lymphoma lymph nodes (FL-LN, n=427) was compared with normal tonsils (TONSIL, n=30) according to GEP public databases (GSE3526, GSE7307, GSE31311, GSE39503, GSE43346, GSE65136, GSE71810, GSE53820, GSE55267, GSE86622, GSE93261, GSE12453, GSE12195, GSE35426 and GSE132929). This selected data was all generated with Affymetrix Human Genome U133 Plus 2.0. Briefly, CEL files were normalized using the Expression Console TM Software v1.4.1.46 (Affymetrix, Santa Clara, CA, USA). To take in consideration the batch effect, joint data was normalized using the Limma package included in Transcriptome Analysis console (Applied Biosystems, Waltham, MA, USA).

Statistical analysis

Data were analyzed using Prism Software 9.0 (GraphPad Software, San Diego, CA, USA). We used non-parametric test t-test, paired (Wilcoxon test) or unpaired (Mann-Whitney test) depending on the experiment. Likewise, ordinary one-way ANOVA followed by Holm-Sidak post hoc test was used for multiple comparisons. Data were represented as the mean values of the patients analyzed and standard deviation. Pearson correlation coefficient was used to measure linear correlations. Differences between the results of comparative tests were considered significant if the two-sided P value was less than 0.05. The statistical significance convention used along the manuscript was as follows: * $p < 0.05$, ** $p < 0.01$, *** $p < 0.001$ and **** $p < 0.0001$.

BIBLIOGRAPHY

1. McInnes L, Healy J, Melville J. UMAP: Uniform Manifold Approximation and Projection for Dimension Reduction. Arxiv - Cornell Univ [Internet]. 2018 Feb 9; Available from: <http://arxiv.org/abs/1802.03426>
2. Gassen S Van, Callebaut B, Helden MJ Van, Lambrecht BN, Demeester P, Dhaene T, et al. FlowSOM : Using Self-Organizing Maps for Visualization and Interpretation of Cytometry Data. *Cytometry*. 2015;87(7):636–45.
3. Bolger AM, Lohse M, Usadel B. Trimmomatic: a flexible trimmer for Illumina sequence data. *Bioinformatics*. 2014;30(15):2114–20.
4. Kopylova E, Noé L, Touzet H. SortMeRNA: fast and accurate filtering of ribosomal RNAs in metatranscriptomic data. *Bioinformatics*. 2012;28(24):3211–7.
5. Bray NL, Pimentel H, Melsted P, Pachter L. Near-optimal probabilistic RNA-seq quantification. *Nat Biotechnol*. 2016;34(5):525–7.
6. Soneson C, Love MI, Robinson MD. Differential analyses for RNA-seq: transcript-level estimates improve gene-level inferences [version 2; peer review: 2 approved]. *F1000Research*. 2016;4(1521).
7. Love MI, Huber W, Anders S. Moderated estimation of fold change and dispersion for RNA-seq data with DESeq2. *Genome Biol*. 2014;15(12):550.
8. Stephens M. False Discovery rates: a new deal. *Biostatistics*. 2017 Apr 1;18(2):275–294.
9. Subramanian A, Kuehn H, Gould J, Tamayo P, Mesirov JP. GSEA-P: a desktop application for Gene Set Enrichment Analysis. *Bioinformatics*. 2007;23(23):3251–3.

SUPPLEMENTAL FIGURES

Figure S1

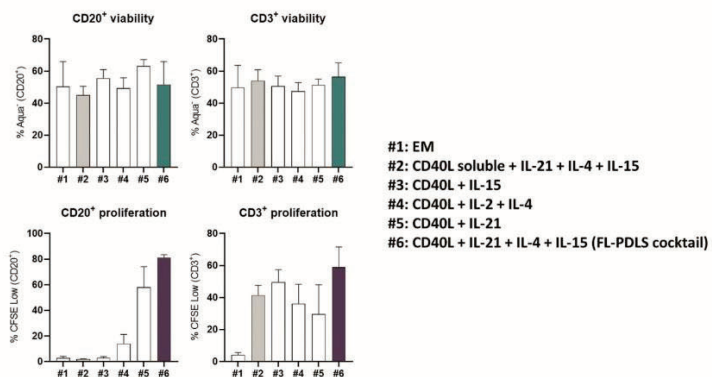


Figure S1. Optimization of PDLS cocktail. PDLS (n=10) including normal donor monocytes were cultured with the indicated cytokine cocktails. CD20⁺ and CD3⁺ population viability (upper panel) was determined by the percentage of Aqua⁺ flow cytometry staining, and proliferation (lower panel) was analyzed by the percentage of CFSE low signal after 7 days of culture.

Figure S2

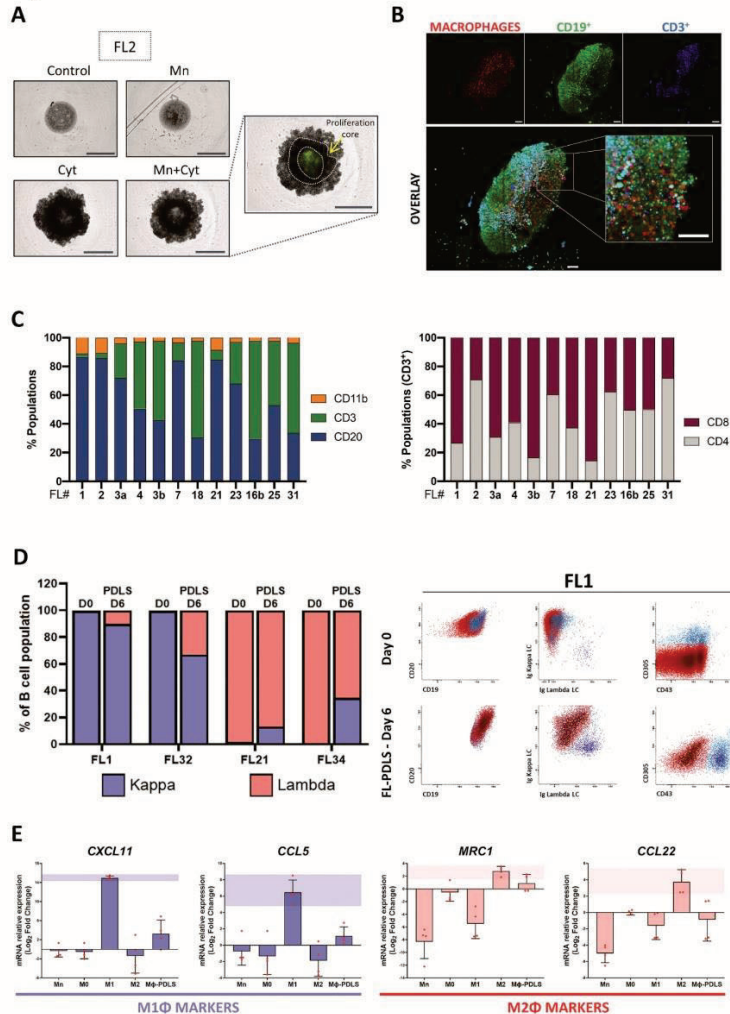


Figure S2. FL-PDLS additional features. (A) Brightfield images superimposed with CFSE (Cytation 1) in FL-PDLS after 7 days of culture with the following conditions: non-stimulated (Control), cytokine cocktail (Cyt), with monocytes (Mn) and the complete condition combining both cytokines and monocyte co-culture (Mn+Cyt). Magnification 4x and 1000 μ m scale. (B) Immunofluorescent capture of CD19⁺ (green), CD3⁺ (blue) or Far Red (macrophages)(red) labeled cells, and merged image of all 3 channels (overlay). Captured in confocal Leica TCS SPE microscope. Scale 100 μ m. (C) CD20⁺, CD3⁺ and CD11b⁺ cell proportions (left panel) and CD4⁺, CD8⁺ out of CD3⁺ (right panel) from day 7-FL-PDLS. (D) Light chain restriction analysis in four representative FL-PDLS. Kappa/lambda percentages are shown in the control sample (D0) and in the corresponding FL-PDLS (day 6). Representative density plots indicating the population (CD19⁺ CD20⁺), the light chain distribution and the expression of CD305 and CD43 in D0 sample and in the corresponding FL-PDLS. (E) Gene expression of M1 and M2 makers by RT-qPCR in CD11b⁺ cells sorted from day 7-FL-PDLS, compared to Mn, M0, M1 or M2 macrophages. Values are relative to M0 macrophages (mean, n=4).

Figure S3

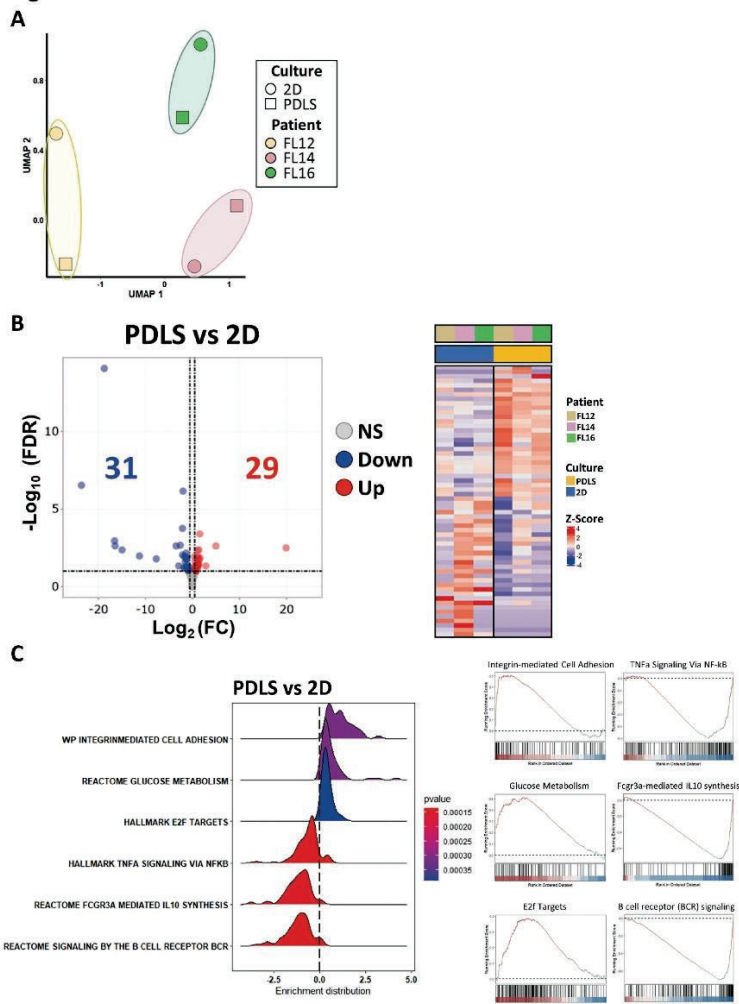


Figure S3. FL-PDLs and 2D comparison. (A) Purified B cells from FL-PDLs (n=3) or cultured in conventional 2D were analyzed by RNAseq. Uniform approximation and projection (UMAP) plot is shown. (B) Volcano plot representing the differentially expressed genes (DEG) comparing purified B cells from FL-PDLs or cultured in 2D (left panel). Heatmaps of DEG for the individual patients (n=3) (right panel). NS: non-significant; Down: Downregulated; Up: upregulated. (C) Gene Set Enrichment Analysis: PDLs vs 2D samples. The ridgeplot visualizes the expression distributions of core enriched genes for selected GSEA enriched gene sets. Gradient color reflects the p-values (left panel). Corresponding enrichment plots are also shown (right panel).

Figure S4

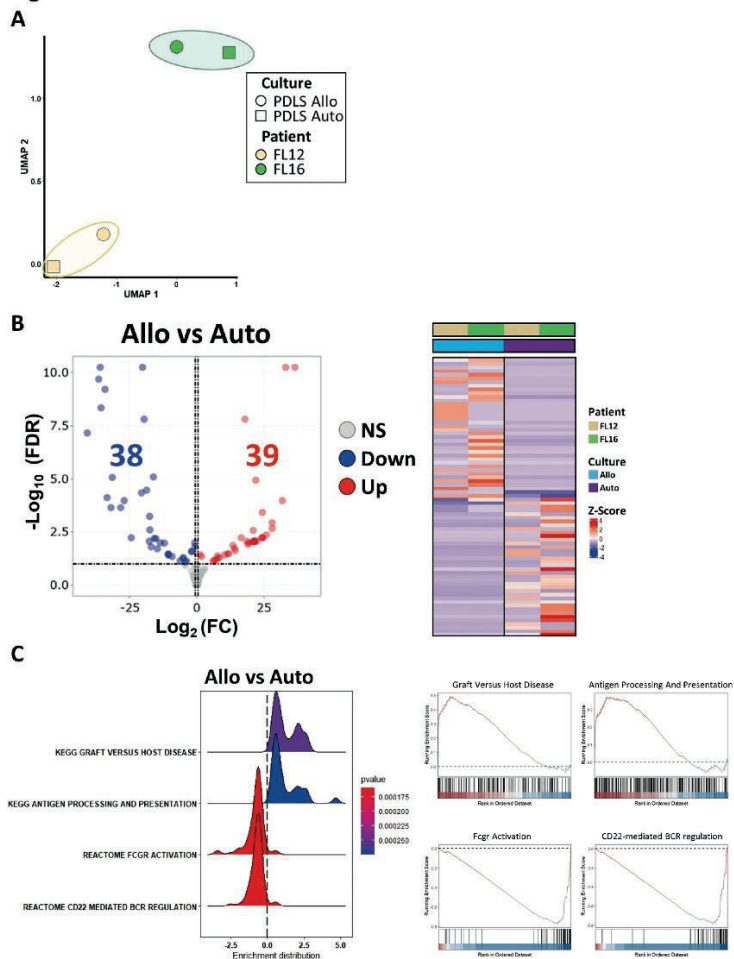


Figure S4. Comparison of FL-PDLS generated with allogenic or autologous monocytes. (A) Purified B cells from FL-PDLS (n=2) generated with allogenic or autologous monocytes were analyzed by RNAseq. Uniform approximation and projection (UMAP) plot is displayed. **(B)** Volcano plot representing the differentially expressed genes (DEG) comparing PDLS with allogenic monocytes (Allo) or containing autologous monocytes (Auto) (left panel). Heatmaps of DEG for the individual patients (n=2) (right panel). NS: non-significant; Down: Downregulated; Up: upregulated. **(C)** GSEA analysis ridgeplot of top 4 significant-enriched GO pathway gene sets. Corresponding enrichment plots are also shown (right panel).

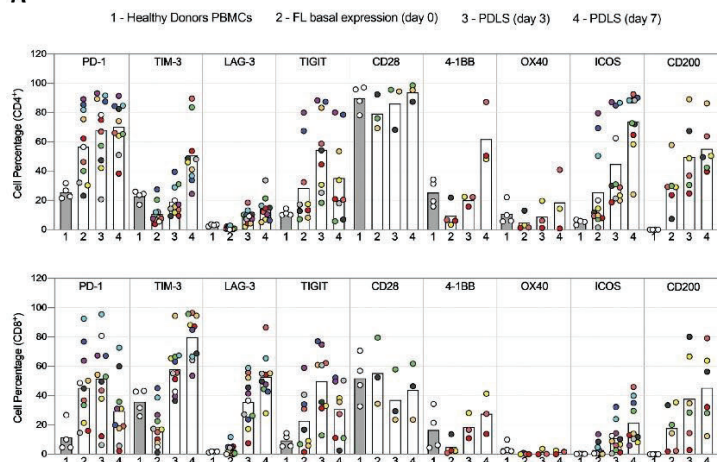
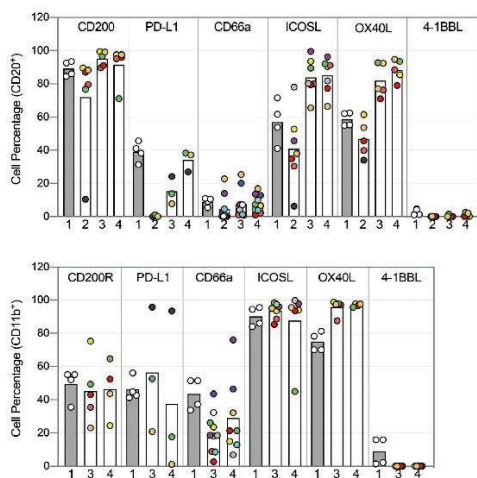
Figure S5**A****B**

Figure S5. Immune regulators expression in autologous T cells from FL-PDLS. (A) Graph bars showing mean percentages of IC expression on CD4 and CD8 T cells, or their ligands in CD20 and CD11b cells **(B)** from (2) baseline (day 0), (3) day 3, and (4) day 7-FL-PDLS. Control expression is measured in healthy donors PBMCs (1). Each colored dot represents a FL-PDLS patient.

Figure S6

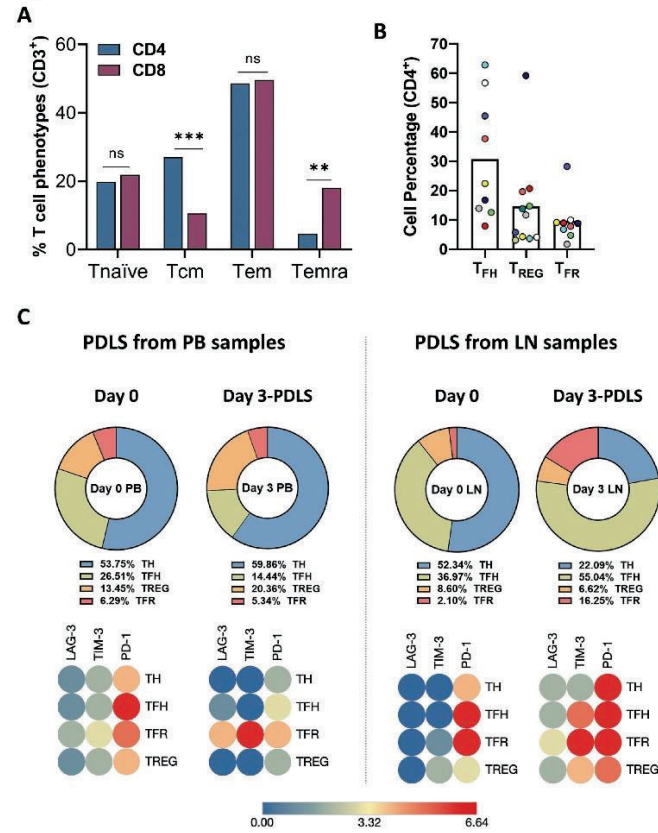


Figure S6. T cell phenotypes present in FL-PDLS. (A) Mean percentage of each CD4⁺ or CD8⁺ phenotype for FL patient measured by CD45RA and CCR7 expression by flow cytometry at day 3-PDLS. Paired t test - Wilcoxon matched-pairs signed rank test was applied. **(B)** Cell percentage of T_{FH}, T_{REG} and T_{FR} measured by FoxP3 and CXCR5 expression by flow cytometry at day 3-PDLS within the CD4 population (as in figure 3F) including patient coding. **(C)** Cell percentage of T_H, T_{FH}, T_{REG} and T_{FR} measured by FoxP3 and CXCR5 expression by flow cytometry at day 0 and day 3-PDLS generated from PB or LN samples. The relative expression of LAG-3, TIM-3 and PD-1 is displayed in these four conditions.

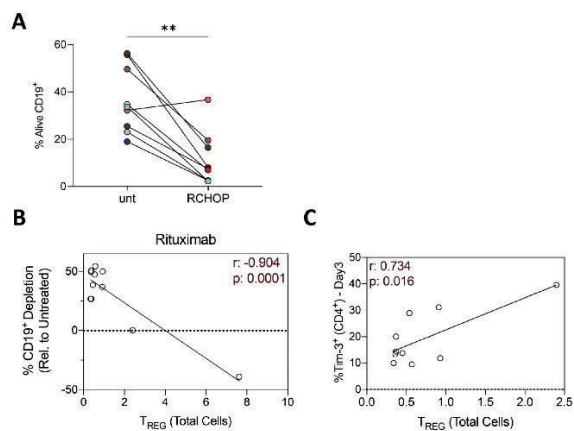
Figure S7

Figure S7. TIM3 expression and rituximab activity. (A) Day 3 FL-PDLS were treated with R-CHOP or remained untreated for 3 days; the percentage of alive B cells is represented. Paired t test - Wilcoxon matched-pairs signed rank test was applied. (B) Correlation plot (simple linear regression) between percentage of total T_{REG} in the autologous day 3-FL-PDLS T population and rituximab depletion. (C) Correlation plot (simple linear regression) between TIM-3 expression at day 3 in CD4⁺ cells and the percentage of T_{REG} cells out of total alive cells from the FL-PDLS.

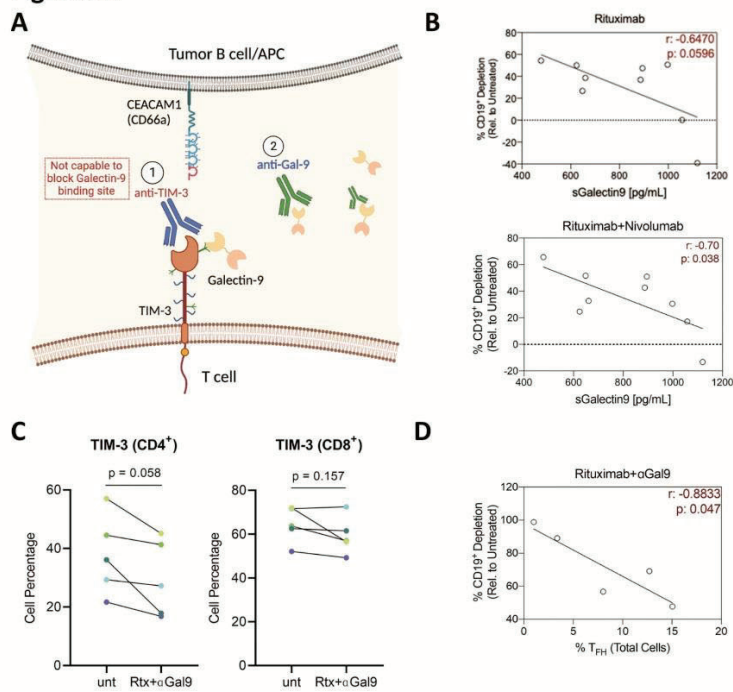
Figure S8

Figure S8. Galectin-9 is a novel target modulating TIM-3 expression. **A)** Schematic representation of receptor TIM-3 and CD66a and galectin-9 ligands and how blocking antibodies interact. Created with BioRender.com. **(B)** Correlation plot (simple linear regression) of tumor B cell depletion in FL-PDLs treated with rituximab (upper panel) or rituximab + nivolumab (lower panel) and the concentration of soluble galectin-9 in the supernatants. **(C)** TIM-3 expression in CD4 and CD8 cells in FL-PDLs untreated (unt) or treated with rituximab + mAb anti-galectin-9 (Rtx+Gal9). Paired t test - Wilcoxon matched-pairs signed rank test was applied. **(D)** Correlation plot (simple linear regression) of tumor B cell depletion in FL-PDLs treated with rituximab + anti-galectin-9 and the percentage of T_{HH} out of total alive cells from the PDLs.

SUPPLEMENTAL MATERIAL STUDY 3

SUPPLEMENTARY TABLES

Code	Sex	Age	Ann Arbor stage	B-cell symptoms	ECOG	FLIPI	High LDH	High B2M	Hemoglobin (g/L)	1st line treatment	Response	Group	PFS (years)
FL01	M	36	II	N	1	0	Y	N	148	R-CHOP	CR	NR	15,8
FL02	M	53	IV	Y	0	NA	NA	NA	118	R-CHOP	CR	NR	15,2
FL03	F	59	IV	Y	1	3	Y	Y	115	R-CHOP	CR	NR	14,5
FL04	F	60	IV	N	0	0	Y	N	120	R-CHOP	CR	NR	13,8
FL05	F	59	II	N	0	0	Y	N	137	R-CHOP	CR	NR	14,3
FL06	M	55	II	N	0	0	Y	N	157	R-CHOP	CR	NR	13,4
FL07	F	26	III	N	0	1	Y	N	135	R-CHOP	CR	NR	13,5
FL08	F	48	II	N	0	0	Y	N	132	R-CHOP	CR	NR	13,0
FL09	F	37	III	N	1	1	Y	N	114	R-CHOP	CR	NR	12,9
FL10	F	52	II	N	0	1	Y	Y	92	R-CHOP	CR	NR	17,7
FL11	M	68	II	N	0	0	1	N	145	R-CHOP	CR	NR	11,5
FL12	M	74	III	N	0	2	Y	N	161	R-CHOP	CR	NR	15,6
FL13	M	51	IV	N	0	3	Y	Y	152	R-CHOP	CR	Rel	4,3
FL14	F	69	IV	N	2	4	Y	Y	129	R-CHOP	CR	Rel	4,1
FL15	F	73	III	N	0	2	Y	N	151	R-CHOP	CR	Rel	3,0
FL16	F	58	IV	N	0	2	Y	N	143	GA-CHOP	CR	Rel	4,1
FL17	F	27	IV	N	0	2	NA	NA	122	R-CHOP	CR	Rel	5,3
FL18	M	63	IV	N	0	2	NA	NA	NA	R-CHOP	PR	Rel	3,5
FL19	F	40	IV	Y	0	3	N	Y	79	R-CHOP	CR	Rel	4,0
FL20	F	78	IV	N	0	3	N	Y	137	R-CHOP	PR	Rel	2,1
FL21	F	52	IV	N	0	1	N	Y	137	R-CHOP	CR	Rel	4,5
FL22	M	48	IV	N	0	3	Y	Y	128	R-CHOP	CR	Rel	7,0

FL23	F	65	IV	N		0	3	Y	N	140	R-CHOP	CR	Rel	4,7
FL24	F	67	IV	Y		0	4	Y	Y	81	R-CHOP	CR	Rel	4,4
FL25	M	66	II	N		0	0	Y	Y	125	R-CHOP	CR	Rel	1,3
FL26	F	52	I	N		0	0	Y	Y	135	R-CHOP	CR	Rel	1,8
FL27	F	55	IV	N		0	1	Y	Y	98	R-CHOP	CR	Rel	1,4
FL28	F	35	IV	Y		1	2	Y	Y	144	R-CHOP	CR	Rel	1,5
FL29	M	42	IV	N		0	2	Y	Y	135	R-CHOP	PR	Rel	1,0
FL30	M	26	III	N		0	NA	NA	NA		R-CHOP	PR	Rel	0,7
FL31	F	52	IV	N		0	4	Y	NA	NA	R-CHOP	CR	Rel	1,7
FL32	M	50	II	N		0	0	N	NA	133	R-CHOP	CR	Rel	2,3

Table S1. Clinical parameters of FL patients. NR = non-relapse; Rel = relapse; ECOG = Eastern Cooperative Oncology Group; FLPI = Follicular Lymphoma International Prognostic Index; CR = complete response; B2M = beta-2-microglobulin; LDH = lactate dehydrogenase; PFS = progression-free survival; F = female; M = male; Y = yes; N = no; NA = not available

FIGURE LEGENDS

Figure S1. Differential immune profile between patients that will or will not relapse. (A) Pre-ranked GSEA analysis showing biological pathways up-regulated or down-regulated in relapse compared to non-relapse patients. (B) GSEA plots showing some of the most representative pathways over-represented in each group. (C) Box-plot representation of mRNA expression levels of *CD27* in each group, expressed in log2 from Nanostring counts, each patient is represented by a single dot. (D) Correlation analysis showing genes that significantly correlate ($\text{abs } R > 0.4$, $p < 0.05$) with *CD70* expression. (E) Biological pathways over-represented by GSEA in genes positively correlating with *CD70*. (F) Dot-plot representation of the correlation between *CD70* and some of the most important genes (*CCL20*, *CCL22*, *IRF4*).

Figure S2. Genetic profile of FL samples (A) Heatmap representing WT or altered status of the most frequently mutated genes in FL, together with the number of mutations, the group (Rel / NR), and *CD70* levels (B) Box-plot representation of *CD70* normalized counts according if the patient has more or less than 8 mutations (median number of mutations). (C) Accumulative number of mutations, expressed in percentage of patients from each group (*CD70* low or high) that reach each certain number of mutations (left panel). Area under curve (AUC) units from each group (right panel). (D) Box-plot representation of mRNA expression levels of *CD70* in each group. Each patient is represented by a single dot. T-test or Mann-Whitney U test were applied for D

Figure S3. *CD70* and *CD27* expression in FL-LN by multiplexed immunofluorescence (A) Merged from a representative Rel and a NR patient stained with Panel 3 antibodies. (B) Summary of the *CD27* and *CD70* expression, represented with box-plots in relapse (red) and non-relapse (blue) patients. (C) Kaplan-meier survival analysis (lower panels) and percentage of *CD70*+ cells (upper panels) in T helper non-follicular cells (left panel) and T follicular regulatory cells (right panel). Each patient is represented by a single dot. (D) Kaplan-meier survival analysis (lower panels) and percentage of *CD27*+ cells (upper panels) in T helper non-follicular cells (left panel) and T follicular regulatory cells (right panel). (E and F) Box-plot representation of density of cells expressing *CD70* (E) or *CD27* (F) in *CD20*+, *CD4*+ or *CD8*+ population. Each patient is represented by a single dot. T-test or Mann-Whitney U test were applied for C-F. (G) Correlation analysis (R spearman) between density of *CD20*+*CD70*+ cells and density of T regulatory cells.

Figure S4. *CD70* expression in tumor cells correlates with *CD70* in T cells. (A) Bubble-plot showing the correlation between the percentage of *CD70*+ cells in the *CD20*+ population with the expression of *CD70*+ and *CD27*+ in the populations analyzed by multiplexed immunofluorescence. (B and C) Representation of the most relevant correlations between *CD70*+ in B cells with *CD70*+ (B) or *CD27*+ (C) in T cells.

Figure S5. CD70 knock-out in FL cell lines and primary samples. (A) Histogram from flow cytometry data representing expression of CD70 in WSU-FSCCL and SC-1 cell lines. (B) Histogram from flow cytometry data representing transfection efficiency (ATTO-550+) of gCtrl and gCD70, compared to untransfected (UNT) cells. (C) Intracellular expression of CD70 in stable FL cell lines generated by transfection with a gCtrl (red) or a gCD70 (blue). (D) Expression of CD27 in SC-1 cells in different days (D) after electroporation with a gCtrl (red) or a gCD70 (blue). (E) Soluble CD27 (sCD27) levels in supernatants from WT WSU-FSCCL and SC-1 cell lines. (F) Expression of CD27 (in SC-1 cells, left panel) or CD70 (in both SC1, middle panel, and WSU-FSCCL, right panel) at different times after electroporation. Represented as median fluorescence intensity (MFI). (G) Soluble CD27 (sCD27) levels in supernatants from FL cell lines co-cultured with T cells. Represented as the increase in sCD27 compared to the baseline (FL cell lines cultured alone). (H) Percentage of CD70 (left panel) and CD27 (right panel) of FL cells co-cultured with T cells. (I) Histogram representation of CD70 down-regulation in a FL patient 4 days after electroporation with a gCtrl (red) or a gCD70 (blue) (left panel). Percentage of positive CD70 (middle panel) and CD27 (right panel) in CD20+, CD4+ and CD8+ populations, after 4 days of electroporation. Each patient is represented by a single dot. (J) Relative B-cell count after 4 days of electroporation, calculated by flow cytometry techniques. Each patient is represented by a single dot. Paired t-test was applied for G-J.

Figure S6. Determination of the lead anti-CD27 CAR-T construct in follicular lymphoma (A) CAR-T membrane expression, in scFv-based CAR-Ts (left panel) and in ligand-based CAR-Ts (right panel). CD27^{high} population was determined with an arbitrary gate from UTD expression. (B) sCD27 concentration in supernatants at the end of the expansion (day 10). (C) Percentage of specific lysis, represented as mean \pm sd of bioluminescence loss in K562 cells WT cells or transduced with CD19 (K562-CD19) or CD70 (K562-CD70), compared to cells without CAR-T, after 24h of co-culture (n=3). 3 different effector to target (E:T) ratios (3:1, 1:1, 1:3) were used. (D) IL-2 levels in supernatants of K562-WT, K562-CD19 and K562-CD70 cells co-cultured for 24h with CAR-T, in a E:T ratio of 3:1 (E) Specific killing (left panel), T-cell proliferation (middle panel) and B/T cell proportion (right panel) of SC-1 and WSU-NHL cells co-cultured for six days with CAR-T in a E:T ratio of 1:4. Specific killing was calculated as the depletion compared to untransduced (UTD) cells. T-cell proliferation was calculated as the fold change comparing the number of CD3+ cells at endpoint. (n=3). A representative example with SC-1 cells comparing B cells (CD10+) and T cells (CD3+) by flow cytometry is shown. Anova test and Holm-Sidak test for multiple group comparisons was applied in A, B, D and E.

SUPPLEMENTARY FIGURES

Figure S1

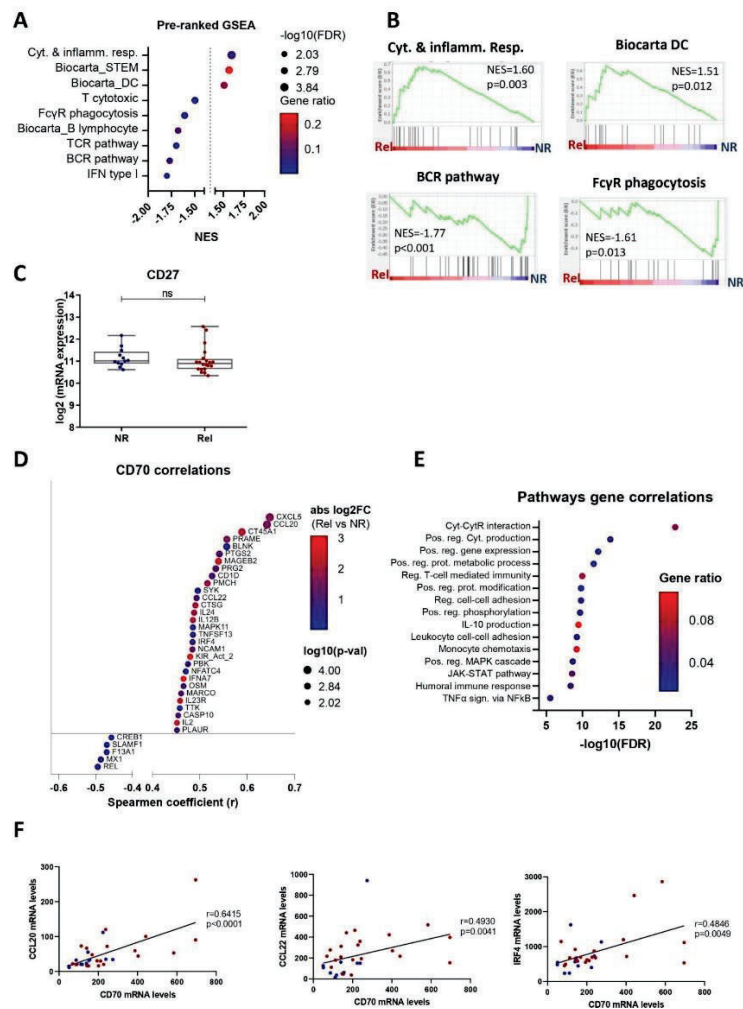


Figure S2

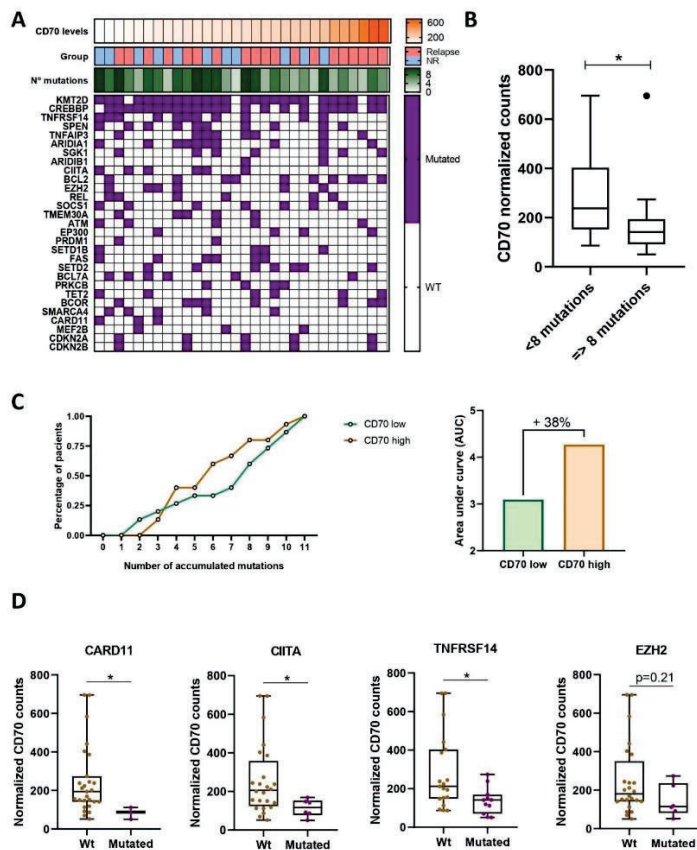


Figure S3

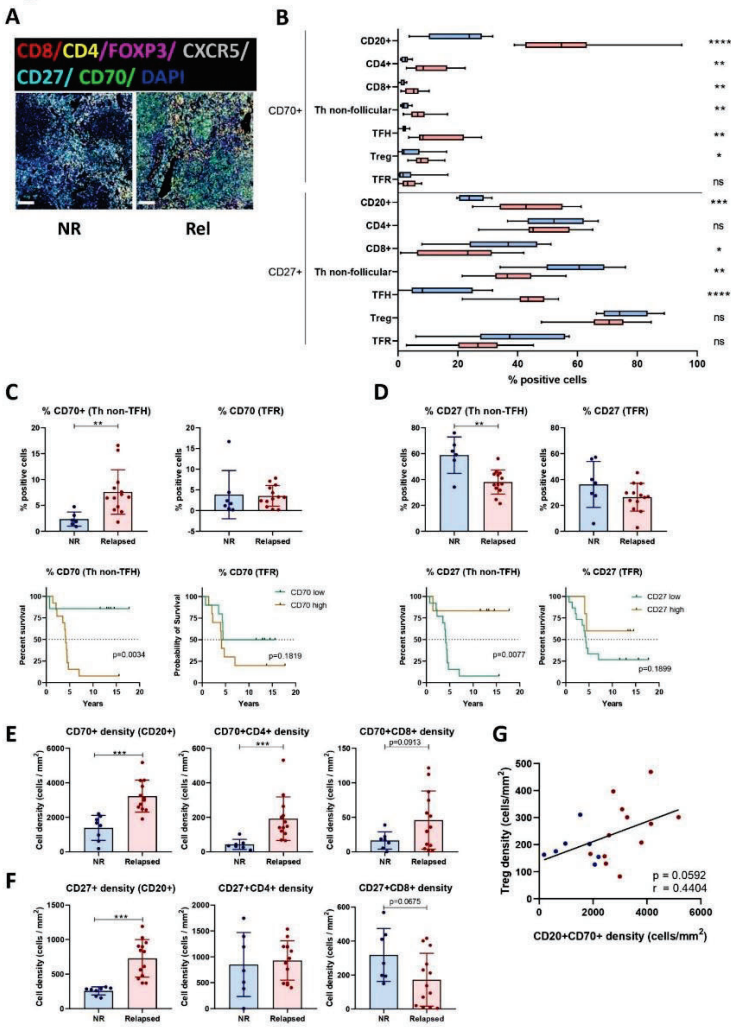


Figure S4

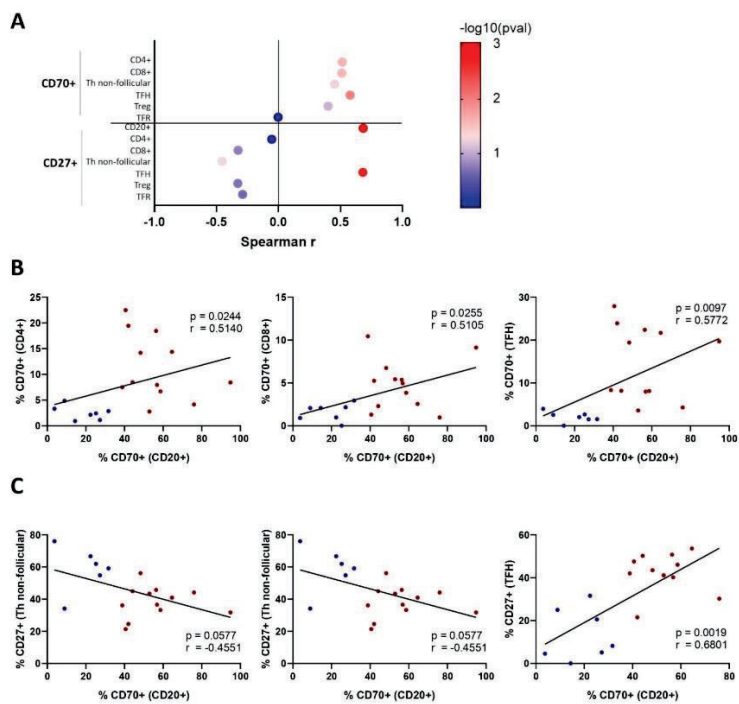


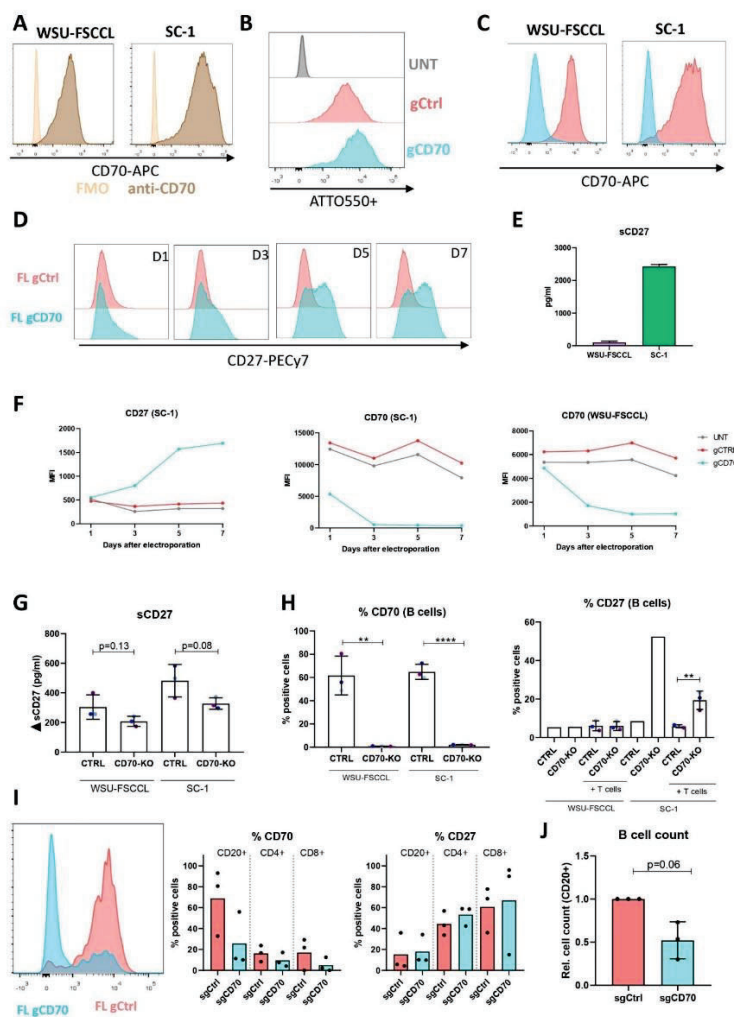
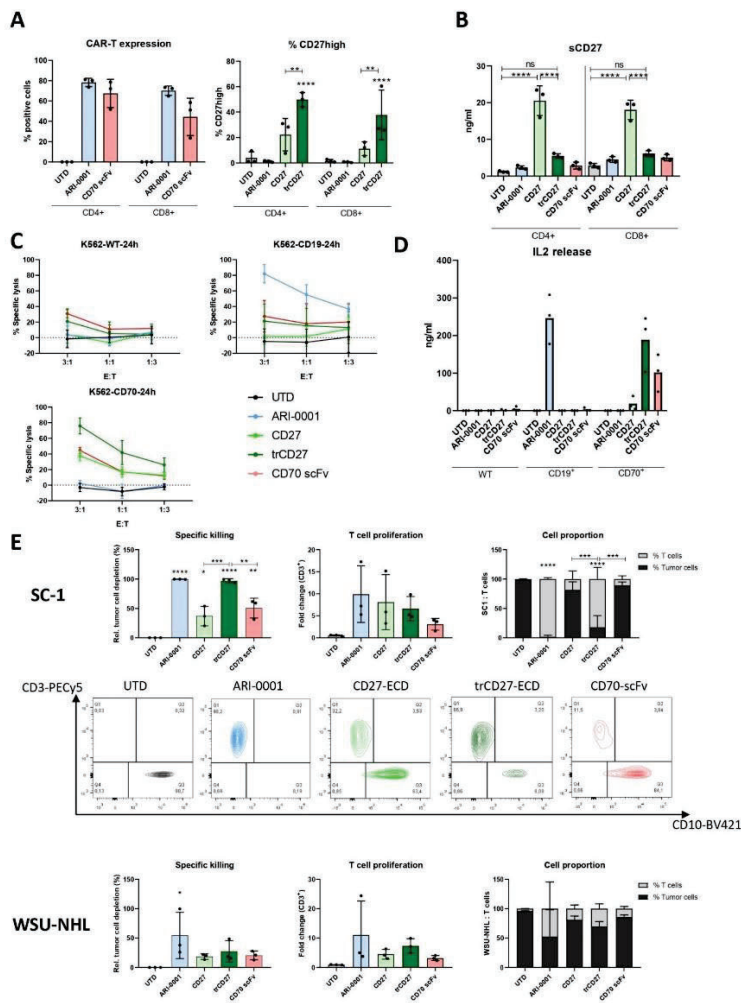
Figure S5

Figure S6



ADDITIONAL PUBLICATIONS

Apart from the studies mentioned above, which represent original research papers, two review works have also been published during this thesis:

1. Dobaño-López C, **Araujo-Ayala F**, Serrat N, Valero JG, Pérez-Galán P. Follicular Lymphoma Microenvironment: An Intricate Network Ready for Therapeutic Intervention. *Cancers (Basel)*. 2021 Feb 5;13(4):641. doi: 10.3390/cancers13040641. PMID: 33562694; PMCID: PMC7915642.
2. **Araujo-Ayala F**, Pérez-Galán P, Campo E. Vulnerabilities in the tumor and microenvironment in follicular lymphoma. *Hematol Oncol*. 2021 Jun;39 Suppl 1:83-87. doi: 10.1002/hon.2855. PMID: 34105816.



Review

Follicular Lymphoma Microenvironment: An Intricate Network Ready for Therapeutic Intervention

Cèlia Dobano-López ¹, Ferran Araujo-Ayala ¹, Neus Serrat ¹, Juan G. Valero ^{1,2} and Patricia Pérez-Galán ^{1,2,*}

¹ Department of Hematology-Oncology, Institut d'Investigacions Biomèdiques August Pi i Sunyer (IDIBAPS), 08036 Barcelona, Spain; cdobanol@clinic.cat (C.D.-L.); faraujo@clinic.cat (F.A.-A.); mnserrat@clinic.cat (N.S.); garcia32@clinic.cat (J.G.V.)

² Centro de Investigación Biomédica en Red-Oncología (CIBERONC), 28029 Madrid, Spain

* Correspondence: pperez@clinic.cat

Simple Summary: Follicular lymphoma is a paradigm of tumors that require the interaction between tumor and microenvironment cells to foster their development from initial steps to progression. Recent large-scale genome studies have uncovered multiple genetic alterations that cooperate with the lymphoma microenvironment to promote cell survival, proliferation and to facilitate tumor evasion from host immune system. Understanding the crosstalk between tumor B-cells and the microenvironment is fundamental to identify vulnerabilities that may offer novel therapeutic targets. This review highlights recent findings showing the effect of common genetic mutations modulating the cell composition and phenotype of the tumor microenvironment and the novel therapeutic perspectives to target these interactions.



Citation: Dobano-López, C.; Araujo-Ayala, F.; Serrat, N.; Valero, J.G.; Pérez-Galán, P. Follicular Lymphoma Microenvironment: An Intricate Network Ready for Therapeutic Intervention. *Cancers* **2021**, *13*, 641. <https://doi.org/10.3390/cancers13040641>

Academic Editors: Victor Peperzak and Marta Cuenca Lopera
Received: 4 November 2020
Accepted: 1 February 2021
Published: 5 February 2021

Publisher's Note: MDPI stays neutral with regard to jurisdictional claims in published maps and institutional affiliations.



Copyright: © 2021 by the authors. Licensee MDPI, Basel, Switzerland. This article is an open access article distributed under the terms and conditions of the Creative Commons Attribution (CC BY) license (<https://creativecommons.org/licenses/by/4.0/>).

Abstract: Follicular Lymphoma (FL), the most common indolent non-Hodgkin's B cell lymphoma, is a paradigm of the immune microenvironment's contribution to disease onset, progression, and heterogeneity. Over the last few years, state-of-the-art technologies, including whole-exome sequencing, single-cell RNA sequencing, and mass cytometry, have precisely dissected the specific cellular phenotypes present in the FL microenvironment network and their role in the disease. In this already complex picture, the presence of recurring mutations, including *KMT2D*, *CREBBP*, *EZH2*, and *TNFRSF14*, have a prominent contributory role, with some of them finely tuning this exquisite dependence of FL on its microenvironment. This precise characterization of the enemy (FL) and its allies (microenvironment) has paved the way for the development of novel therapies aimed at dismantling this contact network, weakening tumor cell support, and reactivating the host's immune response against the tumor. In this review, we will describe the main microenvironment actors, together with the current and future therapeutic approaches targeting them.

Keywords: follicular lymphoma; microenvironment; immunotherapy

1. FL Microenvironment: Friend or Foe?

Follicular lymphoma (FL), the most common indolent non-Hodgkin's lymphoma (NHL), is a biologically heterogeneous disease with clinical variations in patient outcome [1].

The initial oncogenic hit happens in the Pre B/Pro B stage of B cells in the bone marrow (BM) where they acquire the t (14;18) translocation due to an error in V(D)J recombination. Subsequently, these cells home to B cell follicles inside lymph nodes (LNs) where they encounter the antigen (Ag) and undergo, in the germinal center (GC), somatic hypermutation (SHM) and class switch recombination (CSR) (IgM to IgG) of the immunoglobulin that constitutes the B cell receptor (BCR). FL-like cells interact with follicular dendritic cells (FDCs) and are selected to undergo apoptosis or be rescued by follicular helper T cells (T_{FH}), based on the Ag affinity of their BCRs. Overexpression of

BCL2, along with additional anti-apoptotic proteins, allow apoptosis escape independently of BCR affinity. These FL-like B cells then exit the GC and enter circulation where they might be prone to traffic between secondary lymphoid organs and the BM, and they acquire additional genetic changes necessary for transformation to FL, such as *CREBBP*, *KMT2D*, *EZH2*, *TNFRSF14*, among others [2,3].

There is now growing evidence that crosstalk between lymphoma cells and stromal and immune cells in lymphoid compartments is fundamental for disease onset and progression. This crosstalk is dynamic and shapes the tumor microenvironment enhancing the pro-tumoral features of the niche [4,5]. FL represents a paradigm of dependence on the microenvironment. Seminal microarray studies in LN biopsies from the Leukemia and Lymphoma Profiling Project (LLMPP) series established for the first time that FL prognosis was not given by the tumor cell per se but by the composition of non-malignant cells [6–8]. Subsequently, many studies have tried to identify phenotypic markers to stratify patients, although this picture has been more complicated than anticipated, and influenced by treatment.

The main players that support tumors, through a complex set of cytokines, receptors, immune modulators, and pro-angiogenic factors, are follicular dendritic cells (FDCs), fibroblastic reticular cells (FRCs), mesenchymal stromal cells (MSCs), and tumor-associated macrophages (TAMs), together with a rich T cell infiltrate composed of CD4 T follicular helpers (T_{FH}) cells, CD4 T follicular regulatory (T_{FR}) cells, CD4 T regulatory cells (T_{REG}), and CD8 cytotoxic T cells (CTL) [9,10] (Figure 1).

The FL-LN maintains a structure reminiscent of a normal LN, where B cells are supported by T_{FH} and the follicles are delimited for a network of FDCs. These types of dendritic cells are only present in the follicles of primary and secondary lymph organs. FDCs are particular Ag-presenting cells (APCs) as they do not internalize, process, and present Ag, but present intact Ag–Ab complexes on their cell surface that induce survival of FL cells and their differentiation into memory B cells or plasma cells. In vitro studies using a non-immortalized FDC cell line have demonstrated that FDCs preferentially bind to GC B cells and deliver a positive signal for B cell survival, activation, and differentiation [11,12]. Interestingly, FL cells are then able to present this Ag derived from FDC presentation and trigger T_{FH} recruitment. T_{FH} are specialized CD4⁺ T cells located in the GC light zone and are characterized by CD4⁺, CXCR5⁺, PD1⁺, ICOS⁺, and CD25⁺ phenotype. T_{FH} are essential for the formation and maintenance of GC, contributing to B cell fitness by means of CD40L signaling and IL-4 or IL-21 cytokines [13]. It is noteworthy that IL-4 proteins are five-fold more abundant in FL germinal centers than in normal tonsil [14]. Moreover, malignant B cells are involved in the recruitment of T_{REG} (CD4⁺, CD25⁺), present in a higher frequency in FL compared with tonsils, and acting as inhibitors of CD8⁺ T cell effector activity [15].

FRCs are stromal cells present in the T cell zone of the LN that are endowed with functions that create a permissive niche by secreting components of the extracellular matrix (ECM), including laminin, fibronectin, and collagen IV. They organize and regulate immune cell trafficking, differentiation, and migration of T cells through an IL-4/CXCL12 communication axis with T_{FH} , among other signals, and secretion of additional chemokines such as CCL19 and CCL21. FRC also plays a direct role in B malignant cells' activation and survival through BAFF signaling [16–19].

MSCs are present both in the BM niche and LNs, supporting B cell survival through the secretion of numerous factors, such as BAFF, TNF α , lymphotoxin α (LT α) [20], while chemokine CCL2 favors the recruitment of macrophages to the FL niche [21].

Tumor-associated macrophages (TAMs) are highly plastic cells from the myeloid lineage. Depending on the stimuli, macrophages can be polarized into M1 (inflammatory phenotype) or M2 (anti-inflammatory), resulting in distinct cytokine production or T cell function (Th1 and Th2). We have recently demonstrated that FL-FDC niche promotes, via the secretion of CCL2 and CSF-1, monocyte recruitment, differentiation, and polarization towards an M2-like pro-tumoral phenotype, as seen in FL patient biopsies [5], favoring angiogenesis, dissemination, and immunosuppression [22]. Moreover, macrophages

Thus, FL is surrounded by a rich and well-interconnected network of supportive allies that may account for the incurability of this indolent lymphoma. Moreover, this dynamic microenvironment also takes part in the histological transformation (HT) of FL to an aggressive lymphoma. These modifications comprise the disruption of the FDC network [27], changes in the gene expression of CD4/8 T cells leading to decrease motility [28], a decrease in the number and follicular distribution of FoxP3⁺ T_{REG} [29] and PD-1 positive T cells [30].

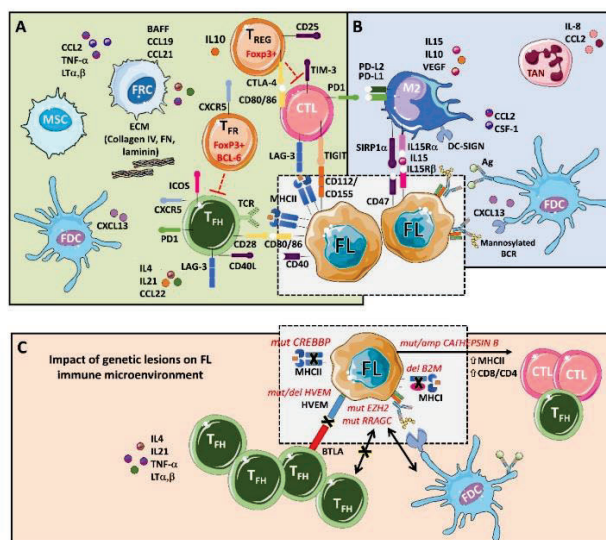


Figure 1. An integrative view of follicular lymphoma (FL) microenvironment and its crosstalk with genetic drivers. (A) FL is highly infiltrated with several T cell subpopulations, where T_{FH} are fundamental players through MHC II and CD40L, while immunosuppressive T_{REG} , hamper cytotoxic T cells (CTLs) activation. Fibroblastic reticular cells (FRCs) also participate in immunosuppression by secreting extracellular matrix (ECM) proteins that regulate T cell trafficking and cooperate with T_{FH} . (B) FL cells favor the recruitment of monocytes through CCL2 and CSF-1 that differentiate and polarize mostly into M2-like macrophages expressing PD-L1 and PD-L2 and dampening CTLs cytotoxic activity. Both macrophages and FDCs activate B cell receptors (BCRs) through lectins binding to mannosylated BCR. Likewise, FDCs also activate BCRs through the presentation of immunocomplexes to FL cells. Neutrophils are recruited through IL8 secretion in the FL niche and support lymphoma growth. (C) Several genetic alterations corrupt the microenvironment to better support FL. Mutations in *CREBBP* and deletions in *B2M* genes reduce MHC II and MHC I expression, respectively. On the contrary, aberrant *CATHEPSIN B* leads to an increase in MHC II expression and CD8 expansion. Both *EZH2* and *RRAGC* mutations reduce the need for T_{FH} help making FL cells more dependent on FDCs, while disruption of the HVEM-BTLA axis allows uncontrolled T_{FH} support to FL cells.

2. FL Mutational Landscape and Microenvironment Interplay

Although t(14;18) (q32;q21) was discovered decades ago [31], it is considered the first oncogenic hit in FL. It is not present in approximately 10% of patients [32,33], and it has been detected in some healthy individuals [34,35]. Therefore, additional mutations must contribute to disease onset. In this genomic era, the FL genome has been fully characterized by whole genome and exome sequencing and, more recently, by single-cell RNA sequencing (sc-RNAseq). In this review, we focus on those mutations with an impact on the FL microenvironment remodeling.

FL is a malignancy addicted to epigenetic mutations [36] where these hits (*KTMD2*, *CREBBP/EP300*, and *EZH2* genes) constitute early oncogenic events present in virtually all FL patients [37–39]. These genes are involved in the post-translational modification of histones [40]. The loss of function of histone K3K4 methyltransferase KMT2D (also known as MLL2) is the most frequent alteration (60–90%), followed by loss of function mutations in the H3K27/H3K18 acetyltransferases CREBBP (50–70%) and EP300 (10–20%), resulting in transcriptional repression [41,42].

Histone-lysine N-methyltransferase 2D (KMT2D) function is related to GC formation and CSR, two critical steps in the maturation process of B cells, and it cooperates with BCL-2 in lymphomagenesis [41,43]. No impact on the immune microenvironment has been described thus far.

CREB-binding protein (CREBBP) is a haploinsufficient tumor suppressor that acts as a major regulator of enhancer networks in the GC, especially in the light zone, and avoids terminal B cell differentiation [42]. CREBBP also acetylates non-histone proteins such as p53 and BCL6. Loss of function CREBBP mutations leads to reduced activation of p53 as well as to diminished inactivation of BCL6 [44,45]. Noteworthy, *CREBBP* mutations have a clear effect on the immune microenvironment. MHC class II is reduced in FL cells at both the transcriptome and protein levels, resulting in a diminished Ag presentation [46]. Recently, this finding has been confirmed by scRNA-seq analysis [47]. Furthermore, *CREBBP* mutations are associated with reduced T cell proliferation and have been identified as early mutations, since they are present in the earliest inferable progenitors [46] and could even be present in hematopoietic stem and progenitor cell compartments [45]. Altogether, there is a large amount of evidence indicating that *CREBBP* mutations may play a major role in the evasion of immune surveillance during the development of FL tumors. In addition, both *mutCREBBP* and *mutEP300* contribute to lymphomagenesis by enabling unopposed suppression of enhancers by BCL6/SMRT/HDAC3 complexes, suggesting HDAC3-targeted therapy as a precision approach for CREBBP-mutant lymphomas [48], and recent results with specific HDAC3 inhibitors have demonstrated the reactivation of immune responses [49]. While specific HDAC3 inhibitors are not at a clinical stage, diminished chromatin acetylation by *mutCREBBP* might be reverted using pan-HDACi. Preclinical data suggest that these families of compounds may be beneficial in combination with immunotherapy in B cell lymphomas [50]. Some clinical trials have explored pan-HDAC in monotherapy. Vorinostat yielded moderate responses (<50%) in two phase II clinical trials [51,52], while abexinostat has shown an improved overall response rate (ORR) [53] (Table 1). The lack of isoform-specificity could lead to immunosuppressive effects by pan-HDACi [54].

Table 1. Current therapies in clinical or preclinical status targeting FL-microenvironment crosstalk.

Drug Family	Target	Status ¹	Combination	Clinical Responses		Ref ⁴
				ORR ² (%)	PFS ³ (Months)	
Epigenetic Regulators						
BRD3308	HDAC3i	PC	Anti-PDL1	NA		[49]
Vorinostat	HDACi	C	None	47	15.6	[51]
			None	49	20	[52]
Abexinostat	HDACi	C	None	63	20.5	[53]
Tazemetostat	EZH2	C	None	<i>mut</i> EZH2: 69 <i>wt</i> EZH2: 35	<i>mut</i> EZH2: 13.8 <i>wt</i> EZH2: 11.1	[55]
Metabolic Regulators						
Temsirolimus	mTOR	C	None	53.8	12.7	[56]
			Bendamustine and rituximab	90	22	[57]
			Bortezomib	56	16.5	[58]
B-Cell Receptor Inhibitors						
Idelalisib	PI3K δ	C	None	57	11	[59]
		PC	Venetoclax	NA		[60]
Copanlisib	PI3K $\alpha\delta$	C	None	58.7	11.2	[61]
		C	Nivolumab	NCT03884998		NA
		C	Rituximab	NCT03789240		NA
Duvelisib	PI3K $\gamma\delta$	C	None	42	9.5	[62]
		C	Venetoclax	NCT03534323		NA
		C	Nivolumab	NCT03892044		NA
Ibrutinib	BTK	C	None	37.5	14	[63]
		C	Rituximab	85	41.9	[64]
Fostamatinib	SYK	C	None	10	4.2	[65]
Entospletinib	SYK	PC	Obinutuzumab	NCT03010358		NA
Cerdulatinib	SYK/JAK	C	None	>50%	NA	[66]
Immune Checkpoints Inhibitors						
CAR-T	HVEM	PC	None	NA		[67]
Nivolumab	PD1	C	None	40	NR	[68]
Pidilifzumab	PDL-1	C	Rituximab	66	18.8	[69]
Sym022	LAG-3	C	None	NCT03489369		NA
		C	Anti-PD1	NCT03311412		NA
Sym023	TIM-3	C	None	NCT03489343		NA
		C	Anti-PD1	NCT03311412		NA
Immune Checkpoint Activators						
Urelumab	CD317	C	Rituximab	21	4.5	[70]
Selicrelumab	CD40	C	Anti-PD-L1	NCT03892525		NA
Macrophage Checkpoint Inhibitors						
Pexidartinib	CSF1-R	PC	Rituximab	NA		[22]
SIRP α -Fc	SIRP α	PC	Rituximab	NA		[71]
Hu5F9-G4 (5F9)	CD47	C	Rituximab	71	NR	[72]

¹ C, Clinical; PC, Preclinical; ² ORR, overall response rate; ³ PFS, progression free survival; ⁴ Ref, reference; NA, not available; NR, not reached.

Enhancer of zeste homolog 2 (EZH2) is a histone methyltransferase that methylates H3K27 and presents monoallelic gain-of-function mutations at three recurrent hotspots (Y646, A682, and A692) in 20–30% of FL [73]. It is the combined function of wt and *mut*EZH2

that causes an increased di- and trimethylation of H3K27 [74]. EZH2 plays a central role during GC formation in cooperation with BCL6 through the formation of bivalent promoters [75,76]. BCL6 is necessary to maintain GC reaction and acts as a transcriptional repressor, antagonizing CREBBP/EP300 function [42]. Noteworthy is EZH2's participation also in the remodeling of the GC immune microenvironment. *mutEZH2* cells in the GC light zone lose dependence on T_H1 cells, while upregulated genes are involved in an interaction with FDC and become dependent on them. As a consequence, these cells are no longer capable of reentering the dark zone of GC but can proliferate as centrocytes [77].

As EZH2 mutations gain function (in contrast to CREBBP/EP300 and KMT2D), they are easily druggable, and several attempts have been made to develop selective inhibitors [78,79]. Nowadays, tazemetostat is the most promising compound (Table 1). FL patients with *mutEZH2* had an objective response of 63% and 71%, higher than in *wtEZH2* patients (28% and 33%, respectively) [80]. These results were confirmed in another phase II study involving 99 patients with relapsed or refractory (R/R) FL, separated in a *EZH2^{mut}* cohort with an ORR of 69% and progression-free survival (PFS) of 13.8 months and a *EZH2WT* cohort presenting a diminished ORR of 35% and PFS of 11.0 months [55], which led to FDA approval in June 2020 for adult patients with R/R FL with EZH2 mutated tumors.

B2-microglobulin (B2M) and CD58 genes are inactivated in some DLBCL cases, uncovering a mechanism of immune evasion, as B2M is involved in the expression of MHC class I, necessary for cytotoxic CD8⁺ T cell recognition and CD58 mediates T and NK cell response [81]. Although initially, no mutations were observed in FL, later studies have shown that mutations and deletions in B2M and CD58 were present in transformed FL [82,83].

Cathepsin S (CTSS), which is aberrant in approximately 20% of FL patients by activating point mutation or amplification [84], has effects opposite to CREBBP mutations regarding Ag presentation since it is required for the binding of MHC to antigenic peptides [85]. When cathepsin S is hyperactivated, it cleaves its substrates more efficiently, including CD74, leading to upregulation of MHC class II genes and a higher CD4⁺ T cell infiltration [84,86]. Furthermore, patients carrying CTSS mutations expressed higher levels of IFN- γ and IFN- γ R1 [84]. Moreover, while CREBBP mutations have been related to bad prognosis [39], cathepsin S activation correlates with a better outcome after chemioimmunotherapy treatment [84]. It could be explained due to the enhanced CD4⁺ T cell response. In addition, in a CTSS KO in vivo model, the modification of the Ag repertoire supported a multiclonal expansion of cytotoxic CD8⁺ T cells, and in FL patients, there was an inverse correlation between CTSS and PD1 expression [86].

Herpesvirus entry mediator A (HVEM), also known as TNFRSF14, is a receptor inactivated by mutations and/or deletions in half of FL patients and associated generally with a bad prognosis [87], although some controversy still remains [88].

This loss of function disrupts the interaction between HVEM and BTLA that normally provides inhibitory signals to BCR signaling. In addition, BTLA does not present mutations, but it is often transcriptionally silenced. The net balance is an increased BCR stimulation. Furthermore, HVEM loss makes TME more tumor-supportive due to the high secretion of stromal activating cytokines (TNF α , LT α , LT β) and increased T_H1 cell recruitment [67]. A therapeutic approach has been proposed to restore HVEM expression using an engineered chimeric antigen receptor T cell (CAR-T) construct directed towards B cell marker CD19, which produces HVEM protein locally and continuously, and promising results have been shown in mouse lymphoma models [67].

Ras-related GTP binding C (RRAGC) activating mutations occur in up to 17% of patients and constitute a mechanism that bypasses amino acid deprivation to activate mTORC1 signaling [89,90]. As recently published by Ortega-Molina et al., engineered mice are able to activate mTORC1 via PI3K-Akt by ligands that mimic paracrine T cell-derived activating signals (IL-4/CD40L axis). Furthermore, mutated RRAGC confers enhanced B cell activation but in an autonomous manner, reducing T_H1 dependence, similar to EZH2

mutation. Intriguingly, RAGC mutation confers an opportunity to target mTORC1 in selected patients by rapamycin [91]. In recent years, several phase I and II clinical trials have been engaged to evaluate the use of temsirolimus or everolimus as single agents [56] and in combination with other drugs. Among these combinations, we highlight temsirolimus with bendamustine and rituximab, achieving an ORR of 90% [57] and with the proteasome inhibitor, bortezomib, resulting in an ORR of 56% [58] (Table 1).

3. T Cells: Fundamental Actors in FL Pathogenesis Modulated with BCR Inhibitors

As described above, FL-infiltrated lymphoid tissues preserve normal follicle architecture in the GC, where FL cells behave like normal B cells, interacting with T cells through the MHC class II and responding to activating signals [92]. Accordingly, FL cells remain dependent on BCR signaling, which has made BCR inhibitors [93] (mainly BTK and PI3K inhibitors) useful drugs for treatment. While BCR stimulation can be achieved by ways other than cognate B–T interaction, such as DC-SIGN binding to mannose residues of BCR [23], FL still requires cell-to-cell interaction with T_{FH} for proliferation and survival [84,85] (Figure 1). Numerous pieces of evidence indicate that FL cells take advantage of T_{FH} function in order to obtain positive signals that fuel tumor growth and actively modify GC composition by recruiting cells or altering their phenotype in a process called microenvironment re-education [86,87]. Another important actor in the FL milieu is the chemokine CCL22, secreted by FL tumor cells as a result of the CD40L–CD40 axis activated by T_{FH} . CCL22 facilitates the active recruitment of T_{REG} and IL-4-producing T cells, which, in turn, may stimulate more chemokine production in a feed-forward cycle [15,94].

The role of T_{REG} FOXP3+ cells in FL prognosis has remained controversial for a long time [29,95]. The discovery of a new T subset called follicular regulatory T cells (T_{FR}), which are present in the germinal center and suppress T_{FH} and B cell activation [96], has finally explained the divergence observed in the results. The FOXP3+ population encompasses two different T cell subsets. Conventional T_{REG} can be attracted to the GC through CCL22 secretion, impairing T CD4+ or CD8+ activation by tumor antigens, with a pro-tumoral consequence. On the contrary, the T_{FR} population probably plays an antitumoral role, as they reduce T_{FH} support to malignant cells.

It is noteworthy that PI3K inhibitors have been shown to disrupt this interactive B–T cell network, blocking this forward-feed cycle efficiently. Idelalisib has been the first-in-class PI3K inhibitor FDA-approved in 2014 for the treatment of relapsed or refractory (R/R) FL. In a phase 1b study for indolent NHL, 47% of patients showed ORR, with one patient demonstrating a complete response [97,98]. Further trials in FL confirmed these values (57% ORR, 6% CR) [59], demonstrating that PI3K inhibition has significant efficacy in FL, although it also has serious side effects, mainly severe diarrhea, hepatotoxicity, or pneumonitis, and, in some cases, made it necessary to stop the treatment [99]. PI3K is a key regulator of T_{FH} differentiation [100] and has deleterious effects on T_{REG} [101], which closely relates with some side effects described for this drug and may be responsible for its therapeutic activity. In this regard, using ex vivo FL-FDC primary co-cultures, we recently uncovered that idelalisib interferes with the CD40/CD40L pathway at the B–T interface, decreasing CD40L-induced proliferation and downregulating the expression of key membrane proteins critical for B–T cell synapses (CD80, SLAMF1, and ICAM1). The net balance of these effects might result in inefficient crosstalk between FL cells and the supportive T_{FH} cells. Moreover, the chemokine CCL22, fundamental in the FL milieu, decreases after idelalisib treatment, and this phenomenon impacts on the composition of FL microenvironment by a decrease in the recruitment of T_{REG} and T_{FH} , but not T_{FR} into FL-FDC niche, which may allow the host to mount superior immune responses against the tumor [60].

In the last few years, new PI3K inhibitors were added to the list: copanlisib that inhibits all class I PI3Ks, including α isoform and duvelisib, a dual PI3K γ , δ inhibitor. In a phase II study, copanlisib ORR was 43.7% in indolent lymphomas [93]. With respect to undesirable effects, copanlisib produces less severe diarrhea or hepatotoxicity than PI3K

inhibitor, but it displays new side effects like hyperglycemia or hypertension, all of them generally manageable. On the basis of its improved safety, there are currently three phase III trials on copanlisib in indolent lymphoma [61]. The advantages of duvelisib are related to γ isoform inhibition, which has a special effect on myeloid cells [102] (Section 5.2.). Finally, combinations of PI3K inhibitors with different agents are under investigation (Table 1).

In addition to PI3K inhibitors, additional BCR inhibitors have been developed and tested in FL.

The BTK inhibitor, ibrutinib, was tested as monotherapy in FL, with modest results (ORR 37.5%) [63]. However, its combination with a Rituximab in a randomized phase III trial has yielded encouraging results in untreated FL patients [64]. In chronic lymphocytic leukemia (CLL), it has been demonstrated that ibrutinib profoundly reshapes the T cell compartment, improving T cell function. Ibrutinib induces expansion of memory T cells, Th1 polarization, reduces the expression of inhibitory receptors (i.e., PD-1 and CTL-4), and improves immune synapse between T cells and CLL cells [103,104]. However, no data are available for FL in this regard. Finally, the SYK/JAK inhibitor cerdulatinib has shown significant tumor responses in refractory B cell lymphoma [105].

Overall, these kinase inhibitors impact not only on BCR signaling but also on other receptors such as CD19, CD40, or IL-4R. In consequence, these drugs can cause indirect inhibition of T_{FH} supportive action. Additionally, they have a direct effect on T cells and macrophages that will contribute to antitumor activity and often to its undesirable effects.

4. Immune Escape in FL and Checkpoint Inhibitors

Immune escape is a hallmark of cancer and FL is not an exception. FL cells have evolved to avoid immune surveillance via multiple mechanisms, including advantageous somatic mutations (described in Section 2), but also through modulation of specific genes to inactivate both innate and cellular immunity.

As described in the previous section, the FL microenvironment is characterized by a heavy infiltration of T cells. However, early functional studies in FL samples determined that tumor-infiltrating T cells (TILs) were not responsive to cytokines such as IL-4, IL-10, or IL-21, in contrast to those of peripheral blood (PB) from the same patients, suggesting that immune-suppressive molecules may be present in the tumor tissue [106]. T cell activity is regulated by immune checkpoint activators (CD40L, OX40, CD27, CD28, and 4-1BB/CD137) and inhibitors (CTLA-4, PD1, LAG-3, TIM-3, and TIGIT) [107]. We briefly described the immune checkpoint inhibitors that may be relevant in FL pathogenesis.

Programmed death 1 (PD-1) is upregulated in a large proportion of tumor-infiltrating lymphocytes (TILs) in many different tumor types, but it is also upregulated in other immune cells. Intracellular PD-1 signaling is activated upon PD-1 binding to its ligands PD-L1 (B7-H1, CD274), or PDL2 (PDCD1LG2, CD273), which induces a reduction in the T cell activation cascade. Thus, by expressing PD-1 ligands on the tumor cell surface and engaging PD-1-positive infiltrating lymphocytes, tumors utilizing the PD-1 pathway can therefore evade an immune response.

Cytotoxic T-lymphocyte-associated protein 4 (CTLA-4/CD152) is a homolog of CD28 and binds to CD80/CD86. CTLA-4 is constitutively expressed in T_{REG} and activated T cells.

Lymphocyte activation gene 3 (LAG3/CD223), a CD4-like molecule, is upregulated on activated CD4+ and CD8+ T cells and a subset of natural killer (NK) cells upon binding to MHC class II molecules, inducing the inhibition of T lymphocyte activity and eventually its anergy [108].

T cell immunoglobulin-3 (TIM-3) is expressed in T_{FH} , CTLs and NKs, and is co-regulated and co-expressed along with PD-1, LAG-3, or TIGIT on CD4+ and CD8+ T cells, and it marks the most dysfunctional or terminally exhausted subset of CD8+ T cells [109].

T cell immunoglobulin and ITIM domain (TIGIT) shifts the cytokine balance by targeting the immune response at multiple levels, namely, through its action on APCs, CTLs, and T_{REG} cells. In DCs, TIGIT ligation induces IL-10 production and dampens type 1 immunity indirectly.

In FL, PD1 is expressed in both intratumoral CD4 and CD8 T cells, but several subsets with different expression levels have been identified [110]. CD4⁺PD-1^{high} T cells predominantly reside in the LN follicles, while PD-1^{low} T cells are mainly located in interfollicular areas. CD8 T cells are mainly PD1^{low}, and a significant portion express TIM-3. Intratumoral CD4⁺PD-1^{high} T cells have a T_{HH} cell phenotype that supports tumor growth with no TIM-3 expression, while CD4⁺PD-1^{low} T cells that have an exhausted phenotype, express TIM-3 and display a reduced cytokine production and cell–signal transduction. Moreover, T cells from the LNs of FL patients present a high percentage of CD8+TIM-3+ showing defective cytokine production upon TCR engagement, despite the presence of ex vivo markers of lytic granule [111].

Regarding PD1 ligands, it is accepted that while FL cells do not express PD-L1 and PD-L2 is moderately expressed in a high proportion of FL cases, these ligands are present in the tumor microenvironment [112]. Precisely, PD-L1⁺ histiocytes have been detected in the T cell-rich zone of the neoplastic follicles [106].

Overall, these studies suggest that in FL, PD-1 expression is not sufficient to distinguish exhausted from activated T cells, and immune escape in FL goes far beyond PD-1. Data mining analysis studies [112] identified genes involved in cancer immune–evasion pathways (immune escape gene set (IEGS)) across FL and normal B cell transcriptomes indicated that the whole IEGS was significantly upregulated in FL samples compared to normal tonsils. These genes include, besides the PD-1 axis genes, additional immune checkpoints (TIGIT and CTLA-4), exhaustion markers (TIM-3, LAG3, Galectin 1 and 3), chemoattractants of immunosuppressive cells (CSF-1, CCL2, and CCL22) M2 macrophages markers (CD206, CD163) and immunosuppressive molecules (IL10, VEGF, IDO1 and 2). Further validation in FL tissue microarray indicated an abundant immune infiltrate expressing PD-L1⁺, PDL2⁺, and LAG3⁺. LAG-3 has been found in intratumoral PD1⁺ T cells, and they are phenotypically heterogeneous, with a predominant effector memory phenotype. Intratumoral PD-1⁺LAG-3⁺ T cells exhibited a reduced capacity to produce cytokines and granules compared to PD-1⁺LAG-3[−] T cells. Moreover, LAG-3 expression may be upregulated on CD4⁺ or CD8⁺ T cells by IL-12, cytokine enriched in the serum of FL patients. Furthermore, simultaneous blockade of both PD-1 and LAG-3 signaling enhances the function of intratumoral CD8⁺ T cells. The relevance of LAG-3 expression on intratumoral T cells correlated with a poor outcome in FL patients [113].

Armed CTLs (CD3⁺CD8⁺Granzyme B⁺) represent a rich infiltrate in FL interfollicular areas and are associated with better outcomes [114]. However, these cells express higher TIM-3 expression than their counterparts in normal tonsil. As expected, these cells show defective responses to TCR activation, and a high percentage of TIM-3⁺ immune cells in the infiltrate was associated with shortened patient PFS, independently of Granzyme B (GrzB) score, highlighting the relevance of this checkpoint inhibitor in FL and the need of scoring both TIM-3 and Grz B in this disease [111].

TIGIT [115,116] also constitutes a common inhibitory receptor in FL, expressed by the majority of CD8 T effector memory cells, which are commonly co-expressed with exhaustion markers such as PD-1 and CD244. These FL CD8⁺ T cells showed significantly reduced TCR-induced distal signaling (pERK) and reduced production of IFN γ , while TCR proximal signaling did not seem to be affected. Interestingly, the TIGIT ligands CD112 and CD155 are expressed by FDCs. Dysfunctional TCR signaling correlated with TIGIT expression in FL CD8 T cells and could be fully restored upon in vitro culture, supporting that TIGIT blockade is a relevant strategy for improved immunotherapy in FL, possibly in combination with blockade of PD-1.

In terms of clinical development, the PD1 axis has been the most explored. Nevertheless, despite the initial encouraging results in early Phase 1b trials [117], later assessment in larger cohorts have demonstrated limited activity of nivolumab in R/R FL [68]. Noteworthy is the combination of anti-PD1 with standard anti-CD20 immunotherapy that has been more successful. In this regard, a phase II trial combining anti-PD-L1 obtained significant OR (66%) and a high proportion of complete responses with manageable adverse

events [69]. Following the experience in melanoma, PD-1 has been combined with CTLA-4. Recent results of the phase Ib have been quite disappointing, as the combination did not provide added benefit other than the single agents [118].

The low responses of the PD-1 blockade may be related to the heterogeneity of PD-1⁺ T cells in FL and the role of PD-1 in restraining T_{HH} cell help to GC B cells. T_{HH} are principal actors in the FL microenvironment. In view of poor clinical responses to anti-PD1, these therapies may unleash PD1 break in T_{HH} and increase helper signals to FL B cells more prominently than the benefit of unleashing existing CD8. This suggests that additional immunotherapy approaches that do not unleash T_{HH} cell helper signals need to be tested in FL.

In this regard, anti-LAG-3 therapy is in phase I trials and based on encouraging preclinical results in MHC II expressing tumors, such as Hodgkin's Lymphoma; anti-LAG3 therapy in combination with anti-PD1 is also under clinical investigation. Similarly, anti-TIM-3 alone and in combination with anti-PD1 is also under clinical investigation (Table 1).

Although preclinical results with anti-TIGIT may support its clinical investigation [119], no trials in lymphoma are registered at the moment of writing this review. Nevertheless, several studies are running in advanced solid tumors or plasma cell neoplasms as multiple myeloma.

A complementary approach is to target the immune checkpoint activators. A recent paper using the anti-CD137 antibody in combination with rituximab has shown a favorable safety profile and clinical activity in patients with R/R FL. However, the combination did not enhance clinical activity relative to rituximab alone or other current standards of care. It is noteworthy that those FL patients with CR showed increased T cell infiltration and cytotoxic activity in tumors [70]. CD40 constitutes another druggable activator; however, to date trials performed with agonist antibodies against CD40 have provided modest results and may need to be further tested in combination therapy [120] as the ongoing trial with anti-PDL1 (Table 1).

5. Maneuvers of Myeloid Companions in FL

Myeloid cells are a major cellular compartment of the immune system composed of a heterogeneous population of cells like mast cells, dendritic cells, monocytes, macrophages, and granulocytes, all of which originate from the bone marrow but mature into subpopulations with diverse and unique properties [121]. Most of these populations are known to be part of the tumor microenvironment in FL. However, in recent years, monocytes, macrophages, and neutrophils have received most of the attention, as they play an important role in disease severity, transformation, clinical outcome, and response to therapy in this disease [122].

5.1. Tumor-Associated Monocytes in FL

As described before, TAMs derive from circulating PB monocytes that originated in the BM. These monocytes are recruited to the tumor tissues and then differentiate locally in response to a variety of cytokines, chemokines, and growth factors produced by the stromal and tumor cells in the tumor microenvironment. For instance, in FL, the chemokine CCL2 from MSCs and macrophage colony-stimulating factor were shown to recruit inflammatory monocytes to the tumor site, and then differentiate into TAMs in response to IL-4, IL-10, IL-13, and other cytokines in the tumor microenvironment and promote lymphoma dissemination [21].

Two studies have analyzed the significance of absolute monocyte count (AMC) in FL. The first study with a large cohort of patients described that AMC was associated with inferior overall survival (OS) in FL independently of FLIPI in a multivariate analysis. The AMC may be most helpful when used in conjunction with the FLIPI, as the AMC was able to identify high-risk patients otherwise identified as low-/intermediate-risk by the FLIPI. Conversely, the AMC was able to identify relatively low-risk patients

classified as high-risk by the FLIPI [123]. In contrast with these results, in a second study in a cohort of 150 follicular lymphoma patients who received rituximab and cyclophosphamide–doxorubicin–vincristine–prednisone regimen (R-CHOP) therapy, PFS did not differ significantly according to the AMC [124].

The lymphocyte-to-monocyte ratio (LMR) constitutes a prognostic factor in different neoplasms, but its potential relevance in FL is not well defined. An initial retrospective cohort study including 88 patients with a histologically proven FL diagnosis demonstrated that LMR played a significant role in predicting PFS; however, the strength of the evidence for OS was weak [125]. More recently, an extensive study analyzed a cohort of 384 FL patients for which the LMR was available at diagnosis. In these series, patients with an $\text{LMR} \leq 2.5$ had a shorter PFS and inferior OS. Furthermore, low LMR was also an independent risk factor for histological transformation. Likewise, patients with a low LMR had a higher rate of second malignancies. The authors concluded that LMR could be an additional tool to improve the prognostic classification of FL patients in order to avoid toxicities of overtreatment low-risk patients and to intensify therapy in patients at a higher risk of early progression or histological transformation [126].

5.2. Tumor-Associated Macrophages in FL

Macrophages are conventionally classified into M1 and M2 subtypes according to their polarization status and functional role in the immune system. M2 macrophages, also known as alternatively activated macrophages, exhibit anti-inflammatory features, downregulating expression of their MHC molecules and interleukin IL-12, while expressing high levels of IL-10, MSR1 (CD204), and arginase. M2 macrophages are involved in wound-healing and angiogenesis. This is in contrast to M1 macrophages associated with antitumor responses and production of high levels of pro-inflammatory cytokines, including TNF α , IL-1, IL-6, IL-12, and inducible nitric oxide synthase [127]. TAMs share some similarities with the M2 macrophage subset because they express a series of markers, such as CD163, the Fc fragment of IgG, C-type lectin domains, and heat shock proteins, some of which are commonly expressed in M2 macrophages. Moreover, the acquisition of an M2-like phenotype is also caused by the secretion of tumor-derived cytokines such as IL4, IL10, and IL13. However, findings suggest that this binary polarization model is becoming obsolete, and there exists a whole spectrum of TAM phenotypes that are yet to be discovered and fully characterized [128].

Since early gene expression studies by Dave et al., highlighting the role of macrophages and other immune cells in FL outcomes [8], subsequent immunohistochemical studies have tried to transfer these findings into the clinical laboratory by associating the cellular composition of the microenvironment and its spatial distribution with the progression of the disease. To date, this issue remains a matter of debate.

The first study in the pre-rituximab era analyzed CD68 in a study group that consisted of uniformly staged FL patients treated with BP-VACOP (bleomycin, cisplatin, etoposide, doxorubicin, cyclophosphamide, vincristine, and prednisone) followed by radiation. In this study, high numbers of lymphoma-associated macrophages predicted inferior survival [129]. However, the introduction of rituximab early changed this view, and high TAMs content correlated with longer survival rates after R-CHOP [130]. These results were later confirmed in patients from the FL-2000 trial, a prospective multicenter study conducted by the GELA (Groupe d'Etude des Lymphomes de l'Adulte) where patients were randomly assigned to receive cyclophosphamide, doxorubicin, etoposide, prednisolone, and interferon (CHVP-I) or rituximab plus CHVP-I. The study demonstrated that high numbers of intratumoral macrophages correlated with poor prognosis in the patients treated with chemotherapy without rituximab [131].

Later on, the identification of TAMs was performed more accurately using the M2 marker CD163, a member of the scavenger receptor cysteine-rich family. In 2010, Clear et al. published an analysis restricted to the interfollicular area from TAMs. Importantly, the treatment was variable during the 35-year period under review, and patients were treated

according to the current protocol during this period. This work demonstrated the existence of a correlation between the number of CD163⁺ TAMs in angiogenic sprouts (CD31⁺) with poor prognosis [132]. More recently, an enlightening study investigated the correlation of TAMs with outcome using automated image analysis, analyzing a single-institution experience with uniform therapy (BCCA cohort, R-CVP) in a cohort of 186 patients and compared the findings with those from a prospective, randomized phase III clinical trial (PRIMA, R-CHOP followed by R maintenance) containing 395 samples. This study showed that most FL samples were infiltrated by few macrophages, and increased staining for CD163 was associated with poor PFS and OS in the BCCA cohort and favorable PFS in the PRIMA cohort. On the other hand, the CD68 staining cells did not predict outcomes in either cohort [133]. These opposing results were concealed by the differences in treatment. The PRIMA trial regimen included doxorubicin (inducer of immunogenic cell death) and R maintenance that may benefit from high macrophage numbers.

In an attempt to solve these discrepancies and integrate the microenvironment in the prognosis algorithms, the Lunenburg Lymphoma Biomarker Consortium confirmed in a homogeneously rituximab-chemotherapy-treated group of patients that lower percentages of CD8⁺ T cells, CD163⁺ M2 macrophage areas, EZH2 wild-type status, and gain of chromosome 18 in the initial tumor biopsy specimen were predictors of poor prognosis FL treated with R-CHOP while refuting the prognostic impact of various other markers [134]. These results validate those of Kridel et al., showing that a higher CD163⁺ pixel count or CD163⁺ area were independent predictors of prolonged PFS in patients treated with R-CHOP, while the CD68⁺ macrophages population did not have a significant impact by pixel count or area [134].

Lately, the CSF1 receptor tyrosine kinase (CSF-1R) has generated attention. The colony-stimulating factor-1 (CSF-1) binds this receptor through autophosphorylation of CSF-1R. Triggering this phosphorylation cascade increases gene transcription and protein translation and induces cytoskeletal remodeling by several signaling pathways, leading to the recruitment, survival, proliferation, and differentiation of monocytes into macrophages. Because CSF-1 regulates the survival, proliferation, and chemotaxis of macrophages and supports their activation, this factor is involved in the pathogenesis of several diseases [135]. CSF-1R protein expression could represent an important tool in the future study of some lymphomas. Martin-Moreno et al. analyzed the distribution of CSF-1R⁺ cells in FFPE samples from reactive lymphoid tissues and different lymphoma types, including FL. The results demonstrated that the CSF-1R⁺ cell population only partially overlapped with the M2-type macrophages detected by CD163 expression, in agreement with previous observations about monocyte differentiation, where the *CSF-1R* gene was not significantly differentially expressed between M1 versus M2 monocyte activation models [136]. In this regard, recent results from our laboratory in FL patients homogeneously treated with R-CHOP yielded an association between high CSF-1R expression (both follicular and Interfollicular) and histological grade or risk of transformation [22].

Finally, an additional interesting checkpoint is CD47, a “do not eat me” antiphagocytic signal that forms a signaling complex with signal-regulatory protein α (SIRP α), enabling the escape of cancer cells from macrophage-mediated phagocytosis and other phagocytes. Virtually all cancers overexpress CD47. A growing number of studies have demonstrated that inhibiting the CD47-SIRP α signaling pathway promotes the adaptive immune response and enhances the phagocytosis of tumor cells by macrophages [137]. In a recent work using FFPE LN biopsies from FL patients, researchers identified three subsets (CD14⁺SIRP α ^{hi}, CD14⁺SIRP α ^{low}, and CD14⁺SIRP α ^{neg}) of monocytes/macrophages (Mo/M Φ) that exhibited specific differentiation, migration, phagocytic or immunosuppressive properties. When using SIRP α -Fc to block the interaction between SIRP α and CD47, alone or in combination with rituximab, phagocytosis of tumor cells was differentially increased in the three Mo/M Φ subsets. Clinically, high numbers of CD14⁺SIRP α ^{hi} cells significantly correlated with poor prognosis in FL patients. In contrast, while not statistically significant, the

number of CD14⁺ SIRP α ^{low} (that stimulate rather than suppress T cells) was associated with a favorable prognosis [71].

Overall, this better characterization of the supportive interactions between FL and TAMs has opened new therapeutic avenues. Four main approaches can be highlighted:

5.2.1. Blockade of DC-SIGN-Mediated BCR Activation

BTK and SYK inhibitors have been demonstrated to reduce the viability of FL cells in vitro [23,25]. However, the clinical benefit of SYKi or BTKi in FL as a single agent are limited [63,65], and better results have been obtained in combination with anti-CD20 antibodies [64].

5.2.2. Blockade of the CSF-1/CSF-1R Pathway Axis Has Been Extensively Investigated in Tumor Models and Is Paradigmatic of the TAM–Cancer Cell Interaction

This strategy represents a selective approach to manipulate macrophages and is well described in solid tumors and, more recently, in hematologic malignancies as mantle cell lymphoma [138] or acute myeloid leukemia [139]. In FL, the inhibition of CSF-1R kinase activity with PLX-3397 (pexidartinib) preferentially affects M2 macrophage viability and induces their repolarization to M1 macrophages, disrupting FL–M2 positive crosstalk. In vivo, CSF1-R inhibition caused M2 reduction and repolarization towards M1 macrophages and antitumor effect cooperating with anti-CD20 rituximab [22].

5.2.3. PI3Ky Inhibitors

Although much attention has been paid to PI3K δ inhibitors, the PI3Ky isoform, highly expressed in leukocytes, plays a major role in cell chemotaxis to inflammation sites. Accordingly, PI3Ky inhibition stimulates p65/RelA phosphorylation, promoting a more prone M1 phenotype in macrophages [140]. In HL and peripheral T cell lymphoma, PI3Ky inhibition resulted in a shift of TAMs from the immunosuppressive M2-like phenotype to the inflammatory M1-like phenotype [141,142]. These additional properties of PI3Ky may explain the good clinical results of the dual PI3K δ y inhibitor duvelisib, currently approved for CLL, SLL, and FL [143].

5.2.4. Blockade of CD47

Anti-CD47 antibodies induce an antitumor T cell response by the cross-presentation of tumor antigens by phagocytes to T cells. Hu5F9-G4 (hereafter, 5F9) is a humanized, IgG4 isotype, CD47-blocking monoclonal antibody [72]. In preclinical xenograft models, 5F9 enabled the phagocytic elimination of FL. CD47 is widely expressed on normal cells; however, 5F9 selectively eliminated malignant cells and not normal cells. Phagocytosis is dependent on unmasking pro-phagocytic “eat me” signals that are expressed only on tumor cells and not on normal cells (with the exception of aging red cells). In this phase 1b study, combination therapy with 5F9 plus rituximab was associated with a good safety profile and produced responses in half the patients with R/R aggressive and indolent lymphomas. The mechanism of antitumor synergy with 5F9 and rituximab therapy depends largely on macrophage-mediated tumor killing through the blockade of the antiphagocytic CD47 signal by 5F9 combined. Although a reduction in NK cell-mediated antibody-dependent cellular cytotoxic effect is a mechanism of rituximab resistance, these clinical data suggest that 5F9 can restore rituximab sensitivity by means of macrophage-mediated, antibody-dependent cellular phagocytosis. A phase II trial is currently ongoing ([ClinicalTrials.gov Identifier: NCT02953509](https://clinicaltrials.gov/Identifier/NCT02953509)).

5.3. Tumor-Associated Neutrophils in FL

Few data are available regarding interactions between FL cells and neutrophils, which are key players in the innate immune system. Although neutrophils are traditionally considered in the context of their antibacterial functions, there is increased awareness that

tumor-associated neutrophils (TANs) may be key mediators of malignant transformation, tumor progression, angiogenesis, and the modulation of antitumor immunity.

Although TANs do not seem to be implicated in the phagocytosis mechanism of rituximab activity [144], in vitro and in vivo studies, have demonstrated that TANs may compromise the cytotoxic effect of common chemotherapeutic agents used through CD11b/ICAM-1 interaction with CD44 of malignant B cells and inhibit FL B cell apoptosis. Interestingly, the expression levels of activation markers (CD11a, CD11b, CD18, CD32, and CD66b) in TANs are significantly increased when neutrophils are co-cultured with FL cells, suggesting that lymphoma cells influence their phenotype and function [145]. In accordance, a clinical study demonstrated a correlation increased between neutrophil counts and reduced response rate to therapy, pointing out that these innate immune cells could be pharmacologically targeted to enhance therapeutic responses [146]. Likewise, the neutrophil-to-lymphocyte ratio (NLR) has been evaluated as a possible prognostic factor, demonstrating that NLR at relapse is associated with post-progression survival (PPS) as a continuous variable, where PPS was defined as the time from progression or relapse to the date of death [125].

6. Concluding Remarks

Over the last decade, thanks to the contribution of high-content techniques, both at genomic and cellular levels, a picture of the FL microenvironment has become much better delineated, providing the basis for the application of precision medicine. However, the road ahead is not completely clear, and a number of important topics remain to be answered. On the one hand, despite being a disease that is addicted to epigenetic mutations, no magic bullet has yet been found, and specific epigenetic modulators are eagerly awaited. On the other hand, in a disease where the immune microenvironment plays such a fundamental role, immunotherapy, besides anti-CD20 antibodies, is still far from being a reality. In this regard, there is an urgent need to better characterize the immune profile in specific clinical scenarios (i.e., early versus late relapse versus histological transformation) and tailor immunotherapies accordingly.

Author Contributions: C.D.-L. revised general concepts on FL microenvironment; F.A.-A. revised genetic alterations in FL; N.S. revised PI3K inhibitors and the T cell compartment; J.G.V. revised data on the myeloid compartment; P.P.-G., design the manuscript, revised immune checkpoint data and the whole details of this review. All authors have read and agreed to the published version of the manuscript.

Funding: Grants that contributed to this work included: Spanish Ministry of Economy and Competitiveness & European Regional Development Fund (ERDF) “Una manera de hacer Europa” for SAF2017/88275R to PP-G, Fundacio la Marató TV3 (TAIFOL 201933-30) to PP-G, PRE2018-083797 to CD-L, IMLINFO-INTERREG (IMLINFO-EFA281/16) to PPG.

Institutional Review Board Statement: Not applicable.

Informed Consent Statement: Not applicable.

Data Availability Statement: Not applicable.

Acknowledgments: To all who donate to Fundació la Marató TV3.

Conflicts of Interest: The authors declare no conflict of interest

References

1. Kahl, B.S. Follicular lymphoma: Are we ready for a risk-adapted approach? *Hematology* **2017**, *2017*, 358–364. [CrossRef] [PubMed]
2. Huet, S.; Sujobert, P.; Salles, G. From genetics to the clinic: A translational perspective on follicular lymphoma. *Nat. Rev. Cancer* **2018**, *18*, 224–239. [CrossRef] [PubMed]
3. Kahl, B.S.; Yang, D.T. Follicular lymphoma: Evolving therapeutic strategies. *Blood* **2018**, *127*, 2055–2064. [CrossRef]
4. Shain, K.H.; Dalton, W.S.; Tao, J. The tumor microenvironment shapes hallmarks of mature B-cell malignancies. *Oncogene* **2015**, *34*, 4673–4682. [CrossRef] [PubMed]
5. Yang, Z.Z.; Ansell, S.M. The tumor microenvironment in follicular lymphoma. *Clin. Adv. Hematol. Oncol.* **2012**, *10*, 810–818.

6. Verdière, L.; Frédéric Mourcin, K.T. Microenvironment signaling driving lymphomagenesis. *Curr. Opin. Hematol.* **2018**, 335–345. [\[CrossRef\]](#)
7. De Jong, D.; Hemato, S.; Fest, T. The microenvironment in follicular lymphoma. *Best Pract. Res. Clin. Haematol.* **2011**, 24, 135–146. [\[CrossRef\]](#)
8. Dave, S.S.; Wright, G.; Tan, B.; Rosenwald, A.; Gascoyne, R.D.; Chan, W.C.; Fisher, R.I.; Braziel, R.M.; Rimsza, L.M.; Grogan, T.M.; et al. Prediction of Survival in Follicular Lymphoma Based on Molecular Features of Tumor-Infiltrating Immune Cells. *N. Engl. J. Med.* **2004**, 2519–2169. [\[CrossRef\]](#)
9. Chraa, D.; Naim, A.; Olive, D.; Badou, A. T lymphocyte subsets in cancer immunity: Friends or foes. *J. Leukoc. Biol.* **2019**, 243–255. [\[CrossRef\]](#)
10. Amé-Thomas, P.; Tarte, K. The yin and the yang of follicular lymphoma cell niches: Role of microenvironment heterogeneity and plasticity. *Semin. Cancer Biol.* **2014**, 24, 23–32. [\[CrossRef\]](#)
11. Matas-Céspedes, A.; Rodriguez, V.; Kalko, S.G.; Vidal-Crespo, A.; Rosich, L.; Casserras, T.; Balsas, P.; Villamor, N.; Giné, E.; Campo, E.; et al. Disruption of follicular dendritic cells-follicular lymphoma cross-talk by the pan-PI3K inhibitor BKM120 (buparlisib). *Clin. Cancer Res.* **2014**, 20, 3458–3471. [\[CrossRef\]](#)
12. Park, C.-S.; Choi, Y.S. How do follicular dendritic cells interact intimately with B cells in the germinal centre? *Immunology* **2005**, 114, 2–10. [\[CrossRef\]](#)
13. Amé-Thomas, P.; Le Priol, J.; Yssel, H.; Caron, G.; Pangault, C.; Jean, R.; Martin, N.; Marafioti, T.; Gaulard, P.; Lamy, T.; et al. Characterization of intratumoral follicular helper T cells in follicular lymphoma: Role in the survival of malignant B cells. *Leukemia* **2011**, 1053–1063. [\[CrossRef\]](#)
14. Pangault, C.; Amé-Thomas, P.; Ruminy, P.; Rossille, D.; Caron, G.; Baia, M.; De Vos, J.; Roussel, M.; Monvoisin, C.; Lamy, T.; et al. Follicular lymphoma cell niche: Identification of a preeminent IL-4-dependent TFH-B cell axis. *Leukemia* **2010**, 24, 2080–2089. [\[CrossRef\]](#)
15. Yang, Z.-Z.; Novak, A.J.; Stenson, M.J.; Witzig, T.E.; Ansell, S.M. Intratumoral CD4+CD25+ regulatory T-cell-mediated suppression of infiltrating CD4+ T cells in B-cell non-Hodgkin lymphoma. *Blood* **2006**, 107, 3639–3646. [\[CrossRef\]](#) [\[PubMed\]](#)
16. Brown, F.D.; Sen, D.R.; LaFleur, M.W.; Godec, J.; Lukacs-Kornek, V.; Schildberg, F.A.; Kim, H.J.; Yates, K.B.; Ricoult, S.J.H.; Bi, K.; et al. Fibroblastic reticular cells enhance T cell metabolism and survival via epigenetic remodeling. *Nat. Immunol.* **2019**, 20, 1668–1680. [\[CrossRef\]](#)
17. Brown, F.D.; Turley, S.J. Fibroblastic Reticular Cells: Organization and Regulation of the T Lymphocyte Life Cycle. *J. Immunol.* **2015**, 23, 1–7. [\[CrossRef\]](#) [\[PubMed\]](#)
18. Pandey, S.; Mourcin, F.; Marchand, T.; Nayar, S.; Guirric, M.; Pangault, C.; Monvoisin, C.; Amé-Thomas, P.; Guilloton, F.; Dulong, J.; et al. IL-4/CXCL12 loop is a key regulator of lymphoid stroma function in follicular lymphoma. *Blood* **2017**, 129, 2507–2518. [\[CrossRef\]](#) [\[PubMed\]](#)
19. Lamaison, C.; Tarte, K. Impact of B cell/lymphoid stromal cell crosstalk in B-cell physiology and malignancy. *Immunol. Lett.* **2019**, 215, 12–18. [\[CrossRef\]](#)
20. Amé-Thomas, P.; Maby-El Hajjami, H.; Monvoisin, C.; Jean, R.; Monnier, D.; Caulet-Maugendre, S.; Guillaudeux, T.; Lamy, T.; Fest, T.; Tarte, K. Human mesenchymal stem cells isolated from bone marrow and lymphoid organs support tumor B-cell growth: Role of stromal cells in follicular lymphoma pathogenesis. *Blood* **2007**, 109, 693–702. [\[CrossRef\]](#)
21. Guilloton, F.; Caron, G.; Ménard, C.; Pangault, C.; Amé-Thomas, P.; Dulong, J.; De Vos, J.; Rossille, D.; Henry, C.; Lamy, T.; et al. Mesenchymal stromal cells orchestrate follicular lymphoma cell niche through the CCL2-dependent recruitment and polarization of monocytes. *Blood* **2012**, 119, 2556–2567. [\[CrossRef\]](#) [\[PubMed\]](#)
22. Perez Galan, P.; Valero, J.G.; Matas-Céspedes, A.; Rodriguez, V.; Arenas, F.; Carreras, J.; Serrat, N.; Guerrero-Hernandez, M.; Corbera, M.; Yahiaoui, A.; et al. Deciphering the contribution of macrophages to follicular lymphoma pathogenesis: New insights into therapy. *Hematol. Oncol.* **2019**, 37, 151–152. [\[CrossRef\]](#)
23. Amin, R.; Mourcin, F.; Uhel, F.; Pangault, C.; Ruminy, P.; Dupré, L.; Guirric, M.; Marchand, T.; Fest, T.; Lamy, T.; et al. DC-SIGN-expressing macrophages trigger activation of mannoseylated IgM B-cell receptor in follicular lymphoma. *Blood* **2015**, 126, 1911–1920. [\[CrossRef\]](#)
24. Hollander, N.; Haimovich, J. Altered N-linked glycosylation in follicular lymphoma and chronic lymphocytic leukemia: Involvement in pathogenesis and potential therapeutic targeting. *Front. Immunol.* **2017**, 8, 1–6. [\[CrossRef\]](#) [\[PubMed\]](#)
25. Linley, A.; Krysov, S.; Ponzoni, M.; Johnson, P.W.; Packham, G.; Stevenson, F.K. Lectin binding to surface Ig variable regions provides a universal persistent activating signal for follicular lymphoma cells. *Blood* **2015**, 126, 1902–1910. [\[CrossRef\]](#)
26. Epron, G.; Amé-Thomas, P.; Le Priol, J.; Pangault, C.; Dulong, J.; Lamy, T.; Fest, T.; Tarte, K. Monocytes and T cells cooperate to favor normal and follicular lymphoma B-cell growth: Role of IL-15 and CD40L signaling. *Leukemia* **2012**, 26, 139–148. [\[CrossRef\]](#)
27. Shiozawa, E.; Yamochi-Onizuka, T.; Yamochi, T.; Yamamoto, Y.; Naitoh, H.; Kawakami, K.; Nakamaki, T.; Tomoyasu, S.; Kushima, M.; Ota, H. Disappearance of CD21-positive follicular dendritic cells preceding the transformation of follicular lymphoma: Immunohistological study of the transformation using CD21, p53, Ki-67, and P-glycoprotein. *Pathol. Res. Pract.* **2003**, 199, 293–302. [\[CrossRef\]](#)
28. Kiaii, S.; Clear, A.J.; Ramsay, A.G.; Davies, D.; Sangaralingam, A.; Lee, A.; Calaminici, M.; Neuberg, D.S.; Gribben, J.G. Follicular lymphoma cells induce changes in T-cell gene expression and function: Potential impact on survival and risk of transformation. *J. Clin. Oncol.* **2013**, 31, 2654–2661. [\[CrossRef\]](#)

29. Carreras, J.; Lopez-Guillermo, A.; Fox, B.C.; Colomo, L.; Martinez, A.; Roncador, G.; Montserrat, E.; Campo, E.; Banham, A.H. High numbers of tumor-infiltrating FOXP3-positive regulatory T cells are associated with improved overall survival in follicular lymphoma. *Blood* **2006**, *108*, 2957–2964. [\[CrossRef\]](#)
30. Lopez-Guillermo, A.; Carreras, J.; Roncador, G.; Villamor, N.; Colomo, L.; Martinez, A.; Hamoudi, R.; Howat, W.J.; Montserrat, E.; Campo, E. High numbers of tumor-infiltrating programmed cell death 1-positive regulatory lymphocytes are associated with improved overall survival in follicular lymphoma. *J. Clin. Oncol.* **2009**, *27*, 1470–1476. [\[CrossRef\]](#)
31. Tsujimoto, Y.; Cossman, J.; Jaffe, E.; Croce, C.M. Involvement of the bcl-2 gene in human follicular lymphoma. *Science* **1985**, *228*, 1440–1443. [\[CrossRef\]](#) [\[PubMed\]](#)
32. Vaandrager, J.W.; Schuurin, E.; Raap, T.; Philippo, K.; Kleiverda, K.; Kluin, P. Interphase FISH detection of BCL2 rearrangement in follicular lymphoma using breakpoint-flanking probes. *Genes Chromosom. Cancer* **2000**, *27*, 85–94. [\[CrossRef\]](#)
33. Roulland, S.; Kelly, R.S.; Morgado, E.; Sungalee, S.; Solal-Celigny, P.; Colombat, P.; Jouve, N.; Palli, D.; Pala, V.; Tumino, R.; et al. t(14;18) translocation: A predictive blood biomarker for follicular lymphoma. *J. Clin. Oncol.* **2014**, *32*, 1347–1355. [\[CrossRef\]](#) [\[PubMed\]](#)
34. Limpens, J.; Stad, R.; Vos, C.; De Vlaam, C.; De Jong, D.; Van Ommen, G.J.B.; Schuurin, E.; Kluin, P.M. Lymphoma-associated translocation t(14;18) in blood B cells of normal individuals. *Blood* **1995**, *85*, 2528–2536. [\[CrossRef\]](#)
35. Roulland, S.; Leblay, P.; Lecluse, Y.; Heutte, N.; Nadel, B.; Gauduchon, P. Long-term clonal persistence and evolution of t(14;18)-bearing B cells in healthy individuals. *Leukemia* **2006**, *20*, 158–162. [\[CrossRef\]](#) [\[PubMed\]](#)
36. Korfi, K.; Ali, S.; Heward, J.A.; Fitzgibbon, J. Follicular lymphoma, a B cell malignancy addicted to epigenetic mutations. *Epigenetics* **2017**, *12*, 370–377. [\[CrossRef\]](#)
37. Green, M.R.; Gentles, A.J.; Nair, R.V.; Irish, J.M.; Kihira, S.; Liu, C.L.; Kela, I.; Hopmans, E.S.; Myklebust, J.H.; Ji, H.; et al. Hierarchy in somatic mutations arising during genomic evolution and progression of follicular lymphoma. *Blood* **2013**, *121*, 1604–1611. [\[CrossRef\]](#)
38. Okosun, J.; Bödör, C.; Wang, J.; Araf, S.; Yang, C.Y.; Pan, C.; Bolter, S.; Cittaro, D.; Bozek, M.; Iqbal, S.; et al. Integrated genomic analysis identifies recurrent mutations and evolution patterns driving the initiation and progression of follicular lymphoma. *Nat. Genet.* **2014**, *46*, 176–181. [\[CrossRef\]](#) [\[PubMed\]](#)
39. Pastore, A.; Jurinovic, V.; Kridel, R.; Hoster, E.; Staiger, A.M.; Szczepanowski, M.; Pott, C.; Kopp, N.; Murakami, M.; Horn, H.; et al. Integration of gene mutations in risk prognostication for patients receiving first-line immunochemotherapy for follicular lymphoma: A retrospective analysis of a prospective clinical trial and validation in a population-based registry. *Lancet Oncol.* **2015**, *16*, 1111–1122. [\[CrossRef\]](#)
40. Morin, R.D.; Mendez-Lago, M.; Mungall, A.J.; Goya, R.; Mungall, K.L.; Corbett, R.D.; Johnson, N.A.; Severson, T.M.; Chiu, R.; Field, M.; et al. Frequent mutation of histone-modifying genes in non-Hodgkin lymphoma. *Nature* **2011**, *476*, 298–303. [\[CrossRef\]](#)
41. Ortega-Molina, A.; Boss, I.W.; Canela, A.; Pan, H.; Jiang, Y.; Zhao, C.; Jiang, M.; Hu, D.; Agirre, X.; Niesvizky, I.; et al. The histone lysine methyltransferase KMT2D sustains a gene expression program that represses B cell lymphoma development. *Nat. Med.* **2015**, *21*, 1199–1208. [\[CrossRef\]](#) [\[PubMed\]](#)
42. Zhang, J.; Vlasevska, S.; Wells, V.A.; Nataraj, S.; Holmes, A.B.; Duval, R.; Meyer, S.N.; Mo, T.; Basso, K.; Brindle, P.K.; et al. The CREBBP acetyltransferase is a haploinsufficient tumor suppressor in B-cell lymphoma. *Cancer Discov.* **2017**, *7*, 323–337. [\[CrossRef\]](#) [\[PubMed\]](#)
43. Zhang, J.; Dominguez-Sola, D.; Hussein, S.; Lee, J.E.; Holmes, A.B.; Bansal, M.; Vlasevska, S.; Mo, T.; Tang, H.; Basso, K.; et al. Disruption of KMT2D perturbs germinal center B cell development and promotes lymphomagenesis. *Nat. Med.* **2015**, *21*, 1190–1198. [\[CrossRef\]](#) [\[PubMed\]](#)
44. Pasqualucci, L.; Dominguez-Sola, D.; Chiarenza, A.; Fabbri, G.; Grunn, A.; Trifonov, V.; Kasper, L.H.; Lerach, S.; Tang, H.; Ma, J.; et al. Inactivating mutations of acetyltransferase genes in B-cell lymphoma. *Nature* **2011**, *471*, 189–196. [\[CrossRef\]](#)
45. Horton, S.J.; Giotopoulos, G.; Yun, H.; Vohra, S.; Sheppard, O.; Bashford-Rogers, R.; Rashid, M.; Clipson, A.; Chan, W.I.; Sasca, D.; et al. Early loss of Crebbp confers malignant stem cell properties on lymphoid progenitors. *Nat. Cell Biol.* **2017**, *19*, 1093–1104. [\[CrossRef\]](#)
46. Green, M.R.; Kihira, S.; Liu, C.L.; Nair, R.V.; Salari, R.; Gentles, A.J.; Irish, J.; Stehr, H.; Vicente-Dueñas, C.; Romero-Camarero, I.; et al. Mutations in early follicular lymphoma progenitors are associated with suppressed antigen presentation. *Proc. Natl. Acad. Sci. USA* **2015**, *112*, E1116–E1125. [\[CrossRef\]](#)
47. Andor, N.; Simonds, E.F.; Czerwinski, D.K.; Chen, J.; Grimes, S.M.; Wood-Bouwens, C.; Zheng, G.X.Y.; Kubit, M.A.; Greer, S.; Weiss, W.A.; et al. Single-cell RNA-Seq of follicular lymphoma reveals malignant B-cell types and coexpression of T-cell immune checkpoints. *Blood* **2019**, *133*, 1119–1129. [\[CrossRef\]](#)
48. Jiang, Y.; Ortega-Molina, A.; Geng, H.; Ying, H.-Y.; Hatzi, K.; Parsa, S.; McNally, D.; Wang, L.; Doane, A.S.; Agirre, X.; et al. CREBBP Inactivation Promotes the Development of HDAC3-Dependent Lymphomas. *Cancer Discov.* **2017**, *7*, 38–53. [\[CrossRef\]](#)
49. Mondello, P.; Tadros, S.; Teater, M.; Fontan, L.; Chang, A.Y.; Jain, N.; Yang, H.; Singh, S.; Ying, H.-Y.; Chu, C.-S.; et al. Selective Inhibition of HDAC3 Targets Synthetic Vulnerabilities and Activates Immune Surveillance in Lymphoma. *Cancer Discov.* **2020**, *10*, 440–459. [\[CrossRef\]](#)
50. Wang, X.; Waschke, B.C.; Woolaver, R.A.; Chen, S.M.Y.; Chen, Z.; Wang, J.H. HDAC inhibitors overcome immunotherapy resistance in B-cell lymphoma. *Protein Cell* **2020**, *11*, 472–482. [\[CrossRef\]](#) [\[PubMed\]](#)

51. Kirschbaum, M.; Frankel, P.; Popplewell, L.; Zain, J.; Delioukina, M.; Pullarkat, V.; Matsuoka, D.; Pulone, B.; Rotter, A.J.; Espinoza-Delgado, I.; et al. Phase II study of vorinostat for treatment of relapsed or refractory indolent non-hodgkin's lymphoma and mantle cell lymphoma. *J. Clin. Oncol.* **2011**, *29*, 1198–1203. [\[CrossRef\]](#)
52. Ogura, M.; Ando, K.; Suzuki, T.; Ishizawa, K.; Oh, S.Y.; Itoh, K.; Yamamoto, K.; Au, W.Y.; Tien, H.F.; Matsuno, Y.; et al. A multicentre phase II study of vorinostat in patients with relapsed or refractory indolent B-cell non-Hodgkin lymphoma and mantle cell lymphoma. *Br. J. Haematol.* **2014**, *165*, 768–776. [\[CrossRef\]](#)
53. Evens, A.M.; Balasubramanian, S.; Vose, J.M.; Harb, W.; Gordon, L.L.; Langdon, R.; Sprague, J.; Sirisawad, M.; Mani, C.; Yue, J.; et al. A phase I/II multicenter, open-label study of the oral histone deacetylase inhibitor abexinostat in relapsed/refractory lymphoma. *Clin. Cancer Res.* **2016**, *22*, 1059–1066. [\[CrossRef\]](#) [\[PubMed\]](#)
54. Kroesen, M.; Gielen, P.R.; Brok, L.C.; Armandari, I.; Hoogerbrugge, P.M.; Adema, G.J. HDAC inhibitors and immunotherapy: A double edged sword? *Oncotarget* **2014**, *5*, 6558–6572. [\[CrossRef\]](#)
55. Morschhauser, F.; Tilly, H.; Chaidos, A.; McKay, P.; Phillips, T.; Assouline, S.; Batlevi, C.L.; Campbell, P.; Ribrag, V.; Damaj, G.L.; et al. Tazemetostat for patients with relapsed or refractory follicular lymphoma: An open-label, single-arm, multicentre, phase 2 trial. *Lancet Oncol.* **2020**. [\[CrossRef\]](#)
56. Smith, S.M.; van Besien, K.; Karrison, T.; Dancy, J.; McLaughlin, P.; Younes, A.; Smith, S.; Stiff, P.; Lester, E.; Modi, S.; et al. Temsirolimus has activity in non-mantle cell non-Hodgkin's lymphoma subtypes: The University of Chicago phase II consortium. *J. Clin. Oncol.* **2010**, *28*, 4740–4746. [\[CrossRef\]](#) [\[PubMed\]](#)
57. Hess, G.; Wagner, K.; Keller, U.; La Rosee, P.; Atta, J.; Hübel, K.; Lerchenmueller, C.; Schoendube, D.; Witzens-Harig, M.; Ruckes, C.; et al. Final Results of a Phase I/II Trial of the Combination Bendamustine and Rituximab With Temsirolimus (BeRT) in Relapsed Mantle Cell Lymphoma and Follicular Lymphoma. *HemaSphere* **2020**, *4*, e398. [\[CrossRef\]](#)
58. Fenske, T.S.; Shah, N.M.; Kim, K.M.; Saha, S.; Zhang, C.; Baim, A.E.; Farnen, J.P.; Onitilo, A.A.; Blank, J.H.; Ahuja, H.; et al. A phase 2 study of weekly temsirolimus and bortezomib for relapsed or refractory B-cell non-Hodgkin lymphoma: A Wisconsin Oncology Network study. *Cancer* **2015**, *121*, 3465–3471. [\[CrossRef\]](#)
59. Gopal, A.K.; Kahl, B.S.; Flowers, C.R.; Martin, P.; Ansell, S.M.; Abella-Dominicis, E.; Koh, B.; Ye, W.; Barr, P.M.; Salles, G.A.; et al. Idelalisib is effective in patients with high-risk follicular lymphoma and early relapse after initial chemoimmunotherapy. *Blood* **2017**, *129*, 3037–3039. [\[CrossRef\]](#) [\[PubMed\]](#)
60. Serrat, N.; Guerrero-Hernández, M.; Hernández, H.; Matas-Céspedes, A.; Yahiaoui, A.; Valero, J.G.; Nadeu, F.; Clot, G.; Di Re, M.; Corbera-Bellalta, M.; et al. PI3Kd inhibition reshapes follicular lymphoma-immune microenvironment cross talk and unleashes the activity of venetoclax. *Blood Adv.* **2020**, *4*, 4217–4231. [\[CrossRef\]](#)
61. Dreyling, M.; Morschhauser, F.; Bouabdallah, K.; Bron, D.; Cunningham, D.; Assouline, S.E.; Verhoef, G.; Linton, K.; Thieblemont, C.; Vitolo, U.; et al. Phase II study of copanlisib, a PI3K inhibitor, in relapsed or refractory, indolent or aggressive lymphoma. *Ann. Oncol.* **2017**, *28*, 2169–2178. [\[CrossRef\]](#)
62. Flinn, I.W.; Miller, C.B.; Ardeshta, K.M.; Tetreault, S.; Assouline, S.E.; Mayer, J.; Merli, M.; Lunin, S.D.; Pettitt, A.R.; Nagy, Z.; et al. DYNAMO: A Phase II study of duvelisib (IPI-145) in patients with refractory indolent non-hodgkin lymphoma. *J. Clin. Oncol.* **2019**, *37*, 912–922. [\[CrossRef\]](#)
63. Bartlett, N.L.; Costello, B.A.; LaPlant, B.R.; Ansell, S.M.; Kuruvilla, J.G.; Reeder, C.B.; Thye, L.S.; Anderson, D.M.; Krysiak, K.; Ramirez, C.; et al. Single-agent ibrutinib in relapsed or refractory follicular lymphoma: A phase 2 consortium trial. *Blood* **2018**, *131*, 182–190. [\[CrossRef\]](#)
64. Fowler, N.H.; Nastoupil, L.; De Vos, S.; Knapp, M.; Flinn, I.W.; Chen, R.; Advani, R.H.; Bhatia, S.; Martin, P.; Mena, R.; et al. The combination of ibrutinib and rituximab demonstrates activity in first-line follicular lymphoma. *Br. J. Haematol.* **2020**, *189*, 650–660. [\[CrossRef\]](#)
65. Friedberg, J.W.; Sharman, J.; Sweetenham, J.; Johnston, P.B.; Vose, J.M.; Lacasce, A.; Schaefer-Cuttillo, J.; De Vos, S.; Sinha, R.; Leonard, J.P.; et al. Inhibition of Syk with fostamatinib disodium has significant clinical activity in non-Hodgkin lymphoma and chronic lymphocytic leukemia. *Blood* **2010**, *115*, 2578–2585. [\[CrossRef\]](#)
66. Hamlin, P.A.; Flinn, I.W.; Wagner-Johnston, N.; Burger, J.A.; Coffey, G.P.; Conley, P.B.; Michelson, G.; Leeds, J.M.; Der, K.; Kim, Y.; et al. Efficacy and safety of the dual SYK/JAK inhibitor cerdulatinib in patients with relapsed or refractory B-cell malignancies: Results of a phase I study. *Am. J. Hematol.* **2019**, *94*, E90–E93. [\[CrossRef\]](#) [\[PubMed\]](#)
67. Boice, M.; Salloum, D.; Mourcin, F.; Sanghvi, V.; Amin, R.; Oricchio, E.; Jiang, M.; Mottok, A.; Denis-Lagache, N.; Ciriello, G.; et al. Loss of the HVEM Tumor Suppressor in Lymphoma and Restoration by Modified CAR-T Cells. *Cell* **2016**, *167*, 405–418.e13. [\[CrossRef\]](#) [\[PubMed\]](#)
68. Armand, P.; Janssens, A.M.; Gritti, G.; Radford, J.; Timmerman, J.M.; Pinto, A.; Mercadal Vilchez, S.; Johnson, P.W.M.; Cunningham, D.; Leonard, J.P.; et al. Efficacy and safety results from CheckMate 140, a phase 2 study of nivolumab for relapsed/refractory follicular lymphoma. *Blood* **2020**. [\[CrossRef\]](#) [\[PubMed\]](#)
69. Westin, J.R.; Chu, F.; Zhang, M.; Fayad, L.E.; Kwak, L.W.; Fowler, N.; Romaguera, J.; Hagemeister, F.; Fanale, M.; Samaniego, F.; et al. Safety and activity of PD1 blockade by pidilizumab in combination with rituximab in patients with relapsed follicular lymphoma: A single group, open-label, phase 2 trial. *Lancet Oncol.* **2014**, *15*, 69–77. [\[CrossRef\]](#)
70. Timmerman, J.; Herbaux, C.; Ribrag, V.; Zelenetz, A.D.; Houot, R.; Neelapu, S.S.; Logan, T.; Lossos, I.S.; Urba, W.; Salles, G.; et al. Urelumab alone or in combination with rituximab in patients with relapsed or refractory B-cell lymphoma. *Am. J. Hematol.* **2020**, *95*, 510–520. [\[CrossRef\]](#) [\[PubMed\]](#)

71. Chen, Y.P.; Kim, H.J.; Wu, H.; Price-Troska, T.; Villasboas, J.C.; Jalali, S.; Feldman, A.L.; Novak, A.J.; Yang, Z.Z.; Ansell, S.M. SIRP α expression delineates subsets of intratumoral monocyte/macrophages with different functional and prognostic impact in follicular lymphoma. *Blood Cancer J.* **2019**, *9*. [\[CrossRef\]](#)
72. Advani, R.; Flinn, I.; Popplewell, L.; Forero, A.; Bartlett, N.L.; Ghosh, N.; Kline, J.; Roschewski, M.; LaCasce, A.; Collins, G.P.; et al. CD47 Blockade by Hu5F9-G4 and Rituximab in Non-Hodgkin's Lymphoma. *N. Engl. J. Med.* **2018**, *379*, 1711–1721. [\[CrossRef\]](#)
73. Bódor, C.; Grossmann, V.; Popov, N.; Okosun, J.; O'Riain, C.; Tan, K.; Marzec, J.; Araf, S.; Wang, J.; Lee, A.M.; et al. EZH2 mutations are frequent and represent an early event in follicular lymphoma. *Blood* **2013**, *122*, 3165–3168. [\[CrossRef\]](#)
74. Sneeringer, C.J.; Scott, M.P.; Kuntz, K.W.; Knutson, S.K.; Pollock, R.M.; Richon, V.M.; Copeland, R.A. Coordinated activities of wild-type plus mutant EZH2 drive tumor-associated hypertrimethylation of lysine 27 on histone H3 (H3K27) in human B-cell lymphomas. *Proc. Natl. Acad. Sci. USA* **2010**, *107*, 20980–20985. [\[CrossRef\]](#) [\[PubMed\]](#)
75. Béguelin, W.; Popovic, R.; Teater, M.; Jiang, Y.; Bunting, K.L.; Rosen, M.; Shen, H.; Yang, S.N.; Wang, L.; Ezponda, T.; et al. EZH2 Is Required for Germinal Center Formation and Somatic EZH2 Mutations Promote Lymphoid Transformation. *Cancer Cell* **2013**, *23*, 677–692. [\[CrossRef\]](#) [\[PubMed\]](#)
76. Béguelin, W.; Teater, M.; Gearhart, M.D.; Calvo Fernández, M.T.; Goldstein, R.L.; Cárdenas, M.G.; Hatzl, K.; Rosen, M.; Shen, H.; Corcoran, C.M.; et al. EZH2 and BCL6 Cooperate to Assemble CBX8-BCOR Complex to Repress Bivalent Promoters, Mediate Germinal Center Formation and Lymphomagenesis. *Cancer Cell* **2016**, *30*, 197–213. [\[CrossRef\]](#) [\[PubMed\]](#)
77. Béguelin, W.; Teater, M.; Meydan, C.; Hoehn, K.B.; Phillip, J.M.; Soshnev, A.A.; Venturutti, L.; Rivas, M.A.; Calvo-Fernández, M.T.; Gutierrez, J.; et al. Mutant EZH2 Induces a Pre-malignant Lymphoma Niche by Reprogramming the Immune Response. *Cancer Cell* **2020**, *37*, 655–673.e11. [\[CrossRef\]](#) [\[PubMed\]](#)
78. Knutson, S.K.; Wigle, T.J.; Warholic, N.M.; Sneeringer, C.J.; Allain, C.J.; Klaus, C.R.; Sacks, J.D.; Raimondi, A.; Majer, C.R.; Song, J.; et al. A selective inhibitor of EZH2 blocks H3K27 methylation and kills mutant lymphoma cells. *Nat. Chem. Biol.* **2012**, *8*, 890–896. [\[CrossRef\]](#) [\[PubMed\]](#)
79. McCabe, M.T.; Ott, H.M.; Ganji, G.; Korenchuk, S.; Thompson, C.; Van Aller, G.S.; Liu, Y.; Della Pietra, A.; LaFrance, L.V.; Mellinger, M.; et al. EZH2 inhibition as a therapeutic strategy for lymphoma with EZH2-activating mutations. *Nature* **2012**, *492*, 108–112. [\[CrossRef\]](#)
80. Italiano, A.; Soria, J.-C.; Toulmonde, M.; Michot, J.-M.; Lucchesi, C.; Varga, A.; Coindre, J.-M.; Blakemore, S.J.; Clawson, A.; Suttle, B.; et al. Tazemetostat, an EZH2 inhibitor, in relapsed or refractory B-cell non-Hodgkin lymphoma and advanced solid tumours: A first-in-human, open-label, phase 1 study. *Lancet Oncol.* **2018**, *19*, 649–659. [\[CrossRef\]](#)
81. Challa-Malladi, M.; Lieu, Y.K.; Califano, O.; Holmes, A.B.; Bhagat, G.; Murty, V.V.; Dominguez-Sola, D.; Pasqualucci, L.; Dalla-Favera, R. Combined Genetic Inactivation of β 2-Microglobulin and CD58 Reveals Frequent Escape from Immune Recognition in Diffuse Large B Cell Lymphoma. *Cancer Cell* **2011**, *20*, 728–740. [\[CrossRef\]](#) [\[PubMed\]](#)
82. Pasqualucci, L.; Khiabani, H.; Fangazio, M.; Vasishtha, M.; Messina, M.; Holmes, A.B.; Ouillette, P.; Trifonov, V.; Rossi, D.; Tabbò, F.; et al. Genetics of Follicular Lymphoma Transformation. *Cell Rep.* **2014**, *6*, 130–140. [\[CrossRef\]](#) [\[PubMed\]](#)
83. Kridel, R.; Chan, F.C.; Mottok, A.; Boyle, M.; Farinha, P.; Tan, K.; Meissner, B.; Bashashati, A.; McPherson, A.; Roth, A.; et al. Histological Transformation and Progression in Follicular Lymphoma: A Clonal Evolution Study. *PLoS Med.* **2016**, *13*, 1–25. [\[CrossRef\]](#)
84. Bararia, D.; Hildebrand, J.A.; Stolz, S.; Haebe, S.; Alig, S.; Trevisani, C.P.; Osorio-Barrios, F.; Bartoschek, M.D.; Mentz, M.; Pastore, A.; et al. Cathepsin S Alterations Induce a Tumor-Promoting Immune Microenvironment in Follicular Lymphoma. *Cell Rep.* **2020**, *31*. [\[CrossRef\]](#)
85. Riese, R.J.; Wolf, P.R.; Brömme, D.; Natkin, L.R.; Villadangos, J.A.; Ploegh, H.L.; Chapman, H.A. Essential role for cathepsin S in MHC class II-associated invariant chain processing and peptide loading. *Immunity* **1996**, *4*, 357–366. [\[CrossRef\]](#)
86. Dheilley, E.; Battistello, E.; Katanayeva, N.; Sungalee, S.; Michaux, J.; Duns, G.; Wehrle, S.; Sordet-Dessimoz, J.; Mina, M.; Racle, J.; et al. Cathepsin S Regulates Antigen Processing and T Cell Activity in Non-Hodgkin Lymphoma. *Cancer Cell* **2020**, *37*, 674–689. [\[CrossRef\]](#) [\[PubMed\]](#)
87. Cheung, K.J.J.; Johnson, N.A.; Affleck, J.G.; Severson, T.; Steidl, C.; Ben-Neriah, S.; Schein, J.; Morin, R.D.; Moore, R.; Shah, S.P.; et al. Acquired TNFRSF14 mutations in follicular lymphoma are associated with worse prognosis. *Cancer Res.* **2010**, *70*, 9166–9174. [\[CrossRef\]](#) [\[PubMed\]](#)
88. Launay, E.; Pangault, C.; Bertrand, P.; Jardin, F.; Lamy, T.; Tilly, H.; Tarte, K.; Bastard, C.; Fest, T. High rate of TNFRSF14 gene alterations related to 1p36 region in de novo follicular lymphoma and impact on prognosis. *Leukemia* **2012**, *26*, 559–562. [\[CrossRef\]](#) [\[PubMed\]](#)
89. Okosun, J.; Wolfson, R.L.; Wang, J.; Araf, S.; Wilkins, L.; Castellano, B.M.; Escudero-Ibarz, L.; Al Seraihi, A.F.; Richter, J.; Bernhart, S.H.; et al. Recurrent mTORC1-activating RRAGC mutations in follicular lymphoma. *Nat. Genet.* **2016**, *48*, 183–188. [\[CrossRef\]](#)
90. Ying, Z.X.; Jin, M.; Peterson, L.F.; Bernard, D.; Saiya-Cork, K.; Yildiz, M.; Wang, S.; Kaminski, M.S.; Chang, A.E.; Klionsky, D.J.; et al. Recurrent mutations in the MTOR regulator RRAGC in follicular lymphoma. *Clin. Cancer Res.* **2016**, *22*, 5383–5393. [\[CrossRef\]](#)
91. Ortega-Molina, A.; Deleyto-Seldas, N.; Carreras, J.; Sanz, A.; Lebrero-Fernández, C.; Menéndez, C.; Vandenberg, A.; Fernández-Ruiz, B.; Marín-Arriaza, L.; de la Calle Arregui, C.; et al. Oncogenic Rag GTPase signalling enhances B cell activation and drives follicular lymphoma sensitive to pharmacological inhibition of mTOR. *Nat. Metab.* **2019**, *1*, 775–789. [\[CrossRef\]](#) [\[PubMed\]](#)
92. Umetsu, D.T.; Esserman, L.; Donlon, T.A.; Dekruyff, R.H.; Levy, R.; Umetsu, D.T. Induction of proliferation of human follicular (b type) lymphoma cells by cognate interaction with cd4+ t cell clones. *J. Immunol.* **1990**, *144*, 2550–2557.

93. Jerkeman, M.; Hallek, M.; Dreyling, M.; Thieblemont, C.; Kimby, E.; Staudt, L. Targeting of B-cell receptor signalling in B-cell malignancies. *J. Int. Med.* **2017**, *282*, 415–428. [\[CrossRef\]](#) [\[PubMed\]](#)
94. Rawal, S.; Chu, F.; Zhang, M.; Park, H.J.; Nattamai, D.; Kannan, S.; Sharma, R.; Delgado, D.; Chou, T.; Lin, H.Y.; et al. Cross Talk between Follicular Th Cells and Tumor Cells in Human Follicular Lymphoma Promotes Immune Evasion in the Tumor Microenvironment. *J. Immunol.* **2013**, *190*, 6681–6693. [\[CrossRef\]](#)
95. Farinha, P.; Al-Tourah, A.; Gill, K.; Klasa, R.; Connors, J.M.; Gascoyne, R.D. The architectural pattern of FOXP3-positive T cells in follicular lymphoma is an independent predictor of survival and histologic transformation. *Blood* **2010**, *115*, 289–295. [\[CrossRef\]](#)
96. Wing, J.B.; Kitagawa, Y.; Locci, M.; Hume, H.; Tay, C.; Morita, T.; Kidani, Y.; Matsuda, K.; Inoue, T.; Kurosaki, T.; et al. A distinct subpopulation of CD25⁺ T-follicular regulatory cells localizes in the germinal centers. *Proc. Natl. Acad. Sci. USA* **2017**, *114*, E6400–E6409. [\[CrossRef\]](#)
97. Flinn, I.W.; Kahl, B.S.; Leonard, J.P.; Furman, R.R.; Brown, J.R.; Byrd, J.C.; Wagner-Johnston, N.D.; Coutre, S.E.; Benson, D.M.; Peterman, S.; et al. Idelalisib, a selective inhibitor of phosphatidylinositol 3-kinase- δ , as therapy for previously treated indolent non-Hodgkin lymphoma. *Blood* **2014**, *123*, 3406–3413. [\[CrossRef\]](#)
98. Gopal, A.K.; Kahl, B.S.; de Vos, S.; Wagner-Johnston, N.D.; Schuster, S.J.; Jurczak, W.J.; Flinn, I.W.; Flowers, C.R.; Martin, P.; Viardot, A.; et al. PI3K δ inhibition by idelalisib in patients with relapsed indolent lymphoma. *N. Engl. J. Med.* **2014**, *370*, 1008–1018. [\[CrossRef\]](#)
99. Smolewski, P.; Rydygier, D. Efficacy and safety of idelalisib for the treatment of indolent B-cell malignancies. *Expert Opin. Pharmacother.* **2020**, *1*–12. [\[CrossRef\]](#) [\[PubMed\]](#)
100. Abboud, G.; Fruman, D.A.; Morel, L.; Schwartzberg, P.L.; Preite, S.; Huang, B.; Cannons, J.L.; McGavern, D.B. PI3K Orchestrates T Follicular Helper Cell Differentiation in a Context Dependent Manner: Implications for Autoimmunity. *Front. Immunol.* **2019**, *1*, 3079. [\[CrossRef\]](#)
101. Chellappa, S.; Kusekhar, K.; Munthe, L.A.; Tjønnfjord, G.E.; Aandahl, E.M.; Okkenhaug, K.; Taskén, K. The PI3K p110 δ Isoform Inhibitor Idelalisib Preferentially Inhibits Human Regulatory T Cell Function. *J. Immunol.* **2019**, *202*, 1397–1405. [\[CrossRef\]](#)
102. Frustaci, A.M.; Tedeschi, A.; Deodato, M.; Zampogna, G.; Cairoli, R.; Montillo, M. Duvelisib: A new phosphoinositide-3-kinase inhibitor in chronic lymphocytic leukemia. *Futur. Oncol.* **2019**, *15*, 2227–2239. [\[CrossRef\]](#)
103. Mhibik, M.; Wiestner, A.; Sun, C. Harnessing the Effects of BTKi on T Cells for Effective Immunotherapy against CLL. *Int. J. Mol. Sci.* **2020**, *21*, 68. [\[CrossRef\]](#)
104. Long, M.; Beckwith, K.; Do, P.; Mundy, B.L.; Gordon, A.; Lehman, A.M.; Maddocks, K.J.; Cheney, C.; Jones, J.A.; Flynn, J.M.; et al. Ibrutinib treatment improves T cell number and function in CLL patients. *J. Clin. Invest.* **2017**, *127*, 3052–3064. [\[CrossRef\]](#)
105. Coffey, G.P.; Feng, J.; Betz, A.; Pandey, A.; Birrell, M.; Leeds, J.M.; Der, K.; Kadri, S.; Segal, J.; Wang, Y.L.; et al. Cerdulatinib Pharmacodynamics and Relationships to Tumor Response Following Oral Dosing in Patients with Relapsed/Refractory B-cell Malignancies. *Clin. Cancer Res.* **2019**, *15*, 1174–1184. [\[CrossRef\]](#)
106. Myklebust, J.H.; Irish, J.M.; Brody, J.; Czerwinski, D.K.; Houot, R.; Kohrt, H.E.; Timmerman, J.; Said, J.; Green, M.R.; Delabie, J.; et al. High PD-1 expression and suppressed cytokine signaling distinguish T cells infiltrating follicular lymphoma tumors from peripheral T cells. *Blood* **2013**, *121*, 1367–1376. [\[CrossRef\]](#)
107. Batlevi, C.L.; Matsuki, E.; Brentjens, R.J.; Younes, A. Novel immunotherapies in lymphoid malignancies. *Nat. Rev. Clin. Oncol.* **2016**, *13*, 25–40. [\[CrossRef\]](#) [\[PubMed\]](#)
108. Anderson, A.C.; Joller, N.; Kuchroo, V.K. Lag-3, Tim-3, and TIGIT: Co-inhibitory Receptors with Specialized Functions in Immune Regulation. *Immunity* **2016**, *44*, 989–1004. [\[CrossRef\]](#) [\[PubMed\]](#)
109. Acharya, N.; Sabatos-Peyton, C.; Anderson, A.C. Tim-3 finds its place in the cancer immunotherapy landscape. *J. Immunother. Cancer* **2020**, *8*, e000911. [\[CrossRef\]](#) [\[PubMed\]](#)
110. Yang, Z.Z.; Grote, D.M.; Ziesmer, S.C.; Xiu, B.; Novak, A.J.; Ansell, S.M. PD-1 expression defines two distinct T-cell sub-populations in follicular lymphoma that differentially impact patient survival. *Blood Cancer J.* **2015**, *5*, e281–10. [\[CrossRef\]](#)
111. Gravelle, P.; Do, C.; Franchet, C.; Mueller, S.; Oberic, L.; Ysebaert, L.; Larocca, L.M.; Hohaus, S.; Calmels, M.N.; Frenois, F.X.; et al. Impaired functional responses in follicular lymphoma CD8⁺TIM-3⁺ T lymphocytes following TCR engagement. *Oncotarget* **2016**, *5*, e1224044. [\[CrossRef\]](#)
112. Laurent, C.; Charmpi, K.; Gravelle, P.; Tosolini, M.; Franchet, C.; Ysebaert, L.; Brousset, P.; Bidaut, A.; Ycart, B.; Fourmié, J.-J. Several immune escape patterns in non-Hodgkin's lymphomas. *Oncotarget* **2015**, *4*, e1026530. [\[CrossRef\]](#)
113. Yang, Z.; Kim, H.; Villasboas, J.C.; Price-Troska, T.; Jalali, S.; Novak, A.J.; Ansell, S.M. Expression of Lag-3 Defines Exhaustion of Intratumoral Pd-1⁺ T Cells and Correlates With Poor Outcome in Follicular Lymphoma. *Hematol. Oncol.* **2017**, *35*, 260–261. [\[CrossRef\]](#)
114. Laurent, C.; Müller, S.; Do, C.; Al-Saati, T.; Allart, S.; Larocca, L.M.; Hohaus, S.; Duchez, S.; Quillet-Mary, A.; Laurent, G.; et al. Distribution, function, and prognostic value of cytotoxic T lymphocytes in follicular lymphoma: A 3-D tissue-imaging study. *Blood* **2011**, *118*, 5371–5379. [\[CrossRef\]](#) [\[PubMed\]](#)
115. Josefsson, S.E.; Beiske, K.; Blaker, Y.N.; Førsund, M.S.; Holte, H.; Østenstad, B.; Kimby, E.; Köksal, H.; Wälchli, S.; Bai, B.; et al. TIGIT and PD-1 Mark Intratumoral T Cells with Reduced Effector Function in B-cell Non-Hodgkin Lymphoma. *Cancer Immunol. Res.* **2019**, *7*, 355–362. [\[CrossRef\]](#) [\[PubMed\]](#)

116. Josefsson, S.E.; Huse, K.; Kolstad, A.; Beiske, K.; Pende, D.; Steen, C.B.; Inderberg, E.M.; Lingjærde, O.C.; Østenstad, B.; Smeland, E.B.; et al. T Cells Expressing Checkpoint Receptor TIGIT Are Enriched in Follicular Lymphoma Tumors and Characterized by Reversible Suppression of T-cell Receptor Signaling. *Clin. Cancer Res.* **2018**, *24*, 870–881. [\[CrossRef\]](#)
117. Lesokhin, A.M.; Ansell, S.M.; Armand, P.; Scott, E.C.; Halwani, A.; Gutierrez, M.; Millenson, M.M.; Cohen, A.D.; Schuster, S.J.; Lebovic, D.; et al. Nivolumab in Patients With Relapsed or Refractory Hematologic Malignancy: Preliminary Results of a Phase Ib Study. *J. Clin. Oncol.* **2016**, *34*, 2698–2704. [\[CrossRef\]](#)
118. Armand, P.; Lesokhin, A.; Borrello, I.; Timmerman, J.; Gutierrez, M.; Zhu, L.; Poppa McKiver, M.; Ansell, S.M. A phase 1b study of dual PD-1 and CTLA-4 or KIR blockade in patients with relapsed/refractory lymphoid malignancies. *Leukemia* **2020**. [\[CrossRef\]](#)
119. Yang, Z.-Z.; Kim, H.J.; Wu, H.; Jalali, S.; Tang, X.; Krull, J.E.; Ding, W.; Novak, A.J.; Ansell, S.M. TIGIT Expression Is Associated with T-cell Suppression and Exhaustion and Predicts Clinical Outcome and Anti-PD-1 Response in Follicular Lymphoma. *Clin. Cancer Res.* **2020**, *26*, 5217–5231. [\[CrossRef\]](#)
120. Fanale, M.; Assouline, S.; Kuruvilla, J.; Solal-Célgny, P.; Heo, D.S.; Verhoef, G.; Corradini, P.; Abramson, J.S.; Offner, F.; Engert, A.; et al. Phase IA/II, multicentre, open-label study of the CD40 antagonistic monoclonal antibody lcatumumab in adult patients with advanced non-Hodgkin or Hodgkin lymphoma. *Br. J. Haematol.* **2014**, *164*, 258–265. [\[CrossRef\]](#)
121. Toh, B.; Abastado, J.P. Myeloid cells prime drivers of tumor progression. *Oncotarget* **2012**, *1*, 1360–1367. [\[CrossRef\]](#)
122. Bolen, C.R.; McCord, R.; Huet, S.; Frampton, G.M.; Bourgon, R.; Jardin, F.; Dartigues, P.; Punnoose, E.A.; Szafer-Glusman, E.; Xerri, L.; et al. Mutation load and an effector T-cell gene signature may distinguish immunologically distinct and clinically relevant lymphoma subsets. *Blood Adv.* **2017**, *1*, 1884–1890. [\[CrossRef\]](#)
123. Wilcox, R.A.; Ristow, K.; Habermann, T.M.; Inwards, D.J.; Micallef, I.N.M.; Johnston, P.B.; Colgan, J.P.; Nowakowski, G.S.; Ansell, S.M.; Witzig, T.E.; et al. The absolute monocyte count is associated with overall survival in patients newly diagnosed with follicular lymphoma. *Leuk. Lymphoma* **2012**, *53*, 575–580. [\[CrossRef\]](#)
124. Watanabe, R.; Tomita, N.; Kishimoto, K.; Koyama, S.; Ogusa, E.; Ishii, Y.; Miyashita, K.; Matsuura, S.; Fujisawa, S.; Hattori, Y.; et al. Absolute monocyte count in follicular lymphoma patients treated with rituximab plus cyclophosphamide, doxorubicin, vincristine, and prednisone. *Leuk. Res.* **2013**, *37*, 1208–1212. [\[CrossRef\]](#) [\[PubMed\]](#)
125. Lee, S.F.; Luque-Fernandez, M.A. Prognostic value of lymphocyte-to-monocyte ratio and neutrophil-to-lymphocyte ratio in follicular lymphoma: A retrospective cohort study. *BMJ Open* **2017**, *7*, 1–8. [\[CrossRef\]](#)
126. Mozas, P.; Rivero, A.; Rivas-Delgado, A.; Nadeu, F.; Clot, G.; Correa, J.G.; Castillo, C.; Bataller, A.; Baumann, T.; Giné, E.; et al. A low lymphocyte-to-monocyte ratio is an independent predictor of poorer survival and higher risk of histological transformation in follicular lymphoma. *Leuk. Lymphoma* **2021**, *62*, 104–111. [\[CrossRef\]](#) [\[PubMed\]](#)
127. Mantovani, A.; Sica, A. Macrophages, innate immunity and cancer: Balance, tolerance, and diversity. *Curr. Opin. Immunol.* **2010**, *22*, 231–237. [\[CrossRef\]](#) [\[PubMed\]](#)
128. Jayasingam, S.D.; Citartan, M.; Thang, T.H.; Mat Zin, A.A.; Ang, K.C.; Ch'ng, E.S. Evaluating the Polarization of Tumor-Associated Macrophages Into M1 and M2 Phenotypes in Human Cancer Tissue: Technicalities and Challenges in Routine Clinical Practice. *Front. Oncol.* **2020**, *9*, 1–9. [\[CrossRef\]](#) [\[PubMed\]](#)
129. Farinha, P.; Masoudi, H.; Skinnider, B.F.; Shumansky, K.; Spinelli, J.J.; Gill, K.; Klasa, R.; Voss, N.; Connors, J.M.; Gascoyne, R.D. Analysis of multiple biomarkers shows that lymphoma-associated macrophage (LAM) content is an independent predictor of survival in follicular lymphoma (FL). *Blood* **2005**, *106*, 2169–2174. [\[CrossRef\]](#)
130. Taskinen, M.; Karjalainen-Lindsberg, M.L.; Nyman, H.; Eerola, L.M.; Leppä, S. A high tumor-associated macrophage content predicts favorable outcome in follicular lymphoma patients treated with rituximab and cyclophosphamide-doxorubicin-vincristine-prednisone. *Clin. Cancer Res.* **2007**, *13*, 5784–5789. [\[CrossRef\]](#)
131. Canioni, D.; Salles, G.; Mounier, N.; Brousse, N.; Keuppens, M.; Morchhauser, F.; Lamy, T.; Sonet, A.; Rousselet, M.-C.; Foussard, C.; et al. High numbers of tumor-associated macrophages have an adverse prognostic value that can be circumvented by rituximab in patients with follicular lymphoma enrolled onto the GELA-GOELAMS FL-2000 trial. *J. Clin. Oncol.* **2008**, *26*, 440–446. [\[CrossRef\]](#) [\[PubMed\]](#)
132. Clear, A.J.; Lee, A.M.; Calaminici, M.; Ramsay, A.G.; Morris, K.J.; Hallam, S.; Kelly, G.; MacDougall, F.; Lister, T.A.; Gribben, J.G. Increased angiogenic sprouting in poor prognosis FL is associated with elevated numbers of CD163+ macrophages within the immediate sprouting microenvironment. *Blood* **2010**, *115*, 5053–5056. [\[CrossRef\]](#)
133. Kridel, R.; Xerri, L.; Gelas-Dore, B.; Tan, K.; Feugier, P.; Vawda, A.; Canioni, D.; Farinha, P.; Boussetta, S.; Moccia, A.A.; et al. The Prognostic Impact of CD163-Positive Macrophages in Follicular Lymphoma: A Study from the BC Cancer Agency and the Lymphoma Study Association. *Clin. Cancer Res.* **2015**, *21*, 3428–3435. [\[CrossRef\]](#)
134. Stevens, W.B.C.; Mendeleville, M.; Redd, R.; Clear, A.J.; Bladergroen, R.; Calaminici, M.; Rosenwald, A.; Hoster, E.; Hiddemann, W.; Gaulard, P.; et al. Prognostic relevance of CD163 and CD8 combined with EZH2 and gain of chromosome 18 in follicular lymphoma: A study by the Lunenburg Lymphoma Biomarker Consortium. *Haematologica* **2017**, *102*, 1413–1423. [\[CrossRef\]](#)
135. Hume, D.A.; MacDonald, K.P.A. Therapeutic applications of macrophage colony-stimulating factor-1 (CSF-1) and antagonists of CSF-1 receptor (CSF-1R) signaling. *Blood* **2012**, *119*, 1810–1820. [\[CrossRef\]](#)
136. Martín-Moreno, A.M.; Roncador, G.; Maestre, L.; Mata, E.; Jiménez, S.; Martínez-Torrecuadrada, J.L.; Reyes-García, A.I.; Rubio, C.; Tomás, J.F.; Estévez, M.; et al. CSF1R protein expression in reactive lymphoid tissues and lymphoma: Its relevance in classical Hodgkin lymphoma. *PLoS ONE* **2015**, *10*, 1–14. [\[CrossRef\]](#) [\[PubMed\]](#)

137. Zhang, W.; Huang, Q.; Xiao, W.; Zhao, Y.; Pi, J.; Xu, H.; Zhao, H.; Xu, J.; Evans, C.E.; Jin, H. Advances in Anti-Tumor Treatments Targeting the CD47/SIRP α Axis. *Front. Immunol.* **2020**, *11*, 18. [\[CrossRef\]](#)
138. Papin, A.; Tessoulin, B.; Bellanger, C.; Moreau, A.; Le Bris, Y.; Maisonneuve, H.; Moreau, P.; Touzeau, C.; Amiot, M.; Pellat-Deceunynck, C.; et al. CSF1R and BTK inhibitions as novel strategies to disrupt the dialog between mantle cell lymphoma and macrophages. *Leukemia* **2019**, *33*, 2442–2453. [\[CrossRef\]](#)
139. Edwards, D.K.; Watanabe-Smith, K.; Rofelty, A.; Damnernasawad, A.; Laderas, T.; Lamble, A.; Lind, E.F.; Kaempf, A.; Mori, M.; Rosenberg, M.; et al. CSF1R inhibitors exhibit antitumor activity in acute myeloid leukemia by blocking paracrine signals from support cells. *Blood* **2019**, *133*, 588–599. [\[CrossRef\]](#)
140. Kaneda, M.M.; Messer, K.S.; Ralainirina, N.; Li, H.; Leem, C.; Gorjestani, S.; Woo, G.; Nguyen, A.V.; Figueiredo, C.C.; Foubert, P.; et al. PI3K γ is a molecular switch that controls immune suppression HHS Public Access. *Nature* **2016**, *539*, 437–442. [\[CrossRef\]](#) [\[PubMed\]](#)
141. Horwitz, S.M.; Koch, R.; Porcu, P.; Oki, Y.; Moskowitz, A.; Perez, M.; Myskowski, P.; Officer, A.; Jaffe, J.D.; Morrow, S.N.; et al. Activity of the PI3K-d,g inhibitor duvelisib in a phase 1 trial and preclinical models of T-cell lymphoma. *Blood* **2018**, *131*, 888–898. [\[CrossRef\]](#)
142. Locatelli, S.L.; Careddu, G.; Serio, S.; Consonni, F.M.; Maeda, A.; Viswanadha, S.; Vakkalanka, S.; Castagna, L.; Santoro, A.; Allavena, P.; et al. Targeting cancer cells and tumor microenvironment in preclinical and clinical models of Hodgkin lymphoma using the dual PI3Kd/G inhibitor RP6530. *Clin. Cancer Res.* **2019**, *25*, 1098–1112. [\[CrossRef\]](#)
143. Flinn, I.W.; O'Brien, S.; Kahl, B.; Patel, M.; Oki, Y.; Foss, F.F.; Porcu, P.; Jones, J.; Burger, J.A.; Jain, N.; et al. Duvelisib, a novel oral dual inhibitor of PI3K-d,g, is clinically active in advanced hematologic malignancies. *Blood* **2018**, *131*, 877–887. [\[CrossRef\]](#) [\[PubMed\]](#)
144. Cartron, G.; Ohresser, M.; Salles, G.; Solal-Célgny, P.; Colombat, P.; Watier, H. Neutrophil role in in vivo anti-lymphoma activity of rituximab: FCGR3B-NA1/NA2 polymorphism does not influence response and survival after rituximab treatment. *Ann. Oncol.* **2008**, *19*, 1485–1487. [\[CrossRef\]](#) [\[PubMed\]](#)
145. Grégoire, M.; Guilloton, F.; Pangault, C.; Mourcin, F.; Sok, P.; Latour, M.; Amé-Thomas, P.; Flecher, E.; Fest, T.; Tarte, K. Neutrophils trigger a NF-KB dependent polarization of tumorsupportive stromal cells in germinal center B-cell lymphomas. *Oncotarget* **2015**, *6*, 16471–16487. [\[CrossRef\]](#)
146. Hirz, T.; Matera, E.-L.; Chettab, K.; Jordheim, L.P.; Mathé, D.; Evesque, A.; Esmenjaud, J.; Salles, G.; Dumontet, C. Neutrophils protect lymphoma cells against cytotoxic and targeted therapies through CD11b/ICAM-1 binding. *Oncotarget* **2017**, *8*, 72818–72834. [\[CrossRef\]](#) [\[PubMed\]](#)



Received: 26 February 2021

DOI: 10.1002/hon.2855

SUPPLEMENT ARTICLE

WILEY

Vulnerabilities in the tumor and microenvironment in follicular lymphoma

Ferran Araujo-Ayala¹ | Patricia Pérez-Galán^{1,2} | Elías Campo^{1,2,3,4}

¹Department of Hematology-Oncology, Institut d'Investigacions Biomèdiques August Pi i Sunyer (IDIBAPS), Barcelona, Spain

²Hematological Neoplasms Program, Centro de Investigación Biomédica en Red-Oncología (CIBERONC), Madrid, Spain

³Hematopathology Unit, Pathology Department, Hospital Clinic of Barcelona, Barcelona, Spain

⁴Department of Basic Clinical Practice, University of Barcelona, Barcelona, Spain

Correspondence

Elías Campo, Hospital Clinic of Barcelona, Calle Villarreal 170, 08036-Barcelona, Spain. Email: ecampo@clinic.cat

Abstract

Follicular lymphoma (FL) is a paradigm of tumors that require the interaction between tumor and microenvironment cells to foster their development from initial steps to progression. Recent large-scale genome studies have uncovered multiple genetic alterations of FL that influence the microenvironment in two main directions, promoting tumor cell survival and proliferation and facilitating their evasion from immune antitumor signals. Understanding the crosstalk between tumor B-cells and the microenvironment will facilitate the identification of vulnerabilities that may offer novel targets for treatment of the patients. This review highlights recent findings showing the effect of common genetic mutations modulating the cell composition of the tumor microenvironment and the novel therapeutic perspectives to target these interactions.

KEYWORDS

follicular lymphoma, genomic alterations, microenvironment, target therapies

1 | INTRODUCTION

Follicular lymphoma (FL) develops in the germinal center (GC) of lymphoid follicles due, in most of the cases, to the acquisition of the t (14;18) translocation in precursor cells of the bone marrow which leads to the overexpression of the antiapoptotic protein BCL2. A second early oncogenic event in FL is the introduction of somatic mutations in the variable regions of immunoglobulin genes creating novel N-glycosylation sites for highly mannoseylated glycans that directly interact with endogenous lectins found in cells of the tumor microenvironment (TME). These interactions activate B-cell receptor signals required for tumor development. The third pillar in early steps of FL is recurrent mutations in epigenetic regulator genes that confer selective growth advantages to the B-cell and promote favorable interactions with the microenvironment.^{1,2} Further, development and progression of FL are associated with subsequent acquisition of additional genomic alterations that target different pathways related to cell differentiation, survival, proliferation, dissemination, and metabolic advantages among others. In addition to the genomic and epigenomic alterations, FL cells modulate the microenvironment to

promote the tumor cell growth.³ Understanding these complex phenomena and the crosstalk between tumor and stromal cells may facilitate the identification of vulnerabilities that will offer novel targets for treatment of the patients.

2 | FL GENOME AND NEW VULNERABILITIES

2.1 | Epigenetic modulators

Large-scale genomic studies combined with functional analysis have elucidated the mutational profile of FL and defined the several altered pathways involved in the pathogenesis of these tumors. The most common aberrations are mutations in the epigenetic regulators *KMT2D* (60%–90%), *CREBBP/EP300* (50%–70%/10%–20%), and *EZH2* (10%–30%). The high frequency of these lesions, their findings in “in situ” follicular neoplasia and acquisition in later steps in the evolution indicate that they are very early events but also favor the progression of the tumors.^{4,5} The loss of function mutations in the histone H3K4 methyltransferase *KMT2D* and in the H3K27

TABLE 1 Genomic and microenvironment alterations in follicular lymphoma as potential targets for novel treatment

Target	Type of alteration	Biological consequence	Targeted drug	Combinations	Status
Genomic aberrations					
<i>CREBBP</i>	Loss-of-function mutations	Downregulation of MHC class II	BRD3308	Anti-PDL1	Preclinical
<i>EZH2</i>	Gain-of-function mutations	Increased dependency on FDC	Tazemetostat	None	Approved
<i>TNFRSF14</i>	Inactivating mutations	Increased T _{FH} recruitment	CAR-T	None	Preclinical
<i>RRAGC</i>	Activating mutations	Insensitivity to nutrient deprivation	Temsirolimus	Bendamustine rituximab	Clinical
Increased B cell responses					
FL-microenvironment crosstalk					
B-cell receptor	FL-FDC	BCR activation	Ibrutinib	Rituximab	Clinical
	FL-DC-SIGN ⁺ Mφ				
PI3Kδ	FL-T _{FH}	CD40-CD40L activation, T _{reg} recruitment	Idelalisib	None	Approved
PI3Kγ	FL-T _{reg}				
	FL-monocyte/Mφ	Myeloid cell recruitment, M2 polarization	Duvelisib	None	Approved
CSF-1R	FL-Mφ	Myeloid cell recruitment and differentiation, M2 polarization	Pexidartinib	Rituximab	Preclinical
CD47- SIRP-α	FL-Mφ	CD47 ⁺ FL cells inhibit phagocytosis by Mφ and neutrophils	Anti-CD47	Rituximab	Clinical
	FL-neutrophils				

Abbreviations: BCR, B-cell receptor; FDC, follicular dendritic cell; FL, follicular lymphoma; MHC, major histocompatibility complex; T_{reg}, T-regulatory cell; T_{FH}, T-follicular helper.

acetyltransferase *CREBBP/EP300* together with the gain of function in the H3K27 methyltransferase *EZH2* tend to confer a repressive functional state of the genes targeted by these chromatin modifiers related to B-cell differentiation and cell cycle regulation that maintain tumor cells in a GC stage (Table 1).^{1,5} Particularly, *CREBBP* mutations silence genes that are direct targets of the BCL6-HDAC3 onco-repressor complex, including those that regulate B-cell signaling and immune responses, such as class II major histocompatibility complex (class II MHC). Other B-cell neoplasias, such as Hodgkin's lymphoma and primary mediastinal large B-cell lymphoma show class II MHC deregulation, but the mechanism is different mainly associated with *CITA* alterations.⁶ *CREBBP*-mutated tumors also seem to have less helper and cytotoxic T-cells in the microenvironment suggesting that these mutations favor tumor cell immune evasion.^{5,6} These crucial alterations in FL pathogenesis support the idea that *CREBBP* may be a gene with high therapeutic potential. In this sense, HDAC3 inhibition restores in part the immune responses and therefore may represent a new therapeutic approach in FL.⁷ Recent studies have also linked *EZH2* mutations to the reprogramming of the tumor and microenvironment interactions. Mutant cells in the light zone of the GC seem to be less dependent on T-follicular helper (T_{FH}) cells while potentiate their interaction and dependence on follicular dendritic cells (FDCs).⁸ On the other hand, *EZH2* also seems to play a role in the development of T and natural killer (NK) cells. The potential benefit of *EZH2* inhibitors independently of its

mutational status may be related to this extra tumor cell activity. Interestingly, Food and Drug Administration has approved the use of the selective *EZH2* inhibitor tazemetostat for adult relapse/refractory (R/R) patients with *EZH2*-mutated tumors and patients with R/R FL who have no satisfactory alternative treatment options.

2.2 | Immune evasion

Mutations and deletions of *TNFRSF14* in 1p36, also known as herpesvirus entry mediator A are a common event in FL (~50%).¹ *TNFRSF14* is the ligand for BTLA expressed in TFH cells and induces inhibitory signals on these cells. The disruption of these interactions results in increased recruitment of the tumor supportive T_{FH} and release of cytokines that also favor a pro-TME. In addition, *TNFRSF14* generates inhibitory signals on the B-cell receptor (BCR) of the B-cells that are released by the oncogenic inactivation. A preclinical CAR-T construct has been developed to continuously produce soluble *TNFRSF14* in the microenvironment that restores its inhibitory function.⁹

Ephrin receptor A7 (EPHA7) is a soluble tumor suppressor inactivated in approximately 70% of FL by mutations and deletions. Loss of expression avoids its binding to EPHA2 receptor, which inhibits extracellular regulated MAP kinase (ERK) and SRC proto-oncogene, non-receptor tyrosine kinase oncogenic signals.

Therapies that restore EPHA7 function or inhibit downstream oncogenic signals activated due to EPHA7 loss might be useful to treat FL-mutated patients.¹⁰

Recent studies have identified mutations in mammalian target of rapamycin complex 1 (mTORC1) pathway. Particularly, RAGC activating mutations are present in 17% of FL patients. These mutations activate mTORC1 bypassing amino acid deprivation and also confer an independent requirement of T_{FH} cells for tumor survival. Concordantly, these tumors have less T_{FH} cells in their stroma.¹¹ Thus, the identification of patients carrying mutations in this metabolic pathway may benefit of selective inhibitors.

Cathepsin S (CTSS) has been found to be mutated (6%) or overexpressed (13%) in FL leading to its hyperactivation.^{12,13} CTSS cleaves CD74, among other targets, which is fundamental for MHC II assembly and antigen (Ag) presentation. Hyperactive CTSS yields a more efficient Ag-specific CD4+ T activation, increased CD4+ T-cell infiltration, and proinflammatory cytokine perturbation in FL mouse models and human FL samples. Interestingly, the subversion of TME by this alteration correlates with high PDL2 expression that yielded FL patients more responsive to anti-PD1 regimens, and also associates with better outcomes to immunochemotherapy (rituximab, cyclophosphamide, doxorubicin, vincristine, and prednisone [R-CHOP]).

Other mutated genes in FL that also target the interactions between tumor cells and microenvironment are B2-microglobulin and CD58 that seem to be more common in transformed FL than in the early steps of the disease.¹ Thus, reactivating their function may improve cytotoxic response via CD8+ T cells.

3 | THERAPEUTIC OPPORTUNITIES FROM TME

Interaction of FL cells with nontumor cells constitutes a key feature in the pathophysiology of the tumor. A precise characterization of the TME could uncover new vulnerabilities to treat these patients. The tumor niche of this lymphoma is composed of different cells types, which create a tumor supportive environment and facilitate the escape from the host antitumor immune responses. The main actors in this TME are different subpopulations of T-cells, myeloid derived cells, mainly tumor-associated macrophages (TAMs), and stroma cells, mainly FDCs and cancer-associated fibroblasts, among others. These cells communicate among them and with tumor cells through a network of cytokines and cell-to-cell interactions.

3.1 | T-cells

T-cells are a heterogeneous group of cells that interplay with FL cells at different levels mediating antitumor responses or, contrarily, providing supportive protumoral signals. CD8+ cytotoxic cells, together with NK cells and probably T γ δ cells, mediate antitumor responses. However, FL cells may counteract this antitumor effect by secreting interleukin 12 (IL-12) that leads to an exhaustion of CD8+

cells and by recruiting T-regulatory cells (Tregs) that inhibit degranulation and cytotoxic activity of CD8+ cells.¹⁴ On the other side of the balance, two subpopulations of CD4+ cell, T_{FH}, and Treg play key roles in providing tumor support and facilitating immune evasion. In this way, T_{FH} stimulate tumor B-cells mediated by CD40L/CD40 and MHC class II interactions.¹⁵ These cells secrete IL-4, which triggers activation of B-cells mediated by ERK and STAT6, and the chemokine CCL22 that recruits immunomodulatory Treg cells. Treg cells are a subset of CD4+ cells characterized by the expression of the transcription factor FOXP3. These cells seem to play a pro-tumor role due to their immunosuppressive activity on CD4 and CD8 cells. However, a subset of T follicular regulatory cells (Tfr) has been also recognized by the additional expression of BCL6, CXCR5, ICOS, and PD1. These cells limit the expansion of the GC reaction and down-regulate the effects of T_{FH} cells. However, there is still some controversy regarding the impact of Tfr FOXP3+ expression patterns on FL survival.^{16,17}

The relevance of T_{FH} and Treg cells in FL has been highlighted by the effect of PI3K δ inhibitors disrupting the crosstalk between FL cells and T_{FH} cells. In vitro studies have shown that the PI3K δ inhibitor idelalisib, diminishes tumor cell proliferation, and reshapes immune microenvironment inhibiting the recruitment of classical Treg cells by downregulating CCL22.¹⁸

Finally, in this context of B-T-cell crosstalk, FL cells present immunoglobulin neoantigens that may play a determinant role in host immune responses, and constitute potential immunotherapeutic targets.¹⁹

3.2 | TAMs and other stromal cells

The role of TAMs in FL has been controversial. In the prerituximab era, some studies suggested that macrophage infiltration correlated with lower survival. Nevertheless, the addition of rituximab to chemotherapeutic drugs modified their prognostic impact. The number of infiltrating macrophages in patients treated with standard immunochemotherapeutic regimens such as R-CHOP was associated with improved overall survival.²⁰

In addition to the influence of new therapies in the possible role of TAM, different subpopulations of these cells may also play different roles in the pathogenesis of FL. Macrophages polarized to a M1 phenotype may exert antitumor properties by producing proinflammatory such as IL-1, IL-6, IL-12, and tumor necrosis factor α , whereas M2-polarized macrophages are protumor since they are able to downregulate MHC and IL-12, as well as expressing anti-inflammatory molecules such as arginase and IL-10, and the scavenger receptor CD163. Moreover, M2 macrophages are also involved in tumor angiogenesis. The protumor effect of TAMs, particularly with an M2 polarization, makes these cells and their interactions with tumor cells an attractive target for therapies.

In is noteworthy, that contrary to other B-cell lymphomas such as diffuse large B-cell lymphoma (DLBCL) or Hodgkin lymphoma, FL cells do not express PD-L1, and PD-L2 is moderately expressed in a

high proportion of FL cases.²¹ However, PD1 ligands are present in the immune infiltrates where PD-L1⁺ histiocytes have been detected in the T-cell-rich zone of the neoplastic follicles,²² justifying the therapeutic targeting of this pathway.

A target to interfere the FL-TAMs crosstalk is the colony-stimulating factor 1 receptor (CSF-1R), also known as macrophage colony-stimulating factor receptor, as it is a relevant element in the differentiation and survival of macrophages. Noteworthy, high levels of CSF-1R expression in FL have been associated with higher histological grade and risk of transformation suggesting that targeting CSF-1R may be relevant in high-risk patients. Although CSF-1R is expressed in both M1 and M2 subtypes, its inhibition by pexidartinib preferentially diminish the viability of M2 macrophages and repolarize them to M1 macrophages suggesting that it may reeducated TAMs toward an antitumor phenotype.

CD47 is a receptor usually expressed in cancer cells that prevents phagocytosis forming a complex with signal-regulatory protein α (SIRP- α). Among other phagocytes (e.g., neutrophils), macrophages may express SIRP- α in their membrane compromising their antitumor phagocytic function when interacting with CD47-positive lymphoma cells (Table 1). By administering a therapeutic antibody that blocks CD47, phagocytosis of tumor cells is increased and adaptive immunity is enhanced.²³ This effect has been explained by the Ag-presenting function of macrophages. After phagocytizing tumor cells, macrophages may present tumor Ag to CD4⁺ T-helper cells triggering an antitumor response. Altogether, anti-CD47 antibodies are now in clinical trials as promising drug candidates to activate the immune system in FL, especially in combined immunotherapeutic regimens including rituximab.

PI3Ky is expressed by microenvironment cells that support tumor growth such as CD4 and M2 macrophages. The dual PI3Ky δ inhibitor duvelisib exerts antitumor effects by targeting both the tumor and microenvironment cells (Table 1). This compound inhibits tumor cell proliferation and survival whereas also promotes the differentiation of M2-like TAMs to a M1 phenotype and inhibits the antitumor effect of T-cells interfering with the tumor supporting properties of the TME. Other drugs that interfere with BCR pathway such as ibrutinib may also affect the crosstalk of tumor cells and macrophages. While BTK inhibitors (BTKi) have not showed optimal results as monotherapy, the combination of the BTKi ibrutinib with the anti-CD20 rituximab has improved clinical trials results.²⁴

FDCs are from mesenchymal origin and build a network to support the GC reaction. They are able to present antibody–Ag complexes on their cell surface engaging BCR activation, survival of malignant cells and recruitment of T_H cells.¹⁸ Moreover, we have recently demonstrated that FL-FDC crosstalk induces monocyte recruitment and their differentiation to M2-protumoral macrophages.²⁵

Other cell types that may play an important role in the disease are different subsets of T-cells, TAMs, mesenchymal stem cells, or follicular reticular cells, among others. Interestingly, the evolution of this TME might be determinant in the transformation of FL to DLBCL.

4 | CONCLUDING REMARKS

Although in most cases FL initially presents as an indolent disease, a significant proportion of cases are primary refractory to standard treatment (R-CHOP or derivatives) and a high percentage of those who initially respond to treatment will eventually relapse. Once the relapse occurs, the prognosis of the patients worsens, especially in those who suffer an early relapse, within the first 24 months of treatment progression of disease within 2 years. Furthermore, those patients are in higher risk of histological transformation to an aggressive lymphoma, mainly DLBCL. The evolution of the patients cannot be precisely predicted exclusively based on single genetic alterations. Recent studies have shown that assays that include multiple genetic aberrations or combining both tumor B-cell biology and tumor microenvironment alterations may be better predictive models. These findings reinforce the need to integrate the mutational profile of the tumor cells together with the complex interactions of the TME to predict the biological risk of the patients. This comprehensive perspective should assist in identifying tumor and microenvironment vulnerabilities that will allow treating them effectively and avoiding early clinical progression.

ACKNOWLEDGMENTS

This study was funded by Ministerio de Ciencia e Innovación, Grant No. RTI2018-094274-B-I00 (to E. C.) and Fundación la Marató TV3 (TAIFOL 201933-30) (to P. P.-G.).

CONFLICT OF INTERESTS

The authors declare that there are no conflict of interests.

DATA AVAILABILITY STATEMENT

Data sharing not applicable to this article as no datasets were generated or analyzed during the current study.

REFERENCES

- Huet S, Sujobert P, Salles G. From genetics to the clinic: a translational perspective on follicular lymphoma. *Nat Rev Cancer*. 2018;18:224–239.
- Küppers R, Stevenson FK. Critical influences on the pathogenesis of follicular lymphoma. *Blood*. 2018;131:2297–2306. <https://doi.org/10.1182/blood-2017-11-764365>
- Kridel R, Sehn LH, Gascoyne RD. Pathogenesis of follicular lymphoma. *J Clin Invest*. 2012;122:3424–3431. <https://doi.org/10.1172/JCI63186>
- Schmidt J, Ramis-Zaldivar JE, Bonzheim I, et al. CREBBP gene mutations are frequently detected in situ follicular neoplasia. *Blood*. 2018;132:2687–2690.
- Green MR. Chromatin modifying gene mutations in follicular lymphoma. *Blood*. 2018;131:595–604. <https://doi.org/10.1182/blood-2017-08-737361>
- Green MR, Kihira S, Liu CL, et al. Mutations in early follicular lymphoma progenitors are associated with suppressed antigen presentation. *Proc Natl Acad Sci USA*. 2015;112:E1116–E1125. <https://doi.org/10.1073/pnas.1501199112>
- Mondello P, Tados S, Teater M, et al. Selective inhibition of HDAC3 targets synthetic vulnerabilities and activates immune surveillance

- in lymphoma. *Cancer Discov.* 2020;10:440-459. <https://doi.org/10.1158/2159-8290.CD-19-0116>
8. Béguélin W, Teater M, Meydan C, et al. Mutant EZH2 induces a pre-malignant lymphoma niche by reprogramming the immune response. *Cancer Cell.* 2020;37:655-673.e11. <https://doi.org/10.1016/j.ccell.2020.04.004>
 9. Boice M, Salloum D, Mourcin F, et al. Loss of the HVEM tumor suppressor in lymphoma and restoration by modified CAR-T cells. *Cell.* 2016;167:405-418.e13. <https://doi.org/10.1016/j.cell.2016.08.032>
 10. Oricchio E, Nanjangud G, Wolfe AL, et al. The Eph-receptor A7 is a soluble tumor suppressor for follicular lymphoma. *Cell.* 2011;147:554-564. <https://doi.org/10.1016/j.cell.2011.09.035>
 11. Ortega-Molina A, Deleyto-Seldas N, Carreras J, et al. Oncogenic Rag GTPase signalling enhances B cell activation and drives follicular lymphoma sensitive to pharmacological inhibition of mTOR. *Nat Metab.* 2019;1:775-789. <https://doi.org/10.1038/s42255-019-0098-8>
 12. Dheilly E, Battistello E, Katanayeva N, et al. Cathepsin S regulates antigen processing and T cell activity in non-Hodgkin lymphoma. *Cancer Cell.* 2020;37:674-689.e12. <https://doi.org/10.1016/j.ccell.2020.03.016>
 13. Bararia D, Hildebrand JA, Stolz S, et al. Cathepsin S alterations induce a tumor-promoting immune microenvironment in follicular lymphoma. *Cell Rep.* 2020;31:107522. <https://doi.org/10.1016/j.celrep.2020.107522>
 14. Amé-Thomas P, Tarte K. The yin and the yang of follicular lymphoma cell niches: role of microenvironment heterogeneity and plasticity. *Semin Cancer Biol.* 2014;24:23-32. <https://doi.org/10.1016/j.semcancer.2013.08.001>
 15. Amé-Thomas P, Le Priol J, Yssel H, et al. Characterization of intra-tumoral follicular helper T cells in follicular lymphoma: role in the survival of malignant B cells. *Leukemia.* 2012;26:1053-1063. <https://doi.org/10.1038/leu.2011.301>
 16. Carreras J, Lopez-guillermo A, Fox BC, et al. High numbers of tumor-infiltrating FOXP3-positive regulatory T cells are associated with improved overall survival in follicular lymphoma. *Blood.* 2006;108:2957-2964. <https://doi.org/10.1182/blood-2006-04-018218.EC>
 17. Farinha P, Al-Tourah A, Gill K, Klasa R, Connors JM, Gascoyne RD. The architectural pattern of FOXP3-positive T cells in follicular lymphoma is an independent predictor of survival and histologic transformation. *Blood.* 2010;115:289-295. <https://doi.org/10.1182/blood-2009-07-235598>
 18. Serrat N, Guerrero-Hernández M, Hernández H, et al. PI3Kd inhibition reshapes follicular lymphoma-immune microenvironment cross talk and unleashes the activity of venetoclax. *Blood Adv.* 2020; 4(17):4217-4231. <https://doi.org/10.1182/bloodadvances.2020001584>
 19. Khodadoust MS, Olsson N, Chen B, et al. B-cell lymphomas present immunoglobulin neoantigens. *Blood.* 2019;133:878-881.
 20. Kridel R, Xerri L, Gelas-Dore B, et al. The prognostic impact of CD163-positive macrophages in follicular lymphoma: a study from the BC Cancer Agency and the Lymphoma Study Association. *Clin Cancer Res.* 2015;21:3428-3435. <https://doi.org/10.1158/1078-0432.CCR-14-3253>
 21. Laurent C, Charmpi K, Gravelle P, et al. Several immune escape patterns in non-Hodgkin's lymphomas. *Oncotarget.* 2015;4:e1026530. <https://doi.org/10.1080/2162402X.2015.1026530>
 22. Myklebust JH, Irish JM, Brody J, et al. High PD-1 expression and suppressed cytokine signaling distinguish T cells infiltrating follicular lymphoma tumors from peripheral T cells. *Blood.* 2013;121:1367-1376. <https://doi.org/10.1182/blood-2012-04-421826>
 23. Zhang W, Huang Q, Xiao W, et al. Advances in anti-tumor treatments targeting the CD47/SIRPα axis. *Front Immunol.* 2020;11:18. <https://doi.org/10.3389/fimmu.2020.00018>
 24. Fowler NH, Nastoupil L, De Vos S, et al. The combination of ibrutinib and rituximab demonstrates activity in first-line follicular lymphoma. *Br J Haematol.* 2020;189:650-660. <https://doi.org/10.1111/bjh.16424>
 25. Valero JG, Matas-Céspedes A, Rodríguez V, et al. The receptor of the colony-stimulating factor-1 (CSF-1R) is a novel prognostic factor and therapeutic target in follicular lymphoma. *Leukemia.* 2021. <https://doi.org/10.1038/s41375-021-01201-9>

How to cite this article: Araujo-Ayala F, Pérez-Galán P, Campo E. Vulnerabilities in the tumor and microenvironment in follicular lymphoma. *Hematological Oncology.* 2021;39(S1):83-87. <https://doi.org/10.1002/hon.2855>

ACKNOWLEDGEMENTS

ACKNOWLEDGEMENTS

El fet d'escriure aquestes línies ajuda a reflexionar sobre la construcció d'aquesta tesi doctoral, de com va començar, on hem arribat i cap a on hem de seguir. Vist en perspectiva, aquests quatre anys i escaig que porto al laboratori han passat força ràpid. Tot i començar d'una manera accidentada, amb una pandèmia que m'enviava a casa sense resultats que analitzar ni el Nanostring en marxa, mica en mica vam anar remuntant, fins aconseguir aquests 3 estudis (encara que un encara estigui a mig fer) dels que hem d'estar molt orgullosos com a equip. Dit això, aniré mencionant, seguint el meu estil sintètic, les persones que han estat al meu costat durant aquest temps i han fet possible la realització d'aquesta tesi.

En primer lugar, como no podía ser de otra manera, tengo que agradecer a Patricia su confianza en mí desde el primer momento. Me diste la oportunidad de hacer una tesis doctoral, cumpliendo así mi sueño por el que tanto había luchado desde hacía muchos años. Luego, volviste a confiar en mí para llevar a cabo el proyecto de los CAR-Ts. Durante este tiempo espero haber aportado lo mejor de mí al crecimiento espectacular de tu grupo. Te contacté al ver la noticia de que había un nuevo grupo en el IDIBAPS y, pocos años más tarde, ya eres una súper PI. Ha sido un placer compartir estos años trabajando juntos y aprendiendo mucho de ti.

En este sentido, también tengo que mencionar a Armando, que ayudó a mi contratación previa a la Marató y, aunque finalmente el inicio del proyecto se retrasó por el COVID, generosamente me siguió apoyando. Me alegra que además hayas podido ser mi tutor universitario durante esta etapa.

ACKNOWLEDGEMENTS

Aquest temps m'he trobat amb grans companys al laboratori, tots ells disposats a donar un cop de mà quan era necessari, però sobretot he treballat colze a colze amb la Cèlia. El temps que hem estat junts fent l'IMLINFO ha estat relativament breu (des del desconfinament fins que ens vam acomiadar a Pamplona) però increïblement intens. Hem viscut tantes coses que seria impossible plasmar-les en aquest capítol. Encara que ara estiguem lluny, sé que en aquesta tesi vaig guanyar una amiga per a tota la vida i que podrem seguir comptant l'un amb l'altre, de la mateixa manera que quan fèiem experiments junts i se'ns acumulaven els marcatges.

Des que vaig arribar, tu i l'Heribert m'heu acollit com al vostre germà petit. Quan vaig començar vosaltres ja éreu uns grans dominadors del lab. Què hauria fet sense els coneixements de citometria de l'Heribert? Encara que a vegades l'hem desesperat una mica amb les nostres compensacions, sempre ens ha seguit donant un cop de mà. Tampoc cal oblidar la seva excel·lent faceta com a “company de viatges”, ja que he recorregut bona part d'Espanya amb ell: Santiago, Sevilla i ara properament Vigo, a més dels grupals com Pamplona i Nova Orleans. És una sort que segueixis al lab encara que ara ja siguis tot un doctor i professor de la uni.

Evidentment, també agrair a tots els altres companys del lab, és una gran sort saber que passi el que passi qualsevol d'ells et cobreix l'esquena. Així, gràcies als postdocs: Juan, nuestro gran consejero de figuras y presentaciones; i Neus, la teva actitud fa que siguis una predoc més però amb els consells i la saviesa d'una gran postdoc. També als predocs que han vingut després, Rubén i Noelia, que us heu integrat perfectament a l'equip i seguiu amb la nostra saga.

Agrair especialment a la Dolors per estar sempre allà cuidant de tots i fer una gran família unida encara que oficialment siguem dos grups. Els teus consells (científics o no) sempre són molt valuosos. Gràcies també a tot el teu equip, entre els que vull destacar la Irene, el Juan i, per sobre de tots, l'Ari, el motor del nostre laboratori, sense la qual res no rutllaria.

Per acabar aquesta part dels agraïments, com a metàfora de la successió, mencionar la Maria, la meva primera estudiant, compartida amb la Cèlia. Vas venir en temps difícils, encara a mig desconfinar (i jo sense haver trepitjat gaire el CEK estava mig perdut). Moltes gràcies per incorporar-te al mini-equip dels CAR-Ts i ajudar-me a acabar la història del CD70. No pateixis que jo sé que deixo el lab en bones mans.

En resum, es pot dir que he caigut en un gran lloc per fer la tesi, però no seria tan bo si no fos perquè a l'altra banda del passadís tenia la Judith, la meva companya de lab durant el TFG i de vida per sempre. Poder compartir l'etapa de tesi amb tu ha estat meravellós, no hi ha preu per sortir de casa junts, anar a la feina plegats i saber que si no tenia un bon dia podia treure el cap pel passadís i allà estaries. Tenir l'oportunitat d'anar a congressos (i retreats) junts i donar-nos suport mutu ha estat únic. Tot això a més de l'ajuda científica que m'has donat aquests anys. Els meus èxits també són teus.

Agradecer també a tu inseparable companyera de tesis, Bea, a la que considero una amiga més, així com al Ferran, que sempre em deixa amb un somriure els anàlisis de bioinformàtica ben macos i preparats. Tampoc em voldria oblidar del personal de citometria de l'IDIBAPS, en especial de la Sara i la Selma.

ACKNOWLEDGEMENTS

I, finalment, donar les gràcies a totes les persones que han col·laborat perquè aquests projectes sortissin endavant. En primer lloc, als hematòlegs, que ens donen una gran visió clínica i suport en els nostres estudis: Eva, Pablo, Andrea i Laura. Une mention spéciale au groupe de Toulouse (Christine, Carla et Fabien), pour votre collaboration et de nous ouvrir les portes de votre laboratoire. Gracias a Carlos y Raluca por acogerme en Pamplona durante un mes y enseñarme las técnicas de patología, así como vuestra paciencia hasta lograr que salieran los paneles más complejos. Per últim, agrair a la Sònia i al seu grup, especialment a les implicades en el projecte (Salut, Mireia, Marta i Alba) per introduir-me en el món dels CAR-Ts i compartir el seu coneixement en la matèria.

En el nostre àmbit, la contribució de tanta gent és necessària per tirar endavant els projectes i fer una petita contribució en el coneixement científic, però també és imprescindible tenir el suport de la gent que ens envolta al nostre dia a dia. Per aquest motiu, m'agradaria acabar aquesta tesi agraint a totes les persones que m'han acompanyat en aquest camí, tant familiars com amics. En aquest capítol, per sobre de tot, agrair el suport que m'han donat des de sempre els meus pares, Pepi i Joan Carles, així com el meu germà Marc i la seva família (l'Eveline i el Biel, que va néixer un dia de buffy) i la meua família política (Elvira, José María i Laura).